IMPACT OF CABLE BACTERIA
ON THE BIOGEOCHEMICAL CYCLING
IN A SEASONALLY HYPOXIC BASIN

Dorina Seitaj

Promotor: Prof. dr. ir. Filip Meysman

Proefschrift ingediend tot het behalen van de graad van
Doctor in de Wetenschappen

Vrije Universiteit Brussel

Darwin Center for Biogeology

NIOZ

DOCTORAATSJURY

Promotor: Prof. dr. ir. Filip Meysman   Vrije Universiteit Brussel

Overige Leden:

Prof. dr. Phillipe Claeys	Vrije Universiteit Brussel
Prof. dr. Frank Dehairs	Vrije Universiteit Brussel
Prof. dr. Mark Kochzius	Vrije Universiteit Brussel
Prof. dr. ir. Eveline Peeters	Vrije Universiteit Brussel
Prof. dr. ir. Caroline Slomp	Universiteit Utrecht
Prof. dr. Heide Schulz	Leibniz Institute for Baltic Sea Research (IOW)
Prof. dr. Nils Risgaard-Petersen	Aarhus University

Contents

Acknowledgements

Summary

Coastal hypoxia refers to the oxygen depletion that occurs in the bottom waters of semi-enclosed and stratified coastal systems. There is evidence for a global increase in the frequency, extent, intensity and duration of coastal hypoxia, which has been linked to an increased anthropogenic input of nutrients into the coastal ocean in combination with climate change. Bottom water hypoxia has major consequences for the functioning of coastal ecosystems, as it has profound effects on the biogeochemical cycling, and on the survival and behavior of marine organisms in coastal systems. Hypoxia reaches a particularly harmful stage when sulfide is released to the bottom water where it can give rise to the establishment of euxinia (i.e. sulfidic bottom waters). As sulfide is highly toxic for marine life, the occurrence of euxinia can have devastating ecosystem consequences. Although coastal hypoxia is relatively common, reports of euxinia are less frequent, and so the question remains why euxinia is uncommon. Sulfide effluxes from the sediment are regulated by microbial and geochemical processes occurring in the sediment compartment. Still, the environmental controls that regulate the onset of hypoxia and euxinia, as well as the effects of these phenomena on coastal ecosystems are poorly understood.

To examine the role of sediments in coastal hypoxia, a detailed study was conducted over multiple years in Lake Grevelingen, a saline and stratified coastal reservoir in the Netherlands. This study involved monthly investigations of the water column chemistry, sediment biogeochemistry and sediment microbiology over two consecutive years, and revealed the major environmental controls of oxygen depletion in the lake. Water column stratification and enhanced respiration of allochthonous organic material were the main drivers of oxygen uptake in the bottom waters. A mass balance for organic carbon suggests that the basin acts as a sediment trap for allochthonous material, likely transported from the adjacent North Sea. A major part of this organic material is respired in the sediment, and consequently the sedimentary oxygen consumption is high and responsible for a major part of the total oxygen uptake from the bottom water. The bottom waters of Lake Grevelingen experience anoxia in summer but do not develop euxinia. This thesis documents that the seasonal appearance of cable bacteria can prevent, or substantially delay, the development of euxinia.

Cable bacteria induce the formation of a large pool of sedimentary iron oxides before the onset of summer hypoxia. This pool of iron oxides acts as a 'firewall' against the release of sulfide to the bottom water in early summer, and likely prevents the development of bottom water euxinia. The iron oxides layer contains also a large stock of bound phosphorus, which is then released to the water column upon the reduction of the iron (hydr)oxides in summer. Hence, cable bacteria appear to be key drivers of iron and phosphorous cycling in seasonal hypoxic basins at the ecosystem scale, which reveals that the biogeochemical impact of sedimentary microbes may extend far beyond the sediment-water interface.

The electrogenic metabolism of cable bacteria provides an efficient way of deep sulfide removal in marine sediments. This way cable bacteria provide another solution to the

"aerobic sulfide oxidation paradox". This paradox states that most sulfide in sediments is removed through oxidation with oxygen, though oxygen and sulfide are never into contact, as they are separated by a wide suboxic zone. Electrogenic sulfur oxidation by cable bacteria is able to connect oxygen and sulfide in distinct sediment horizons, and so enables aerobic sulfide oxidation by means of long-distance electron transport. Here, we also show that the three known mechanisms of suboxic zone formation (cable bacteria, nitrate accumulating *Beggiatoaceae*, metal cycling driven by bioturbation) can be differentiated by their pH imprint on the pore water. This analysis was obtained by combining field observations with reactive transport modelling. These insights provide a better understanding and guidance as to the different mechanisms of sulfide oxidation and suboxic zone formation in the seafloor.

Samenvatting

Seizoenale hypoxie refereert naar het zuurstoftekort dat voorkomt in het bodemwater van halfafgesloten en gestratificeerde kustsystemen. Naast de natuurlijk voorkomende zuurstofloosheid, is er bewijs voor een wereldwijde toename in de frequentie, omvang, intensiteit en duur van hypoxie als gevolg van eutrofiëring en klimaatverandering. Zuurstoftekort in het bodemwater heeft grote gevolgen voor het functioneren van kustecosystemen, vanwege de grote effecten op de biogeochemische cycli en de impact op de overlevingskansen en het gedrag van mariene organismen. Een bijzonder schadelijk stadium van hypoxie is de zogeheten euxinie. Deze fase treedt op als sulfide, een stof die erg toxisch is voor mariene levensvormen, vrijkomt in het water (zwavelhoudend bodemwater). Hoewel hypoxie relatief veel voorkomt, is de frequentie van euxinie veel lager. Dat roept de vraag op waarom euxenie zeldzamer is. Sulfide concentraties in het sediment en het bodemwater worden sterk gereguleerd door microbiële en geochemische processen in het sediment. Maar er is tot nu toe weinig kennis over welke processen hypoxie en euxinie reguleren en wat de gevolgen van deze vormen van zuurstoftekort zijn op kustecosystemen.

Om de rol van sedimenten in de hypoxie van kustwateren te bestuderen, hebben we een gedetailleerde studie uitgevoerd, over meerdere jaren. Deze studie vond plaats in het Grevelingenmeer, een gestratificeerd zoutwatermeer in het zuidwesten van Nederland. De studie betrof maandelijkse metingen van de chemie van de waterkolom, de biogeochemie van het sediment, en de microbiologie van het sediment over de loop van twee jaar. Zo werden de belangrijkste oorzaken van zuurstofgebrek in het Grevelingenmeer duidelijk. Het grootste aandeel in het zuurstofgebruik van het systeem is toe te schrijven aan stratificatie van de waterkolom en de toename in respiratie door allochtoon organisch materiaal. Een massabalans van organische koolstof suggereert dat het Grevelingenbekken een sedimentval vormt voor organisch materiaal dat waarschijnlijk uit de ondiepere gedeeltes van het meer of uit de naburige Noordzee afkomstig is. Een groot gedeelte van dit organische materiaal wordt in de bodem van de Grevelingen afgebroken, en deze afbraak zorgt voor een groot gedeelte van de zuurstofconsumptie in het bodemwater. Dit bodemwater is des zomers zuurstofloos, maar ontwikkelt geen euxinie. In dit proefschrift laat ik zien dat de seizoenale aanwezigheid van zogeheten kabelbacteriën de ontwikkeling van euxinie kan voorkomen of in elk geval substantieel vertragen.

De recent ontdekte kabelbacteriën maken een groot reservoir aan van sedimentaire ijzeroxides voor de start van de zomerhypoxie. Dit reservoir capteert vervolgens vrije sulfide, wat geproduceerd wordt door sulfaatreductie in de bovenste sedimentlaag. Dit mechanisme werkt als een 'branddeur' tegen het vrijkomen van sulfide uit het sediment en voorkomt waarschijnlijk de ontwikkeling van euxinie tijdens de zomer. De gevormde ijzeroxide-laag heeft daarbij ook een grote voorraad aan ijzergebonden fosfaat, die in de waterkolom vrijkomt tijdens de reductie van de ijzer(hydr)oxides in de zomer. Zodoende zijn kabelbacteriën sleutelfactoren in de ijzer- en fosforcyclus op de schaal van het gehele ecosysteem, niet alleen in de Grevelingen, maar ook in andere seizoenaal zuurstofarme

bassins. Dit laat zien dat de biogeochemische impact van microben in de bodem veel verder strekt dan het dunne laagje waar sediment en water elkaar raken.

In de stofwisseling van de kabelbacteriën speelt elektriciteit een belangrijke rol. Dat zorgt voor een efficiënte manier om sulfide uit de bodem van zouterwatermeren of de zee te verwijderen. De bacteriën leveren daarmee ook een andere mogelijke verklaring voor de zogeheten 'aerobe sulfideoxidatie paradox'. Het sulfide in het sediment verdwijnt omdat het reageert met zuurstof, maar de zuurstof en het sulfide zijn nooit met elkaar in contact: ze worden van elkaar gescheiden door een "geochemisch niemandsland", waar zowel zuurstof als sulfide ontbreken. De kabelbacteriën kunnen dit niemandsland echter overbruggen door elektronentransport over langere afstand. Ik laat hier ook zien dat de drie mechanismen een dergelijke zone kunnen veroorzaken (kabelbacteriën, nitraatstapelende *Beggiatoaceae*, en het vrijkomen van metalen doordat organismen het sediment omwoelen). Deze mechanismen kunnen van elkaar onderscheiden worden, doordat ze een andere chemische vingerafdruk achterlaten: de pH van het poriënwater is bij alledrie anders. Deze analyse ontstond door het combineren van veldwaarnemingen met geochemische modellen. Deze inzichten zorgen voor een beter begrip van de verschillende mechanismen van sulfide-oxidatie in kustgebieden en geven beter inzicht in de vorming van zuurstofloze zones nabij de zeebodem.

10

Lake Grevelingen

Photo: Silvia Hidalgo Martinez

GENERAL INTRODUCTION

1.1. Oxygen distribution in the ocean

Oxygen (O_2) is essential for the functioning of marine ecosystems, as this reactive compound is involved in the major processes that regulate the biogeochemical cycling in these systems. The oxygen concentration in marine waters is essentially controlled by a balance between supply and removal, driven by various biological and physical processes that occur both in the water column and in the sediment compartment. Oxygen supply is linked to the gas transport from the atmosphere and primary production in the photic zone or within the benthic zone by microphytobenthos (Glud 2008). On the other side, oxygen is rapidly consumed via respiration during the mineralization of organic matter, or upon chemical reaction with reduced compounds (Glud 2008; Testa and Kemp 2011).

As this balance between O_2 supply and O_2 removal differs between locations, the global distribution of oxygen is not homogenous, and the ocean hosts areas that exhibit high oxygen concentrations ($\geq$ air saturation), and zones where oxygen levels are low ($\leq 20\%$ air saturation) (Fig. 1a) (Falkowski et al. 2011). Highly oxygenated waters are found mostly at high latitudes, both in the northern and southern hemispheres (Fig. 1a). Here, oxygen is produced by photosynthesis in the photic zone, and the cold waters have a high solubility for oxygen. Oxygen-rich surface water is subsequently downwelled to deeper depths.

Oxygen deficiency ($[O_2] < 90$ µmol L^{-1}) occurs in specific areas, referred to as Oxygen Minimum Zones (OMZs), which combine sluggish ocean circulation with high surface productivity (Codispoti 2005; Paulmier and Ruiz-Pino 2009). The largest OMZs are located in mid-water layers between 200-1000 m water depth in the eastern Pacific Ocean off Peru, Chile and Mexico, the southeastern Atlantic Ocean off Namibia and Angola, and in the northern Indian Ocean (Stramma et al. 2008; Paulmier and Ruiz-Pino 2009). Within these OMZs, the upwelling of nutrient-rich deep water stimulates primary production in the photic zone. The organic material resulting from this enhanced productivity subsequently sinks to deeper water layers (typically between 200 and 1000 m water depth), where it is consumed in biological respiration, thus creating a high oxygen demand and oxygen depletion (Helly and Levin 2004).

In a restricted number of oceanic regions, the oxygen concentration drops below detection limits and gives rise to anoxia, as observed in the Black Sea (Konovalov and Murray 2001), the deep basins of the Baltic Sea (Carstensen et al. 2014a), and the Cariaco basin (Scranton et al. 2014) (Fig. 1a). In these basins, the combination between topography and stratification strongly impedes the renewal of the bottom waters, thus leading to the establishment of permanent anoxic conditions.

1.2. Coastal hypoxia

Oxygen limitation is not a feature of the open ocean alone, but it also affects shallow waters in shelf regions and coastal zones, where it is referred to as coastal hypoxia (Fig. 1b). Enclosed basins and land-locked fjords, characterized by limited bottom water renewal
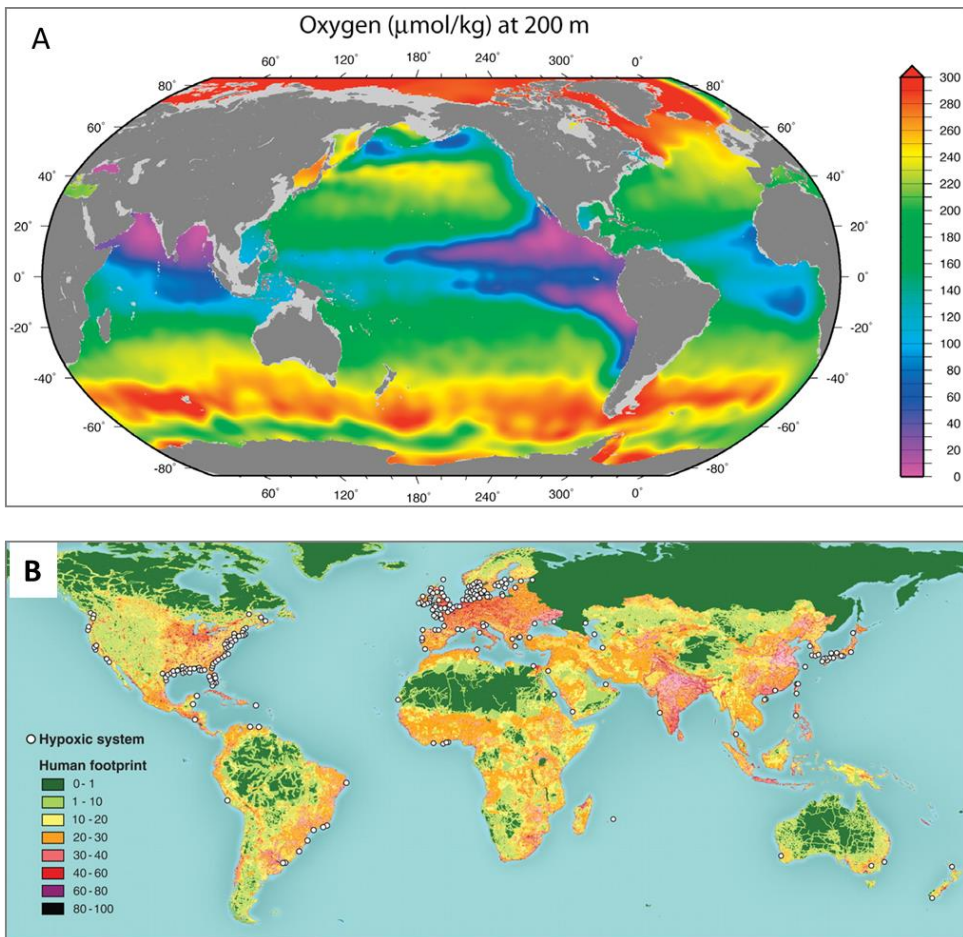
Figure 1. (A) Mean global ocean oxygen concentrations at 200 meters below the surface. Note the extensive regions of low oxygen (oxygen minimum zones) throughout the low- latitude oceans and the subarctic Pacific. Data from the World Ocean Circulation Experiment Global Hydrographic Climatology. Modified from Falkowski et al. 2011. (B) Global distribution of 400-plus systems that have scientifically reported accounts of being eutrophication-associated dead zones (Diaz and Rosenberg 2008).

and long residence times, are naturally prone to oxygen depletion. Alongside this natural occurrence of oxygen depletion, the ongoing increase of coastal hypoxia has been linked to anthropogenic activity such as enhanced nutrient input to the coastal zone and climate change (Kemp et al. 2005, 2009; Turner et al. 2008; Diaz and Rosenberg 2008; Middelburg and Levin 2009). Well studied hypoxic systems occur in the southwestern Louisiana coast and Texas shelf (Boesch and Rabalais, 1991; Ritter and Montagna, 1999), the lower

Chesapeake bay (Holland et al. 1987; Dauer et al. 1992; Llans 1992), the Northern Adriatic Sea (Justić et al. 1987; Stachowitsch 1991; Rabalais et al. 2007), Arhus bay (Jørgensen 1980), fjords along the Swedish coast (Rosenberg 1990; Rosenberg et al. 2001, 2002; Karlson et al. 2002; Rosenberg and Nilsson 2005), in the southern Kattegat (Andersson and Rydberg 1988) and in the deeper basins of the Baltic Sea (Conley et al. 2009; Carstensen et al. 2014a).

Like in the OMZs, stratification and enhanced oxygen consumption from respiration are the two principal drivers of coastal hypoxia (Testa and Kemp 2014; Figure 2a). However the timing is rather different, especially in temperate regions (Figure 2b). While O_2 deficiency in the open ocean is a more permanent phenomenon, coastal hypoxia typically follows a seasonal or ephemeral temporal pattern. In temperate systems, phytoplankton blooms typically occur in spring (Figure 2A). In the following months, the bloom-derived organic material is respired in the water column or within the sediment, creating a high oxygen demand in the lower layers of the water column. Stratification also becomes strongest in the same period, when the warming of the surface waters isolates the surface layer from the denser and colder water below the picnocline (Levin et al. 2009). As the ongoing respiration of organic matter consumes oxygen, in the absence of water renewal, hypoxic ($[O_2] < 63$ µmol L^{-1}) and sometimes even anoxic conditions ($[O_2] < 1$ µmol L^{-1}) are established in the bottom water (Fig. 2B). This condition ceases in fall, as the disruption of the water column stratification allows the reoxygenation of the bottom waters.

1.3. Oxygen distribution in a changing world

At present, there is growing evidence that the prevalence and intensity of oxygen deficiency in marine waters is increasing worldwide, both in the open ocean (Stramma et al. 2008) and in the coastal zone (Diaz and Rosenberg, 2008). There is consensus that this phenomenon is tightly linked to human-induced global changes, most notably climate change and coastal eutrophication (Stramma et al. 2008; Diaz and Rosenberg 2008; Keeling et al. 2010).

The loss of dissolved oxygen from the open ocean is referred to as ocean de-oxygenation (Keeling et al. 2010). Changes in the oxygen content of the ocean interior are mainly driven by climate effects (Keeling et al. 2010). Oxygen is less soluble in warmer water, and hence, an increase in the temperature will decrease the inventory of oxygen within the ocean. Combined with changes in wind and precipitation patterns, higher temperatures will also increase stratification and reduce ventilation, thereby reducing the downward transport of oxygen to deeper waters and seafloor ecosystems. Finally, higher seawater temperatures enhance the respiratory and metabolic rates of organisms, thus stimulating the biological demand for oxygen.

As noted above, the increased prevalence of low-oxygen conditions in coastal and shelf waters is referred to as coastal hypoxia (Diaz and Rosenberg, 2008). In addition to climate effects, the coastal zone is affected by another component of global change, that is, the

A

Non-stratified system

N+P

Pelagic
production

O₂

Pelagic
respiration

Benthic respiration

Stratified system

N+P

Pelagic
production

Pycnocline

O₂

Pelagic
respiration

High O₂

Low O₂

B

winter   spring   summer   fall - winter

Bottom water [O₂]

H₂S
efflux

Stratification Hypoxia   Anoxia   Reventilation
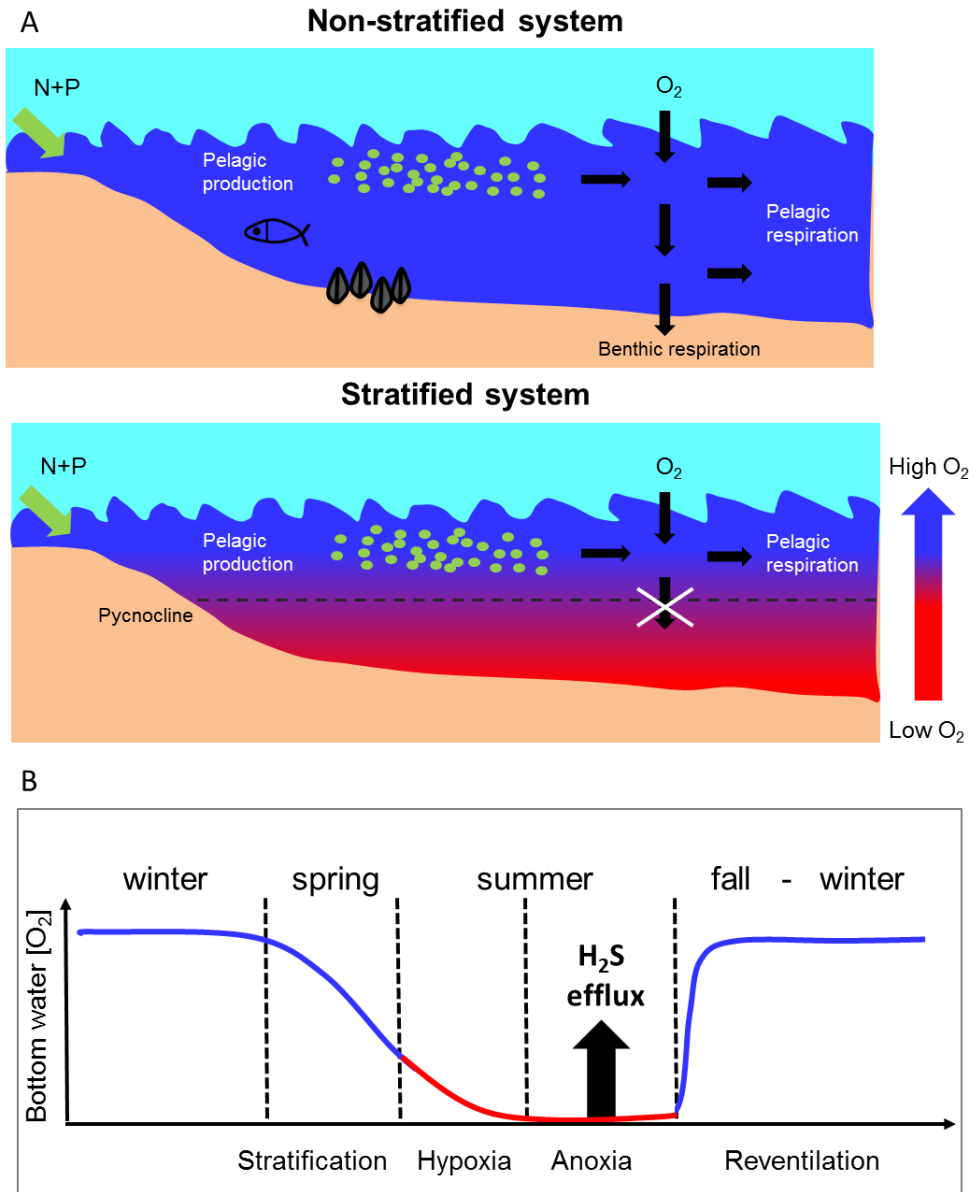
Figure 2. (A) Simplified scheme of coastal hypoxia. Water column stratification and intensified respiration of organic matter are the main drivers of oxygen depletion in the bottom water. (B) Oxygen concentrations in the bottom water (blue and red line) exhibit a pronounced seasonal pattern.

15

increased nutrient delivery from land. Human activity has greatly accelerated the flow of nutrients to estuaries and coastal ecosystems over the past half century, thus stimulating primary production in the coastal zone. This results in a larger supply of organic material to deeper water layers and sediments, stimulating respiration and causing a lower oxygenation in bottom waters (Diaz and Rosenberg, 2008; Conley et al., 2009). At the same time, climate change is anticipated to increase the temperature of the surface waters in summer, and the resulting intensification of water column stratification and decrease in oxygen solubility may exacerbate coastal hypoxia in the upcoming decades (Meire et al., 2014).

1.4. Coastal hypoxia in the Marine Lake Grevelingen

Lake Grevelingen is a former estuary within the Scheldt-Meuse-Rhine delta area of The Netherlands, which was closed off from the North Sea after a devastating storm surge ravaged the Dutch delta region in 1953 (Fig. 3). This coastal marine lake was formed by the construction of a landward dam in 1965 and later a seaward dam in 1971.
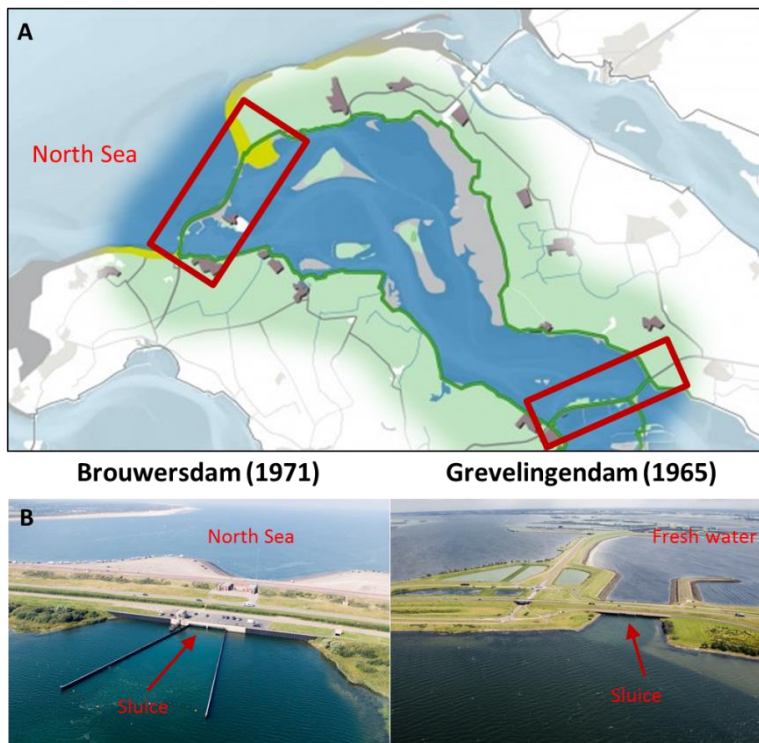
Figure 3. (A) Lake Grevelingen map; (B) seaward and landward dams in the Lake Grevelingen.

Currently, Lake Grevelingen covers a surface area of around 115 km^2, and consists mostly of shallow water areas <12.5 m water depth. However, deep basins which extend down to 45 m water depth are found in the former estuarine channels, and are separated from each other by sills. An underwater sluice is located at 10 m water inside the seaward dam (Paulij et al., 1990), which enables a water exchange with the open sea (Fig. 3b). The sluice operates daily since 1999, and as a result, the salinity in the lake approaches marine values (29-32). In the main gully, stratification develops in the water column each spring and summer (Hagens et al., 2015). The isolation of the bottom waters due to the summer stratification leads to the development of seasonal hypoxia in the bottom waters of the deeper basins in the gully (Wetsteyn 2011). In fall, wind-induced currents and storms disrupt the stratification (Nienhuis and De Bree, 1977), and the water column remains mixed and oxygenated until the end of winter.

Starting from the closure of the lake from the North Sea in 1971, fine-grained, organic rich sediments have accumulated in the deep basins located in the main gully (Table 1).

Table 1. Geochemical characteristics and composition of the sediment in Lake Grevelingen. Values are provided in mean value ± standard deviation calculated over *n* number of replicates.

Parameters	Value	*n*	Units
Solid phase density	2.6 ± 0.03	4	g cm^{-3}
Porosity	0.89 ± 0.01	10	-
Median grain size	16 ± 0.01	3	μm
Organic C (C$_{org}$)	3.4 ± 0.2	23	%
N total	0.42 ± 0.02	23	%
C/N ratio	8.1 ± 0.1	3	%
Total C	6 ± 0.2	23	%
Inorganic C	2.6 ± 0.2	23	%
Ca	8.69 ± 0.01	3	%
Mg	1.33 ± 1.33	3	%
Fe	3.15 ± 3.15	3	%
Mn	0.042 ± 0.001	3	%
P	0.099 ± 0.001	3	%
S	1.27 ± 0.02	3	%
CaCO$_3$	21.7		%
AVS	130		μmol g^{-1}
S^0	64 ± 21		μmol g^{-1}

These muddy, silt deposits overlay the older sand layer, which originated during the estuarine phase of the area. Currenlty, due to the high sedimentation rates taking place in Den Osse basin (up to 2 cm y^{-1}), the dark mud layer forms up to 100 cm of the top sediment at the deepest sites within the basin. These deposits contain $CaCO_3$ (~ 20%; Table 1), and appear dark due to the high content of iron sulfides, which were quantified as acid volatile sulfir (AVS). Benthic fauna is scarce below 15 m water depth, and hence, in the deepest parts of the basin, limited or no bioturbation activity takes place in the sediment. The macrofauna that colonizes this area is typically composed of small individuals (mainly polycheates) which are able to burrow only within the top 1 cm of the sediment. Accordingly, sediments appear laminated, and with no signs of heavy bioturbation.

1.5. Impact of coastal hypoxia on macrofaunal communities

Oxygen depletion in the bottom water of coastal systems has a strong impact on the macrofaunal communities (Diaz and Rosenberg 1995; Levin et al. 2009). Once the oxygen levels drop below a certain "hypoxia" threshold, marine organisms suffer from a variety of stresses, ultimately leading to the disappearance of the species as oxygen levels approach anoxia (Diaz and Rosenberg 1995; Vaquer-Sunyer and Duarte 2008; Steckbauer et al. 2011). The conventional reference level for hypoxia is ~63 $\mu mol \, L^{-1}$, although thresholds vary widely between different organism groups, with crustaceans and fish being the most sensitive taxa (Vaquer-Sunyer and Duarte 2008). Hypoxia also specifically affects the composition of the faunal communities within sediments (the benthos) and their associated bioturbation and bioirrigation activities (Diaz and Rosenberg 1995; Levin et al. 2009).

In seasonally hypoxic coastal systems, the benthic macrofaunal community is typically depauperate and composed of small-sized, short-lived and opportunistic species (Diaz and Rosenberg 1995; Levin et al. 2009). The benthic communities undergo seasonal changes that strongly depend on the oxygen availability in the bottom water (Jørgensen 1980; Holland et al. 1987; Ritter and Montagna 1999). During the hypoxic or anoxic period, the macrofauna abundance and biomass, as well as the species richness, rapidly declines, due to emigration of larger mobile species (e.g. crustaceans) or the mortality of sedentary species as a result of oxygen depletion (Diaz and Rosenberg, 1995; Levin et al., 2009 and references therein). After the anoxic period, when bottom waters are replenished with oxygen, the benthic environment is recolonized by mainly juvenile macrofauna. This recolonization process follows a successional pattern, with small-sized opportunistic species establishing first, and larger, deeper burrowing fauna only arriving in a later stage (Pearson and Rosenberg, 1978; Rosenberg et al., 2002; Steckbauer et al., 2011; Van Colen et al., 2008). Finally, when the following hypoxic event occurs, the succession pattern is started again.

1.6. Effect of hypoxia on nutrient cycling

Oxygen exerts a powerful control on the nitrogen (N) cycle by affecting key processes such as nitrification (the oxidation of ammonia to nitrate) and denitrification (the reduction of nitrate to nitrogen gas) (Fig. 4). The nitrification pathway requires oxygen, and low oxygen concentrations are known to inhibit nitrification. As a consequence, low O_2 concentrations limit coupled nitrification-denitrification, and ultimately inhibit denitrification (Kemp et al. 1990; Middelburg and Levin 2009). In addition, the presence of free sulfide inhibits nitrification as well (Joye and Hollibaugh 1995), and promotes dissimilatory nitrate reduction to ammonium (DNRA) (McCarthy et al. 2008).

The processes involved in N cycling under hypoxic or anoxic conditions have been largely studied in the water column of OMZs (Lam and Kuypers 2011) and in the sediments of seasonally hypoxic systems (Vahtera et al. 2007; Neubacher et al. 2011; Roberts et al. 2012; Testa and Kemp 2012; Jäntti and Hietanen 2012). Within the water column of the OMZs, the reduction of nitrate to gaseous products N_2O or N_2 via canonical denitrification, or to N_2 via anammox (anaerobic ammonium oxidation; Mulder et al. 1995), leads to loss of nitrogen from the oceans to the atmosphere. This way the OMZs are important sites for loss of bio-available nitrogen (Lam and Kuypers 2011). Globally, it has been estimated that OMZ waters are responsible for approximately 30–50% of nitrogen loss from the world's oceans, or 16–27% from land and oceans combined (Codispoti et al. 2001; Gruber 2008). Sediments are also known to be sites of active N cycling (Middelburg et al. 1996). High ammonium effluxes have been reported under hypoxic conditions for a number of settings; e.g. Chesapeake Bay (Kemp et al. 1990, 2005), the Louisiana shelf (McCarthy et al. 2008) and Danish coastal systems (Conley et al. 2007), and have been explained by limited nitrification due to oxygen deficiency, and elevated levels of DNRA.

Phosphorus (P) is an essential element for phytoplankton growth in the ocean, and is taken up during photosynthesis and incorporated into the organic matter. In the water column, P is present as dissolved form (HPO_4^{2-}), which is also the most readily utilizable form of P in nature (Cembella et al. 1982). Under oxic conditions, dissolved P may also be adsorbed by particulate Mn and Fe (hydr)oxides, and thus transported through the water column (Follmi 1996; Delaney 1998) (Fig. 4). In reverse, anoxic conditions in the water column enable the reduction of such metal oxides (Landing and Bruland 1987; Lewis and Landing 1992) and result in the concomitant release of P (Fig. 4). P cycling has been extensively studied also in the sediments of hypoxic systems e.g (Slomp et al. 1996; Mort et al. 2010; Reed et al. 2011; Carstensen et al. 2014b) and is equally redox-sensitive as in the water column e.g. (Slomp 2011). Under oxic conditions, inorganic phosphorous is bound to insoluble oxides and hydroxides of Fe and Mn (Froelich et al. 1988; Slomp et al. 1996) and hence, retained in the sediment. During low oxygen in the bottom waters the reduction of these metal hydroxides results in the release of the phosphate to the porewater (Mort et al. 2010; Reed et al. 2011; Jilbert et al. 2011), where it can accumulate and further diffuse into the water column (Sundby 1992; Slomp et al. 1997). In this way, hypoxic and
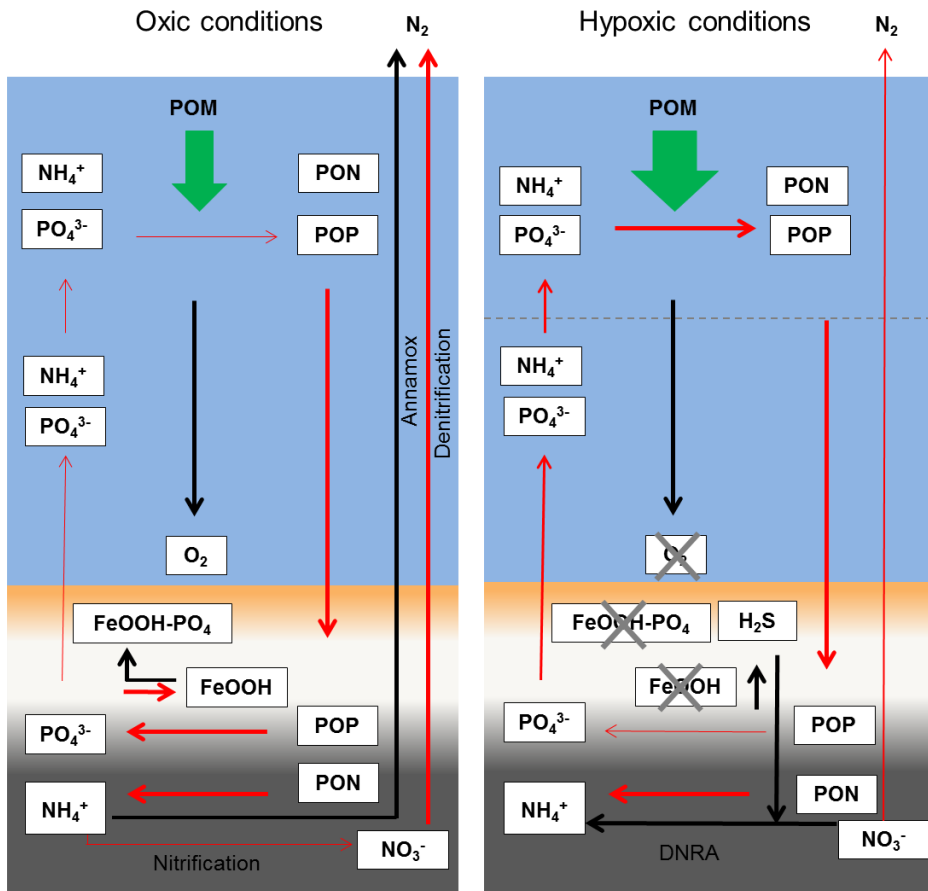
Figure 4. Simplified conceptual diagram of nitrogen and phosphorus cycling in a coastal ecosystem under oxygenated (left panel) and hypoxic/anoxic conditions (right panel). POM: particulate organic matter, PON: particulate organic nitrogen, POP: particulate organic phosphorus. Modified after Jantti et al. 2012, Testa and Kemp 2014.

anoxic conditions lead to enhanced phosphorus release from the sediment, and hence, results in the regeneration of phosphorous in the system (Ingall et al. 1993; Ingall and Jahnke 1994; Jilbert et al. 2011).

1.7. Effect of hypoxia on the distribution of electron acceptors (classic redox cascade)

Oxygen concentrations regulate the biogeochemical cycles in marine systems by affecting the metabolism of microorganisms involved in the mineralization of organic

matter, and also by impacting the secondary redox reactions that take place within the sediment or the porewater (Glud 2008; Conley et al. 2009; Kemp et al. 2009; Reed et al. 2011; Carstensen et al. 2014a).

In aquatic systems, organic matter is mineralized by an array of biogeochemical pathways mediated by prokaryotes that harvest energy by catalyzing redox reactions, whereby electrons are transferred from a reduced electron donor to an oxidized electron acceptor. These microorganisms are able to use a variety of electron acceptors as well as various organic and inorganic electron donors. Thermodynamically, oxygen is the most favorable electron acceptor, providing the highest energy yield (ΔG). In the absence of oxygen, microorganisms use other electron acceptors, which in order of energy yield are NO_3^-, Mn(IV), Fe(III), and SO_4^{2-} (Froelich et al. 1979). These metabolic requirements are reflected in the distribution of the electron acceptors in oxygen deficient systems, where they typically show a spatial (often vertical) distribution (Fig. 5). The distribution of redox species controls the spatial distribution of the associated redox reactions, which follow the so-called redox cascade (Fig. 5). When a favorable electron acceptor is depleted, the next favorable will be used, although there may be some vertical overlap. Accordingly, oxic respiration is the first process to occur, and the zone where oxygen is present defines the oxic zone. In the following horizon, mineralization processes are governed by nitrate and manganese and iron (hydr)oxides reduction. When all these oxidants are depleted, then sulfate reduction takes place, generating sulfide, hence, creating the sulfidic zone. The reduced products of mineralization (NH_4^+, H_2S, Fe^{2+}, Mn^{2+}) can be used by chemolithotrophic bacteria as electron donors in further re-oxidation processes.

The spatial zonation of electron acceptors and donors follows a similar vertical distribution in the water column and the sediment, as both these systems can be regarded as diffusion-reaction environments. Both in the water column and the sediment, the horizon devoid of both oxygen and sulfide is referred to as "suboxic zone". Note that in this thesis, the term "suboxic zone" defines the layer where both oxygen and sulfide are not detectable ($[O_2]$ and $[H_2S] < 0.2$ µM), but does not specify the reactions that take place (Canfield and Thamdrup 2009). The suboxic zone is a common feature of marine waters and sediments, and in hypoxic systems this horizon hosts crucial biogeochemical processes that mineralize most of the organic matter.

In most of the ocean, oxygen is present throughout the water column down to the sediment. However, in oxygen deficient water bodies, a suboxic zone and even a sulfidic zone can develop. For instance, in the Black Sea (Oguz et al. 2001; Glazer et al. 2006; Murray et al. 2007), the deeper basins of the Baltic Sea (Conley et al. 2009), the Cariaco basin (Scranton et al. 2014), the Saanich Inlet (Manning et al. 2010; Zaikova et al. 2010) and the Namibian shelf (Brüchert et al. 2006), oxygen concentrations can fall below detection limit at various water depths and a suboxic zone is detected in the water column of these systems. Frequently the formation and sustainment of such layer is enabled by a dynamic nitrogen cycling (Lam and Kuypers 2011; Ulloa et al. 2012), which also
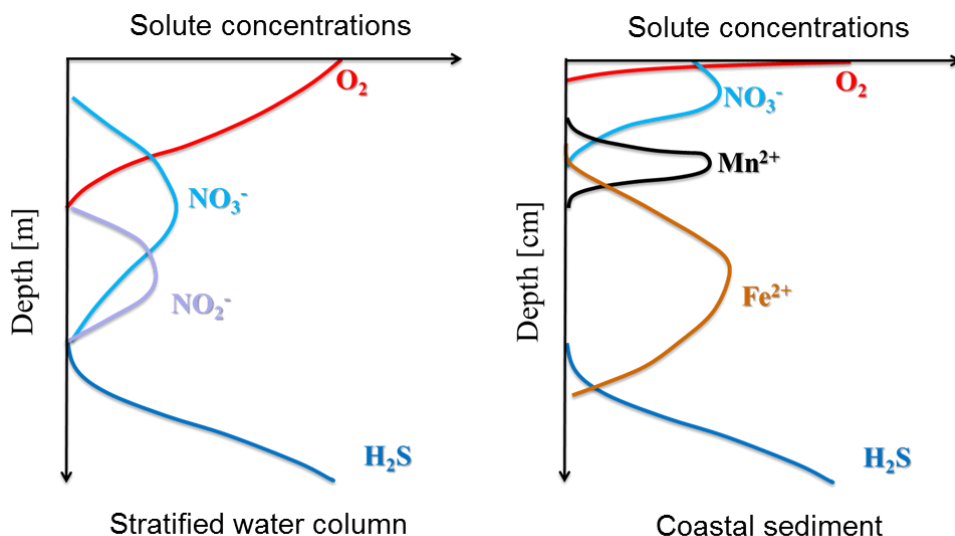
Figure 5. Schematic redrawn after (Ulloa et al. 2012; right panel), shows porewater distribution of O_2 (red), nitrate (light blue), nitrite (light purple) and sulfide (blue) in the water column of stratified systems such as Black Sea, Cariaco Basin, Saanich Inlet, Namibian Shelf. Schematic redrawn after (Froelich et al. 1979; left panel), shows porewater distribution of O_2 (red), nitrate (light blue), dissolved manganese (black), dissolved iron (brown) and sulfide (blue) in surface marine sediments.

dominates the geochemistry and microbial ecology throughout the water column (Lam and Kuypers 2011). Within the suboxic zone, nitrate is rapidly reduced to nitrite (Morrison et al. 1999). Nitrite is further converted to N_2 or N_2O gas via canonical denitrification, to N_2 via the anammox process (Thamdrup et al. 2006) or to NH_4 through dissimilative nitrate reduction to ammonium (Kartal et al. 2007).

In the water column of OMZs the processes forming the suboxic zone occur over ~ 100-1000 m depths, whereas in marine sediments the suboxic zone is compressed over a few millimeters to centimeters depth. In productive coastal systems the suboxic zone extends for only a few centimeters deep within the sediment. In the traditional view, the suboxic zone in sediment is formed in a similar way as in the water column of OMZs, i.e., by means of the redox cascade (as illustrated in Fig. 5). In this view, the suboxic zone is characterized by sequential "suboxic" pathways of organic matter mineralization, which use nitrate, manganese oxides and iron (hydr)oxides as electron acceptors in the degradation of organic matter (Froelich et al. 1979; Jørgensen 1983).

As it happens, an important part of this thesis will be devoted to putting the traditional redox cascade concept into question. In other words, is the suboxic zone in marine sediments really predominantly formed by redox cascade?

The redox cascade is typically described in relation to the vertical distribution of electron acceptors in the water column or the sediment. A similar succession of electron acceptors can occur not only in space, but also through time. For instance, in the bottom waters of seasonally hypoxic systems, the availability of electron acceptors exhibits a temporal pattern, affecting the type of the respiration processes taking place. During winter (prior to potential phytoplankton blooms) in the presence of oxygen and nitrate (Fig. 2b), oxic and nitrate-based respiration are the dominant mineralization pathways. As the oxygen concentrations drop down, nitrate will be subsequently used, followed by Mn and Fe-reduction. Finally, if all these electron acceptors are exhausted, sulfate reduction will prevail, and sulfide will appear.

1.8. Development of euxinia

Oxygen concentrations in marine waters also affect the sulfur cycle, which in turn is strongly coupled to the biogeochemical cycling of iron (Jørgensen and Nelson 2004). Sulfate concentrations in marine waters are high compared to fresh water systems, and although the energy harvested by the reduction of sulfate is low compared to other electron acceptors such as O_2 and NO_3^-, the high concentrations of sulfate in the ocean allow this pathway to be responsible for up to 50% of the organic matter mineralization in the seafloor (Jorgensen 1979). Sulfate reduction generates sulfide, which is a versatile electron donor, as it can be exploited by a variety of microbes to fuel their growth, or react chemically with oxidized species present in the system (Jørgensen and Nelson 2004). Sulfide oxidation can be coupled to the reduction of oxygen, nitrate, manganese and iron oxides, and iron sulfides (Jørgensen and Nelson 2004).

These oxidized species are abundant in marine systems, and free sulfide can only accumulate in the water once these species are exhausted. The accumulation of free sulfide and its persistence in marine waters leads to the establishment of euxinia (Fig. 2b). Free sulfide is rarely found in the water column of marine systems, and only under specific conditions. Euxinic water columns are known to occur in permanently anoxic bottom waters of the Black Sea (Murray et al. 2007), the deep basins of the Baltic Sea (Noffke et al. 2016), and Cariaco basin (Scranton et al. 2014). In these systems, the sulfide results from sulfate production within the water column and also from diffusion out of the sediments. Euxinic bottom waters occur only seasonally in the bottom waters of the Saanich Inlet during anoxia in the bottom water (Anderson and Devol 1987), or occasionally in the Benguela upwelling systems, where sediments have been reported to release high amounts of free sulfide (Lavik et al. 2009; Brüchert et al. 2009).

1.9. Sedimentary sulfur cycling in marine sediments

The development of euxinia is crucially dependent on the sulfur cycling within the sediment. Sedimentary sulfur cycling is highly dynamic as it is regulated by processes that rely on chemical reactions or are mediated by bacteria (Fig. 6). Such processes are
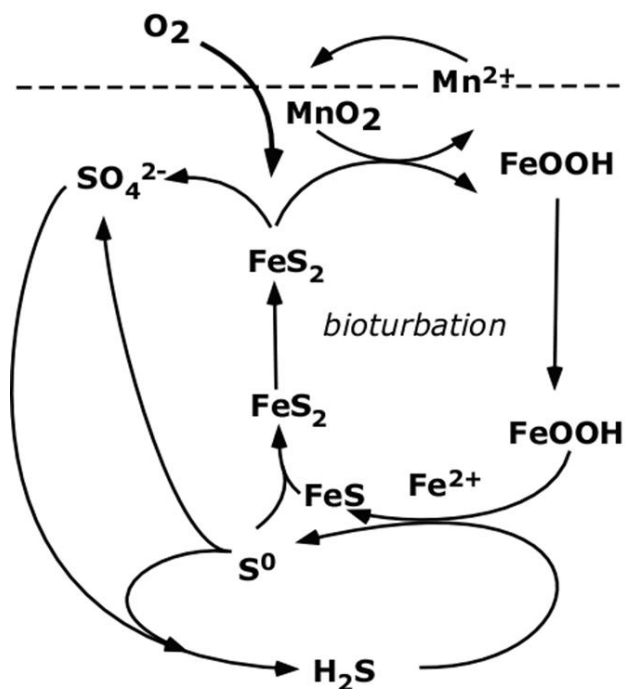
Figure 6. The principal sulfur and iron cycle in bioturbated marine sediments. Sulfide produced from sulfate reduction reacts with iron-oxides to form iron-sulfide minerals, elemental sulfur or other sulfur intermediates. Oxygen and manganese-oxides are typically consumed during the re-oxidation of the iron-sulfide minerals. Bioturbation is crucial in transporting the iron sulfides from the anoxic zone to the oxic zone near the sediment surface (Jørgensen and Nelson 2004).

modulated by diffusional transport, and reactions that include the solid phase of the sediment, but also the mixing activity of bioturbating macrofauna.

Sulfate reduction is the dominant pathway of organic matter mineralization in organic rich sediments, ultimately leading to the accumulation of a large pool of solid metal sulfides and/or high levels of free sulfide in the pore water (Jørgensen 1982). Sulfide is a highly reactive compound and can rapidly react with oxygen both chemically and biologically. Purely chemical sulfide consumption with oxygen has a time scale in the range of several hours, depending on the temperature, pH and ionic strength of the seawater and the presence of a probable catalyst, e.g. metals (Millero et al. 1987).

Biological oxidation of sulfide can proceed much faster (Luther et al. 2011), as for instance within microbial mats of sulfide-oxidizing bacteria, where the microbial turnover of sulfide can occur in less than a second (Jørgensen and Postgate 1982).

The sedimentary sulfur cycle interacts strongly with the biogeochemical cycling of iron. Free sulfide reacts with iron (hydr)oxides and precipitates as iron sulfide (reaction 1; Canfield, 1993; Thamdrup et al., 1994)

$$3 \ H_2S + 2 \ FeOOH \rightarrow S^0 + 2 \ FeS + 4 \ H_2O \hspace{3cm} (1)$$

This initially formed amorphous iron-sulfide can be converted to pyrite (FeS_2), which is the stable form, and get buried (Rickard and Luther 2007).

Alternatively, the iron sulfides produced in the sulfidic zone may be transported upwards to the oxic zone by bioturbating fauna and re-oxidized back to iron (hydr)oxides upon contact with oxygen reaction 2 (Aller and Rude 1988; Canfield et al. 1993b).

$$FeS + 9/4 \ O_2 + 3/2 \ H_2O \rightarrow FeOOH + SO_4^{2-} + 2H^+ \hspace{2cm} (2)$$
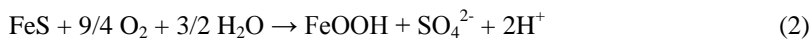
Accordingly, the accumulation of free sulfide within the sediment can start only upon exhaustion of the metal oxide pool and the saturation of the sediment with iron sulfides (Heijs et al. 1999; Giordani et al. 2008). If the accumulation process persists, sulfide may migrate upwards in the sediment, until reaching the surface and diffusing to the bottom water. Provided that the bottom water is devoid of oxidants, the diffusion of sulfide will give rise to euxinic conditions, which are toxic for marine life.

1.10. Sulfur oxidizing bacteria in marine sediments

Sulfur (S) oxidation in marine sediments is mainly catalyzed by microorganisms (Luther et al. 2011), Sulfur oxidizing bacteria comprise a wide range of microorganisms, ranging from free-living single cells, to mat-forming filamentous microbes.

Single cell sulfur-oxidizers. Single-cell sulfur-oxidizing microorganisms necessarily require the presence of both electron acceptor and electron donor within the same sediment horizon to fuel their growth. These type of bacteria are often found in gradient environments, for instance in sulfidic sediments at the narrow (micrometer scale) interface between oxygen and sulfide.

Large *Beggiatoaceae*. The large, sulfur oxidizing *Beggiatoaceae* have been reported to occur in a wide range of environments that host sulfidic sediments, such as coastal sediments, hydrothermal vents, and deep sea mud volcanos (Schulz and Jørgensen 2001). *Beggiatoaceae* are motile gradient bacteria, which position themselves at the interface between oxygen and sulfide, where they efficiently oxidize sulfide using oxygen as electron acceptor. The oxidation of sulfide produces elemental sulfur which is stored intracellularly by the bacteria (reaction 3)

$$2HS^- + 2O_2 \rightarrow 2S^0 + 2OH^- \hspace{4cm} (3)$$

The *Beggiatoaceae* populations that utilize oxygen as electron acceptor, and that hence, are found at the oxic-anoxic interface, are typically composed by thin filamnets (< 10-20 μm of diameter). However, some members of the *Beggiatoaceae* family are also capable of storing nitrate in internal vacuoles (Schulz and Jørgensen 2001; Jørgensen and Nelson 2004), that is used to oxidize sulfide in the anoxic zone of the sediment (reaction 4). These are typically thicker filaments (> 20 μm of diameter) that are found below the sediment oxic zone. In both cases, the intracellular elemental sulfur may be oxidized further to sulfate (reaction 5).

$$4HS^- + NO_{3\;intracell}^- + 6H^+ \rightarrow 4S^0_{intracell} + NH_4^+ + 3H_2O \qquad (4)$$

$$2S^0 + 2H_2O + 3O_2 \rightarrow 2\;SO_4^{2-} + 4\;H^+ \qquad (5)$$
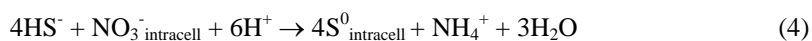
Beggiatoaceae can dominate sulfide oxidation and outcompete the chemical oxidation of sulfide with oxygen, when they occur in dense populations forming microbial mates. Sulfide oxidation by *Beggiatoaceae* may be the dominant process not only in gradient environments, but also within the suboxic zone of marine sediments (Sayama et al. 2005).

Cable bacteria. Recently, a new type of long filamentous bacteria, called "cable bacteria", belonging to the family *Desulfobulbaceae*, have been discovered in marine sediments (Nielsen et al. 2010; Pfeffer et al. 2012). These bacteria perform a novel "electrogenic" type of sulfur oxidation (Pfeffer et al. 2012; Vasquez-Cardenas et al. 2015), by connecting spatially separated redox half reactions via electron transport over centimeter-long distances (Nielsen et al. 2010). In deep sediment layers, sulfide is oxidized in a first redox half-reaction and, the resulting electrons are transported along the longitudinal axis of the filaments, upwards to the oxic zone, where the electrons are consumed in the second redox half-reaction, the reduction of oxygen (Nielsen et al. 2010; Pfeffer et al. 2012). Cable bacteria have recently been found in a wide range of marine environment, in particular the Lake Grevelingen site reported in this study (Malkin et al. 2014; Vasquez-Cardenas et al. 2015).

OBJECTIVES AND THESIS OUTLINE

This objective of this thesis was (1) to document the influence of seasonal hypoxia on the biogeochemical cycling in the water column and sediments of coastal systems, (2) to investigate the role of sediments in the development of coastal hypoxia and (3) identify the key microbial pathways of sedimentary sulfur oxidation in the sediments of seasonally hypoxic coastal systems.

To investigate the multiple effects of coastal hypoxia at an ecosystem scale, a detailed field assessment was conducted in a seasonally hypoxic basin. Coupled water column and benthic data allow to evaluate the role of sediments in the development of hypoxia. Additional, high-resolution sediment analyses were conducted to identify the major microbial pathways that control the sulfide distribution in the sediment and bottom water. A combination of field observations with reactive transport modelling finally allowed a better understanding and guidance as to the different mechanisms of sulfide oxidation and suboxic zone formation in the seafloor.

The impacts of coastal hypoxia on the water column chemistry and sediment geochemistry were investigated in **Chapter 2**. A detailed study was conducted over multiple years in Lake Grevelingen, a seasonally hypoxic coastal reservoir in the Scheldt-Rhine-Meuse delta of the Netherlands. Monthly sampling of physical and chemical parameters in the water column showed the seasonal cycle in primary production and water column stratification, the ensuing development of summer hypoxia and associated response of the biogeochemical cycling in the bottom waters. Benthic flux measurements allowed to assess the response of the sediment biogeochemistry to seasonal hypoxia.

In **Chapter 3**, we performed a detailed yearlong study of the sediments in Lake Grevelingen, which demonstrated how summer hypoxia strongly impacts the sedimentary oxygen consumption as well as the abundance and diversity of the benthic communities. Sedimentary oxygen consumption was quantified based on closed-core incubations and microsensor profiling. The response of the macrofauna communities was investigated by core sampling and sediment profile imaging.

In **Chapter 4**, we performed a detailed investigation of the role of cable bacteria in the natural sediment biogeochemistry of Lake Grevelingen. This investigation revealed – for the first time – how cable bacteria are key players in the iron and sulfur cycling of seasonally hypoxic systems. Microsensor profiling (O_2, pH and H_2S) of sediment cores and microscopy were used to determine the abundance of cable bacteria in Lake Grevelingen on a monthly basis for a whole year. Sediment geochemical data suggest that cable bacteria induce the formation of a large pool of sedimentary iron oxides before the onset of summer

hypoxia, which acts as 'firewall' against the release of sulfide to the bottom water in early summer, and likely prevents the development of bottom water euxinia.

In **Chapter 5**, we performed a detailed investigation of the role of cable bacteria in the phosphorus cycling at Lake Grevelingen. Microscopic analysis with nanoSIMS of individual filaments of cable bacteria indicates the presence of intracellular polyphosphate accumulations within the bacterial cells. However, the strong effect of cable bacteria on phosphorus cycling was not linked to this polyphosphate accumulation, but rather to the indirect formation of the iron oxides layer which contained a large stock of bound phosphorus, and hence increased P retention during spring.

Chapter 6 provides a review of three known mechanisms (cable bacteria, nitrate accumulating *Beggiatoaceae*, and metal cycling driven by bioturbation) that enable aerobic sulfide oxidation in marine sediments by creating a suboxic zone devoid of both oxygen and sulfide. Field observations combined with reactive transport modelling demonstrated that these mechanisms of suboxic zone formation can be differentiated by their pH imprint on the pore water. These insights provide guidance as to the different mechanisms of sulfide oxidation and suboxic zone formation in the seafloor, give a better understanding of redox shuttling and cryptic cycling in the coastal zone, and show how the traditional redox cascade does not hold in many marine sediments.

Photo: Ilja Kocken

Biogeochemical cycling in a seasonally hypoxic coastal basin (Lake Grevelingen, The Netherlands)

Dorina Seitaj, Mathilde Hagens, Bart Veuger, Caroline P. Slomp, Filip J. R. Meysman

ABSTRACT

Low oxygen concentrations in the bottom water of coastal systems alter the biogeochemical cycling both in the water column and sediment compartments, by affecting key mineralization processes.

Here we present a seasonal study that investigates the water column chemistry over two consecutive years, and the sediment biogeochemistry during the first year. Chlorophyll a and carbonate species distribution in the water column depicted the occurrence of three yearly phytoplankton blooms during periods of stratification of the water column. Summer anoxia was accompanied by accumulation of nutrients, dissolved inorganic carbon and alkalinity, and acidification of the bottom water. Benthic fluxes showed that a substantial part of this accumulation was related to release of respiration end-products from the sediment. A mass balance of organic carbon burial and sediment mineralization suggested that the basin acts as a sediment trap for organic material, likely originating from shallower areas within the basin or from the adjacent North Sea.

2.1. INTRODUCTION

Coastal areas worldwide are increasingly affected by oxygen depletion (hypoxia) in the bottom waters (Diaz and Rosenberg 2008), and there is growing evidence that such bottom water hypoxia is linked to anthropogenic nutrient input to the coastal zone (Diaz and Rosenberg 2008; Conley et al. 2009). Oxygen depletion in the bottom water has major impacts on biogeochemical cycling both in the water column and sediment (Turner et al. 2008; Conley et al. 2009; Middelburg and Levin 2009; Kemp et al. 2009; Rabalais et al. 2010; Testa and Kemp 2011).

In shallow coastal environments sediments are crucial in regulating elemental cycling in the water column (Therkildsen and Lomstein 1993; Soetaert and Middelburg 2009), and are responsible for the mineralization of up to 50% of the organic matter produced in the water column (Jørgensen 1977, 1982). The mineralization of this organic material consumes oxygen and results in the release of dissolved inorganic carbon (DIC) and nutrients, and also affects the distribution of alkalinity (A_T), pH and other carbonate species in the porewater. After accumulating in the porewater these by-products can then diffuse to the water column.

Bottom water oxygen concentrations strongly control the dominant mineralization pathways taking place and as a consequence affect the type of by-products that are produced in the sediment, and hence, that may diffuse to the water column. Hypoxia has been shown to strongly affect biogeochemical processes related to the nitrogen (N) and phosphorus (P) cycles (Conley 2009; Kemp et al. 2009; Reed et al. 2011; Carstensen et al. 2014). Low oxygen concentrations in the bottom water inhibit nitrification, and consequently limit coupled nitrification-denitrification in the sediment, and ultimately restrict denitrification (Kemp et al. 1990; Middelburg and Levin 2009). When oxygen concentrations in the bottom water fall below the hypoxia threshold, P is released in the porewater upon reduction of the iron and manganese hydroxides (Mort et al. 2010; Reed et al. 2011; Jilbert et al. 2011), and may diffuse into the water column leading to regeneration of phosphorus in the system (Ingall et al. 1993; Ingall and Jahnke 1994; Jilbert et al. 2011). Hypoxia is associated with a domination of anoxic pathways which are accompanied by release of DIC, and A_T, but also acidification of the bottom water (Cai et al. 2011; Hagens et al. 2015).

Lake Grevelingen is a coastal marine basin that experiences summer anoxia in the bottom waters, and such oxygen depletion has been shown to strongly affect the carbonate system in the water column (Hagens et al. 2015), and the sedimentary oxygen dynamics (chapter 3).The research objective here was to document the effect of seasonal hypoxia on carbon and nutrient cycling in seasonally hypoxic basin within the lake. What is the effect of hypoxia on biogeochemical cycling, and how do sedimentary processes affect the concentrations of elements in the water column? To this end we conducted a detailed seasonal study investigating the water column chemistry monthly, over two years. In addition, during the first year of investigations, we determined the benthic fluxes of

nutrients at three sites, in order to elucidate the role of the sediments on the element dynamics observed in the water column.

2.2. MATERIALS AND METHODS

2.2.1. Study site and sampling procedure

Lake Grevelingen (Fig. 1) is a marine basin within the Rhine-Meuse-Scheldt delta area in the southwest of the Netherlands. The basin was originally an open estuary, but has been closed from the North Sea in 1971 by dam constructions at both the seaward and landward sides. The lake extends over 115 km^2 and is relatively shallow with an average depth of 5.1 m. The shallow areas are intersected by deep gullies, which are the remnants of the former estuarine channels. The main gully within Lake Grevelingen consists of a sequence of deep basins, which extend down to 45 m water depth, and are separated from each other by sills.
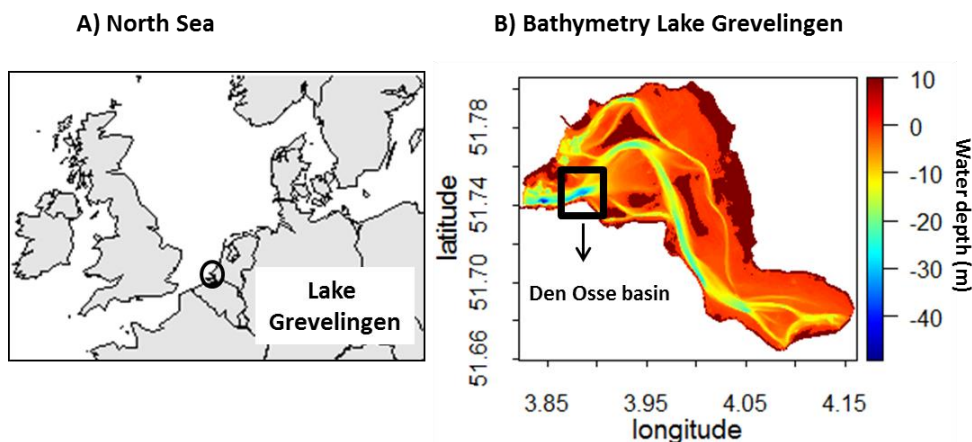
Figure 1. (A) Map of the Southern North Sea; (B) bathymetry of Lake Grevelingen (deepest site 34 m depth: S1; 51.747°N. 3.890°E)**.**

Our investigations were carried out in Den Osse basin, one of the deeper basins (maximum water depth 34 m) in the central gully. In spring and summer, the water column of Lake Grevelingen becomes stratified, which isolates the water within the deep basins from the surface layer (see Hagens et al. 2015; chapter 3). This seasonal stratification is accompanied by the development of bottom water hypoxia, which differs in extent and severity between years (Wetsteyn 2011; chapter 3). During two consecutive years (2012 and 2013), we performed monthly sampling campaigns on board of the R/V Luctor, examining the water column biogeochemistry in the Den Osse basin. Water column sampling took place at station S1, located at the deepest point of the basin (51.747°N, 3.890°E; 34 m water depth). A CTD instrument (YSI 6600) was deployed to record the

depth profiles of temperature (T), salinity (S), pressure (p), oxygen (O_2) and chlorophyll a (Chl a). The seawater density (kg m^{-3}) and the stratification index σ (J m^{-3}), which denotes the amount of energy required to fully homogenise the water column through vertical mixing (Simpson 1981), were calculated from the CTD data (see Hagens et al. 2015 for details). The CTD was lowered at 1 m depth intervals, and allowed to stabilize at each depth for two minutes (to allow sufficient stabilization time for the O_2 optode).

CTD profiling was complemented with discrete water-column sampling at eight different depths (1, 3, 6, 10, 15, 20, 25 and 32 m). Water samples were analysed for the concentrations of oxygen (O_2), dissolved organic carbon (DOC), the carbonate system parameters pH, total alkalinity (A_T), and dissolved inorganic carbon (DIC), and nutrients (NO_3^-, NH_4^+, PO_4^{3-} and $SiOH_4$). Water samples were drawn from a 12L Niskin bottle using gas-tight Tygon tubing, to avoid gas exchange with the surrounding atmosphere.

Throughout 2012 we also investigated the sediment geochemistry by determining benthic fluxes of nutrients, and benthic N_2 production rates. Sediment sampling took place at three stations along a depth gradient within the Den Osse basin: S1 (as above), S2 at 23 m (51.749°N, 3.897°E) and S3 at 17 m (51.747°N, 3.898°E). Intact sediment cores were retrieved with a single core gravity corer (UWITEC, Austria) using PVC core liners (6 cm inner diameter, 60 cm length). All cores were inspected upon retrieval and only visually undisturbed sediment cores were used for further analysis.

2.2.2. Sediment incubations

Ship-board, closed core sediment incubations were performed to determine the fluxes of nutrients (NO_3^-, NH_4^+, PO_4^{3-} and $SiOH_4$) across the sediment-water interface. Incubations were performed in triplicate following the procedure as described in detail in Chapter 3. Hence, only a brief account is given here. After core collection, the overlying water was replaced with ambient bottom water using a gas-tight Tygon tubing, the cores were sealed with gas-tight polyoxymethylene lids and transferred to a temperature controlled incubator (LT650; Elbanton) operating at the *in situ* bottom water temperature. The core lids contained a central stirrer to ensure that the overlying water remained well mixed, as well as two sampling ports to enable discrete water subsampling. Core incubations were started within 30 minutes after sediment collection. A non-invasive Oxygen Spot Sensor (OXSP5; Pyroscience) was used to monitor oxygen concentrations in the bottom water during the incubation. The total oxygen uptake (TOU) of the sediment was determined from the change in O_2 concentration as a function of time (procedure and results reported in (chapter 3).

To monitor the change in nutrients in the overlying water of the incubations, water samples were collected at regular time intervals (5 times). Samples (~3 mL) were withdrawn using a plastic syringe via one sampling port, and concurrently, an equal amount of ambient bottom water was added through a replacement syringe attached to the other

sampling port. The water sample was filtered (0.45 µm Millex-HA syringe filter) and stored in the dark at 4°C.

The flux (mmol m^{-2} d^{-1}) was calculated from the concentration change in the overlying water ΔC_{ow} over the time period Δt, taking into account the enclosed sediment area A and the overlying water volume V_{ow}:

$$J = \left(\frac{\Delta C_{ow}}{\Delta t} \right) \frac{V_{ow}}{A} \tag{1}$$

In March, May, August and November, the concentration change was calculated from the 5 data points by linear regression. In the other months, no subsampling was performed, but fluxes were calculated from the concentration difference in samples taken at the start and end of the incubation.

2.2.3. Benthic N_2 production rates

N_2 production rates were determined on intact sediment cores in triplicates. Right after recovery, the sediment cores were transferred to a nearby laboratory and stored in a temperature-controlled room, at *in situ* temperature. After an overnight equilibration period the cores were sealed with gastight lids, and closed core incubations were started. Overlying water was carefully withdrawn into 12 mL Exetainers via gas tight Tygon-tubing, at the start and end of the incubations (n=3 replicates per core). The incubation time varied between 28 and 65 hours. The N_2 production rate (mmol m^{-2} d^{-1}) was estimated as difference in N_2 at the beginning and end of the incubation. The N_2 water concentration was determined as the N_2/Ar ratio using membrane inlet mass spectrometry (Kana et al. 1994, 1998) on a quadrupole mass spectrometer (HIDEN Analytical, Warrington, UK). Measured N_2/Ar ratios were calibrated using distilled water standards at *in situ* salinity, after adding sodium sulfite to remove oxygen.

2.2.4. Analytical methods

Water samples for DOC analysis were collected in glass syringes and filtered over pre-combusted Whatman GF/F filters (0.7 µm) into 10 mL glass headspace vials. Samples were analysed using a Formacs Skalar-04 by automated UV-wet oxidation to CO_2, of which the concentration is subsequently measured with a non-dispersive infrared detector (Middelburg and Herman, 2007).

Samples for the determination of pH were collected in 100 mL glass bottles. pH measurements were done immediately after collection at *in situ* temperature using a glass/reference electrode cell (Metrohm 6.0259.100) following standard procedures (Dickson et al., 2007; SOP 6a). Both National Institute of Standards and Technology (NIST) and TRIS (2-amino-2-hydroxymethyl-1,3-propanediol) buffers were used for calibration. The temperature difference between buffers and samples never exceeded 2°C. pH values are expressed on the total hydrogen ion scale.

DIC analysis was determined using an AS-C3 DIC analyzer (Apollo SciTEch), in which a sample is acidified and the released CO_2 detected using a solid state infra-red CO_2 detector (Licor LI 7000). Three replicate measurements were carried out for each sample analysed (accuracy & precision: < 3 µmol kg^{-1}). All DIC measurements were calibrated using Certified Reference Material (CRM Batch 116, supplied by A.G. Dickson).

Non-filtered water samples for A_T (~ 10 mL) were collected in 25 mL centrifuge tubes and stored in the dark at 4°C. A_T was determined using the standard operating procedure for open cell potentiometric titration (accuracy & precision: < 5 µmol kg^{-1}), using an automatic titrator (Metrohm 888 Titrando), and a combined Metrohm glass electrode (Unitrode) following the procedure SOP3a as described in Dickson et al. (2007).

Concentrations of nutrients (NO_3^-, NH_4^+, PO_4^{3-} and $Si(OH)_4$) were determined by automated colorimetric techniques using a Seal QuAAtro autoanalyzer.

2.2.5. Numerical and statistical analysis

In general, results are reported as the mean ± 1 standard deviation (s.d.) of n replicate measurements. The Pearson correlation coefficient was used as a measure of the statistical dependence between two variables. All statistical analyses were conducted in the open source software framework R.

Based on the water depth of the three stations, the basin was divided into three separate depth zones. The associated sediment areas and depth zone volumes were calculated based on bathymetric data at 5 by 5 meter resolution (Table 1). Averaged sediment fluxes over the basin were calculated as the areal mean $J = \sum_i \left(A_i/A_T \right) J_i$, where J_i is the flux measured within the zone, A_i is the sediment area of the zone, and A_T is the total area of the basin.

Table 1. Sediment area (km^2) and water volume (km^3) calculated for three different zones within Den Osse basin that are relative to each station. Values were calculated based on bathymetry data provided by the Dutch Environmental Agency.

	Start depth	End depth	Sediment Area (km^2)	Water Volume (km^3)
Zone S3	15	20	0.44	5.27 x 10^{-3}
Zone S2	20	28	0.49	4.88 x 10^{-3}
Zone S1	28	38	0.35	0.83 x 10^{-3}
Total basin	15	38	1.28	10.98 x 10^{-3}

2.3. RESULTS

2.3.1. Physical parameters in the water column

Water temperatures followed a clear seasonal pattern during both years, with lowest temperatures (< 4°C) between January and February and warmest waters (up to ~20 °C) in July and August (Fig. 2a). With the exception of some winter months, bottom waters always exhibited lower temperatures than the surface waters. The warming of the bottom water in summer showed a clear interannual variation. In August 2013, the thermocline was steeper, and the temperature difference between surface and bottom waters was larger (10.2°C) compared to August 2012 (4.5 °C).

Salinity did not exhibit pronounced variations over the investigated two-year period (Fig. 2b). In general, the salinity was higher in the bottom waters (mean value of 31.3 ± 0.8 at the 10-34 m layer over two-year period) compared to the surface layer (mean value 30.4 ± 0.9 in 0-10 m layer over two- year period), reflecting a surface input of fresh water through precipitation or terrestrial runoff. The degree of freshening of the upper part of the water column varied through time (range: 29.2 - 32.7), but did not follow a seasonal pattern. In July 2013, an exceptional freshening event was encountered (salinity decreased to 20.3). Salinity variations in the surface waters are likely governed by terrestrial runoff linked to precipitation in the area. The salinity of the bottom waters also fluctuated through time (range: 25.5 - 32.7), but also a clear seasonal pattern was lacking. Salinity changes in the deep waters are likely linked to bottom water ventilation through irregular inflows of North Sea water via the seaward sluice.

The water column at the field site is prone to stratification, a phenomenon that isolates the bottom layer from the surface layer of the water column. The stratification index shows two distinct stratification periods per year, and this pattern was repeated in both years (Fig. 1d). In late winter and early spring (March 2012, February-March 2013) the stratification is driven by salinity, as fresh water input into Lake Grevelingen creates a fresher surface layer (salinity 29-30) that sits on top of more saline bottom waters (salinity ~32; Fig. 2b). A second and longer stratification period occurs from May to September. This time, the stratification is driven by temperature (Fig. 2a) and creates a stronger picnocline (Fig. 2c). Higher air temperatures warm the surface waters in late spring, and subsequently, the heat is gradually transported to deeper waters. In September the surface waters cool down again, and the water column becomes unstable, given rise to overturning events and a full mixing of the water column (Fig. 2c).

2.1.1. Phytoplankton biomass and oxygen

Oxygen concentrations in the water column showed pronounced seasonal variations, both in the surface layer and in the deeper bottom waters, (Fig. 3a). The surface water exceeded air saturation levels from February/March to the end of August, and periods of strong oversaturation correlated well with increased Chl-a concentrations.
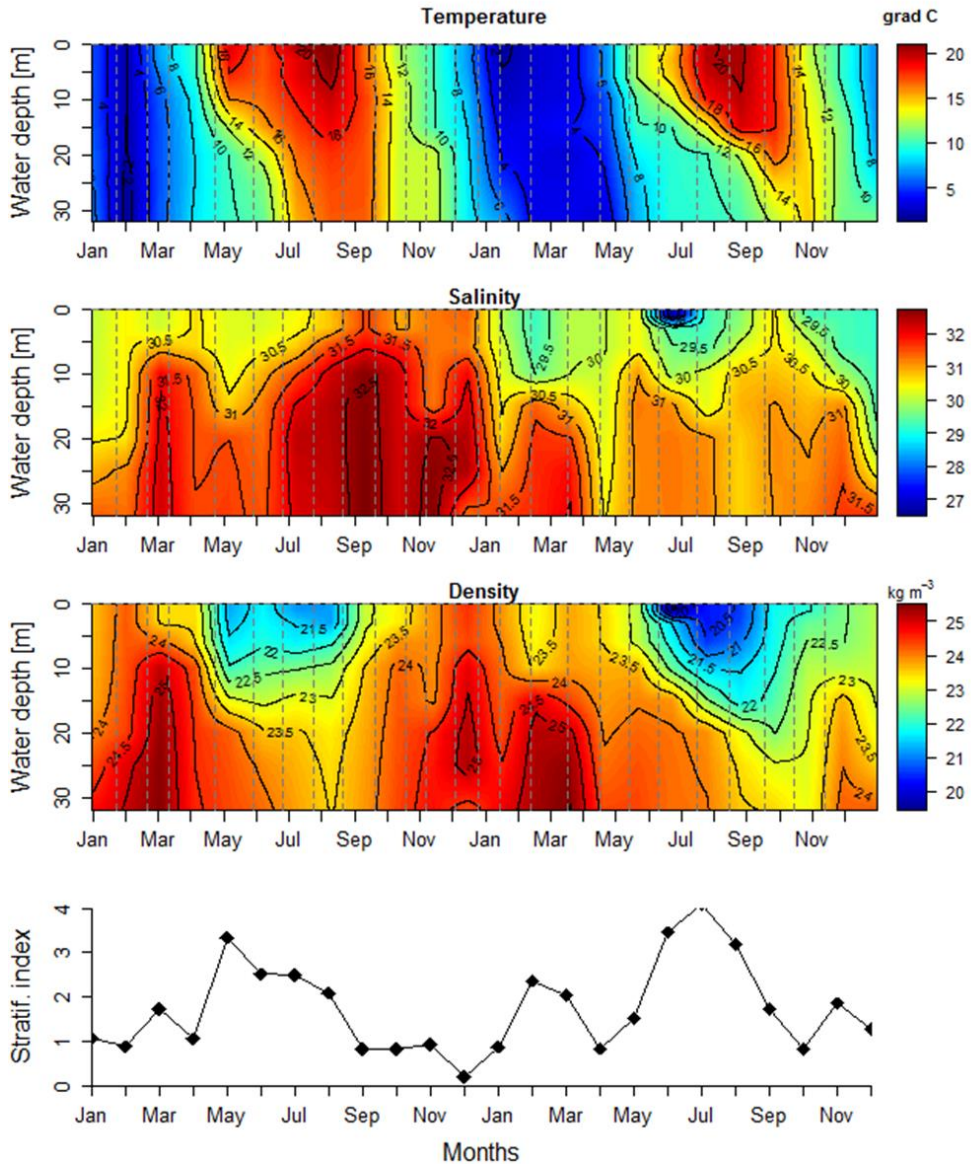
Figure 2. (A) Temperature (°C), (B) density anomaly (kg m-3) (C) salinity, and (D) stratification parameter (J m-3) at the Den Osse basin in 2012 and 2013. Data from (A) – (C) were linearly interpolated in space and time, and dashed lines indicate sampling dates.

During fall and winter the surface waters remained slightly below air saturation (range: 87 - 97%). This seasonal pattern was very consistent between both sampling years. In February 2012 the 100 % air saturation-isocline extended to ~19 m water depth, and progressively moved upwards between 5 and 10 m in the following months. During 2012, three consecutive phytoplankton blooms were recorded, with elevated Chl-a concentrations throughout the first 10 m in March, a subsurface Chl-a maximum at 8-10 m in May, and a strong surface bloom at 0-2 m water depth in July (Fig. 3b). These peaks in Chl-a corresponded closely with the presence of oversaturated waters, reaching 150% oversaturation during the intense summer bloom. This bloom pattern was repeated in 2013, though Chl-a and oversaturation values were generally lower compared to the previous year. In April 2013 the upper 22 m of the waters column was oversaturated, corresponding to elevated Chl-a levels over the first 20 m. In May 2013 a second bloom was observed, but not as intense as the previous year, although this discrepancy could be due to the course resolution of our monthly sampling scheme. In the summer of 2013, surface blooms were recorded in the top 5 m in June and August, coinciding again with oversaturated surface waters. The deeper waters of the Den Osse basin also showed a repeatable pattern in oxygenation over the two sampling years. In concert with the onset of stratification of the water column (Fig. 2c), the oxygen concentrations in the water layers below 15 m water depth started to decrease from April onwards (Fig. 3a). In 2012, the bottom waters at 34 m water depth reached the hypoxia threshold (< 63 μmol L^{-1}) at the end of June (11.1% saturation), and became anoxic (< 0.1 μmol L^{-1}) in August. In 2013 however, the oxygen depletion progressed faster, thus leading to more extensive hypoxia, as can be seen by the larger area under the 20% oxycline in Fig. 3a. In this year, the bottom waters at 34 m water depth reached the hypoxia threshold at the end of June, and oxygen remained below 2-3% saturation until September, but complete absence of oxygen was not reached. The bottom water depletion extended approximately one month longer in 2013 (due to the water column overturning in October) compared to 2012 (overturning in September). Also note that in winter and fall, the bottom waters still show excursions in their oxygen concentration. Irregularly, the O_2 concentration of the bottom water drops beneath 80% (November 2012, March 2013, December 2013), indicating sporadic bottom water isolation. These isolation events can be linked to a short periods of salinity stratification, or periods with a reduced inflow of oxygenated North Sea water to the Den Osse basin.

Dissolved Organic carbon (DOC) data were only recorded in 2012 (Fig. 3c). DOC concentrations in the surface water ranged between 153 and 237 μmol L^{-1}, and increased from May onwards until November. At depths below 15 m water depth, the DOC concentrations remained lower compared to the surface values, were elevated in August, and exhibited a peak at 20 m water depth in October.
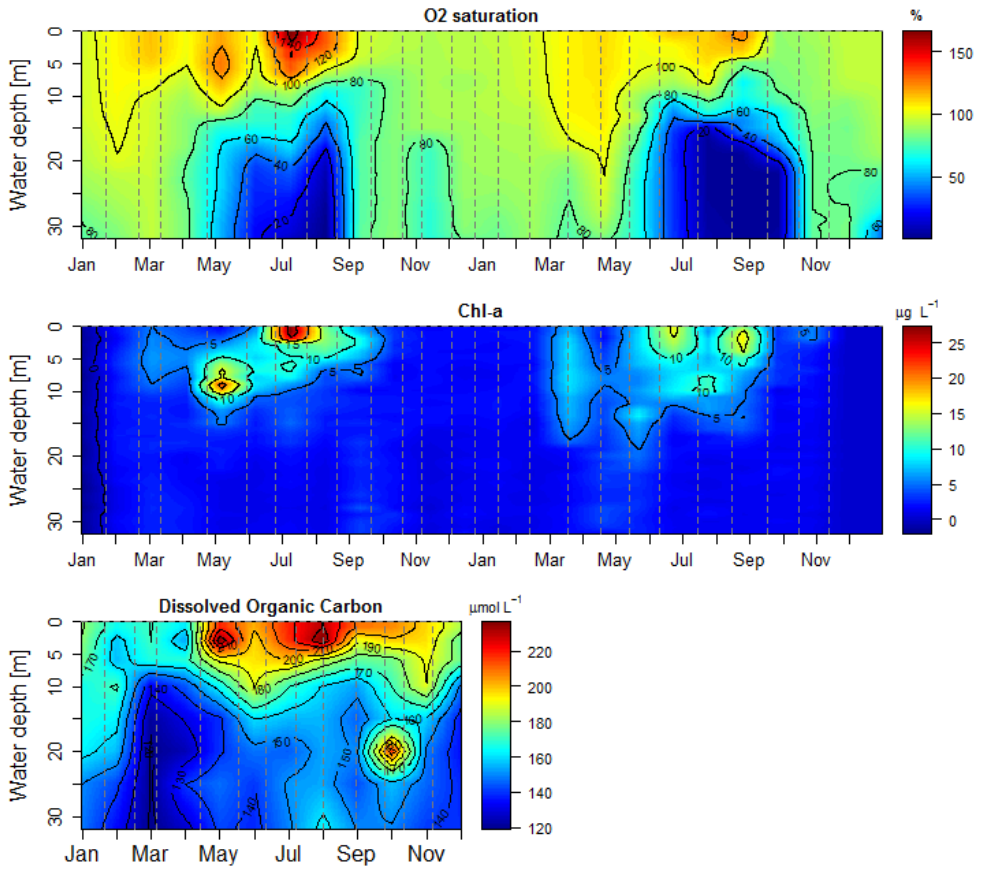
Figure 3. (A) Oxygen saturation (%), (B) Chlorophyll a (μg L^{-1}) and (C) Dissolved Inorganic Carbon (DOC; μmol L^{-1}) at Den Osse basin in 2012 and 2013. Data from were linearly interpolated in space and time, and dashed lines indicate sampling dates.

2.1.2.   Carbonate system

The carbonate system (DIC, A_T and pH) showed a recurrent pattern over the two years that were investigated (Fig. 4). As observed in the O_2 and DOC distributions, there is a clear difference in response between the surface layer above 10 m of water depth, and the underlying waters.

DIC in the surface layer became depleted from April to October (Fig. 4a), corresponding to or following periods of primary production, suggesting CO_2 uptake by phytoplankton. The decrease in DIC was lower in 2013 compared to 2012, which is consistent with the higher O_2 oversaturation and the greater Chl-a values observed in 2012.
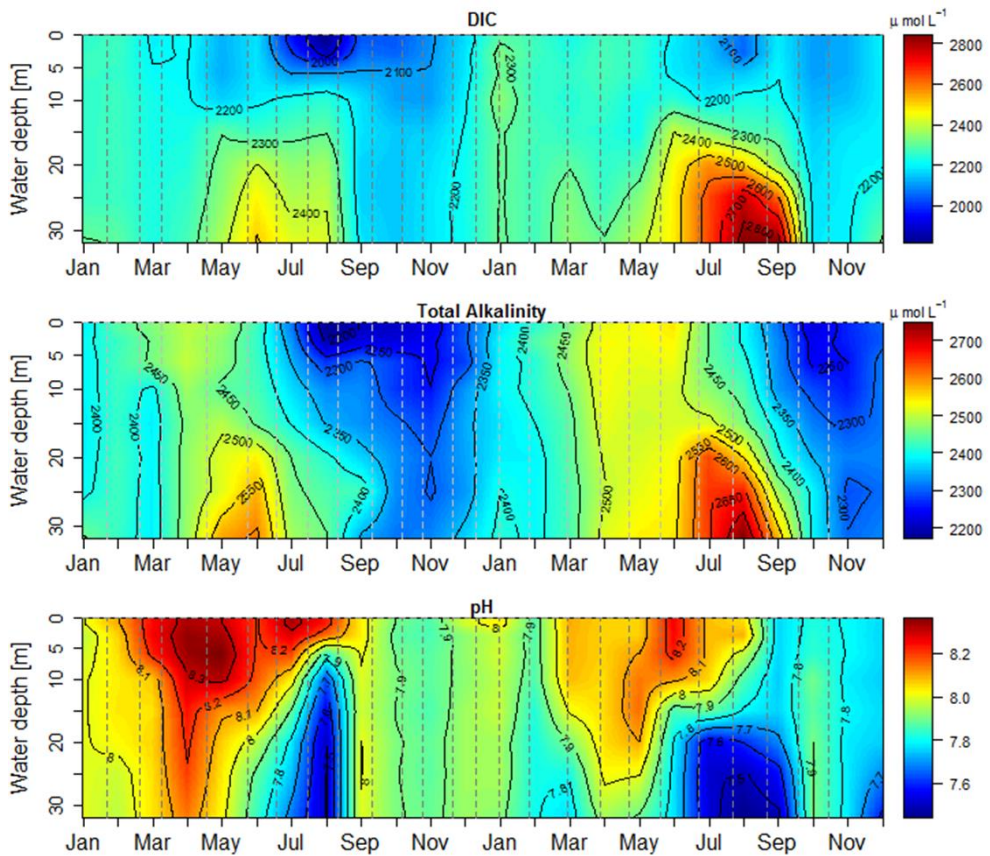
Figure 4. (A) DIC (µmol L^{-1}), (B) A$_T$ (µg L^{-1}) and (C) pH at Den Osse basin in 2012 and 2013. Data from (A) – (C) were linearly interpolated in space and time, and dashed lines indicate sampling dates.

In July 2012 a strong DIC depletion (< 2000 µmol L^{-1}) occurred within the top 5 m in association with a dinoflagellate bloom. In late fall and winter, DIC values increased homogeneously throughout the whole water column. In the deeper water layers, the DIC concentrations increased from April onwards, when the water column became stratified (Fig. 2d). The accumulation of DIC in bottom water was tightly linked to the strength of hypoxia, as DIC reached substantially higher values in 2013 (> 2800 µmol L^{-1}) compared to the previous year (up to 2500 µmol L^{-1}). The alkalinity in the surface layer also showed a clear seasonal pattern (Fig. 4b). A$_T$ gradually decreased during fall and increased again during spring. Quite surprisingly, the dinoflagellate bloom within the top 5 m in July 2012 also coincided with a strong decrease in surface alkalinity. Like DIC, bottom water A$_T$

showed an accumulation during periods of stratification, and this accumulation was substantially higher in 2013 compared to 2012 (Fig. 4b).

The pH in the surface 10 meters was generally high during periods of primary production (March to September Fig. 4c), in accordance with the pH effect of CO_2 uptake by phytoplankton. Notable pH maxima were recorded in May 2012 (at 6 m), July 2012 (at 1 m) and June 2013 (at 6 m). pH values were higher throughout 2012, when higher Chl-a and O_2 concentrations were higher, thus corroborating the link between primary production and high surface pH. In summer, the bottom waters showed a pronounced acidification (pH values < 7.5), and the acidification period closely corresponded to the period of bottom water oxygen depletion. Overall, water column pH was positively correlated with oxygen saturation (Pearson correlation: r=0.6, p<0.001).

2.1.3.   Nutrients in the water column

Nitrate concentrations in the water column showed a clear seasonal pattern, with concentrations being highest in winter and lowest in summer (Fig. 5a). In 2012 high nitrate concentrations (up to 33.0 µ L^{-1}) were observed from January to end of March, whereas the following year this enrichment persisted only from December to the beginning of February. Nitrate consumption took place in spring in the surface layer (Fig. 5a), as the NO_3^- decrease in the surface layer (up to 10 m) preceded that of the deeper layers. This nitrate decrease co-occurred with the first and second phytoplankton blooms (Fig. 3b). In 2013, the whole water column became depleted in nitrate in early summer, when concentrations fell below detection limit (< 0.01 µ L^{-1}). The peak in nitrate concentrations observed in the bottom water in July 2012 was unusual and did not occur during the following summer. Although the nutrient analysis was double checked, we hypothesize this is likely an anomalous observation that could be linked to a sampling error. Throughout the fall, the NO_3^- levels gradually build up again throughout the water column.

During most of the sampling period ammonium concentrations were relatively low (< 10 µmol L^{-1}; Fig. 5b) throughout the entire water column. However, a clear increase was observed in the waters layers below 10 m water depth during April-July 2012 and April-October 2013. During 2013, NH_4^+ concentrations were substantially higher (up to 88 µmol L^{-1}) than the previous summer (up to 40 µmol L^{-1}) and affected a bigger water mass, in accordance with the longer hypoxia period in 2013.

In general, phosphate concentrations showed a similar seasonal water column distribution as ammonium (Fig. 5c). High phosphate concentrations (up to 11 µ L^{-1}) accumulated in the bottom water, and this accumulation was stronger in 2013 compared to 2012. However, in contrast to ammonium, phosphate was also apparently upwelled in summer, giving increased concentrations in the surface layer. This indicates that primary production in summer was likely nitrogen limited, rather than phosphorus limited.

During both years, silicic acid concentrations were high in winter, throughout the entire water column (Fig. 5d), and showed depletion in spring in the upper water layer (< 5 µ L^{-1}),
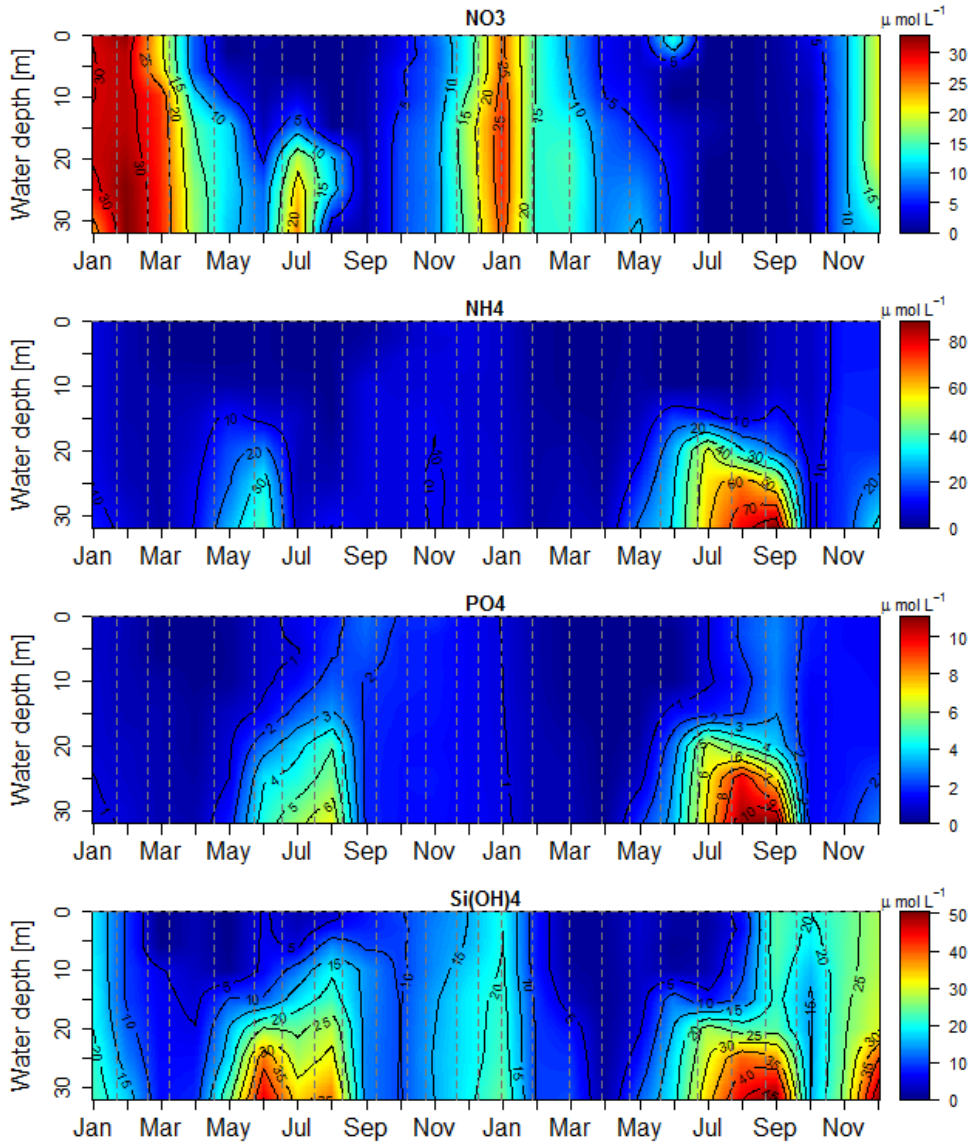
Figure 5. (A) NO$_3^-$ (μmol L^{-1}), (B) NH$_4^+$ (μmol L^{-1}), (C) PO$_4^{3-}$ (μmol L^{-1}), and (D) SiOH$_4$ (μmol L^{-1}) at Den Osse basin in 2012 and 2013. Data were linearly interpolated in space and time, and dashed lines indicate sampling dates.

likely induced by the phytoplankton blooms that occurred in both years (Fig. 3b). During the stratification period, the deeper water layers exhibited high silicic acid concentrations (Fig. 5d).

2.1.4. Benthic nutrient fluxes and denitrification rates

Ammonium fluxes were directed from the sediments towards the water column (Fig. 6a), followed a clear seasonal pattern as well as an increasing trend with water depth (mean annual flux in Table 2). The NH_4^+ fluxes were relatively low from January to April, but showed a clear increase in May, and exhibited the highest rates throughout summer, with 20.9 ± 2.5 mmol m^{-2} d^{-1} at S1 (August), 6.1 ± 0.9 mmol m^{-2} d^{-1} at S2 (September) and 3.9 ± 0.7 mmol m^{-2} d^{-1} at S3 (July). The ammonia release remained high till October at all stations, and afterwards showed a marked decrease in concert with the cooling of the bottom waters (Fig.2a). Ammonia fluxes were positively correlated with the bottom water temperature (Pearson correlation: $r=0.5$, $p<0.001$) and negatively correlated with oxygen saturation (Pearson correlation: $r=-0.5$, $p<0.001$).

Nitrate fluxes at the deepest site S1 varied between -7.4 and 1.1 mmol m^{-2} d^{-1} and were mostly directed from the water towards the sediment, with the exception of February, April and June when a low efflux was observed (Fig. 6b). At site S2 a seasonal pattern was observed, where nitrate escaped from the sediment in winter in (0.8 ± 0.2 in January and and 0.6 ± 0.1 mmol m^{-2} d^{-1} February) and sedimentary nitrate uptake was observed throughout the rest of the year with a maximum influx reached in July (-2.7 ± 0.7 mmol m^{-2} d^{-1}). The seasonal pattern at the shallowest site S3 resembled that at S2, as nitrate escaped the sediment during winter and spring, while it showed an efflux from July to November.

Like ammonium, phosphate followed an increasing trend with water depth (mean annual flux in Table 2). Benthic fluxes of phosphate were positively correlated with temperature (Pearson correlation: $r=0.4$, $p<0.001$) and negatively correlated with bottom water oxygen concentrations (Pearson correlation: $r=-0.7$, $p<0.001$).

Phosphate was released from the sediments from May (2.9 ± 1.3 mmol m^{-2} d^{-1}) to November (1.0 ± 1.0 mmol m^{-2} d^{-1}) at S1 (Fig. 6c), in co-occurrence with high temperatures in the bottom water and bottom water anoxia (July-August). At S2 the phosphate fluxes were detectable from April to September, and showed a peak in August (2.4 ± 0.4 mmol m^{-2} d^{-1}) during bottom water anoxia. At the shallowest S3 phosphate was released from the sediment only during July (0.6 ± 0.1 mmol m^{-2} d^{-1}) and August (1.6 ± 0.2 mmol m^{-2} d^{-1}).

All silicic acid fluxes were directed towards the water column and the seasonal pattern tracked the ammonia flux fairly well, with release rates being higher in summer and fall (Fig. 6d). The silicic acid e release varied between 2.1 ± 0.2 (Feb) and 46.5 ± 17.2 (May) mmol m^{-2} d^{-1} at S1 (for annual mean see Table 2). At the other two stations low rates were observed from January to in March, after which the flux increased and the highest release occurred in August (22.6 ± 1.3 and 18.8 ± 0.8 mmol m^{-2} d^{-1} at S2 and S3, respectively).
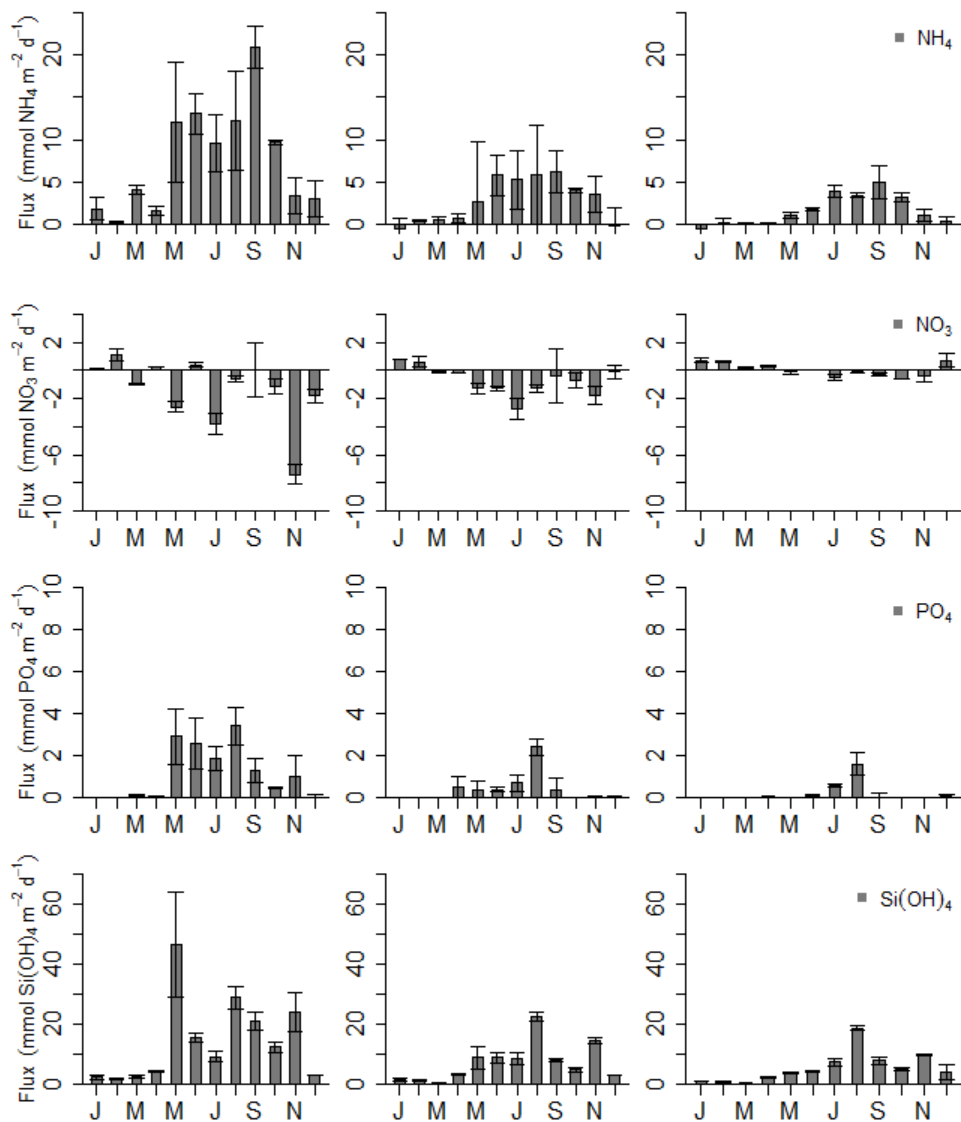
Figure 6. Sediment-water exchange flux of NH_4^+, NO_3^-, PO_4^{3-}, and $Si(OH)_4$ (mmol m^{-2} d^{-1}) at S1(left), S2 (middle), and S3 (right) in Den Osse basin in 2013. Core incubations were executed on replicate or triplicate cores.

Unlike the benthic fluxes, N_2 production rates were generally similar across the 3 stations At S1, N_2 production peaked in June (3.8 ± 0.5 mmol m^{-2} d^{-1}; Fig. 7) and the release remained high until October. In general, S1 exhibited higher rates throughout most
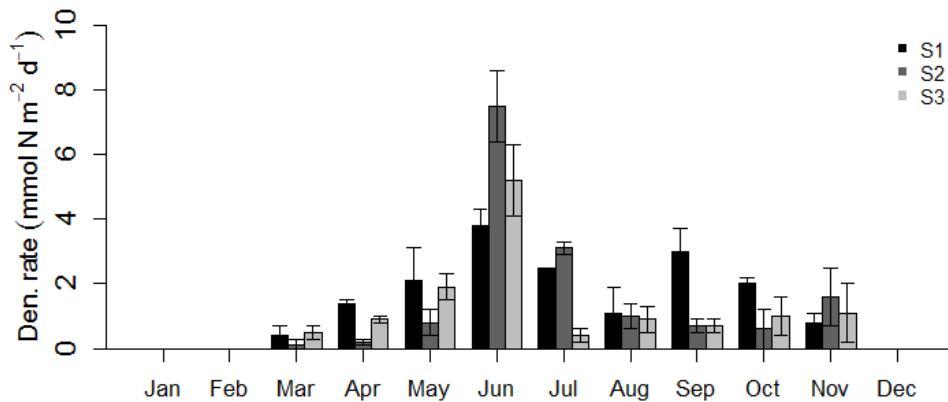
Figure 7. N_2 production rate (mmol N m^{-2} d^{-1}) based on N_2/Ar ratio at all three stations in Den Osse basin in 2012. Core incubations were executed on replicate or triplicate cores.

of the year, except during June-July in concert with the onset of hypoxia in the bottom waters of the basin. S2 showed the highest N_2 production rated measured in the basin, which amounted to 7.5 ± 1.1 mmol m^{-2} d^{-1} in June.

2.2. DISCUSSION
2.2.1. <u>Pelagic primary production</u>

In Lake Grevelingen, primary production exhibits a clear seasonal pattern, and the timing and rate of the phytoplankton activity appears to be regulated by light and nutrients (Hagens et al., 2015; Hagens 2015). The Chl-a distribution in the water column showed three distinct maxima throughout the year (March, May, July-August) suggesting that three separate blooms occurred in surface waters (Fig. 3a). This bloom pattern was seen in both years, and all three phytoplankton blooms occurred during periods of water column stratification. The first phytoplankton bloom of the year took place in early spring (March) and had a lower intensity (lower Chl-a concentrations; Fig. 3b) compared to the following blooming events. The combination of an increase in solar radiation, with the accumulation of nutrients in surface waters throughout winter, and the establishment of a weak salinity-driven stratification, likely triggered the development of this early bloom. The stratification of the surface waters is needed in order to prevent that cells are transported out of the euphotic zone below a critical depth (Sverdrup 1953). In concert with this high phytoplankton activity, the nitrate, silicic acid and DIC concentrations in the surface waters declined (Fig. 4, 5), suggesting nitrate uptake by diatoms (Hagens, 2015). The second bloom took place in late spring (May), when a deep Chl-a maximum was observed at 10 m. Concurrently, nitrate was depleted (< 2.0 µmol L^{-1}) from the surface 10 m layer (Fig. 5a),

but remained at relatively high concentrations ($\sim$ 11 µmol L^{-1}) in the water layer below the Chl-a peak. The May bloom was associated with a DIC decrease within the surface waters, due to CO_2 fixation, and a DOC enrichment, likely due to organic carbon release by sinking phytoplankton. The last phytoplankton bloom occurred in summer (July-August) and was restricted to the top 5 meter water layer. By this time, nitrate was fully depleted throughout the entire water column, the DIC further decreased within the top 5 meters, whereas the DOC remained high and exhibited a maximum in August, following the peak in primary production.

The ratio of dissolved inorganic nitrogen, DIN = ($[NO_3^-]$ + $[NH_4^+]$), over dissolved inorganic phosphorus, DIP = $[PO_4^{3-}]$, remained above the predicted Redfield value (N:P = 16:1) during winter and spring throughout the entire water column. As nitrate decreased at the surface waters in May due to phytoplankton uptake, the DIN:DIP ratio rapidly declined, and remained lower (range: 0.1 and 13) than the Redfield ratio from June to November, at all depths. Phosphate upwelled in summer, generating increased concentrations in the surface layer (Fig. 5c). This indicates that primary production in summer was likely nitrogen limited, rather than phosphorus limited. The winter concentration of DIN in Lake Grevelingen amounts to around 40 µmol L^{-1}. Assuming that nitrogen is the limiting nutrient for primary production throughout the year, the winter inventory of DIN in Lake Grevelingen determines the scope for new production (as opposed to regenerated production based on internal recycling of DIN). If we multiply winter concentration of DIN ($\sim$40 µmol L^{-1}) with the mean depth of the lake (5.1 m) and the Redfield C:N ratio (6.6), we obtain a new production of 16.2 g C m^{-2} yr^{-1}. Hagens et al. (2015) estimated a mean annual net primary production in Den Osse basin of 225 g C m^{-2} y^{-1}. So, only $\sim$7% of the primary production is "new", and hence, most of the primary production within Lake Grevelingen is supported by internal recycling in both water column and sediment.

The phytoplankton community was dominated by diatom species during the first two blooms (Hagens et al., 2015; Hagens 2015). The depletion of silicic acid in the photic zone from May onwards, likely led to a shift in the community composition, as non-siliceous flagellate species dominated in July (Hagens et al., 2015; Hagens 2015). This community was composed mainly of dinoflagellates (*Prorocentrum micans*) and the haptophyte *Phaeocycstis globosa*, which is known to cause blooms in spring in the southern part of the North Sea (Peperzak and Poelman, 2008). Hence, the *Phaeocystis* may have been laterally transported from the North Sea into Lake Grevelingen.

2.2.2. <u>Seasonal hypoxia and oxygen balance</u>

Over the last three decades, the field site (Den Osse basin in Lake Grevelingen) has experienced a regular pattern of summer oxygen depletion in the bottom waters (chapter 4). However, the duration of the hypoxic event varies from year to year. In 2012, the oxygen concentration in the bottom waters of the Den Osse basin (water depth 34 m) fell below the hypoxia threshold (63 µmol L^{-1}) for $\sim$60 days, while the following summer, the hypoxic

period lasted for ~90 days. Given the interannual variability recorded in the government monitoring program over the last three decades, where the hypoxia period ranges between 20 and 90 days (Wetsteyn 2011), the 2013 summer can be categorized as one with rather intense hypoxia.

The temperature driven stratification was stronger in the summer of 2013 compared to the year before, which likely led to the more severe hypoxia, isolating the bottom water for longer time, and thus impeding the renewal of these water masses with oxygenated waters. The development of coastal hypoxia results from an imbalance between local consumption and external supply of oxygen. Oxygen is externally supplied by turbulent mixing from overlying, well-oxygenated water layers, where O_2 is either taken up from the atmosphere or produced via benthic and pelagic photosynthesis. Local oxygen consumption in the bottom water is fuelled both by respiration in the water column and oxygen uptake by the sediments. Yet, at present, the role of sediments in the development of hypoxia is poorly constrained (Middelburg and Levin 2009). To determine the contribution of sediments, we constructed an oxygen budget for the deeper waters of the Den Osse basin. The model includes the zone experiencing hypoxia (water depth > 15 m) and considers the stratified period from April to June, which defines the period of declining O_2. The observed decrease in the water column O_2 concentration (dC/dt) can be related to the respiration rate in the water R_{WC} and the sedimentary O_2 uptake J_{sed}, via the mass balance (Livingstone and Imboden 1996)

$$V_{WC}\left(dC/dt\right) = -V_{WC}R_{WC} - A_{sed}J_{sed} + V_{WC}T_{WC} \qquad (2)$$

where V_{WC} = 1.10 x 10^7 m^3 is the water volume below 15 m (Table 1), A_{sed} = 1.28 x 10^6 m^2 is the sediment area in the hypoxia-affected zone (Table 1), and T_{WC} is the external supply of O_2 to the bottom water by transport. In 2012, the bottom water oxygen decreased from 247 to 61 µM over a period of 64 days, thus providing an average oxygen decrease rate dC/dt = 2.9 mmol m^{-3} d^{-1}. In 2013, the bottom water oxygen decreased at a similar rate of dC/dt = 3.2 mmol m^{-3} d^{-1}, dropping from 282 to 14 µM in 84 days. This observed oxygen decrease rate (~3.1 mmol m^{-3} d^{-1}) is comparable with rates reported for other seasonally hypoxic systems, which range from 0.75 to 5 mmol m^{-3} d^{-1} (Cowan 1996; Boynton and Kemp 2000; Glud et al. 2003; Greenwood et al. 2010; Testa and Kemp 2014).

The pelagic respiration rate was measured during the 2012 sampling campaigns via closed bottle incubations (Hagens et al. 2015), and the yearly average respiration in the photic zone amounted to R_{WC} = 10 mmol O_2 m^{-3} d^{-1}. The deeper bottom waters of Lake Grevelingen are characterized by marine snow formation, which hence keeps substantial amounts of organic matter in suspension. These marine snow flocs are known to be hotspots of mineralisation (Ploug and Jørgensen 1999), which could thus explain the large

pelagic respiration rate. Similarly, the total oxygen uptake (TOU) of the sediment was also measured during the 2012 sampling campaigns (chapter 3). The mean TOU value over the stratified period from April to June was estimated at $J_{sed} = 25.5$ mmol m^{-2} d^{-1} (Table 1) and provides a sediment contribution of $R_{SED} = A_{sed} J_{sed} / V_{WC}$ = 3.0 mmol O$_2$ m^{-3} d^{-1} to the oxygen consumption in the bottom water. This benthic O$_2$ consumption rate already equals the observed O$_2$ decrease in the water column, hence suggesting that sediments could play a crucial role in the hypoxia dynamics of the bottom waters of Lake Grevelingen.

The oxygen mass balance at the field site however still shows some uncertainty. If we add the pelagic contribution (R_{WC} = 10 mmol O$_2$ m^{-3} d^{-1}) and benthic contribution (R_{WC} = 3.0 mmol O$_2$ m^{-3} d^{-1}), we arrive at a total oxygen consumption rate of 13.0 mmol O$_2$ m^{-3} d^{-1}. This would imply that 23 % of the O$_2$ demand originates from the sediment and 77 % occurs in the water column. By means of the oxygen mass balance (Eq. 2) it also implies an external supply of T_{WC} = 10 mmol O$_2$ m^{-3} d^{-1}. This external oxygen supply can occur either by turbulent mixing through the thermocline, or alternatively, via the input of oxygenated North Sea water through the sluice. To examine whether thermocline mixing alone is sufficient, we can estimate the turbulent eddy diffusion coefficient K_z that would be needed to sustain the estimated oxygen transport T_{WC}.

$$K_z = -\frac{V_{WC}}{A_{sed}} \frac{T_{WC}}{(\partial C / \partial z)} \approx -\frac{V_{WC}}{A_{sed}} \frac{T_{WC} \Delta H}{\Delta C} \qquad (3)$$

Here, ΔH represents the thickness of the pycnocline (~ 10 m; see Fig. 2c) and ΔC the oxygen concentration difference over the picnocline (~250 μmol L^{-1}; see Fig. 2c). The resulting value K_z = 4 x 10^{-5} m^2 s^{-1} is slightly above of the range of typical values for K_z observed in thermally stratified lakes (10^{-7} to 10^{-5} m^2 s^{-1}), and 8 times higher than the K_z-value in an hydrodynamic model simulation of Lake Grevelingen (5x10^{-6} m^2 s^{-1}; (Zijl and Nolte 2006). This discrepancy can be resolved in two possible ways. One option is that the pelagic respiration rate could be overestimated (i.e. too high R_{WC} value). The alternative explanation is that the external O$_2$ supply is not alone due to thermocline mixing, but also due to input of oxygenated North Sea water through the sluice. To resolve the current uncertainty in the oxygen budget, future studies should target a more tightly constrained oxygen balance, including field measurements of Kz and turbulence, as well as permanent moorings to document North Sea inflows via depth profiles of temperature, salinity and O$_2$.

2.2.3. <u>Nutrient accumulation in the bottom water</u>

The oxygen budget examined in the previous section indicates that substantial respiration, and hence organic matter mineralization, occurs in both the water column and

sediment compartments of the deeper basins in Lake Grevelingen. This is clearly seen by the accumulation of the end-products of organic matter mineralisation (DIC, NH_4^+, PO_4^{3-} and $Si(OH)_4$) in the bottom water during the stratified period. Similarly to oxygen, we estimated the increase rates dC/dt of these mineralization end-products during the stratified periods of both 2012 and 2013 (Table 2). By adopting a standard stoichiometric composition of organic matter (C:N:P:Si = 106:16:1:16), we recalculated all accumulation rates into corresponding C-units (Table 2). In the summer of 2012, the resulting accumulation of oxygen, DIC, ammonium and silicic acid agree very well with each other (<10% difference; Table 2), indicating that the accumulation in the bottom water showed a consistent signal of organic matter respiration. The same consistent pattern was seen in 2013, except for the accumulation of DIC, which was twice as high as expected.

Table 2. Accumulation rate (dC/dt) of biogeochemical variables in the water column below 15 m water depth. The accumulation rate was calculated from the maximum slope of concentration versus time plot during the stratification period (the exact period varied slightly for each parameter, depending on the occurrence of the maximum slope). Rates were converted to C units using Redfield ratio (C:N:P of 106:16:1). The ratio O_2: DIC was assumed to be 1:1. The sediment flux (J_{sed}) is the mean value at the three stations over the period used for the dC/dt estimation. R_{SED} is the increase/decrease rate calculated as $R_{SED} = A_{sed} J_{sed} / V_{WC}$, where A_{sed} is the sediment area (m^2) enclosed under 15 m water depth, and V_{WC} (m^3) is the relative water volume. Negative values indicate fluxes directed towards the sediment.

	2012		2013		2012	2012
	dC/dt	C-units	dC/dt	C-units	J_{SED}	R_{SED} (C-units)
Parameter	mmol m^{-3} d^{-1}		mmol m^{-3} d^{-1}		mmol m^{-2} d^{-1}	mmol m^{-3} d^{-1}
O_2	-3.0	-3.0	-3.2	-3.2	-25.5	-3.0
DIC	2.7	2.7	5.8	5.8	33.2	3.9
TA	2.6	1.3	3.3	1.7	19.2	1.1
NH_4	0.5	3.1	0.6	4.0	4.3	3.4
PO_4	0.06	6.7	0.12	12.6	1.6	20.1
$Si(OH)_4$	0.6	3.9	0.4	2.7	11.1	8.9

2.2.4. Fluxes from the sediment

To estimate the role of the sediment compartment on the water column DIC and nutrient concentrations, we compared the accumulation rate of the end products of mineralization in the bottom water (dC/dt) with the sediment release rate $R_{SED} = A_{sed} J_{sed}/V_{WC}$ for the year 2012 (Table 2). As was the case for oxygen, the sediment release rate for DIC and ammonium in summer are comparable to the observed accumulation rates, suggesting an important sediment contribution to the accumulation of mineralization products in the bottom water.

Table 3. Annual mean of sediment fluxes at the three stations and averaged for the entire basin taking into account the sediment area.

	Annual mean (mmol m^{-2} d^{-1})			
	S1	S2	S3	Basin mean
TOU	32.1 ± 19.9	23.4 ± 4.7	23.3 ± 3.6	25.7
DIC	54.9 ± 30.5	20.3 ± 9.5	17.3 ± 7.0	28.8
NH$_4^+$	7.6 ± 6.2	2.8 ± 2.5	1.6 ± 1.7	3.7
NO$_3^-$	-1.4 ± 2.2	-0.7 ± 1.0	0.0 ± 0.4	-0.6
PO$_4^{3-}$	1.2 ± 1.2	0.4 ± 0.6	0.2 ± 0.4	0.5
SiOH$_4$	14.5 ± 13.0	7.4 ± 6.1	5.7 ± 4.8	8.7
N$_2$	1.9 ± 1.0	1.7 ± 2.2	1.4 ± 1.4	1.7

We now analyse the sediment-water interface fluxes of the nitrogen species in relation to benthic mineralization on an annual basis (Table 3). If we multiply the mean annual NH$_4^+$ efflux from the sediment (~3.7 mmol m^{-2} d^{-1}) with the Redfield C:N ratio (6.6), and convert this to carbon units, we find that the NH$_4^+$ release from the sediment could sustain a primary production of 107 g C m^{-2} yr^{-1}, which could account for 48% of the observed annual primary production. The deeper basins within Lake Grevelingen only cover 10% of the area, but as the NH$_4^+$ efflux substantially increases with depth (Fig. 6), the sediments in these deep basins appear as important locations of nutrient remineralization. Assuming that the N$_2$ production is equal to the denitrification rate (i.e. neglecting annamox or DNRA) the mean annual benthic denitrification rate (BDR) from the sediment amounted to 1.7 mmol m^{-2} d^{-1}. The nitrate influx towards the sediment was lower, and amounted to 0.6 mmol m^{-2} d^{-1}, and could support up to 35% of the benthic denitrification. Hence, 65% of the denitrification activity observed was due to coupled nitrification-denitrification (calculated as 1-NO$_3^-$ flux/BDR).

Another way to estimate benthic carbon mineralization is to consider ammonification taking place in the sediment. The total ammonification rate in the sediment (AR) was

calculated as AR = NH_4^+ flux + BDR − NO_3^- flux and amounted to 4.8 mmol m^{-2} d^{-1}, which would give a carbon mineralization rate (AR*6.6) of 31.4 mmol m^{-2} d^{-1}. From here we can estimate that 36% of the bioavailable N produced by ammonification is lost by denitrification (BDR/AR), suggesting that denitrification impacts N cycling in Lake Grevelingen sediments.

The observed accumulation of phosphate in summer was however about 3 times higher than expected from mineralisation (Table 2). This pattern was observed in both sampling years. This enhanced P release during summer was recently explained by the sedimentary P dynamics in Lake Grevelingen (chapter 5). Cable bacteria are abundant at S1 in winter and spring, and their metabolism induced the formation of an iron (hydr)oxides layer below the sediment surface in spring (chapter 4). The iron (hydr)oxides pool contained also a large stock of iron-oxide-bound phosphorus, and in this way, cable bacteria indirectly enhanced P retention in the sediment during spring. In summer, during reducing conditions in the sediment, and no oxygen in the bottom water P was released to the porewater upon reduction of the iron (hydr)oxides, and diffused to the bottom water (chapter 5), as observed also in Fig. 5c.

DIC is produced during the mineralization of organic matter in the bottom water and within the sediment. At the field site, sediments are a major source of DIC, releasing a mean annual average of 31.6 mmol C m^{-2} d^{-1} (chapter 3 and Table 1). In chapter 3 we concluded that organic matter mineralization provides the major source of DIC production in the sediment. Alkalinity concentrations are regulated by the dissolution or precipitation of carbonates as well as respiration processes. In marine sediments, A_T is mainly affected by anaerobic mineralization processes: denitrification, iron reduction, and sulfate reduction are the main pathways responsible for alkalinity generation. A_T in the bottom water increased in summer, during anoxia, and in co-occurrence with high denitrification rates (Fig. 8), and substantial sulfide generation which is indicative of enhanced sulfate reduction (chapter 4). Although benthic fluxes of A_T were lower than the DIC efflux (Chapter 3), the associated R_{SED} shows that sediments could provide up to around 85% of the alkalinity found in the bottom water.

2.2.5. Effect of hypoxia on bottom water acidification

The depletion of oxygen in the bottom water was accompanied by a notable acidification of these water layers, and a concomitant accumulation of DIC and A_T in the bottom water. In summer 2012 the bottom water pH decreased up to 0.53 units over 82 days. Over the same period, the accumulation of DIC in the bottom water (132 µmol L^{-1}) was more than 5 times higher than the increase in A_T (23 µmol L^{-1}). In the summer of 2013, the acidification of the bottom waters was slightly lower, as the pH dropped by 0.45 units, accompanied by a substantial release of DIC (447 µmol L^{-1}) and A_T (213 µmol L^{-1}). This time the accumulation of DIC was only 2 times higher than the A_T. A rise in bottom water DIC (at constant A_T) leads to lower pH conditions, whereas the release of A_T (at constant

DIC) will increase the pH. Accordingly, the lower DIC: A_T accumulation ratio in the bottom water in 2013 might explain the reduced increase in pH compared to 2012.

The observation of lower pH values during bottom water anoxia is in accordance with previous studies reporting an effect of hypoxia on the acidification of marine waters (Cai et al. 2011; Mucci et al. 2011). Hagens et al. (2015) studied in detail the biogeochemical processes affecting the carbonate system during 2012 at the field site, and concluded that the pH fluctuations in the bottom water in summer were due to a substantial reduction of the acid–base buffering capacity, which was linked to the occurrence of hypoxia. Such findings are in accordance with previous model analyses which predict pronounced fluctuations in bottom-water pH in seasonal hypoxic systems (Sunda and Cai 2012). Alongside with this increased ocean acidification, the occurrence and intensity of hypoxic events is also expected to increase (Diaz and Rosenberg, 2008). Hence, the reinforcement of bottom water acidification by seasonal hypoxia might reinforce the ecosystem impact of both phenomena in coastal systems (Keeling et al. 2010).

2.2.6. <u>Organic matter dynamics</u>

Given the information above we can compile an organic carbon budget for the bottom water below 15 meter in Den Osse basin (Fig. 8). In order to estimate the yearly mean mineralization rate in the water column (R_{min}), we used the mean respiration rate in the water column ($R_{WC} = 10$ mmol O_2 m^{-3} d^{-1}), the water volume (m^3) and the sediment area of the basin (m^2; Table 1), and adopting a respiratory quotient of 1 (i.e. 1 mole O_2 is consumed per mole of organic carbon mineralized). Accordingly, the pelagic mineralization rate amounts to $R_{min} = 375$ g C m^{-2} y^{-1} ($R_{min}= R_{WC}$·water volume·365.25·12/sediment area).

The basin is characterized by relatively steep slopes on all sides. The sediments consist of dark fine-grained mud with high carbonate content (21 %), high organic matter (C_{org}: 3.9 %), and high respiration activity. The mean TOU across the three stations and across all months amounts to 25.7 mmol O_2 m^{-2} d^{-1} (Table 3 and chapter 3), which corresponds to a benthic respiration rate of 113 g C m^{-2} y^{-1} (adopting a respiratory quotient of 1). Furthermore, we can calculate the burial rate of organic carbon as $F_b = 112$ g C m^{-2} y^{-1} (calculated as $F_b = C_{OM}\rho_S\left(1-\phi\right)v_S$, where $C_{OM} = 0.039$ g C g^{-1} is the concentration of organic carbon at 10 cm depth, $\rho_S = 2.6$ g cm^{-3} is the solid phase density, $\phi = 0.89$ is the porosity at 10 cm depth, and $v_S = 1.0$ cm y^{-1} is the mean sediment accumulation velocity across the Den Osse Basin. Accordingly, the sediments of the Den Osse basin form an important location for carbon burial: about 50 % of the total organic matter reaching the sediment surface (112 + 113 = 225 g C m^{-2} y^{-1}) is buried in the sediment. Assuming a net annual primary production in Den Osse basin of 225 g C m^{-2} y^{-1} (Hagens et al. 2015), direct deposition of all the organic matter locally produced by primary production above the field
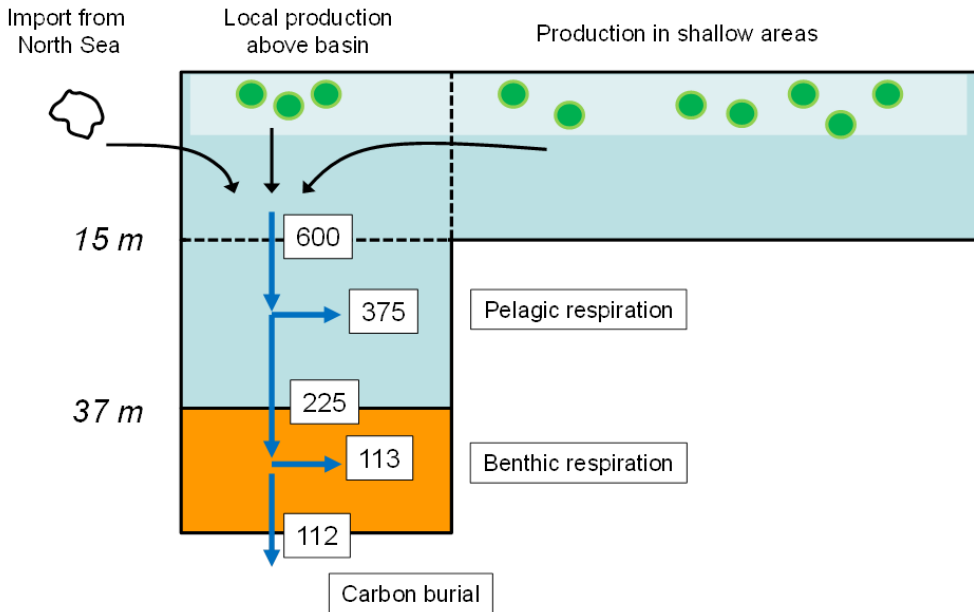
Figure 8. A tentative organic carbon budget for the bottom waters below 15 m in the Den Osse basin in Lake Grevelingen. All fluxes are expressed in g C m^{-2} yr^{-1}.

site is needed to sustain the organic matter input into the sediment. However, pelagic respiration in the deep basin (10 mmol O$_2$ m^{-3} d^{-1}; Hagens et al., 2015) provides a necessary pelagic mineralization rate of 375 g C m^{-2} y^{-1}.

Accordingly, an organic carbon flux of 600 g C m^{-2} y^{-1} is needed across the 15 m horizon to sustain the sum of pelagic respiration, benthic respiration and benthic organic carbon burial (Fig. 8). As a result, local primary production in the surface waters directly above the basin is not able to account for this required export flux. There are two ways to explain this discrepancy. Firstly, Lake Grevelingen contains substantial shallow areas, and the local primary production in these shallow areas can be exported into the deeper basins via so-called "focusing" of suspended matter.

The sedimentation rate in the Den Osse basin strongly increases with water depth (from 0.38 cm y^{-1} at S3 to 2.0 cm y^{-1} at S1; chapter 3), and hence, this corroborates that the deeper basins of Lake Grevelingen are sites of extensive sediment focusing. Secondly, there may be substantial lateral import of particulate organic material (POC) originally produced in the North Sea. Such an import was already suggested by Hagens et al. (2015) to explain the large pelagic respiration rate they recorded. The southern North Sea is a highly dynamic environment with strong tidal currents (tidal range ~ 4 m and bottom currents up to 90 cm s^{-}

[1]; Tryggestad et al., 1983), which keeps fine material in suspension. Once this North Sea water enters the Lake Grevelingen through the sluice gate, it arrives in a much more tranquil environment (no tides and bottom currents up to 0.5 cm s^{-1}; Hamerlynck et al. 1992). Accordingly, Lake Grevelingen acts as a sediment trap for allochtonous material. Particulate organic material (POC) originally produced in the North Sea settles within the calmer waters of the Grevelingen, thus contributing to the high sedimentation rates observed (Fig. 8). At present it is unclear how much of the organic input to the sediment originates from internal redistribution of primary production within the lake and how much originates from import from the North Sea. To this end, a more detailed carbon budget is needed for the entire Lake Grevelingen, which is outside the scope of this study.

2.3. CONCLUSIONS

This work constitutes a comprehensive study on the role of hypoxia on the biogeochemical cycling in both water column and sediments of Lake Grevelingen, a temperate coastal basin. Long-term data series of oxygen concentration in seasonally hypoxic coastal systems demonstrate that the oxygen depletion occurring in the summer months is due to stratification in the water column and enhanced algal production driven by increased nutrient inputs to the coastal zone (Justić et al. 1987; Testa and Kemp 2014). Hence, eutrophication appears to be a major driver of hypoxia in the coastal zone (Diaz and Rosenberg 2008).

Within Lake Grevelingen, the Den Osse basin departs from this trend, as the nutrient concentrations in the water column are relatively low compared to coastal systems. However, strong water column stratification during spring and summer impedes the O$_2$ transport to the bottom waters and thus causes oxygen depletion. Unlike other systems, we found that a substantial part of the organic material entering the basin does not result from in situ primary production, but is rather laterally transported from the North Sea. The respiration of this allochthonous organic material is source of enhanced oxygen utilization, which contributes strongly to the oxygen demand in the basin. When such enhanced respiration occurs in conjunction with water column stratification it leads to the establishment of summer hypoxia.

A carbon budget suggested that the deep basins on the seaward side of the lake act as a sediment trap that accumulate the large amounts of organic material transported from the North Sea of shallower water depths. Such accumulation affects the fate of oxygen in the water column, and hence, must be considered in future managing projects which aim to alter (i.e. enhance) the exchange rate with the adjacent North Sea. The accumulation of these organic rich deposits leads also to the regeneration of nutrients to the water column, which might potentially fuel local primary production, and hence, exacerbate seasonal hypoxia.
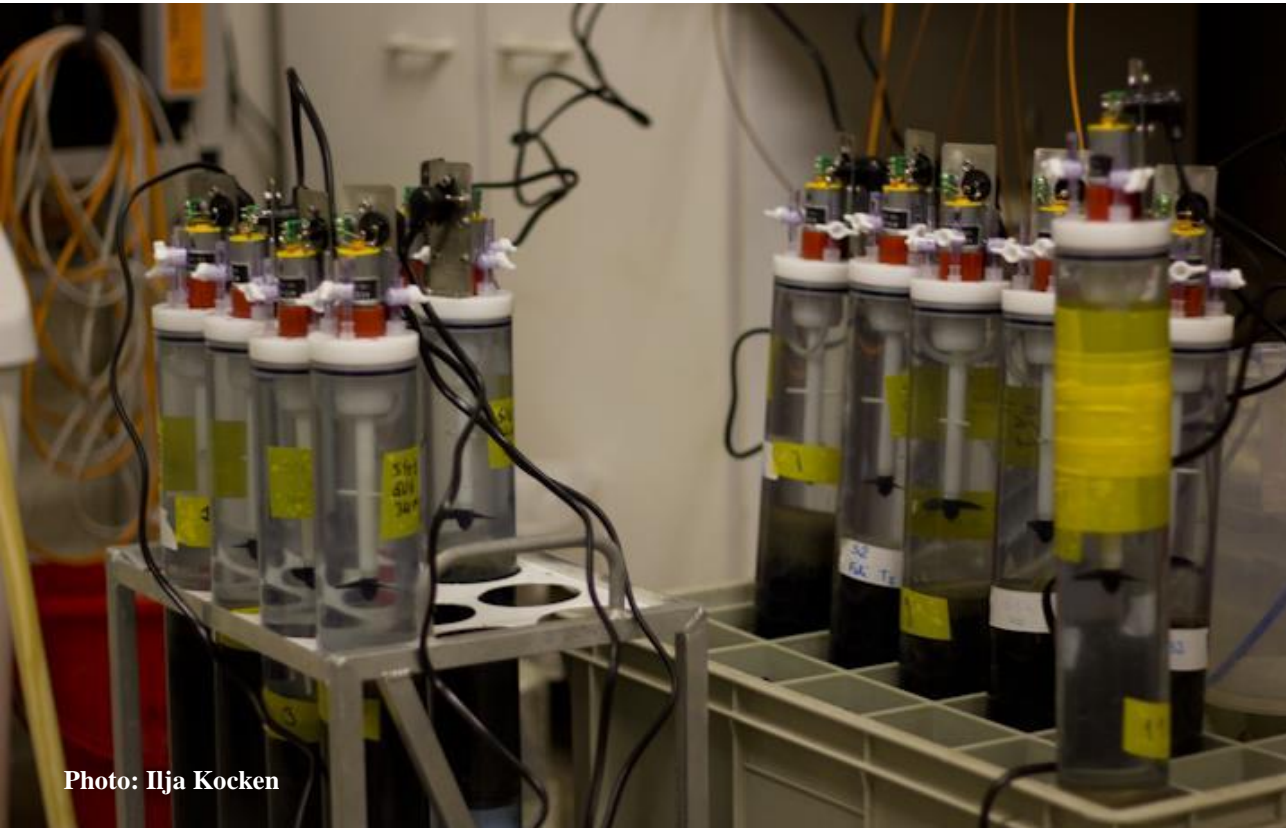
Photo: Ilja Kocken

Sedimentary oxygen dynamics in a seasonally hypoxic basin

Dorina Seitaj, Fatimah Sulu-Gambari, Laurine D.W. Burdorf, Alicia Romero-Ramirez, Olivier Maire, Sairah Y. Malkin, Caroline P. Slomp, Filip J.R. Meysman

ABSTRACT

Seasonal hypoxia refers to the oxygen depletion that occurs in summer in the bottom water of stratified systems, and is increasingly observed in coastal areas worldwide. The process induces a seasonal cycle on the biogeochemistry of the underlying sediments, which remains poorly quantified. Here, we investigated the sedimentary oxygen consumption within Lake Grevelingen (The Netherlands), a saline coastal reservoir that is impacted by yearly recurrent bottom water hypoxia. Monthly sampling campaigns were conducted throughout 2012 at three sites along a depth gradient. Macrofauna sampling and sediment profile imaging demonstrated how summer hypoxia strongly impacts the benthic communities below 15 meters of water depth. Benthic fluxes of oxygen, dissolved inorganic carbon, total alkalinity and ammonium were determined by closed core incubations, while oxygen depth profiles were recorded by microsensor profiling of sediment cores. Our results reveal a pronounced seasonality in the sedimentary oxygen consumption. Low uptake rates in summer were caused by oxygen limitation, and resulted in a build-up of an "oxygen debt" through the accumulation of reduced iron sulfides. Highest oxygen uptake rates were recorded in fall, linked to reoxidation of the pool of iron sulfides in the top layer. However, uptake rates remained unexpectedly high during winter and early spring, likely associated with the oxidation of iron sulfides down to centimeters depth due to the electrogenic sulfur oxidation by cable bacteria. Overall, our results suggest that the sedimentary oxygen dynamic in seasonally hypoxic coastal systems is characterized by a strongly amplified "oxygen debt" dynamic induced by cable bacteria.

3.1. INTRODUCTION

Semi-enclosed and stratified coastal areas can experience a yearly pattern of oxygen depletion in their bottom waters, a phenomenon that is referred to as seasonal hypoxia (Diaz 2001; Middelburg and Levin 2009). The observed increase of the duration, and intensity of seasonal hypoxia (defined as $O_2 < 63$ µmol L^{-1}) in the coastal ocean is recognized as an environmental problem of worldwide concern (Diaz and Rosenberg 2008). The phenomenon is primarily linked to the anthropogenic input of nutrients (Conley et al. 2009), which enhances primary production and export of organic matter from surface waters, thus resulting in increased microbial respiration and oxygen consumption in the bottom water (Rabalais et al. 2002; Kemp et al. 2005; Conley et al. 2009). At the same time, climate change is anticipated to increase the temperature of the surface waters in summer, and the resulting intensification of water column stratification and decrease in oxygen solubility may exacerbate coastal hypoxia in the upcoming decades (Meire et al. 2013).

Seasonal hypoxia has profound effects on the biogeochemical cycling (Turner et al. 2008; Conley et al. 2009; Middelburg and Levin 2009; Kemp et al. 2009; Rabalais et al. 2010; Testa and Kemp 2011) and on the survival and behavior of marine organisms in coastal systems (Diaz and Rosenberg 1995; Rosenberg et al. 2002; Vaquer-Sunyer and Duarte 2008; Levin et al. 2009). Benthic faunal communities inhabiting seasonally hypoxic areas typically exhibit low diversity and abundance, as well as limited sediment reworking activity (Diaz and Rosenberg 1995; Levin et al. 2009). A reduced faunal activity may result in a higher accumulation of reduced compounds and a reduced remineralization and an increased burial of organic matter (Berner and Westrich 1985; Middelburg and Levin 2009).

The oxygen depletion in the bottom waters of stratified systems is ultimately caused by an imbalance between the oxygen supply from surface waters (resulting from atmospheric input and primary production in the photic zone), and the removal of oxygen within the bottom waters (Testa and Kemp 2011). Sediments can account for up to 80% of the total oxygen consumption in shallow coastal systems (Middelburg and Levin 2009), and hence, the sediment likely forms an important sink of oxygen in seasonally hypoxic basins, as has been previously demonstrated for freshwater lakes (Cornett and Rigler 1987; Pace and Prairie 2005).

The coupling between benthic and pelagic compartments is a fundamental feature of shallow coastal ecosystems, and the geochemical cycling in sediments is crucial in regulating this benthic-pelagic exchange (Soetaert and Middelburg 2009). Seasonal patterns in sedimentary oxygen consumption and benthic mineralization are often complex, and affected by simultaneous and interdependent processes (Glud, 2008). Seasonality in benthic mineralization, and consequently in sedimentary oxygen consumption, may result from a variety of factors, such as variations in bottom water temperature (Thamdrup et al. 1998), organic matter input to the sediment (Canfield et al. 1993a), and bottom water oxygen

concentration (Cai and Reimers 1995) as well as seasonality in the activity and abundance of benthic fauna (Aller 1988). Another factor affecting the seasonality in oxygen uptake is the so-called "oxygen debt" (Pamatmat 1971), which represents the oxygen required to re-oxidize reduced compounds (defined as oxygen demand units, ODU; Soetaert et al. 1996) that have accumulated in the sediment during previous months (typically summer). In seasonally hypoxic systems, the fulfillment of the oxygen debt occurs mainly in fall via the oxidation of ODUs, that have accumulated in the sediment throughout summer (Martens and Klump 1984; Chanton et al. 1987; Boynton et al. 1990; Rasmussen and Jorgensen 1992; Moeslund et al. 1994; Brady et al. 2013).

The formation of an "oxygen debt" has been principally linked to the transient accumulation of iron sulfides (FeS) in surficial coastal sediments (Jørgensen 1977). These reduced sulfur compounds can be further transformed to pyrite and become buried (Berner 1970), or undergo oxidation upon contact with oxygen (Luther et al. 1982; Thamdrup et al. 1994). In some coastal sediments, the reoxidation of iron sulfides can account for up to one third of the sedimentary oxygen consumption (Jørgensen 1996), hence, iron sulfide reoxidation represents a major oxygen sink (Glud 2008). Recently, it has been shown that the iron sulfide reservoir can exhibit a marked seasonality in sediments of seasonally hypoxic basins (chapter 4; chapter 5). This seasonal variation was attributed to the metabolic activity of cable bacteria (chapter 4; chapter 5). These filamentous bacteria, which induce long-distance electron transport in the sediment (Nielsen et al., 2010), are thought to be widespread in the sediments of seasonally hypoxic systems (Malkin et al. 2014), and their metabolism has been shown to exert a powerful impact on the sediment geochemistry (Risgaard-Petersen et al. 2012; Rao et al., 2016). However, the impact of cable bacteria metabolism on the sedimentary oxygen dynamics in seasonally hypoxic basins remains to be determined.

The principal research objective here was to document the sedimentary oxygen dynamics in a seasonally hypoxic environment. Building upon two studies examining the microbiology and geochemistry of the sediment within Lake Grevelingen (The Netherlands; chapter 4; chapter 5), our study was conducted at the same seasonally hypoxic basin. To determine the drivers of the seasonality in the sedimentary oxygen consumption, we investigated both the bottom water chemistry and sediment geochemistry at three stations along a depth gradient within the zone affected by hypoxia. Benthic fluxes of oxygen (O_2), dissolved inorganic carbon (DIC), ammonium (NH_4^+) and total alkalinity (TA) were determined in closed chamber incubations, and microsensor profiling was used to quantify the diffusive oxygen uptake (DOU). Sediment profile images and benthic macrofauna data were collected in relation to oxygen conditions in the water column. By combining all measurements, we documented the seasonal variations of the sedimentary oxygen consumption and assessed the role of cable bacteria in these dynamics.

3.2. **MATERIALS AND METHODS**

3.2.1. <u>Study site and sampling procedure</u>

Lake Grevelingen is a former estuary within the Scheldt-Meuse-Rhine delta area of The Netherlands (Fig. 1a, b), which has been closed off by dams at the landward side and seaward side since 1971. Lake Grevelingen (surface area 115 km^2) consists mostly of shallow water areas less than 12.5 m water depth, but in the former estuarine channels, deeper basins are found, which extend down to 45 m water depth. These deeper basins are separated from each other by sills. A sluice on the seaward side enables a limited exchange of water with the open North Sea. Hagens et al. (2015) estimated that the inflow from the North Sea could replenish the water in the entire basin in 30 days. Due to the exchange with the North Sea, the waters approach coastal salinity values (range 29-32).
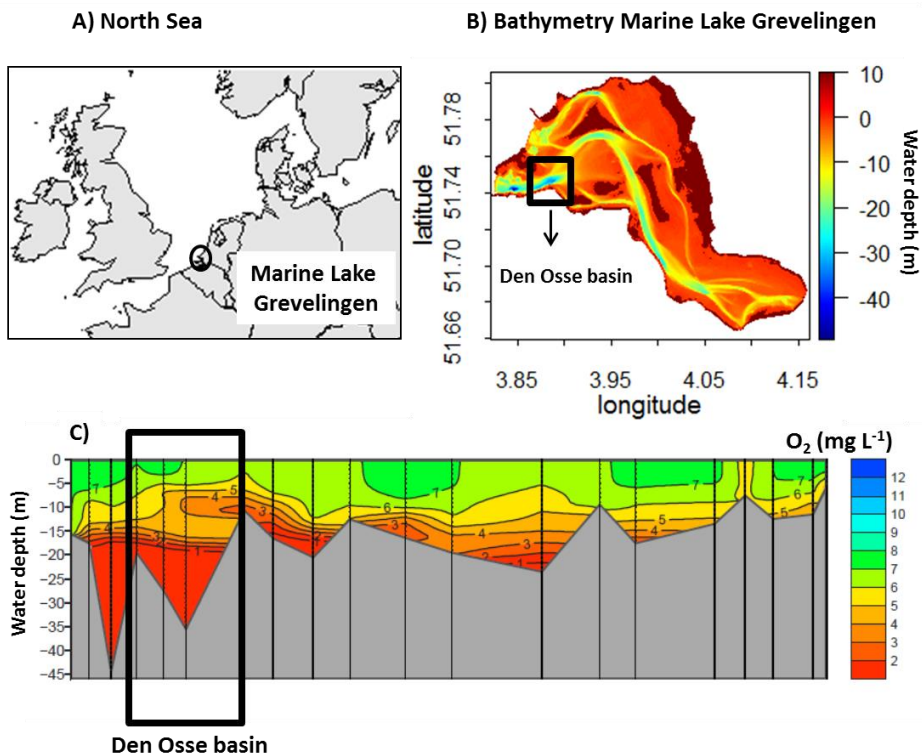
Figure 1. (A) Map of the Southern North Sea; (B) bathymetry of Lake Grevelingen (deepest site 34 m depth: S1; 51.747°N. 3.890°E); (C) depth-map showing the oxygen concentrations in the water column in August 2012 (data from the executive arm of the Dutch Ministry of Infrastructure and the Environment). The black rectangle indicates the area of the Den Osse basin, object of investigation in this study.

Due to the absence of both tides and strong currents, the water column becomes stratified each summer, thus leading to seasonal hypoxia ($O_2 < 63$ µmol L^{-1}) in the bottom waters of the deeper basins (Wetsteyn, 2011; Fig. 1c).

During 2012, we performed monthly sampling campaigns on board of the R/V Luctor, examining both the water-column chemistry and sediment biogeochemistry. Sampling took place in the Den Osse basin, which is located in the western (seaward) part of Lake Grevelingen (Fig. 1c). This basin has a maximum water depth of 34 m, and is enclosed by sills at the landward (10 m) and seaward side (20 m). Sediment sampling was performed at three stations along a depth gradient within the basin: S1was located in the deepest point of the basin at 34 m water depth (51.747°N, 3.890°E), S2 at 23 m (51.749°N, 3.897°E) and S3 at 17 m (51.747°N, 3.898°E). Intact sediment cores were retrieved with a single core gravity corer (UWITEC, Austria) using PVC core liners (6 cm inner diameter, 60 cm length). All cores were inspected upon retrieval and only visually undisturbed sediment cores were used for further analysis.

Water-column sampling was performed at station S1. The three stations S1-S3 were located within around 500 m of each other, and available water quality monitoring data (Wetsteyn, 2011; Fig. 1c) show that the water column is laterally homogenous over such short distances (Fig 1). Accordingly, the bottom water parameters at stations S2 and S3 were derived from the corresponding water depths at S1. A CTD instrument (YSI 6600) was deployed to record the depth profiles of temperature (T), salinity (S), pressure (P), and oxygen concentration. The stratification parameter σ (J m^{-3}) represents the amount of energy required to fully homogenise the water column through vertical mixing (Simpson 1981), and was calculated from the CTD data as (Hagens et al. 2015):

$$\sigma = \frac{1}{H} \int_H^0 (\rho - \rho_W) gz dz \quad \text{where} \quad \rho = \frac{1}{H} \rho_W z dz \qquad (1)$$

Here, H is the total height of the water column (m), z is depth (m), g is gravitational acceleration (m s^{-2}), and and ρ_w denotes the water density (kg m^{-3}), calculated from T, S and P according to Feistel (2008) using the R package CRAN: AquaEnv.

In addition to the CTD profiling, discrete bottom water samples were collected at 2 m above the sediment surface at S1 with a 12 L Niskin bottle to assess the concentrations of oxygen (O_2), dissolved inorganic carbon (DIC), total alkalinity (TA) and ammonium (NH_4^+). In summer, the Niskin bottle was held stationary in the bottom water for at least 10 minutes before retrieval, to allow complete flushing of the Niskin bottle and hence enable an unbiased sampling of the low-oxygen bottom water. Water samples were drawn from the Niskin bottle using Tygon tubing to avoid gas exchange with the surrounding atmosphere.

3.2.2.   Sediment incubations

Shipboard closed core incubations were performed to determine the fluxes of O_2, DIC, TA and NH_4^+ across the sediment-water interface. Incubations were performed in the dark and in triplicate, using intact sediment cores taken by the gravity corer. Upon collection, these sediment cores were of variable height, and to obtain comparable flux results, the water level was adjusted to a fixed level of 18-20 cm above the sediment surface by carefully pushing the sediment upwards in the core liner via the insertion of inert polyurethane disks from below. The core incubations were started within 30 minutes after sediment collection. To ensure that the boundary conditions at the sediment-water interface closely resembled in situ conditions, the overlying water was replaced with bottom water (collected with the Niskin bottle as described above) prior to the start of the incubations. This water replacement was executed via a Tygon tubing, and during the procedure, a floating plastic sheet was placed inside the core, in order to avoid sediment resuspension and disturbance of the sediment water interface during water replacement. Immediately thereafter, the cores were sealed with gas-tight polyoxymethylene lids and transferred to a temperature controlled incubator (LT650; Elbanton) operating at the in situ bottom water temperature. The core lids contained a central stirrer to ensure the overlying water remained well mixed, as well as two sampling ports to enable discrete water subsampling. The incubation time was determined such that the change in oxygen concentration $[O_2]$ would remain nearly linear during the incubation. Under oxic bottom water conditions, we allowed $[O_2]$ to maximally decrease to 50% air saturation, whereas during the hypoxic period, we ensured that the waters would not become anoxic and $[O_2]$ remained above 5% air saturation. As a result, incubation times varied between stations and sampling campaigns, from 6 hours at S1 during summer, up to 65 hours at S3 during winter.

The Total Oxygen Uptake (TOU) of the sediment was determined by following the decrease of the O_2 concentration non-invasively in the overlying water of the closed cores, using Oxygen Spot Sensors (OXSP5; Pyroscience), which were attached to the inner wall of each core liner. The optode signal was read out by an Optical Fiber (SPFIB; Pyroscience) connected to the outer wall of the core liner for the entire duration of the incubation, using a Basic Spot Adapter (SPADBAS; Pyroscience) and a Lens Spot Adapter (SPADLNS; Pyroscience). This procedure enabled a continuous (30 sec interval) measurement of the oxygen concentration in the overlying water, avoiding the gas bubble intrusion that often accompanies the insertion of sensors into chamber incubations. A temperature sensor (TSUB21; Pyroscience) was placed inside the incubator near the cores, to continuously monitor the incubation temperature. The four oxygen sensors and the temperature sensor were connected to a FireStingO2 oxygen meter (Pyroscience), located outside the incubator. Prior to sediment sampling, the Oxygen Spots were calibrated via a two-point calibration at 0% O_2 saturation (saturated Na_2SO_3 solution) and 100% O_2 saturation (artificial seawater bubbled with air at in situ temperature and salinity).

To monitor the DIC and NH_4^+ change in the overlying water of the incubations, water samples were collected at regular time intervals (5 times). Samples were withdrawn using a syringe via one sampling port, and concurrently, an equal amount of ambient bottom water was added through a replacement syringe attached to the other sampling port. DIC samples (~7 mL) were withdrawn using a glass syringe, and a subsample was transferred to a headspace vial, poisoned with 5 μL $HgCl_2$ and stored submerged at 4°C. Samples for NH_4^+ (~3 mL) were collected using a plastic syringe, and afterwards were filtered (0.45 μm Millex-HA syringe filter) and stored in the dark at 4°C. Non-filtered water samples for TA (~ 10 mL) were collected in 25 mL centrifuge tubes only at the beginning and end of the incubation, and stored in the dark at 4°C. Each subsampling total volume of 10 mL was less than 5% of the water mass, so no correction factor was applied to account for dilution.

The TOU, DIC, TA and NH_4^+ fluxes (mmol m^{-2} d^{-1}) were calculated from the concentration change in the overlying water ΔC_{ow} over the time period Δt, taking into account the enclosed sediment area A and the overlying water volume V_{ow}:

$$J = \left(\frac{\Delta C_{ow}}{\Delta t} \right) \frac{V_{ow}}{A} \qquad (2)$$

In all months, the oxygen concentration change ($\Delta C_{ow} / \Delta t$) was determined by linear regression as the initial slope (i.e. the part when the oxygen decrease remained linear) of the recorded oxygen time series. Similarly, in March, May, August and November the DIC and NH_4^+ concentration changes were calculated from the 5 data points by linear regression. In the remaining months, no subsampling was performed, but fluxes were calculated from the concentration difference between start and end of the incubation. DIC fluxes were determined in March, and then monthly from May onwards. TA flux measurements were performed in March, May, August and November, and the flux was calculated from the concentration change in the overlying water between start and end of the incubation.

3.2.3.   Analytical methods

DIC was determined using an AS-C3 DIC analyzer (Apollo SciTEch), in which a sample is acidified and the released CO_2 detected using a solid state infra-red CO_2 detector (Licor LI 7000). Three replicate measurements were carried out for each sample analyzed. All DIC measurements were calibrated using Certified Reference Material (CRM Batch 116 - accuracy & precision: 3 μmol kg^{-1}, supplied A.G. Dickson).

TA was determined using the standard operating procedure for open cell potentiometric titration, using an automatic titrator (Metrohm 888 Titrando), and a combined Metrohm glass electrode (Unitrode) following the procedure SOP3a as described in Dickson et al. (2007). Concentrations of NH_4^+ were determined by automated colorimetric techniques using a Seal QuAAtro autoanalyzer.

3.2.4. **Microsensor profiling**

Oxygen depth profiles were recorded by microsensor profiling using commercial O_2 micro-electrodes with 25- or 50-µm tips (Unisense A.S., Denmark), a Multimeter amplifier system (Unisense A.S., Denmark) and a motorized micromanipulator (Unisense A.S., Denmark). The microsensor profiling was always started within two hours of core collection, Measurements took place in the dark, in a thermo-regulated room, which was set to the temperature of in situ bottom water. To enable profiling in the core liner, the sediment was first pushed upwards until ~ 10 cm of overlying water remained (procedure as detailed above). During profiling, the overlying water was gently stirred using a custom-made propeller to ensure the establishment of a suitable diffusive boundary layer. Oxygen depth profiles were recorded at 50 µm resolution. Micro-electrodes were calibrated using a 2-point calibration made in air-saturated seawater (100 %) and the anoxic zone of the sediment (0 %). A single depth profile was collected in three replicate cores at each of the three stations during each monthly sampling campaign. The diffusive oxygen uptake (DOU) was calculated from the oxygen depth profiles using Fick's first law:

$$DOU = - \frac{\phi}{(1-2\ln\phi)} D_{O_2} \frac{d[O_2]}{dx} \qquad (3)$$

where x represents the depth into the sediment and, ϕ denotes the porosity, and the term $(1-2\ln \phi)$ is a correction for sediment tortuosity (Boudreau 1996). The concentration gradient $d[O_2]/dx$ was calculated via linear regression as the slope of the O_2 depth profile just below the sediment-water interface. Depending on the thickness of the oxic sediment layer, between 4 and 12 data points were included in the regression. The diffusion coefficient D_{O_2} was calculated from salinity (S) and temperature (T) using the R package CRAN: marelac (Soetaert et al. 2012).

3.2.5. **Sediment parameters**

Porosity was determined at 2 mm resolution over the first 40 mm, in one sediment core collected at each site in March, May, August and November. Sediment layers were collected via slicing, with the exception of August, when a syringe and a plexiglass ring (2 mm thick) were used to withdraw the first 2 mm layer, due to the high fluffiness of the upper sediment layer. Porosity was calculated from water content and solid phase density measurements. Water content was determined by drying sediment samples to a constant weight at 60 $^{\circ}$C accounting for the salt content of the pore water. The solid phase density was obtained from the volume displacement after adding a known mass of dry sediment to a graduated cylinder. The sediment grain size distribution was determined by laser diffraction using a Malvern Mastersizer 2000 (McCave et al. 1986). Different horizons within the top sediment showed a distinct coloration, and the thickness and color type of these layers were recorded directlyafter core collection. Furthermore, a custom-made

plexiglass device was used to longitudinally cut and remove one half of the top 20 cm of a sediment core, so that the mid-plane section was exposed and could be photographed.

For organic carbon and nitrogen analysis, one sediment core per site was sliced at 0.5 cm resolution over 10 cm in a N_2-purged glove-bag in March, May, August and November. Sediment samples were freeze-dried and ground to a fine powder. A 0.3 g subsample was acidified with 1M HCl to remove inorganic carbon (Van Santvoort et al. 2002) and then analyzed to determine organic carbon (C_{org}) and organic nitrogen (N_{org}) (% dry weight; Fison Instruments, NA 1500 NCS element analyzer). A second subsample (0.1g) of freeze-dried, ground sediment was dissolved in HF (40 %) and a 2.5 ml mixture of $HClO_4/HNO_3$. This digested sample was analyzed for selected elemental concentrations by ICP-OES (Perkin Elmer Optima 3000 Inductively Coupled Plasma-Optimal Emission Spectroscopy). The measured Ca concentration (total Ca) was used to calculate the $CaCO_3$ content (% dry weight) of the solid phase.

The average sedimentation rate was estimated based on an assessment of the accumulated sediment inventory. As noted above, Lake Grevelingen was closed off from the North Sea by a dam in 1971, and since then, fine-grained, dark silt has accumulated within deeper lying areas. This sediment horizon is clearly distinguishable from the underlying grey estuarine sand, and hence, this transition can be used as a time marker (i.e., 41 years of sedimentation in 2012). A large number of sediment cores (>20) were taken at each station and the depth L of the transition horizon was measured with a ruler (precision ~5%). The sedimentation rate was subsequently calculated as $v = L/T$ where T = 41 years.

3.2.6. Macrofauna

To determine the abundance (individuals m^{-2}) and diversity (number of species) of macrofauna, at each site 8 sediment cores were collected, during each monthly campaign (for a total surface area of ~0.02 m^2 for each site). The sediment from all cores was pooled and directly sieved (mesh size 1.0 mm) on board. Subsequently, macrofauna were carefully handpicked and preserved in a 4% formalin solution stained with rose bengal. All individuals were identified to species level when possible using a stereo-microscope (Leica MZ16). Macrofauna functional diversity was estimated using the Shannon-Wiener diversity index ($H´$). Sediment Profile Images (SPIs) were collected in August 2011 using an Ocean Imaging® SPI-lander system fitted with a Nikon DS 90 digital camera. The SPI system was deployed at four sites (34, 23, 16, and 10 m) along a line transect starting from S1, and 6 images were taken at each station. The average penetration depth of the SPI-wedge was 19 cm for the stations deeper than 20 m and 9 cm for the stations shallower than 20 m. SPIs were analyzed using the SpiArcBase software (Romero-Ramirez et al. 2013).

3.2.7. Statistical analysis

In general, results are reported as the mean and standard deviation (s.d.) of n replicate measurements. Porosity, C_{org} and N_{org} values are reported as mean ± s. d. in the uppermost 2 cm of sediment, as this sediment layer is prone to seasonal variation, given the maximum sedimentation rate within the basin of 2 cm yr^{-1}. Temporal and spatial statistical differences relative to these parameters were tested with a 2-way ANOVA, where values from March, May, August and November were used as representative of the four seasons. Differences in TOU, DOU, DIC, TA, NH_4^+, oxygen penetration depth (OPD), and macrofauna abundance across seasons and stations were analysed using a 2-way ANOVA, after pooling months together in a "season" factor. Additionally, a post-hoc Tukey's test was used to compare seasonal differences for TOU, DOU and OPD, and spatial differences for DIC and NH_4^+. Within-station differences between TOU and DOU across time were identified with the paired Student's t-test. All statistical analyses were conducted in the open software R.

3.2.8. Numerical models

The shape of the oxygen depth profiles was described using two end-member models. In a first model, we assume a homogenous consumption of oxygen within the oxic zone. The resulting relation between the oxygen penetration depth (δ) and the diffusive oxygen uptake (DOU) is $\delta = 2\phi D_s C_0 / DOU$, while the associated oxygen depth profile is given by $C(x) = C_0 \left(1 - x/\delta\right)^2$ (Bouldin 1968; Cai and Sayles 1996). In a second model, we assume that all the oxygen consumption takes place right at the oxygen penetration depth. The resulting relation between for the ODP and DOU becomes $\delta = \phi D_s C_0 / DOU$, while the depth profile is given by $C(x) = C_0 \left(1 - x/\delta\right)$ (Meysman et al. 2010b). In these equations, C_0 denotes the bottom water oxygen concentration, x is the sediment depth, ϕ is the mean porosity within the oxic zone, and D_s is the oxygen diffusion constant in the pore water.

3.3. RESULTS

3.3.1. Water column conditions

The temperature of the bottom water (depth = 32 m) varied throughout the year between 1.5 ^{o}C in February and 16.9 ^{o}C in September, whereas the temperature of the surface water (depth = 3 m) showed a larger seasonal amplitude, varying between 2.0 ^{o}C in February and 21.0 ^{o}C in August (Fig. 2a). In January, the surface water was colder than the bottom water, but the salinity near the bottom was higher, thus stabilizing the water column. From February to April, the temperature of the surface and bottom water increased simultaneously, and as a result, their temperature difference remained within 1ºC. A strong
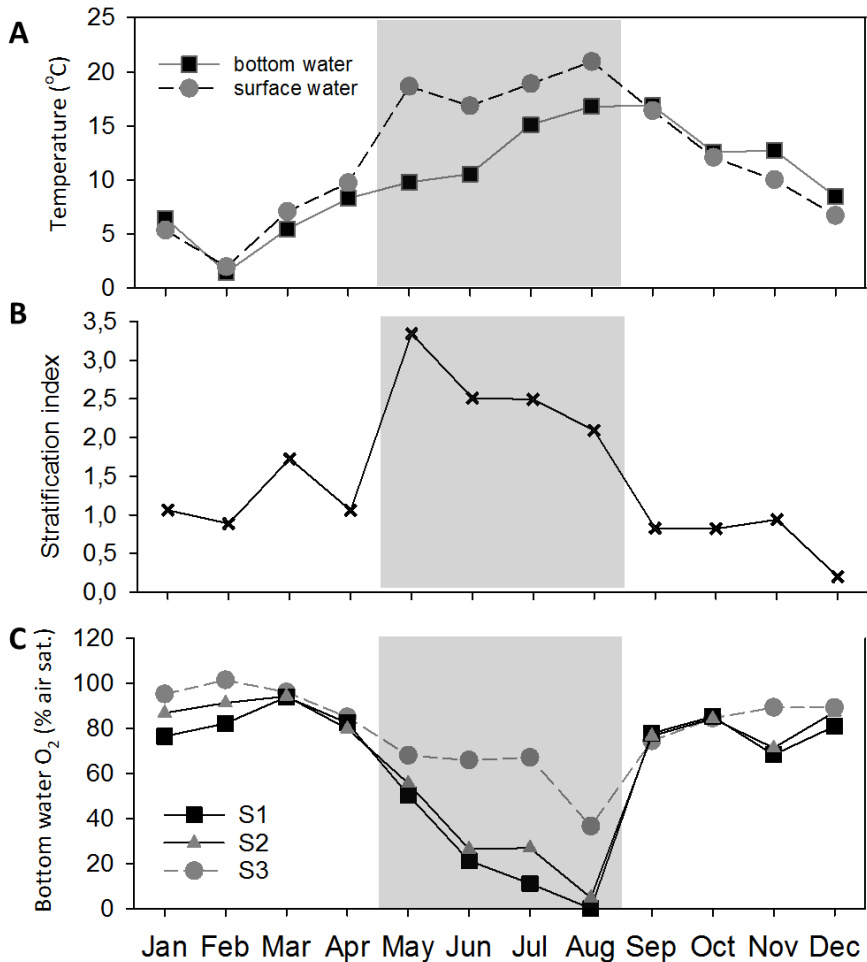
Figure 2. (A) Surface and bottom water temperature at S1 (depth 34 m), S2 (depth 23), and S3 (depth 17 m); (B) stratification index, sigma and (C) oxygen saturation in the bottom water at S1-3, measured during each sampling campaign. Gray area indicates stratification period.

warming of the surface water occurred in late spring, which established a larger temperature gradient between surface and deep water, thus leading to a stratified water column as indicated by the increased stratification index σ (Fig. 2b). In July and August, the bottom water temperature increased, and so, the difference between surface and bottom water decreased again. The stratification index σ remained high, although it was slightly lower than in previous months, decreasing from 3.3 J m^{-3} in May to 2.1 J m^{-3} in August (Fig. 2b). Stormy weather conditions and strong winds in September led to the disruption of

the stratification, and the mixing of the water column (Hagens et al. 2015). In September and October, the stratification index σ was low and there was no temperature difference between surface and bottom water, indicating a well-mixed water column, while in November and December, surface waters were again cooler than bottom waters.

The seasonal variation in the bottom water oxygen concentration was highly correlated with the seasonal stratification pattern, with greatest bottom water O_2 in winter and fall, and lowest values in summer (Fig. 2c). The temporal evolution of the oxygen concentration at the intermediate depth station (S2) was similar to the deep station (S1) throughout the year, while the O_2 evolution at the shallower station (S3) was distinct, with higher oxygen concentrations in summer. In early winter, the bottom water oxygen concentrations varied between 239 and 299 µmol L^{-1} (76-94% saturation) at S1, and from 255 to 357 µmol L^{-1} (85-102 % saturation) at S3. The stratification of the water column in May isolated the bottom waters, and limited the downward-mixing of oxygen-rich surface waters. Consequently, the oxygen concentrations dropped progressively, and at the end of June hypoxic levels were reached at S1 (28.8 µmol L^{-1}, corresponding to 11.1% saturation) and near-hypoxia was attained at S2 (68.5 µmol L^{-1} or 26.9 %), whereas at S3 the oxygen saturation remained above 60% (165.9 µmol L^{-1}). More extensive oxygen depletion occurred in August, when the bottom water at S1 became anoxic (< 0.1 µmol L^{-1}), S2 exhibited very low oxygen concentrations (12 µmol L^{-1}), whereas the oxygen levels at S3 remained just above the hypoxia threshold (88 µmol L^{-1} or 36% saturation). The disruption of the stratification in September led to water renewal in the deep layers of the basin, resulting in a re-oxygenation of these water masses, and as a result, similar bottom water O_2 concentrations were observed in the three stations (74-78 % saturation). In November, the oxygen concentrations slightly decreased at S1 and S2 to 68 % saturation, whereas they remained high at S3 (89 % saturation).

3.3.2. Sediment characteristics

The sediments at all sites in the Den Osse basin consist of fine mud (median grain size 16 µm; silt content 94%), with a solid phase density of 2.60 ± 0.03 g cm^{-3} ($n = 4$), which is a typical value for siliciclastic sediments. The porosity in the uppermost 2 cm was different among stations (2-way ANOVA, $F_{2,48}$=10.4, p<0.01), and also showed a seasonal variation (2-way ANOVA, $F_{3,48}$=17.4, p<0.001), with minimum values (0.92) reached in spring and maximum values (0.98) in summer (Fig. 3a). The porosity slightly decreased from the surface to 4 cm depth (Fig. 3a). This high porosity in the first few centimeters (0.92-0.98) was associated with a fluffy surface layer at all sites in summer, which was easily re-suspended upon disturbance.

Sediment cores showed a notable transition between the older grey estuarine sand and the overlying dark accumulated silt horizon. This transition depth (L) strongly differed between stations (S1: 81 ± 5 cm; S2: 33 ± 7 cm; S3: 15 ± 3 cm), and the resulting estimate of a mean sedimentation rate over the 41 year enclosure period increased with water depth
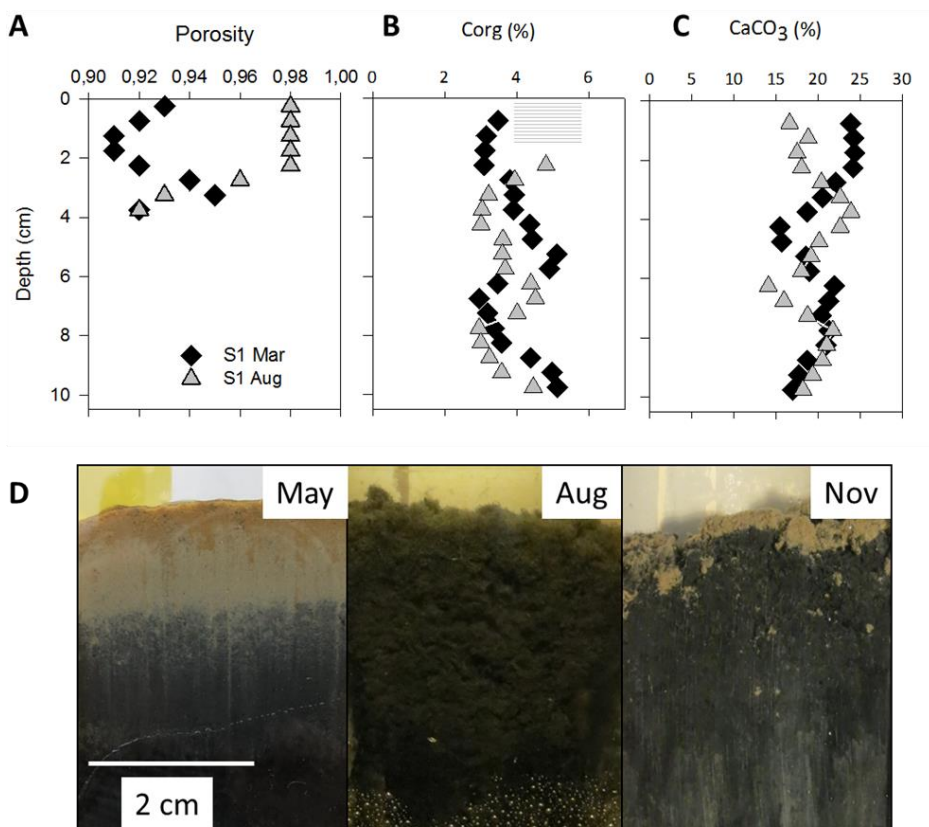
Figure 3. (A) Depth profiles of porosity, (B) C_{org} (%), and (C) $CaCO_3$ for S1 in March (black diamonds) and August (grey triangles); (D) Cross cut of intact sediment cores from May, August and November. Note that C_{org} values at 0-2 cm in Aug are not available (gray dashed area) as samples were lost during core handling.

(S1: 2.0 ± 0.1 cm yr^{-1}; S2: 0.80 ± 0.17 cm yr^{-1}; S3: 0.36 ± 0.07 cm yr^{-1}). The estimated sedimentation rate at S1 was consistent with a previous assessment via ^{137}Cs and ^{210}Pb radionuclide dating, which provided a similar estimate of 2.2 cm yr^{-1} (Donders et al. 2012).

Overall, the sediment showed a high organic carbon content, which revealed clear variations with depth over the first 10 centimeter (Fig 3b). The sediment organic carbon content in the upper 2 cm significantly differed with seasons (2-way ANOVA, $F_{3,51}=4.6$, $p<0.01$), but not across stations (2-way ANOVA, $F_{2,51}=1.1$, $p=0.33$), and ranged between 3.3 % and 5.4 % (mean value across stations, depth and time: 4.0 ± 0.6 %; Table 1). Throughout the seasons, the mean molar C:N ratio in the upper 2 cm of sediment decreased with water depth, from 6.9 ± 0.1 at S1, over 7.1 ± 0.1 at S2 and 7.2 ± 0.1 at S3. All stations

Table 1. Sediment characteristics at the three sites. N_{org}, C_{org} and $CaCO_3$ numbers indicate mean value (±s.d.) in the first 2 cm of sediment. The thickness of the brown layer was identified visually.

		C/N	Corg	CaCO$_3$	DOU	TOU
			%		mmol m^{-2} d^{-1}	
Mar	*S1*	6.9	3.3 ± 0.3	23.8 ± 0.8	18.2 ± 1.7	30.1 ± 0.6
	S2	7.1	3.7 ± 0.4	20.7 ± 0.1	15.8 ± 3.1	26.5 ± 0.2
	S3	7.2	3.3 ± 1.5	20.7 ± 2.5	17.1 ± 5.7	26.1 ± 1.7
May	*S1*	6.9	5.4 ±0.4	23.7 ± 2.4	20.9 ± 3.4	29.8 ± 2.0
	S2	7.1	3.8 ±0.3	22.7 ± 1.0	17.6 ± 3.2	26.1 ± 1.3
	S3	7.2	3.7 ± 0.1	21.8 ± 4.1	23.5 ± 2.0	26.0 ± 1.3
Aug	*S1*	6.6	4.4 ± 0.4	18.3 ± 1.3	-	-
	S2	7.1	3.9 ± 0.4	21.0 ± 0.3	-	12.2 ± 1.2
	S3	7.3	4.2 ± 0.2	19.5 ± 1.2	13.9 ± 2.1	18.9 ± 1.0
Nov	*S1*	6.9	3.5 ± 0.4	21.8 ± 0.8	58.1 ± 1.3	68.3 ± 6.0
	S2	7.0	3.9 ± 0.4	21.3 ± 0.4	22.68 ± 5.3	22.3 ± 0.1
	S3	7.3	4.0 ± 0.2	19.3 ± 1.2	26.0 ± 5.3	19.4 ± 0.7
Yearly average	*S1*	-	-	-	23.6 ± 14.8	32.1 ± 19.9
	S2	-	-	-	18.6 ± 7.1	23.4 ± 4.7
	S3	-	-	-	19.1 ± 5.9	23.3 ± 3.6

showed a similarly high $CaCO_3$ content with a mean of 21.6 ± 1.6 % across stations, depth and time (Table 1; Fig 3c). The oscillations with depth of organic carbon and $CaCO_3$ are inversely correlated, and suggest a seasonal shift in the composition of the deposited sediment.

The visual appearance and coloration of the surface sediment layer changed substantially throughout the year, suggesting marked changes in redox conditions and geochemical cycling (Fig. 3b). From January to May we observed a brown oxidized surface layer of approximately 2 cm (Fig. 3d) at all stations, which gradually decreased in thickness in May, as the sediments were evolving to a more reduced state. In summer a highly porous "fluffy" layer was present on top (Fig. 3d), the thickness of which increased with water depth (40 mm at S1, 23 mm at S2 and 11 mm at S3 in August). In fall, patches of light-brown oxidized sediment appeared, which were distributed heterogeneously within the surface fluffy layer. Marine snow was abundant in the deep bottom waters of Lake Grevelingen (video observations via GoPro camera attached to sediment corer; data not shown), and so these light-brown sediment patches might have resettled after being resuspended and oxidized in contact with oxic water, or might have been transported laterally (Fig. 3d).

3.3.3. Benthic fauna

Sediment profile images (SPIs) were taken along a depth transect (Fig. 4a) during a period of severe bottom water oxygen depletion (August 2011). SPIs clearly revealed an increasing impact of hypoxia on geochemistry and infauna with water depth. The sediments at the two deepest stations (34 and 23 m depth) were entirely black, did not show any sign of an apparent redox potential discontinuity (aRPD), and had no signs of biogenic structures. These sediments also had a sizeable fluffy layer, the thickness of which increased with water depth (from 9.7 mm at 10 m depth to 32 mm at 34 m depth). SPIs from the station located at 16 m water depth showed a thin aRPD of around 8mm, but did not exhibit visible burrow structures or other indications of macrofauna. SPIs from the shallowest station (10 m water depth) revealed a larger oxidized layer and sediments that were colonized by epifauna, suggesting bioturbation activity.

The benthic fauna at the study site in 2012 was generally sparse, with a dominance of small polychaetes such as *Streblospio benedicti*, *Scoloplos armiger*, *Chone duneri* and *Capitella capitata* and juvenile bivalves such as *Corbula gibba* and *Abra nitida*. Overall, the macrofauna abundance and number of species exhibited strong seasonal variation (2-way ANOVA, $F_{3,29}$=2.4, p=0.09 and $F_{3,29}$=8.9, p<0.001, respectively), but values were not significantly different among stations (2-way ANOVA, $F_{2,29}$=2.5, p =0.10 and $F_{2,29}$=2.8, p =0.07, respectively). The population density showed a clear seasonal pattern, which was similar across the three stations (Fig. 4b). In September, right after the summer hypoxia, no
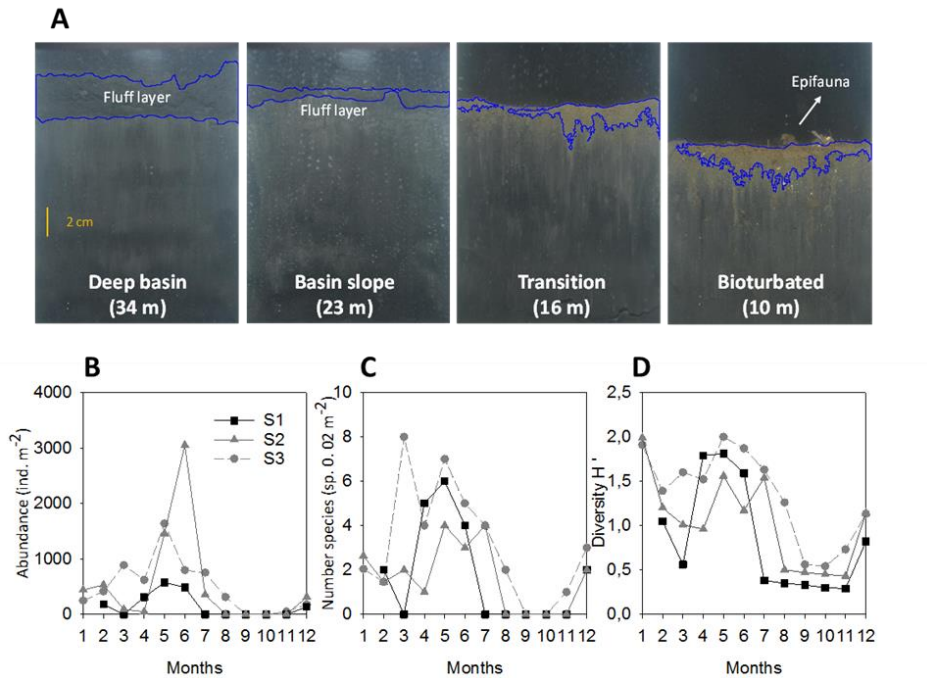
Figure 4. (A) SPI-images at 4 stations distributed along a depth transect in Den Osse basin in August 2011. Area delimited by the blue line indicates the distribution of the fluffy layer (at 34 and 23 m), the oxidized layer (at 6 m), and the zone colonized by epifauna (at 10 m). (B) Macrofauna abundance, (C) number of species and (D) Shannon-Wiener diversity index (H') over the year at the three stations.

macrofauna were found in the sediments, and the sediments remained devoid of fauna until November. When repopulation began in December, the small deposit-feeding polychaetes *Scoloplos armiger* and *Capitella capitata* were the first species to re-appear. Population densities remained very low in winter and early spring, and only in late spring did the macrofauna abundance start to increase (Fig. 4b). At S1 and S3, greatest densities were observed in May (of 575 ind. m^{-2} and 1636 ind. m^{-2} respectively), whereas at S2 the community reached its peak in June at a density of 3050 ind. m^{-2}. In summer, the macrofauna entirely disappeared, first in July the deepest station S1, then followed by S2 in August. At station S3, where the bottom water remained above the hypoxia threshold, the population also declined, but more slowly and here macrofauna were gone by September.

The macrofaunal diversity was generally low with 26 species detected in total, and at most 8 species were present conjointly in one station at the same time point. The seasonal pattern in number of species (Fig. 4c) was similar to that of population density, although the number of species present showed high fluctuations in spring. The Shannon-Wiener

diversity index ($H´$) showed a clear seasonal pattern, with highest values from May to June (Fig. 4d). The highest $H´$= 2.0 was obtained in May at S3.

3.3.4. Seasonality in sedimentary oxygen uptake

Throughout 2012, the deepest station (S1) showed the strongest seasonality in the total oxygen uptake (TOU). The TOU remained fairly constant from January to June, ranging between 20.4 and 29.8 mmol O_2 m^{-2} d^{-1}, with slightly lower values in February (Fig. 5). The advent of low bottom water oxygen conditions in July was accompanied by a substantial drop in TOU at S1, which - as expected - approached zero in August when the bottom water became completely devoid of oxygen. The re-introduction of oxygen to the bottom layers, generated a surge in the TOU at S1 in September, which lasted until November, when the highest TOU value (68.3 mmol m^{-2} d^{-1}) was recorded over the year 2012. The TOU values decreased again in December, and approached the level observed in January 2012, thus completing the yearly cycle.

The TOU at the other two sites, S2 and S3, showed less pronounced seasonal fluctuations compared to the deepest site. As observed for S1, the TOU remained fairly constant from January to May (mean value over this period at S2: 25.0 ± 2.2 mmol m^{-2} d^{-1}; and at S3: 25.7 ± 0.4 mmol m^{-2} d^{-1}). At both S2 and S3, the TOU dropped slightly in June, increased in July, and then decreased again in August, though with a larger drop at S2 compared to S3. Similar to station S1, the sediment responded to the re-introduction of oxygen in September by an increase in TOU, after which the values decreased again in the following months. The yearly mean TOU values were 32.1 ± 3.6 mmol O_2 m^{-2} d^{-1} at S1, 23.4 ± 1.0 mmol O_2 m^{-2} d^{-1} at S2, and 24.3 ± 1.8 mmol O_2 m^{-2} d^{-1} at S3. Two-way ANOVA indicated that the TOU rates were not different between stations ($F_{2,24}$=1.9, p=0.16), but significantly differed over the four seasons ($F_{3,24}$=11.2, p <0.001). A post hoc test revealed that TOU was higher in fall (Tukey's HSD test, p<0.001).

The diffusive oxygen uptake (DOU) scaled with the TOU at all three sites, suggesting that most of the oxygen uptake was sustained by diffusive transport across the sediment-water interface. At station S1, the DOU showed the same strong seasonality as the TOU (Fig. 5). No systematic difference between TOU and DOU was apparent in spring and summer, but TOU exceeded DOU from September until November. This difference between TOU and DOU in fall can be either due to the high consumption (strong gradients in pore water O_2 make the DOU estimate less precise) or due heterogeneous microtopography created by surficial mats of sulfur-oxidizing bacteria (as further discussed below). At sites S2 and S3, the TOU/DOU ratio showed the reverse response compared to S1: the TOU exceeded DOU in late spring, when the highest macrofauna abundance was recorded (thus suggesting a small faunal respiration and bio-irrigation effect), but no systematic difference was apparent in fall, when macrofauna was absent. Theoretically, the TOU should always be larger than the DOU, as the TOU incorporates all sources of oxygen
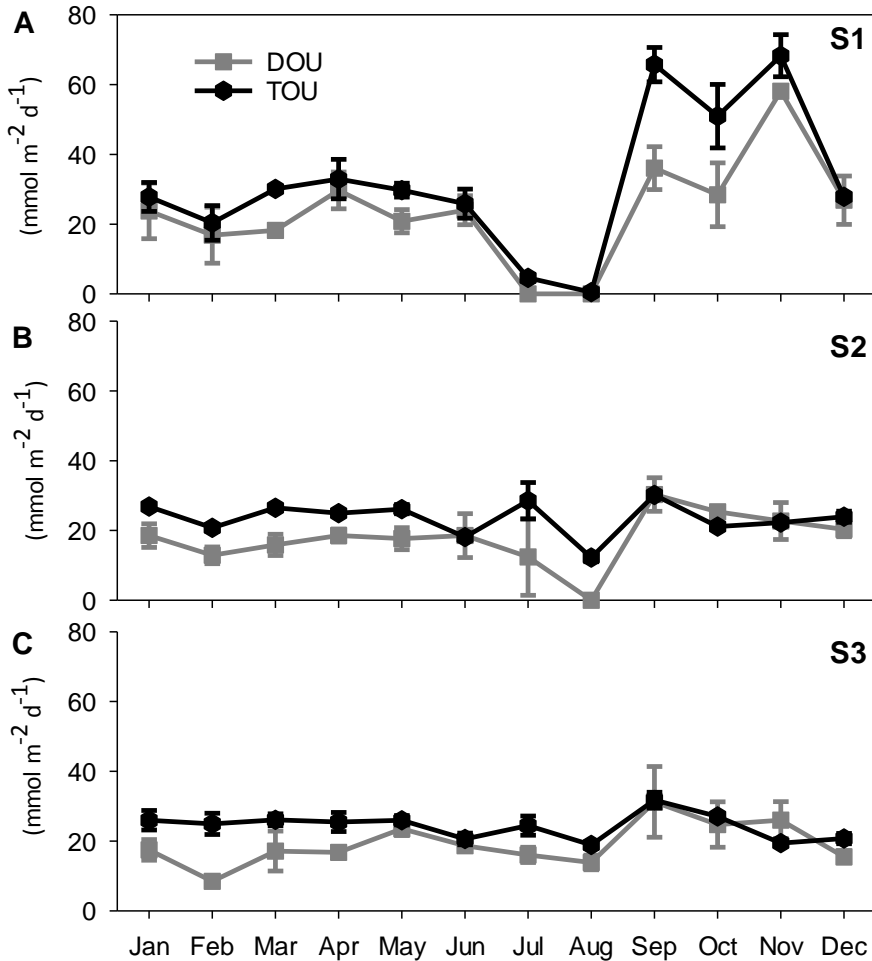
Figure 5. Sedimentary oxygen consumption measured as TOU (black) and DOU (gray) throughout 2012 at (A) S1, (B) S2, and (C) S3. Error bars indicate the standard deviation calculated over three TOU and DOU replicates.

demand (i.e. due to physical advection, diffusion, bio-irrigation and faunal respiration). This condition was fulfilled for all stations and months, except for three instances (April S1, October S2, and November S3). However, a student T-test showed that also in these latter three cases, the values of TOU and DOU were not statistically different (t=-0.6, df=2.4, p=0.62).

The yearly mean DOU values were 23.6 ± 14.8 mmol O_2 m^{-2} d^{-1} at S1, and 18.6 ± 7.1 and 19.1 ± 5.9 mmol O_2 m^{-2} d^{-1}, at S2 and S3, respectively (Tab. 1). The DOU rates differed between stations (2-way ANOVA, $F_{2,95}$=3.5, p <0.05), and were also different among seasons (2-way ANOVA, $F_{3,95}$=26.0, p <0.001), with fall showing higher rates (Tukey's HSD test, p<0.001).

3.3.5. DIC, TA and NH4+ fluxes

The seasonal pattern of the fluxes of DIC, TA and NH_4^+ across the sediment-water interface is shown in Figure 6. The DIC flux at S1 was generally high and showed strong variations throughout the year (Fig. 6a). Fluxes increased from March to June, and showed a small decrease during hypoxia (Fig. 6a). The DIC efflux peaked again in September (139 mmol m^{-2} d^{-1}), when the bottom water got re-oxygenated, and decreased from October onwards, in concert with the decline in bottom water temperature (Fig. 2a). At S2 and S3, the seasonal pattern of the DIC efflux tracked the bottom water temperature (Fig. 2a), with values being higher in spring-summer and lower in winter. The release of DIC significantly differed with water depth (2-way ANOVA, $F_{2,54}$=25.6, p <0.001), with higher fluxes at the deepest station S1 (Tukey's HSD test, p<0.001).

The seasonal pattern of the NH_4^+ flux resembled well that of the DIC flux at the three stations (Fig. 6b). Seasonal variation in the NH_4^+ flux was significant (2-way ANOVA, $F_{3,72}$=18.2, p <0.001), and there was a significant difference among stations (2-way ANOVA, $F_{2,72}$=28.4, p <0.001), with S1 showing the highest NH_4^+ release from the sediment (Tukey's HSD test, p<0.001).

Alkalinity (TA) was released from the sediment over the entire year 2012, with only one exception, in November at S1, where was observed an uptake rather than a release of TA (Fig. 6c). Although TA fluxes did not exhibit a strong spatial variation (2-way ANOVA, $F_{2,24}$=3.1, p =0.06), the seasonal variations were pronounced (2-way ANOVA, $F_{3,24}$=8.6, p <0.001).

3.1.1. Mineralization rate and respiratory coefficient

The effluxes of DIC and NH_4^+ from the sediment provide two independent proxies for the mineralization rate (i.e. the rate of organic matter decomposition), assuming that (1) the sediment resides in a steady state and (2) that no other consumption or production processes of DIC (e.g. carbonate precipitation/ dissolution) or NH_4^+ (e.g. nitrification) are taking place (Canfield 1993; Glud 2008). The efflux of NH_4^+ can be converted into an equivalent mineralization rate by multiplication with the C:N ratio of sedimentary organic matter (Table 1). The NH_4^+-based mineralization rate closely matches the measured DIC flux (Fig. 6), suggesting that carbonate precipitation or dissolution are likely not important. This is confirmed by the alkalinity effluxes (-10 to 45 mmol m^{-2} d^{-1}; Fig 6c), which are generally much smaller than DIC effluxes (26 to 139 mmol C m^{-2} d^{-1}). Assuming the TA flux is entirely generated by carbonate dissolution, then 0.5 times the TA flux would represent the
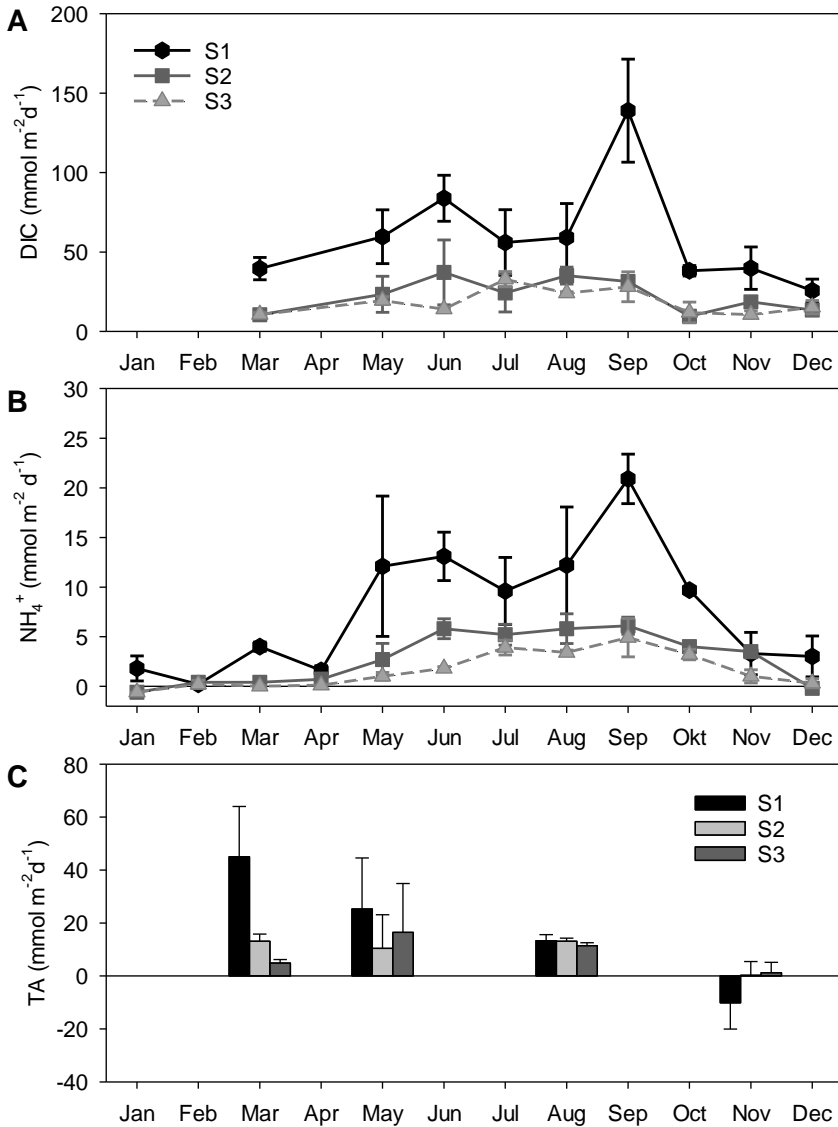
Figure 6. Benthic fluxes of (A) DIC, (B) NH_4^+ and (C) TA at the three stations throughout 2012. Error bars indicate standard deviation among 2-3 replicates. Measurements were performed in March and from May onwards for DIC, monthly for NH_4^+, and in March, May, August and November for TA.
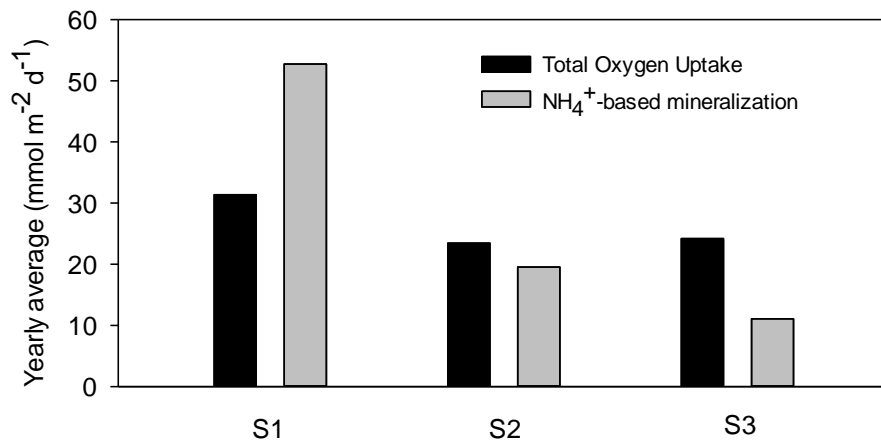
Figure 7. Yearly average of Total Oxygen Uptake and NH_4^+-based mineralization at S1-S3. The NH_4^+-based mineralization was estimated based on measured NH_4^+ flux*C/N ratio of 6.9.

DIC release by carbonate dissolution. The latter only provides a relatively small contribution to the total DIC flux (21 % in May, 11 % in August), and hence, we conclude that organic matter mineralization provides the major source of DIC production in the sediment.

The respiratory quotient RQ is defined as the ratio of sedimentary DIC production over sedimentary O_2 consumption. Figure 7 plots the average DIC and NH_4^+-based mineralization rate and TOU over 2012 for the three stations. There is a remarkable depth dependency of the yearly average RQ, which is high at S1 (RQ = 1.6 ± 0.9), nearly one at S2 (RQ = 1.1 ± 0.8) and low at S3 (RQ = 0.8 ± 0.3). Accordingly, the deepest site S1, shows an apparent deficit in oxygen consumption compared to mineralization, which may be explained by the high mineralization and the high sediment accumulation at this site. An oxygen deficit can be created when iron mono-sulfide (FeS) and pyrite (FeS_2) escape reoxidation by oxygen through burial in deeper sediment horizons. Sulfide burial is stimulated by high sediment accumulation combined with high mineralization, which favors anoxic mineralization pathways (thus inducing high sulfide production through sulfate reduction). Recently, we calculated an average burial rate of solid sulfur compounds of 3 mmol S m^{-2} d^{-1} at S1, which hence provides an oxygen deficit of 6 mmol S m^{-2} d^{-1} (chapter 4).

In contrast, the shallowest site S3 shows an apparent surplus of oxygen consumption compared to both DIC and NH_4^+-based mineralization. As station S3 experiences

oxygenated bottom waters throughout the year, one explanation for this could be nitrification, which results in a lowered NH_4^+ efflux from the sediment, and hence leads to an underestimation of the NH_4^+-based mineralization rate. Overall, the strong depth dependency of the respiratory quotient in the sediments of Lake Grevelingen remains incompletely understood and requires further study.

3.1.2.   Oxygen penetration depth

Sediments at the Lake Grevelingen site exhibited a shallow oxygen penetration depth (OPD), ranging between 0.8 and 4.5 mm across seasons and sites (Fig. 8 a, b). Station S1 showed the lowest mean OPD (1.1 ± 0.6 mm), and the OPD increased at shallower water depths (S2: 1.6 ± 0.8 mm and S3: 1.9 ± 1.0 mm). The OPD significantly varied between stations (2-way ANOVA, $F_{2,96}$=17.6, p <0.001) and seasons (2-way ANOVA, $F_{3,96}$=38.0, p <0.001), with higher OPDs present in winter (Tukey's HSD test, p<0.001).

3.2. DISCUSSION

3.2.1.   Impact of seasonal hypoxia on benthic fauna

Over the last three decades, Lake Grevelingen has experienced a regular pattern of bottom water oxygen depletion occurring in summer (chapter 4). Such seasonal hypoxia strongly impacts the benthic fauna community composition in coastal systems (Diaz and Rosenberg 1995; Levin et al. 2009). As oxygen levels drop animals may suffer from a variety of stresses, ultimately leading to their disappearance as oxygen levels approach anoxia (Diaz and Rosenberg 1995; Vaquer-Sunyer and Duarte 2008; Steckbauer et al. 2011). The conventional threshold level for hypoxia is 2 mg L^{-1} or 63 µmol L^{-1}, although thresholds vary widely between different organism groups, with crustaceans and fish being among the most sensitive taxa (Vaquer-Sunyer and Duarte 2008).

As also observed here (Fig. 4), the benthic macrofaunal communities undergo seasonal changes that depend on the oxygen availability in the bottom water (Jørgensen 1980; Holland et al. 1987; Ritter and Montagna 1999), and the response of benthic faunal community to oxygen depletion appears to follow a systematic successional pattern. During the hypoxic or anoxic period, the macrofauna abundance and biomass, as well as the species richness, rapidly declines, due to emigration of larger mobile species (e.g. crustaceans) or the mortality of sedentary species as a result of oxygen depletion (Diaz and Rosenberg, 1995; Levin et al., 2009 and references therein). After the anoxic period, when bottom waters are replenished with oxygen, the benthic environment is recolonized by mainly juvenile macrofauna. This recolonization process classically follows a successional pattern, with small-sized opportunistic species establishing first, and larger, deeper burrowing fauna only arriving in a later stage (Pearson and Rosenberg, 1978; Rosenberg et al., 2002; Steckbauer et al., 2011; Van Colen et al., 2008). Finally, when the following hypoxic event occurs, the succession pattern is started again.

The actual recovery pattern of the benthic faunal community depends on the frequency of the hypoxic events. In a seasonally hypoxic system, such as Lake Grevelingen, the oxygen depletion develops each year in the bottom waters, which impedes the establishment of a well-developed macrofauna community. Due to the frequency of stressors, the community is kept in an early successional state, and is typically depauperate and composed of small-sized, short-lived and opportunistic species (Diaz and Rosenberg 1995; Rosenberg et al. 2002). These small fauna only create shallow dwelling zones, and hence, they are capable of limited bioturbation (Diaz and Rosenberg 1995; Levin et al. 2009). This pattern was clearly documented in our SPI imaging, which revealed a sharp transition in communities (Fig. 4a) above and below the water depth affected by seasonal hypoxia (~15 m). The shallower areas of the lake (<15 m) host a rich faunal community (Wetsteyn 2011), while the deeper areas host a poor community that is only present during a limited period. Our results show that the deeper sediments remain devoid of macrofauna until November, and that small polychaetes and juvenile bivalves start colonizing the sediment in spring. However, overall abundances and species number remain low. Low oxygen conditions in summer disrupt the recolonization, and impede the establishment of large burrowing or deep-irrigating animals, which require multi-annual recruitment cycles.

Although the bioturbation intensity was not quantified directly, our macrofauna and SPI data provide a qualitative estimation of the seasonal sediment reworking. At all stations located below 15 m water depth, the dominant individuals were small, surface deposit-feeding polychaetes, which only burrow in the first 1-2 cm of the sediment and have low particle processing rates per individual (Diaz and Rosenberg 1995). Bivalve individuals were also typically small, suggesting a recent settlement of juveniles with a limited capacity to rework the sediment. Accordingly, only in late spring and early summer, there may be some moderate biological working of the sediment. Still, during video observations in winter and spring (GoPro camera attached to the gravity corer; data not included), we were able to observe large crabs (*Cancer pagurus*) moving along the sediment surface at all sites as well small shrimp burrowing. In addition, ample trail marks of large crustaceans were visible in the video footage, as faunal imprints exposed the underlying black sediment. These large epifauna were not captured by our coring procedure, and most likely migrated to deeper water depths at times of sufficient bottom water oxygenation. These epifauna could therefore increase the rate of surficial sediment mixing in winter and spring.

3.2.2. Impact of fauna and large bacteria on sedimentary oxygen uptake

Burrow construction and other sediment reworking by fauna (re)expose anoxic sediments to oxygen, and extend the oxic-anoxic interface area (Fenchel 1996; Kristensen 2000), and this increases the reoxidation rates of reduced compounds in sediments (Banta et al. 1999; Kristensen 2001). In studies on sedimentary O_2 uptake, the decomposition TOU = DOU + FR + IOU may be used, which includes the Diffusive Oxygen Uptake (DOU) across the sediment-water interface, the faunal respiration (FR), and the Irrigational Oxygen

Uptake (IOU), representing the O_2 consumption in the oxygenated zone around burrows (Archer and Devol 1992; Wenzhöfer and Glud 2004; Meysman et al. 2010b). The contribution of fauna is termed the fauna-mediated oxygen uptake (FMOU = FR + IOU), which can be a dominant component in coastal sediments, accounting for 50-90% of the TOU (Wenzhöfer and Glud 2004).

Nevertheless, at the three sites investigated, the FMOU contribution was not substantial. As noted above, the macrofauna community exhibited low abundances compared to other coastal habitats and mainly consisted of small polychaetes that created small and shallow burrows (e.g. *Scoloplos armiger* and *Capitella capitata*). Accordingly, the respiration of the fauna was likely small (FR << DOU), whereas no large bio-irrigators species were recorded in the faunal analysis, and so oxygen uptake by bio-irrigation was likely unimportant (IOU << DOU). Overall, the contribution of fauna to the sedimentary oxygen uptake within sediments below 15 m water depth cannot be substantial, and hence, seasonality in macrofaunal activity does not seem to strongly affect the TOU.

Moreover, a substantial faunal imprint would create a discrepancy between DOU and TOU (Wenzhöfer and Glud 2002; Glud 2008), which was not observed (Fig. 5). Even in late spring, when faunal densities were the highest, DOU and TOU were similar. In general, the TOU and DOU followed a similar seasonal pattern and were not significantly different from each other (Fig. 5), suggesting a low bio-irrigation activity of the benthic community (Rabouille et al. 2003). One notable exception was the period from September to October at station S1 (DOU/TOU ratio ~ 0.6). These low DOU/TOU ratios coincided with the presence of *Beggiaotaceae* mats on the sediment surface, i.e. large filamentous sulfur oxidizing bacteria, that were extensively present from September to November (chapter 4). The surface mats of *Beggiaotaceae* filaments alter the sediment microtopography, and as a consequence they affect the thickness of the diffusive boundary layer (DBL) and increase the overall area of the sediment-water interface (Jørgensen and Marais 2008). A higher surface area leads to an increase of the oxygen flux across the sediment-water interface (detected via the TOU measurement) which is not captured in the one-dimensional flux calculated from the oxygen depth profiles (DOU) (Jørgensen and Marais 2008). As DOU values were calculated from concentration gradients inside the sediment, any O_2 consumption by *Beggiaotaceae* above the sediment-water interface would lead to a difference between TOU and DOU. Accordingly, this mechanism could explain the low DOU/TOU ratio observed at S1 in the fall of 2012.

3.2.3. <u>Contribution of reoxidation to sedimentary oxygen consumption</u>

The sedimentary oxygen dynamic in Lake Grevelingen is driven by two main types of oxygen consumption: aerobic respiration of organic matter versus reoxidation of reduced compounds. To assess the relative contribution of these two mechanisms, we performed a model analysis of the oxygen depth profiles recorded by micro-sensor profiling. The shape of the oxygen depth profile, and also the OPD, is determined by the actual location where
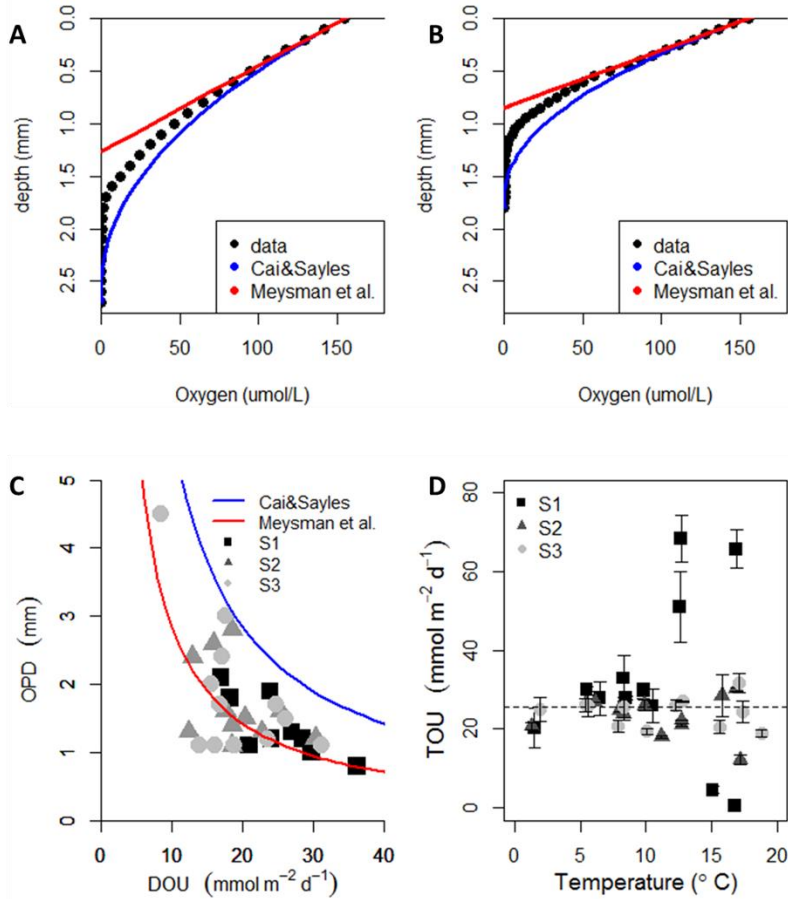
Figure 8. Measured oxygen depth profiles in (A) February and (B) November. Red lines indicate the simulated oxygen depth profile, where $C(x) = C_0 (1 - x/\delta)^2$ (Cai and Sayles 1995). Blue lines indicate the simulated oxygen depth profile, where $C(x) = C_0 (1 - x/\delta)$. (C) OPD - DOU relation. The solid blue line indicates the relation as predicted from $\delta = 2\phi D_s C_0 / DOU$ (Cai and Sayles 1995). The solid red line indicates $C(x) = C_0 (1 - x/\delta)$ (Meysman et al., 2010). (D) TOU versus bottom water temperature. Dashed line indicates yearly average temperature over the three stations (T=13.8°C). Error bars indicate the standard deviation calculated over three TOU replicates. Abbreviations: C_0 denotes the yearly average bottom water oxygen concentration over the three stations (223.8 µol L^{-1}), ∂ indicates the calculated OPD, and x is the sediment depth, $\phi = 0.95$ is the yearly average porosity, and D_s oxygen diffusion constant in sediments.

oxygen consumption takes place within sediment. Effectively, one can think of two end-member models (corresponding expressions for the O_2 depth profile and the OPD are provided in Methods section – Fig. 8 a, b). In a first model, the O_2 consumption is uniformly distributed throughout the oxic zone (Bouldin 1968; Cai and Sayles 1996). This situation is expected when heterotrophic respiration of organic matter is the dominant O_2 consuming process. As the oxic zone is narrow, likely the reactivity of organic matter does not vary with depth, and so to a first approximation, the rate of aerobic respiration can be assumed to remain constant with depth. In a second model, all the O_2 consumption is concentrated near the OPD (Meysman et al. 2010b). This situation is expected when reoxidation of reduced mineralization products (e.g oxidation of ammonium or free sulfide) is the dominant O_2 consuming process. Typically, reoxidation reactions have fast kinetics and are concentrated in a narrow zone around the oxic-anoxic transition depth. In this reoxidation end-member model, the O_2 depth profile becomes a straight line down to the OPD.

As illustrated for two representative examples (Fig. 8 a, b), the observed O_2 depth profiles resided typically in between the depth profiles predicted by the two end-member models. The observed depth profiles showed more curvature than the 100% reoxidation model, but were also more linear than the 100% aerobic respiration model, implying that the observed O_2 consumption was a mix of these two O_2 consumption modes. The intensification of the O_2 consumption near the oxic-anoxic transition causes a straightening of the concentration depth profile and a reduction in the OPD (Fig. 8 a, b).

Figure 8c plots the OPD versus the DOU for all sampling dates and stations, and adds the two model predictions (using an average porosity $\varphi = 0.95$ and mean bottom water concentration across all stations $[O_2]_{bw} = 223.8$ µmol L^{-1}). The data show an inverse relation between OPD and DOU, as has been noted in previous investigations (Cai and Sayles 1996; Glud 2008; Glud et al. 2009). Most data points fall in between the two end-member model curves (Fig. 8c), although there is a tendency towards the 100% reoxidation model line, suggesting that reoxidation is a larger component of the O_2 consumption, compared to aerobic respiration. Accordingly, we conclude that under oxic bottom water conditions, reoxidation of secondary metabolites is the principal driver of benthic oxygen consumption in the sediments of Lake Grevelingen below 15 m water depth. This is not unexpected for these organic-rich sediments, which support high rates of anaerobic mineralization, and thus sustain high rates of reoxidation (chapter 4). Note that some points fall below the 100% reoxidation model line. These points were recorded during the stratification period in late spring, when the bottom water oxygen was low (and hence lower than the yearly averaged bottom water $[O_2]_{bw}$ used in the calculation of the model predictions).

3.2.4. Seasonality in alkalinity efflux

Although TA fluxes are relatively small (compared to DIC fluxes), there is a marked seasonality in these fluxes. The largest TA efflux is observed in spring, especially at S1, while in contrast, the sediment shows a small TA influx in fall (Fig. 6c). This seasonality can be explained in terms of the dominant microbial populations that are present in the sediment. In spring, cable bacteria were active at S1 (chapter 4) and the metabolism of these bacteria (electrogenic sulfur oxidation) is known to acidify the first centimeters of the sediment. This acidification induces carbonate dissolution (Risgaard-Petersen et al. 2012), and thus explains the alkalinity efflux (Rao et al. 2016). In contrast, in fall, nitrate-accumulating *Beggiatoaceae* are abundant at site S1 (chapter 4), which generate alkaline conditions in the surface sediment (increase the pH), thus favoring carbonate precipitation, and hence explaining the observed influx of alkalinity.

3.2.5. Seasonality in benthic mineralization

The seasonal mineralization pattern (both NH_4^+-efflux based and DIC-efflux based) shows a clear correlation with the seasonal signal in bottom water temperature (Fig. 9a), as has been previously reported for sediments in a shallow Danish fjord (Jørgensen 1977). Temperature is known to exert an important environmental control on benthic mineralization rates as it regulates both microbial activity (Thamdrup et al. 1998) and faunal respiration (Smith 1973). The effect of temperature on mineralization is traditionally expressed by the Q_{10} factor, which quantifies the change in a process rate for a temperature difference of 10 ^{o}C. The bottom water temperature at the Lake Grevelingen field site varied between 2 ^{o}C in winter and 17 ^{o}C in summer (Fig. 2a). Adopting $Q_{10} = 2.5$ for aerobic respiration (Thamdrup et al. 1998), and assuming a temperature increase of 15 ^{o}C, the mineralization rate would increase by a factor of ~4. Our data shows that the DIC efflux increased from March to September by a factor of 3.5, which closely matches the predicted temperature effect, and is consistent with a regulating role of temperature in organic matter mineralization.

A second factor known to affect benthic mineralization rates is the temporal variation in the organic carbon flux to the seafloor (Jørgensen 1977; Archer and Devol 1992; Soetaert et al. 1998; Zilius et al. 2012). Typically, phytoplankton blooms occurring in spring and summer lead to a deposition of reactive organic matter onto the sediment (Rasmussen and Jorgensen 1992; Therkildsen and Lomstein 1993; Glud et al. 2003), which then promotes sulfate reduction, and increases the sedimentary oxygen consumption (Jørgensen,1977). For example, in Aarhus Bay, the DOU was found to significantly increase after the onset of the phytoplankton bloom (Rasmussen and Jorgensen, 1992; Glud et al., 2003). During 2012, two main phytoplankton blooms occurred at the field site, which happened in March and July (Hagens et al. 2015). Given a water depth of ca. 30 m, and a sinking velocity of 1 m d^{-1} (Soetaert et al. 2000), the organic material produced in the photic zone should reach the sediment around 1 month after a phytoplankton bloom. Accordingly, one would expect an

increased oxygen uptake in April and August, which was however not observed in the mineralization rate (Fig. 9a). During September, there was a notable increase in the NH_4^+-based and DIC-based mineralization rates, as well as in the TOU. The coincident increase in these three fluxes, points towards a surge in mineralization, which is likely linked to the decomposition of labile organic material that settled after the phytoplankton bloom in July.

In addition, this peak in sedimentary mineralization occurred after a period of anoxia in the bottom water, which may have delayed the mineralization of organic matter that settled on the surface during low O_2 conditions. Previous studies have shown that hypoxic conditions in bottom waters enhance the preservation of organic matter (Moodley et al. 2005), and hence, suppress the mineralization rate compared to oxic conditions (Hedges and Keil 1995; Middelburg and Levin 2009). Here, the oxygen concentrations in the bottom water at S1 fell below the hypoxia threshold right after our sampling in June. This oxygen decline was followed by a drop in the mineralization rate, which in July decreased by 33% (based on the DIC flux) and 27% (based on the NH_4^+ flux) compared to the previous month. Hence, we hypothesize that the decrease in mineralization rates in summer could be due to oxygen depletion in the bottom water during this time.

3.2.6.   Bottom water O2 concentrations control TOU

Seasonal variations in benthic mineralization are translated in fluctuations of the sedimentary oxygen uptake (Glud 2008). At the deepest station (S1), we observed a strong seasonal fluctuation in the total oxygen uptake (an excursion of around 68 mmol O_2 m^{-2} d^{-1} between maximum and minimum TOU). A similar excursion was observed also in the DOU, where the highest DOU recorded (58 mmol m^{-2} d^{-1} in Nov 2012) is 3.4 times higher than the lowest DOU recorded during oxic conditions (17 mmol m^{-2} d^{-1} in Feb 2012). However, pronounced variations in the sedimentary oxygen uptake were not observed at shallower water depths. In contrast with S1, station S2 showed a seasonal cycle with lower amplitude, while S3 showed no seasonality at all. The absence of a clear seasonal pattern in the TOU and DOU recorded at stations S2 and S3 (Fig. 5b, c) speaks against a major influence of temperature. Overall, the TOU showed no significant correlation with bottom water temperature ($R^2 = 0.001$; $p = 0.83$ Fig. 8d), suggesting that temperature is not a major driver of the observed seasonal variation in sedimentary oxygen uptake in the Lake Grevelingen.

Water column oxygenation, and more specifically oxygen limitation, is another factor that may affect sedimentary oxygen uptake. Prolonged chamber incubations have given insight into the relation between sedimentary oxygen consumption rate and oxygen concentration in the enclosed bottom water (Hall et al. 1989; Glud 2008). During the initial phase of an incubation, the oxygen decrease in the water overlying the sediment is approximately linear over time (Glud 2008), indicating that the consumption rate does not depend upon the oxygen availability. However, when the oxygen concentrations in the water passes the hypoxia threshold, this relation becomes non-linear, as the oxygen uptake

slows down at decreased O_2 levels (Glud 2008). This might explain why the sediment oxygen consumption is usually depressed under hypoxic to anoxic conditions in systems such as Chesapeake Bay (Boynton et al. 1990; Brady et al. 2013) and the Louisiana continental shelf (Rowe et al. 2002; Lehrter et al. 2011). Similarly, at the field site here, the TOU was reduced by oxygen availability in early summer at stations S1 and S2 (Fig. 5), but not at station S3 (which remained above the hypoxia threshold). Hence, we conclude that bottom water oxygen availability exerted the dominant control on the TOU in summer in the deeper basins of Lake Grevelingen.

3.2.7.   The importance of the oxygen debt mechanism

Among the three sites investigated, the deepest site (S1) experiences the longest and most intense period of hypoxia, and so its response most strongly exemplifies the impact of seasonal hypoxia on sediment oxygen dynamics. To analyze this seasonality, Figure 9b compares the seasonal patterns of the "expected TOU" versus the "observed TOU".

The "expected TOU" is the sedimentary oxygen consumption that is expected if mineralization of organic matter is the sole, instantaneous driver of the oxygen consumption. This model hence assumes that the TOU always linearly scales with the mineralization rate.

To calculate the "expected TOU", we divided the monthly values of the NH_4^+ flux- based mineralization rate by the mean annual respiratory quotient RQ (blue curve; Fig. 9b). The "observed TOU" simply represents the measured TOU values at S1 (red curve; Fig. 9b).

There are clear discrepancies between the "expected" and "observed" TOU, and we hypothesize that these differences can be largely explained by the concept of the so-called "sedimentary oxygen debt" (Pamatmat 1971).

In coastal sediments, the mineralization of organic matter is dominated by anaerobic pathways, which lead to the accumulation of reduced by-products (i.e. NH_4^+, H_2S and FeS) that can be viewed as oxygen demand units (ODUs) (Soetaert et al. 1996a). Upon transport to the sediment water interface, these ODUs come into contact with O_2, and are re-oxidized again. In a balanced sedimentary system, the production of ODUs through mineralization is exactly matched by the consumption of ODUs through reoxidation. In this situation, the seasonal oxygen uptake of the sediment would closely track the seasonal pattern in sedimentary mineralization (i.e., the "observed" TOU tracks the "expected" TOU). However, when reduced compounds (e.g. ODUs like FeS) are not immediately re-oxidized and transiently accumulate in the sediment, the oxygen consumption becomes out of phase with the mineralization. Under these conditions, the TOU is temporarily lower than expected from the ongoing mineralization (creation of the oxygen debt). Later in the seasonal cycle, the reverse situation can occur, when the pool of reduced compounds is re-oxidized, and the TOU is higher than required by the ongoing mineralization (fulfilment of the oxygen debt). An increased TOU compared to mineralization in fall, associated with the fulfilment of an "oxygen debt", has been previously reported in geochemical studies of
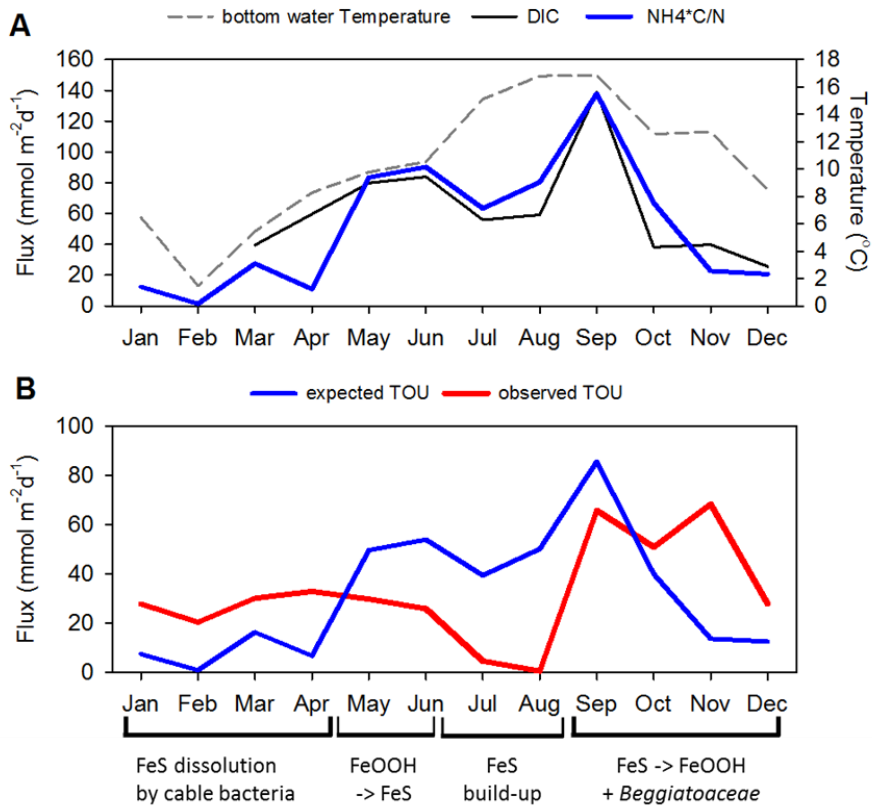
Figure 9. (A) Bottom water temperature, benthic DIC efflux and NH_4^+-based mineralization at S1 throughout 2012. (B) Seasonal variation of "expected" vs "observed" TOU at S1. The "expected TOU" was calculated from the NH_4^+-based mineralization divided by the mean annual respiratory quotient (RQ), whereas the "observed TOU" is the measured total oxygen uptake. During Jan-April the sedimentary oxygen consumption was affected by oxidation of FeS promoted by cable bacteria metabolism; during spring and summer accumulation of FeS occurs; from September onwards *Beggiatoaceae* affect sedimentary oxygen consumption.

seasonally-hypoxic sites, including Aarhus Bay (Rasmussen and Jorgensen 1992; Moeslund et al. 1994), Cape Lookout Bight (Martens and Klump 1984; Chanton et al. 1987), and Chesapeake Bay (Boynton et al. 1990; Brady et al. 2013). Seasonal hypoxia within the Den Osse basin induces a strong oxygen debt dynamic in the sediments at S1, with oscillations between periods of oxygen debt fulfilment and periods of oxygen debt creation (Fig. 9b). Here we put forward the hypothesis that the oxygen debt dynamic is closely linked to the activity of cable bacteria, which enable electrogenic sulfur oxidation via electrical currents (Nielsen et al. 2010; Pfeffer et al. 2012). As described in detail in (chapter 4), these cable

bacteria are abundant and active in spring at S1, and their presence exerts a strong impact on the seasonality of the sediment geochemistry. The sedimentary iron and sulfur cycling in the sediments at S1 is described in detail in (chapter 4; chapter 5), and taking advantage of this dataset, it is possible to distinguish four distinct periods in terms of sedimentary O_2 cycling over 2012 (Fig. 9b). At the beginning of the year, from January to April, electrogenic sulfur oxidation by cable bacteria generated a large pool of iron (hydr)oxides (950 Fe mmol m^{-2}) in the uppermost 3.5 cm of the sediment (chapter 4; chapter 5), via the reoxidation of FeS to FeOOH. The reoxidation of this FeS by oxygen (FeS + 5/4O_2 + 3/2$H_2$0 $\rightarrow$ FeOOH + SO_4^{2-} + 2H$^+$; (Meysman et al. 2015)) would induce an extra O_2 consumption of 1188 mmol O_2 m^{-2}, corresponding to an additional oxygen consumption of ~9 mmol O_2 m^{-2} d^{-1} (assuming cable bacteria are active over a period of 130 days). This way, the metabolic activity of cable bacteria in spring induces a period of "oxygen debt fulfilment" (Fig. 8b), which increases the sedimentary O_2 consumption in winter and spring above the level expected from mineralization alone (from 13 mmol O_2 m^{-2} d^{-1} expected to 21 mmol O_2 m^{-2} d^{-1} observed, where the latter is the observed average DOU at S1 over January-May).

From May onwards, the iron (hydr)oxides formed during spring, become reduced and precipitate as iron sulfides upon contact with free sulfide (chapter 4; chapter 5) as described by the overall reaction 8FeOOH + 9HS$^-$ + 7H$^+$ $\rightarrow$ 8FeS + SO_4^{2-} + 12H_2O. This process hence creates two consecutive periods of oxygen debt. In a first period, the iron oxides formed close to the sediment surface could be mixed downwards into deeper sulfidic horizons (1 to 2 cm) by small bioturbating fauna, which attained the highest abundances in May and June (Fig. 4). This FeOOH to FeS transformation continued – and most likely accelerated – throughout summer, when the bottom water oxygen decreased towards anoxia (Fig. 2c), and free sulfide accumulated to high levels in the upper sediment layers (chapter 4).

In fall, when bottom waters become oxygenated again, another period of oxygen debt fulfilment was started. At this time, *Beggiatoaceae* filaments colonized the sediment, but in contrast to cable bacteria, the *Beggiatoaceae* do not directly affect the FeS pool in the sediment. Hence during this period, the FeS in the surface layer will be re-oxidized only by O_2 diffusing into the sediment. Adopting an OPD of 2 mm, the transient reoxidation of all FeS in contact with oxygen (113.4 µmol S g^{-1}; chapter 4) would consume 83 mmol O_2 m^{-2}. Assuming this FeS reoxidation takes place within 60 days, this would only increase the sedimentary oxygen uptake by 1.4 mmol O_2 m^{-2} d^{-1}. However, substantially larger increases in the TOU are observed in fall, which could be due to high sulfate reduction rates associated with an increased temperature of the bottom water and sediment in fall (Fig. 2A). But it is also possible that the intensity of the oxygen debt fulfilment is higher, as for example, due to resuspension effects on TOU. During core inspection, we observed oxidized sediment patches within the surface layer of the sediment (up to 0.5 cm; Fig. 3d), which might have resettled after being resuspended and oxidized in contact with oxygen.

We do not have observational data to quantify the importance of resuspension at the field site. It is however possible that strong winds and stormy conditions, which typically occur in late fall and winter, may cause the resuspension of the fluffy surface sediments present at the study site. This mixing by resuspension might bring anoxic sediment to the sediment surface, where it is exposed to oxic bottom water. In the eventuality that the upper 1.5 cm of sediment would be mixed by resuspension, and the entire FeS pool contained in this layer (49 µmol S cm^{-2}) would be re-oxidized in 60 days, this would add ~ 10 mmol O_2 m^{-2} d^{-1} to the TOU. It must be noted that the oxidation of NH_4^+ released from the sediment to the bottom water in fall could additionally contribute to the observed high TOU rates.

The high TOU in winter, and the absence of a clear response of TOU to bottom water temperature, were also observed in S2 and S3. Still, the seasonal pattern of oxygen debt dynamic was not as clear as at S2 and S3, possibly due to the lower intensity of hypoxia compared to S1. Especially at station S3 (17 m water depth), summer hypoxia is less intense compared to S1 (Fig. 2c), and so reduced compounds accumulate to lower concentrations in the surface sediment (chapter 5). Hence, these layers form a lower oxygen debt during summer, which could explain why the TOU increases less in fall (Fig. 5 b, c). Station 2 is influenced more by oxygen limitation in summer (though still less than S1), but as argued above, the oxygen debt dynamics is particularly amplified by the activity of cable bacteria in spring. Cable bacteria have a patchy distribution in the Lake Grevelingen (chapter 4), and were not detected at S2 in spring 2012, which could explain the less pronounced fluctuations of the TOU and DOU throughout 2012 at this station. Overall, based on our results, we forward the hypothesis that cable bacteria could substantially amplify the oxygen debt dynamics in the sediments of seasonal hypoxic coastal systems, but the extent to which this occurs requires more detailed quantification, as well as confirmation in coastal systems other than Lake Grevelingen.

SUPPLEMENTARY INFORMATION

Oxygen uptake by *Beggiaotaceae*

Beggiaotaceae filaments, which were colonizing the sediment in fall at S1, are known to oxidize sulfide to sulfate via two-step reactions consuming oxygen and/or nitrate. Firstly sulfide is oxidized to elemental sulfur ($4HS^- + NO_3^-{}_{intracell} + 6H^+ \rightarrow 4S^0{}_{intracell} + NH_4^+ + 3H_2O$), which is afterwards oxidized to sulfate ($2S^0{}_{intracell} + 3O_2 + 2H_2O \rightarrow 2SO_4^{2-} + 4H^+$) (Schulz and Jørgensen 2001). Based on the *Beggiaotaceae* biovolume (chapter 4), and adopting a biomass-specific sulfide oxidation rate (Preisler et al. 2007) it is possible to estimate the oxygen consumption related to the sulfur oxidation by these bacteria. Combining the estimated biomass-specific conversion rate (13 mM day^{-1}) (Preisler et al. 2007) and the measured biomass (2.64 mm^3 cm^{-2}) (chapter 4) , the areal rates of sulfide oxidation to sulfate by *Beggiatoaceae* amounts to 0.34 mmol S m^{-2} d^{-1}, as free sulfide rapidly reacts with oxygen ($0.5H_2S + O_2 \rightarrow 0.5\ SO_4^{2-} + H^+$). The oxidation of this amount of sulfide corresponds to 0.34*2=0.68 mmol O$_2$ m^{-2} d^{-1}. If the *Beggiatoaceae* oxidize sulfide via the two-step reactions (reported above) using nitrate as electron acceptor, the biomass-specific conversion rate reported by Preisler et al. (2007) is 52 mM day^{-1}. Hence, this would yield an areal sulfide oxidation rate of 1.37 mmol S m^{-2} d^{-1}, which would be a sink for oxygen (1.37*2=2.7 mmol O$_2$ m^{-2} d^{-1}).

Photos: Sairah Y. Malkin, Filip J.R. Meysman

Cable bacteria in the sediments of seasonally hypoxic basins: a microbial firewall against euxinia

Dorina Seitaj, Regina Schauer, Fatimah Sulu-Gambari, Silvia Hidalgo-Martinez, Sairah Y. Malkin, Laurine D.W. Burdorf, Caroline P. Slomp, Filip J.R. Meysman

ABSTRACT

Seasonal oxygen depletion (hypoxia) in coastal bottom waters can lead to the release and persistence of free sulfide (euxinia), which is highly detrimental to marine life. Although coastal hypoxia is relatively common, reports of euxinia are less frequent, which suggests that certain environmental controls can delay the onset of euxinia. However, these controls and their prevalence are poorly understood. Here we present field observations from a seasonally-hypoxic marine basin (Grevelingen, The Netherlands), which suggest that the activity of cable bacteria , a recently discovered group of sulfur oxidizing microorganisms inducing long-distance electron transport, can delay the onset of euxinia in coastal waters. Our results reveal a remarkable seasonal succession of sulfur cycling pathways, which was observed over multiple years. Cable bacteria dominate the sediment geochemistry in winter, while after the summer hypoxia, *Beggiatoaceae* mats colonize the sediment. The specific electrogenic metabolism of cable bacteria generates a large buffer of sedimentary iron oxides before the onset of summer hypoxia, which captures free sulfide in the surface sediment, thus likely preventing the development of bottom water euxinia. As cable bacteria are present in many seasonally-hypoxic systems, this euxinia-preventing firewall mechanism could be widely active, and may explain why euxinia is relatively infrequently observed in the coastal ocean.

4.1. INTRODUCTION

The depletion of oxygen in bottom waters (hypoxia) is a naturally-recurring phenomenon in some coastal systems (Middelburg and Levin 2009), such as basins with restricted water circulation (Jørgensen et al. 1991), and shelf regions subject to strong nutrient upwelling (Thamdrup et al. 1996). Alongside this natural hypoxia, there is evidence for a global increase in the frequency, extent, intensity and duration of coastal hypoxia, which is linked to an increased anthropogenic input of nutrients into the coastal ocean in combination with climate change (Turner et al. 2008; Conley et al. 2009; Middelburg and Levin 2009; Kemp et al. 2009). The development of bottom water hypoxia has major consequences for the functioning of coastal ecosystems, sometimes leading to the formation of "dead zones" characterized by a complete absence of benthic fauna and fish. Areas sensitive to hypoxia are typically major fishing grounds, so the resulting economic and biodiversity losses make the global expansion of coastal hypoxia a subject of growing concern (Ekau et al. 2010; Zhang et al. 2010).

The ecosystem impacts of coastal hypoxia are particularly amplified when bottom water oxygen depletion progresses to a critical transition, termed euxinia, when free sulfide escapes from the sediment and accumulates in the bottom water (Vaquer-Sunyer and Duarte 2008). Even low levels of free sulfide are toxic to metazoan life, and therefore euxinia can induce mass-mortality events, even among highly motile fauna like fish and large crustaceans (Diaz and Rosenberg 1995; Vaquer-Sunyer and Duarte 2008; Levin et al. 2009). Although strong oxygen depletion, or even a complete removal of oxygen (anoxia), is often reported, concomitant reports of euxinia in coastal bottom waters are much scarcer. This suggests that certain sedimentary processes delay the onset of euxinia relative to anoxia, but at present, the environmental controls on the timing and formation of coastal euxinia are poorly understood.

Here we document a microbial mechanism that can delay or even prevent the development of euxinia in seasonally-hypoxic basins. The mechanism is based on the metabolic activity of a newly discovered type of electrogenic micro-organisms, named cable bacteria (*Desulfobulbaceae,* Deltaproteobacteria*)*, which are capable of inducing electrical currents over centimeter-scale distances in the sediment (Nielsen et al. 2010; Pfeffer et al. 2012). Cable bacteria have recently been suggested to be abundant in seasonally-hypoxic coastal systems (Malkin et al. 2014), but their impact on the biogeochemical cycling in these systems is unknown. These filamentous bacteria possess a unique respiratory metabolism, in which the oxidative removal of sulfide in deeper sediment layers is electrically coupled to the reductive consumption of oxygen just below the sediment-water interface (Nielsen et al. 2010), a process referred to as electrogenic sulfur oxidation (e-SOx) (Meysman et al. 2015). In laboratory experiments, e-SOx has been shown to exert a strong impact on sedimentary iron and sulfur cycling, leading to a conversion of iron sulfides into iron oxides (Risgaard-Petersen et al. 2012). Here we demonstrate that the same interconversion process of iron minerals occurs in the sediments

of a seasonally-hypoxic marine basin, and that the large pool of iron oxides can act as a "firewall", which can substantially delay the development of euxinia.

4.2. MATERIALS AND METHODS

4.2.1. Sampling

We performed monthly sampling campaigns on the R/V Luctor in 2012, in the seasonally hypoxic Lake Grevelingen (The Netherlands) (Hagens et al. 2015). Investigations took place in the Den Osse basin, a deep gully located in the south-western part of the lake (max water depth 34 m; 51.747°N, 3.890°E), and we examined the water-column chemistry and sediment biogeochemical processes. Discrete bottom water samples were collected with a 12L Niskin bottle to assess the O_2 and H_2S concentrations. Water samples from the Niskin bottle were collected via gas-tight Tygon tubing. Bottom water oxygen concentrations were measured using an automated Winkler titration procedure with potentiometric end-point detection (Mettler Toledo DL50 titrator and a platinum redox electrode). Bottom water ΣH_2S concentrations were determined spectrophotometrically (Cline 1969). Intact sediment cores (6 cm Ø) were retrieved with a UWITEC gravity corer in triplicates. All cores were inspected on retrieval and only undisturbed cores were used for measurements. Immediately after collection, sediment cores were transported to a nearby laboratory, where microprofiling was started within two hours from collection and conducted under climate-controlled conditions (temperature of in situ bottom water).

4.2.2. Microsensor profiling

Microsensor profiling was performed using commercial micro-electrodes (Unisense A.S., Denmark) for O_2 (25 or 50-µm tip; Unisense), pH (200-µm tip diameter), H_2S (50-µm tip diameter). Oxygen microprofiles were made at 25-50 µm resolution, with a 2-point calibration made in air-saturated seawater (100% saturation) and at depth in anoxic sediment (0% saturation). For H_2S and pH, depth profiles were made at 200 µm resolution in the oxic zone, and 400 or 600 µm resolution below. Calibrations for pH were made with three NBS standards and a TRIS buffer to correct for salinity effects, and pH is reported on the total scale. For H_2S, a 5-point calibration was made using Na_2S standards. Total free sulfide ($\Sigma H_2S = H_2S + HS^-$) was calculated from H_2S based on pH measured at the same depth using the R package AquaEnv (Hofmann et al. 2010). The oxygen penetration depth (OPD) is operationally defined as the depth below which $[O_2] < 1$ µM, while the sulfide appearance depth (SAD) is operationally defined as the depth below which $[H_2S] > 1$ µM. The diffusive oxygen uptake (DOU) was calculated from the oxygen depth profiles as in reference (Malkin et al. 2014).

4.2.3.   Pore water and solid phase geochemistry

Pore water was extracted from the sediment using centrifugation (15 min. at 4500 g) and was filtered (0.45 µm) and subsampled under N_2. Centrifuged pore water was sub-sampled for sulfide, where samples were fixed with zinc-acetate and stored at 4°C. Sulfide was measured spectrophotometrically (Cline 1969). Centrifuged sediment samples were freeze-dried, then ground in a N_2-purged glove-box. Sediment sulfur fractions were separated using the extraction described in reference (Burton et al. 2008), and modified as in reference (Kraal et al. 2013) to include an extraction step for elemental sulfur. Acid volatile sulfur (AVS) and chromium reducible sulfide (CRS) were quantified using iodometric titration. Solid phase Fe phases were also extracted and separated according to reference (Poulton and Canfield 2005), where Fe-oxides were measured as the total of the non-sulfidized Fe pools.

4.2.4.   Microscopy.

Beggiatoaceae filaments were identified via inverted light microscope (Olympus IM) within 24 hrs of retrieval. Intact sediment cores were sectioned at 5 mm intervals over the top 4 cm from which subsamples (20-30 mg) were used to count living *Beggiatoaceae* filaments. The biovolume was determined by measuring length (10x) and width (40x) of all filaments found in the subsample, according to reference (Jørgensen et al. 2010). Microscopic identification of cable bacteria was achieved by FISH, using a *Desulfobulbaceae*-specific oligonucleotide probe (DSB706; 5′-ACC CGT ATT CCT CCC GAT-3′), according to Schauer et al. (2014) (Schauer et al. 2014). The depth distribution of cable bacteria was quantified in March, May, August and November 2012. Cable bacteria biovolume per unit of sediment volume (mm^3 cm^{-3}) was calculated based on measured filament length and diameter, as well as the areal biovolume of cable bacteria (mm^3 cm^{-2}) by depth integration over all eight sediment layers. For macrofauna analysis, sediment collected from 8 cores (for a total surface area of ~0.02 m^2) was wet-sieved (mesh size 1.0 mm) on board. Subsequently, macrofauna were carefully handpicked and preserved in 4% formalin solution stained with rose bengal. All individuals were identified to species level where possible using a stereo-microscope (Leica MZ16), and macrofauna abundance (individuals m^{-2}) was calculated.

4.3. RESULTS and DISCUSSION

4.3.1.   Response of pore water geochemistry to seasonal oxygenation

The sediment geochemistry, sediment fauna and sedimentary microbial communities were surveyed in Marine Lake Grevelingen (The Netherlands), a coastal water body (salinity ~30) with restricted water exchange with the open North Sea. Over the last decade, Marine Lake Grevelingen has experienced a regular pattern of summer stratification and bottom water oxygen depletion (Fig. S1a), which was also observed in monthly sampling

campaigns performed throughout 2012 (Fig S1b). Bottom water oxygen concentrations (Winkler method; Fig.1a) were near air saturation in winter and early spring, started to decline in April at the onset of stratification, became hypoxic ($O_2 < 63$ µM) by the end of May, and declined below the detection limit in August ($O_2 < 1$ µM; anoxia). In September, the overturning of the water column resulted in a re-oxygenation of the bottom water.

Due to sediment focusing, the deeper basins in Marine Lake Grevelingen experience a strong accumulation (~ 2 cm yr^{-1}) of dark, organic-rich, fine-grained sediment (Malkin et al. 2014). Free sulfide ($\Sigma H_2S = [HS^-] + [H_2S]$) accumulates in the pore water to high levels ($\sim$ 2 mM at 10 cm depth; Fig. S2), suggesting that intensive organic mineralization takes place in the surface sediment and that sulfate reduction is the major mineralization pathway (estimated to be ~ 30 mmol S m^{-2} d^{-1} in August; Supplementary Information, *SI*). The burial of pyrite and iron sulfides only scavenges ~ 39 % of the sulfide production (*SI*), and bottom water concentrations of nitrate (the alternative electron acceptor) are generally low in Marine Lake Grevelingen (Fig. S1b). Accordingly, oxygen appears to be the main electron acceptor for the oxidation of the large amount of free sulfide that is produced by sulfate reduction (*SI*).

Nevertheless, micro-sensor profiling revealed that O_2 and H_2S were almost never in direct contact in the pore water, as a well-developed suboxic zone was present throughout most of the year (Fig. 1b), i.e., a distinct sediment horizon where neither O_2 nor ΣH_2S were present in detectable concentrations. This suboxic zone was widest in the first part of the year (annual maximum of 17.6 ± 4.6 mm in April), and its width decreased in a stepwise fashion by ~ 50% in late spring (May: 8.9 ± 2.1, June: 7.0 ± 5.2 mm). When the oxygen saturation of the bottom water dropped below 11% (corresponding to 29 µmol L^{-1}; July and August, Fig. 1a), the H_2S front started to move towards the sediment surface (Fig. 1b). However, free sulfide remained undetectable in bottom water samples collected at 2 meters above the sediment surface during the stratified season ($\Sigma H_2S < 0.2$ µM; June, August). We additionally determined the ΣH_2S concentration in the overlying ~ 10 cm water of retrieved sediment cores, which confirmed that euxinia did not occur.

Figure 1. (A) Oxygen concentration (µmol L^{-1}) in the bottom water, measured at 1 m above the sediment surface throughout 2012. (B) Depth distribution of the oxic zone (red), suboxic zone (brown), and sulfidic zone (black) within the sediment throughout 2012. The data were obtained from microsensor measurements in intact sediment cores. (C) Pore water pH values in the upper 30 mm of the sediment measured monthly during 2012, in intact sediment cores. Gray lines indicate sampling dates. (D) Biovolume (cm^3 cm^{-2}) of cable bacteria (pink bars) and *Beggiatoaceae* (blue bars), and macrofauna abundance (100* individualsm^{-2}; orange line) recorded throughout 2012. Cable bacteria were enumerated in March, May, August, and November; *Beggiatoaceae* were counted monthly over the entire year 2012; macrofauna were determined monthly from February to December.
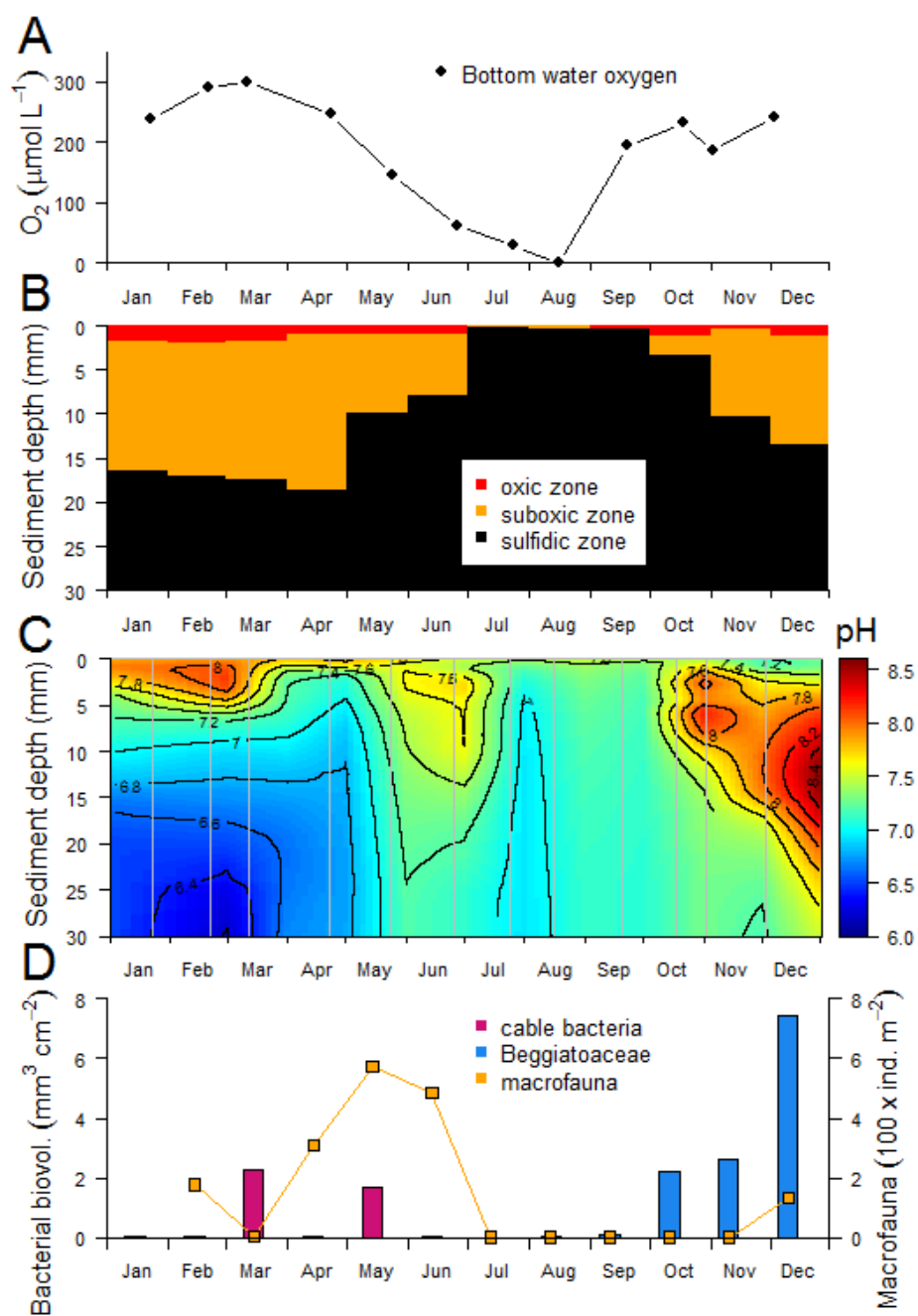
After the overturning of the basin, the oxygen penetration depth was small (0.7 ± 0.1 mm), indicative of strong oxygen uptake caused by re-oxidation of reduced compounds. September was also the only month when the pore water depth profiles O_2 and H_2S showed an overlap (Fig. 1b), allowing the direct aerobic oxidation of sulfide ($H_2S + 2O_2 \rightarrow SO_4^{2-} + 2H^+$). A small suboxic zone reappeared in October (2.2 ± 0.9 mm) and gradually expanded (12.2 ± 1.6 mm in December).

4.3.2.   <u>Mechanisms of suboxic zone formation</u>

To elucidate the underlying mechanisms of sulfide oxidation and suboxic zone formation, we developed a pH typology for three known mechanisms of aerobic sulfide oxidation (*SI*): (1) the electrogenic sulfur oxidation metabolism of the recently discovered cable bacteria (Nielsen et al. 2010; Risgaard-Petersen et al. 2012; Pfeffer et al. 2012), (2) the cycling of iron between reduced and oxidized mineral forms, which is crucially dependent on solid-phase mixing (Aller and Rude 1988; Canfield et al. 1993a) and (3) the respiratory metabolism of nitrate-accumulating *Beggiatoaceae* (Mussmann et al. 2003; Sayama et al. 2005; Lichtschlag et al. 2010). Each of these three pathways is associated with a characteristic pH depth-profile (Fig. 2 and *SI*), which reveals when these mechanisms dominate the pore water geochemistry and are responsible for the formation of the suboxic zone (Fig. 1c). This pH typology predicted that electrogenic sulfur oxidation by cable bacteria was dominant from January to April, while metal cycling dominated in May and June, and respiration of nitrate-accumulating *Beggiatoaceae* created the suboxic zone in fall, after the ventilation and re-oxygenation of the bottom water (Fig. 1c).

This temporal succession of sulfur oxidation pathways as predicted by the pH typology analysis was confirmed by direct microscopic observation of microbial and macrofaunal communities. Cable bacteria were enumerated on a seasonal basis by Fluorescence *In Situ* Hybridization (FISH), which revealed that cable bacteria were abundant in March and May (filament density 402-480 m cm^{-2}; biovolume 1.8-2.5 mm^3 cm^{-2}), but remained below the detection limit in August and November (Fig. 1d). When present, cable bacteria were found throughout the upper 40 mm of the sediment, with the maximum density near the sediment surface, high densities in the suboxic zone, and low densities declining into the sulfidic zone (Fig. 2a, March). The filament diameter did not differ significantly (t-test; n = 15, p = 0.29) between March (1.3 ± 0.3 µm) and May (1.2 ± 0.3 µm), suggesting that cable bacteria populations were phenotypically similar.

Quantitative microscopic enumeration of *Beggiatoaceae* was conducted each month (Fig. 1d), and showed low densities in spring (biovolume B: 0.02-0.05 mm^3 cm^{-2}), when only a few filaments were found dispersed throughout the upper 2 cm of sediment, and a virtual absence from May to August (B $\leq$ 0.001 mm^3 cm^{-2}). In September, a population of thin *Beggiatoaceae* filaments (diameter d: 2.4 µm; mean filament length L: 70 µm; B: 0.08 mm^3 cm^{-2}) was found concentrated right at the O_2-H_2S interface, which likely catalyzed the direct aerobic oxidation of free sulfide. Laboratory studies have estimated that sulfide
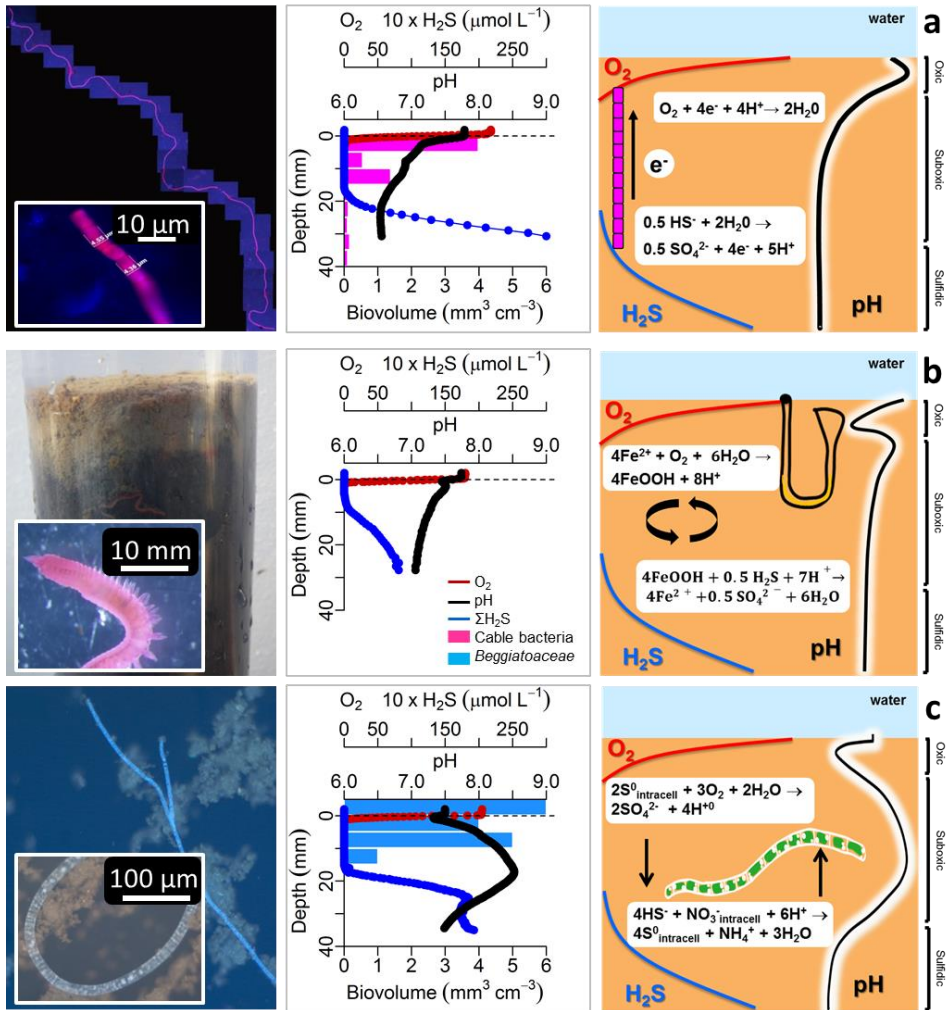
Figure 2. Three mechanisms of suboxic zone formation were active during 2012 at the study site. (A) FISH image of cable bacterium (DSB706 probe) and close-up of a cable bacterium (Left); depth profiles of O_2 ($\mu mol\ L^{-1}$, red line), pH (black line), and ΣH_2S ($\mu mol\ L^{-1}$, blue line) and biovolume ($cm^3\ cm^{-2}$) of cable bacteria (pink bar) in March (Middle); and schematic representation of geochemical signature and e-SOx carried out by cable bacteria (Right). (B) Sediment core picture and microscope picture of the polychaete Scoloplos armiger (Left); microsensor depth profiles in May (Middle); and schematic view of effect of the macrofauna on sedimentary iron and sulfur cycling (Right). (C) *Beggiatoaceae* filament image and close up of a filament (light microscope, stained with DAPI) (Left); microsensor depth profiles and *Beggiatoaceae* biovolume ($cm^3\ cm^{-2}$, pink bar) in December (Middle); and schematic view of geochemical signature and sulfur oxidation carried out by *Beggiatoaceae* (Right).

oxidation at the oxic-anoxic interface by *Beggiatoaceae* may be up to three times faster than the autocatalytic aerobic chemical oxidation of sulfide (Jørgensen and Postgate 1982; Jørgensen and Revsbech 1983; Schulz and Jørgensen 2001), thus enabling an efficient competition with the abiotic pathway. From October onwards, the biovolume of *Beggiatoaceae* filaments drastically increased (B: 2.2 - 7.5 mm^3 cm^{-2}), and the depth-distribution of the *Beggiatoaceae* closely tracked the progressive widening of the suboxic zone (Fig. 2c). In addition, the filament diameter and length increased significantly compared to September (t-test; n = 672, p < 0.001, regarding both length and diameter) suggesting that a different population of *Beggiatoaceae* was active in late fall, which had a metabolism based on intracellular nitrate respiration. Bacterial cell-lysing experiments confirmed that the large *Beggiatoaceae* filaments observed at the field site were storing nitrate into intracellular vacuoles (*SI*).

The pH typology analysis predicted that suboxic zone in May and June was no longer formed by cable bacteria, but that metal cycling caused the separation of O_2 and H_2S horizons in the upper first centimeter of the sediment (Fig. 2b). This coincided with a sharp rise in the abundance and diversity of the macrofauna in the surface sediment (Fig. 1d), suggesting that bioturbation could provide the sediment mixing needed to sustain the metal cycling. An alternative explanation would be that mixing via sediment resuspension is specifically intense during May and June, which is unlikely however, as meteorological conditions at the field site are typically calm in early summer. With the onset of hypoxia in late June, the macrofauna vanished abruptly and the sediment remained devoid of macrofauna until December, when recolonization started, although population densities remained low throughout winter. Upon recolonization in spring, the fauna was dominated by small polychaetes and juvenile bivalves, which only have a shallow burrowing depth, consistent with the limited suboxic zone of 7-9 mm observed in May and June. Since fauna are highly sensitive to free sulfide (Diaz and Rosenberg 1995; Vaquer-Sunyer and Duarte 2008; Levin et al. 2009), the deep removal of sulfide by cable bacteria in early spring may have promoted faunal re-colonization.

4.3.3. <u>**Microbial competition for reduced sulfur compounds**</u>.

In Marine Lake Grevelingen, we observed that cable bacteria were dominant throughout spring, whereas sulfur oxidation was largely carried out by nitrate-accumulating *Beggiatoaceae* throughout fall.

This pattern was not only observed in 2012, when detailed monthly sampling was conducted, but was confirmed by seasonal surveys over the period 2011-2015 (*SI*). Combining micro-sensor profiling and pH-signature analysis, we found that the geochemical signature of cable bacteria is significantly more present in spring, while the activity of *Beggiatoaceae* is more likely encountered in fall (Fig. 3). For example, in spring 2015, all sampled sediment sites below 15 meter water depth showed the cable bacteria signature, while in fall 2011 and 2014, all sediment revealed the geochemical signature of
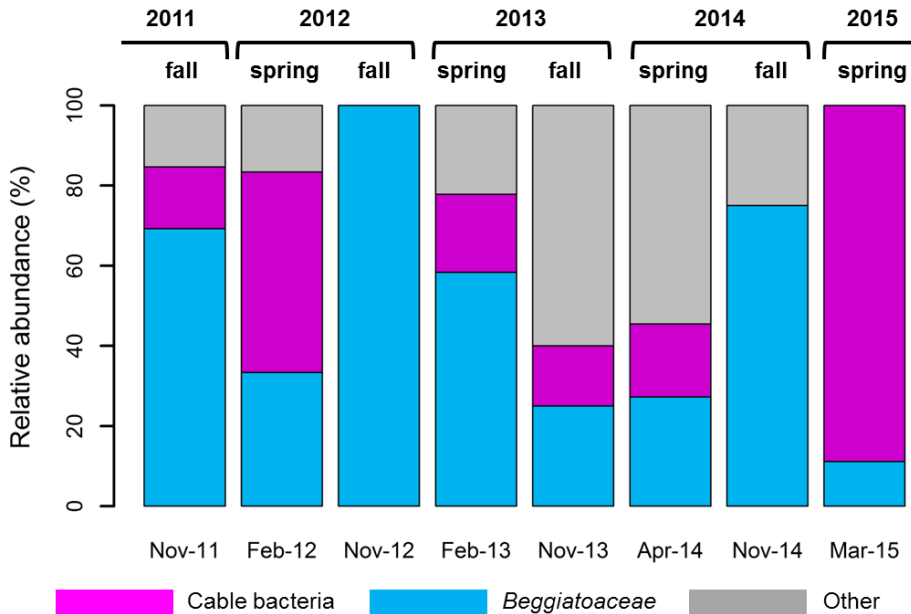
Figure 3. Relative abundance of the dominant sulfur oxidation pathways carried out by cable bacteria (pink bar), Beggiatoaceae (blue bar), and other processes (gray bar) during each fall and spring from November 2011 to March 2015. The geochemical signature (characteristic depth profiles of O_2, pH, and H_2S recorded by microsensor profiling) was used to determine the dominant pathway of sulfur oxidation at any given time at different sites within Lake Grevelingen (Supplementary Information).

nitrate accumulating *Beggiatoaceae*. This implies that two distinct types of filamentous S-oxidizing bacteria were competing for the same geochemical niche, but that each type was competitively successful during a distinct period of the year.

The development of *Beggiatoaceae* after summer suggests a better survival of the anoxic period, which could be due to the use of nitrate as an alternative electron acceptor to oxygen. Although both cable bacteria (Marzocchi et al. 2014) and *Beggiatoaceae* (Mussmann et al. 2003; Sayama et al. 2005; Lichtschlag et al. 2010) can use nitrate for respiration, cable bacteria reach lower population densities when nitrate is the sole electron acceptor (Marzocchi et al. 2014). Moreover, the nitrate concentration in the bottom water was low (< 1.7 µM) during summer (Fig. S1b), and thus, nitrate reduction was likely insignificant in sustaining microbial metabolism during anoxia. However, nitrate accumulation prior to anoxia could have played a role. Presently, there are no indications that cable bacteria can accumulate electron acceptors, while *Beggiatoaceae* can store nitrate in intracellular vacuoles (Schulz and Jørgensen 2001; Mussmann et al. 2003; Sayama et al.

103

2005; Lichtschlag et al. 2010), which can be used as an electron acceptor reservoir to survive the summer period of low bottom water oxygenation (Schulz and Jørgensen 2001).

Our seasonal surveys indicate that cable bacteria replace the *Beggiatoaceae* population in winter, yet the reasons for this population switch are not fully understood. One intriguing question is how cable bacteria can "invade" a sediment where a suboxic zone is already established by *Beggiatoaceae*, as recent laboratory experiments show that cable bacteria filaments progressively extend downwards from an initial overlap of oxygen and sulfide near the sediment-water interface (Schauer et al. 2014; Vasquez-Cardenas et al. 2015). A pre-existing suboxic zone thus poses a barrier for sediment colonization by cable bacteria. Future research should hence clarify the drivers and controls of what appears to be a yearly recurrent, and hence predictable, switch between two groups of filamentous S-oxidizing bacteria.

4.3.4.   Impact of cable bacteria on geochemistry

Cable bacteria and nitrate-accumulating *Beggiatoaceae* are both capable of efficient sulfide oxidation leading to the creation of a wide suboxic zone. Hence, with regard to biogeochemical cycling in seasonally-hypoxic basins, one could ask to what extent it matters whether one or the other is the dominant sulfur oxidizing microbial population? Solid phase data collected at the field site reveal a notable difference in the iron mineral phases between spring and fall (Fig. 4a), and suggest that cable bacteria induce a strong seasonal iron cycling. In March, when cable bacteria were active, a strong depletion of Acid Volatile Sulfides (AVS, interpreted to be mostly iron monosulfides; FeS) occurred in the suboxic zone (11.9 ± 7.3 µmol S g^{-1} over the first 3.3 cm; Fig. 4a), compared to high values in November (117.0 ± 26.4 µmol S g^{-1} over the first 3.3 cm; Fig. 4a), when nitrate-accumulating *Beggiatoaceae* were abundant. Exactly the opposite trend was seen in the extractable iron (hydr)oxides (FeOOH), which showed a much higher accumulation in spring (163 ± 52 µmol Fe g^{-1}; Fig.4a) than in fall (99 ± 27 µmol Fe g^{-1}). Together with our micro-sensor and microscopy data, these solid phase data suggest the following seasonal iron cycle (Fig. 4b): (1) conversion of FeS to FeOOH in spring by cable bacteria, (2) the downward-mixing of the FeOOH-rich surface sediment layer in late spring by the newly colonizing fauna, thus enhancing the observed S oxidation by metal oxide reduction, (3) the conversion of FeOOH back to FeS when free sulfide rises to the sediment-water interface during the summer hypoxia period, and (4) the persistence of an FeS pool in the suboxic zone during fall when nitrate-accumulating bacteria are active. Alternative mechanisms, such as winter resuspension events or a strong sedimentation of allochtonous iron (hydr)oxides in winter, cannot suitably explain the observed conversion of FeS to FeOOH in spring (SI).
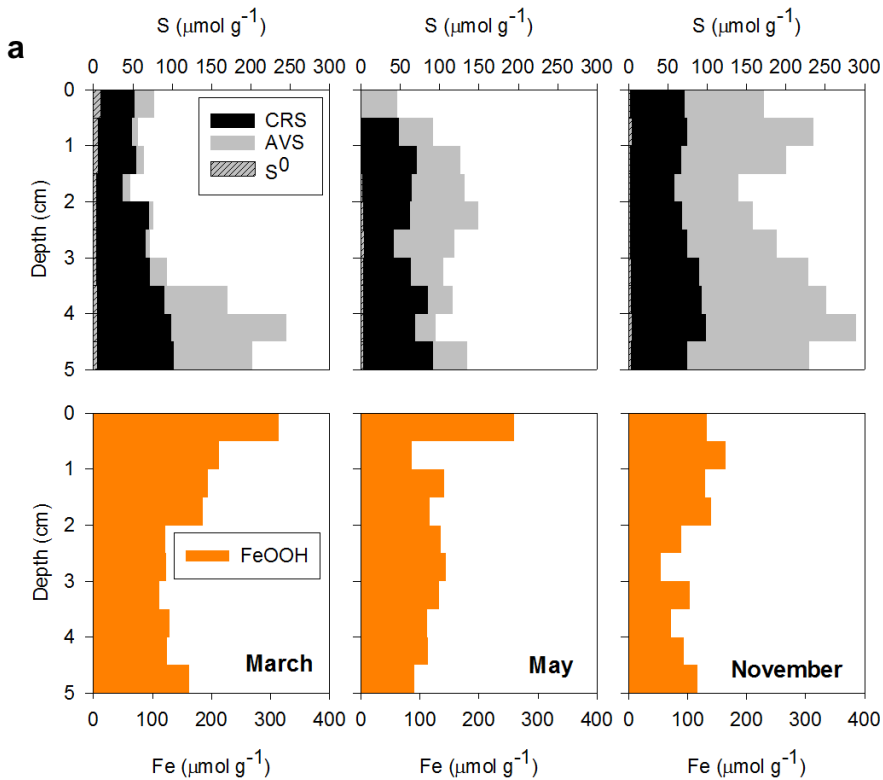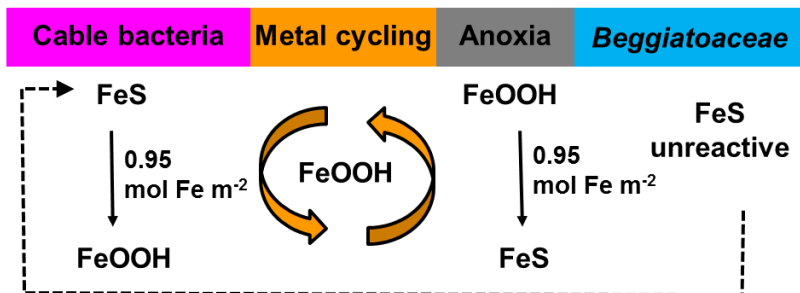
Figure 4. (A) Solid-phase geochemistry in the top 5 cmof the sediment. Depth profiles of S^0, CRS, and AVS (μmol S g^{-1}, Top) and iron (hydr)oxides (μmol Fe g^{-1}, Bottom) measured in March (Left), May (Middle), and November (Right). The iron (hydr)oxides represent the total of the nonsulfidized iron. (B) Illustration of interconversion between FeS and FeOOH during four time periods in 2012, when the sediment geochemistry was dominated by cable bacteria, metal cycling promoted by sediment mixing, anoxia, and *Beggiatoaceae*.

Accordingly, we conclude that observed seasonal iron cycling is principally driven by the FeOOH-forming activity of cable bacteria in spring, and this iron cycle would not occur if nitrate-accumulating *Beggiatoaceae* were dominant throughout the year. Our study therefore demonstrates that not only external environmental factors, such as bottom water oxygen availability, are driving the sedimentary iron and sulfur cycling in seasonally-hypoxic basins, but that the intrinsic population dynamics of the microbial community, and particularly rapid shifts in sulfur oxidizers, can be equally important.

The metabolic activity of cable bacteria exerts a profound impact on the sediment geochemistry through its effect on pore water pH (Meysman et al. 2015). The electrogenic metabolism induces a spatial uncoupling of sulfide oxidation and oxygen reduction (Fig. 2a), and accordingly, the production and consumption of protons occur widely segregated in space. The establishment of acidic conditions within the deeper suboxic zone promotes the dissolution of iron sulfides, which provides an extra H_2S-supply to the cable bacteria in addition to sulfate reduction (Risgaard-Petersen et al. 2012), and the oxidation of this extra H_2S generates more protons, thus establishing a positive feedback (15). In laboratory experiments, it has been shown that FeS dissolution provides up to 40-94% of the sulfide for e-SOx (Risgaard-Petersen et al. 2012; Meysman et al. 2015), and can completely exhaust the sedimentary FeS pool over a period of weeks (Schauer et al. 2014), while generating a surface enrichment of FeOOH. The observed FeS depletion in the top 4 cm in March shows that cable bacteria also induce strong FeS dissolution in the field, and we speculate that the depletion of the sedimentary FeS stock (Fig. 4a) may have limited the electron donor supply causing the demise of the cable bacteria population in late spring (Nielsen and Risgaard-Petersen 2015).

4.3.5. <u>Cable bacteria in seasonally-hypoxic systems and euxinia.</u>

Conventionally, the formation of sulfidic bottom waters is considered to be closely linked to the exhaustion of energetically-favorable electron acceptors in the water column, such as oxygen and nitrate (Middelburg and Levin 2009). Once these electron acceptors are depleted in the bottom water, the oxidation of sulfide in the surface sediment layer is halted, thus enabling a release of sulfide to the overlying water. However, laboratory sediment incubations (Kristiansen et al. 2002; Kristensen et al. 2003) have previously shown that the disappearance of oxygen and nitrate (anoxia) is not necessarily synchronous with the appearance of free sulfide (euxinia). In sediments that contain a large pool of reactive iron (hydr)oxides prior to the onset of anoxia, this pool can act as a "firewall" against the release of free sulfide from the sediment, thus delaying the onset of euxinia (Kristiansen et al. 2002; Kristensen et al. 2003). Iron (hydr)oxides have a high binding capacity for free sulfide (Rozan et al. 2002), therefore the efflux of free sulfide only starts after exhaustion of the iron (hydr)oxide pool, which can delay euxinia by several weeks, depending on the size of the initial reactive iron pool (Kristiansen et al. 2002; Kristensen et al. 2003).

At present, this iron-oxide mediated "firewall" mechanism has not been demonstrated to occur in seasonally-hypoxic basins. Moreover, it is also not expected to occur, as the mechanism requires a yearly build-up of an iron (hydr)oxides pool prior to the onset of summer anoxia, which is not obvious in seasonally-hypoxic environments. Coastal sediments typically accumulate sizeable pools of iron (hydr)oxides only when subjected to strong levels of bioturbation by infauna (Kristensen and Kostka 2005). The ventilation of macrofaunal burrows with oxygen-rich overlying water promotes the oxidation of dissolved ferrous iron (Fe^{2+}) in the pore water (Aller 2001), while particle reworking enhances the oxidation of deeply-buried iron sulfides by transporting them upwards to the oxic zone of the sediment (Meysman et al. 2006). However, as shown here, such large and deep-burrowing fauna are typically absent from seasonally-hypoxic sediments, because the yearly recurrent oxygen depletion increases mortality and decreases recruitment success (Rosenberg et al. 2002; Levin et al. 2009). For this reason, the sediments of seasonally hypoxic coastal systems are generally thought to have a low buffer-capacity towards the release of free sulfide (Jørgensen and Nelson 2004).

Although sampling at monthly-resolution is not sufficient to accurately document the magnitude of the time lag, we observed that anoxia did not coincide with euxinia. Even when the bottom water was devoid of oxygen in August, and nitrate was fully depleted, no free sulfide (concentrations were below the detection limit of $< 0.2\mu M$) was detected in the bottom water. Two potential mechanisms could explain this delay in the formation of euxinia relative to anoxia. The presence of a deep suboxic zone prior to the onset of bottom water anoxia is one potential mechanism. Before free sulfide can escape the sediment, the suboxic zone has to be transiently replenished with free sulfide, either through local production of sulfide via sulfate reduction, or via diffusion of sulfide from deeper sediment horizons. As both cable bacteria and *Beggiatoaceae* induce a suboxic zone, they both induce this form of euxinia delay. Analysis of the curvature of the ΣH_2S depth profile provides an estimate of the sulfide production rate of 0.3 mol H_2S m^{-3} d^{-1} within the first 10 cm of sediment, Accordingly, ~ 6 days are required for sulfide to accumulate in the suboxic zone up to the ΣH_2S ~ 2 mM level observed in August (porosity of 0.9). In reality, this accumulation of sulfide in the suboxic zone will proceed faster as molecular diffusion also supplies free sulfide from beneath the suboxic zone. Accordingly, the formation of a deep suboxic zone only delays euxinia for a short period of time, on the order of a few days at most.

The iron-oxide mediated "firewall" mechanism is a more effective mechanism for H_2S removal, and has been previously shown to delay sulfide effluxes from sediments for a period of weeks (Kristiansen et al. 2002; Kristensen et al. 2003). Our results show that cable bacteria generated a large pool of reactive iron (hydr)oxides prior to the onset of summer hypoxia (0.95 mol Fe m^{-2}, as calculated from the difference in FeS and FeOOH inventories over 0-4 cm between spring and fall, SI. Given a depth-integrated sulfide production rate of 30 mmol H_2S m^{-2} d^{-1}, this iron (hydr)oxide pool could potentially buffer

H$_2$S production up to ~ 36 days. This period is considerably longer than the observed period of anoxia at the study site in 2012 (<20 days), and hence may explain the observed absence of bottom water euxinia in August 2012.

4.4. CONCLUSION

Cable bacteria have only recently been discovered (Nielsen et al. 2010; Pfeffer et al. 2012), and hence, little is known about their ecology, life cycle and natural distribution. Our results demonstrate that cable bacteria can have a major impact on sedimentary biogeochemical cycling in a seasonally-hypoxic basin, with potential basin-scale impacts on water column chemistry. In a first report on the occurrence of cable bacteria under natural conditions, it was demonstrated that cable bacteria thrive globally in a wide range of marine sediment habitats, such as coastal mud plains and salt marshes, but that they particularly seem abundant in seasonally-hypoxic basins (Malkin et al. 2014). If cable bacteria in other coastal systems follow a similar seasonal cycle to that of Marine Lake Grevelingen, the iron-oxide "firewall" mechanism proposed here could be widely prevalent, and may explain the relatively rare reports of euxinia in coastal systems affected by seasonal hypoxia. However, to accurately document the magnitude and efficiency of this buffer mechanism, a comparison of the sediment geochemistry and microbiology is needed across multiple seasonally-hypoxic systems at a higher-than-monthly resolution. Such investigations are crucial, given that seasonal hypoxia in coastal areas is increasing worldwide due to anthropogenic nutrient input and climate change (Middelburg and Levin 2009).

Acknowledgments:

4.5. SUPPLEMENTARY INFORMATION: RESULTS AND DISCUSSION

4.5.1. Study site description and seasonal water column chemistry

Lake Grevelingen (surface area 115 km^2) is a former estuary in the Delta region, in the south-west of The Netherlands. In 1971 this water body was closed off from the North Sea by a dam, turning the estuary into a marine lake, which consists of separate basins. Most areas of the impoundment are shallow consisting of < 12.5 m water depth. Due to limited water exchange with the open sea, water column stratification develops each summer, leading to seasonal hypoxia in the bottom waters of the deeper basins (Fig. S1). A comprehensive overview of stratification and the water circulation in Lake Grevelingen is given in ref. (Hagens et al. 2015).

Water column temperature and salinity data were used to calculate the stratification parameter ϕ (J m^{-3}) (Fig. S1), which is defined as the amount of energy required to fully homogenize the water column through vertical mixing (Hagens et al. 2015):

$$\phi = \frac{1}{H} \int_{-H}^{0} (\rho_{av} - \rho_W) gz dz \quad \text{where} \quad \rho_{av} = \frac{1}{H} \int_{-H}^{0} \rho_W \, z dz$$

where H is the total height of the water column (m), z is depth (m), g is gravitational acceleration (m s^{-2}), ρ_w is water density (kg m^{-3}) and ρ_{av} is the average water column density (kg m^{-3}).

4.5.2. Sulfur cycling budget

The sulfate reduction rate was estimated from the production and accumulation of total free sulfide ($\Sigma H_2 S = [HS^-] + [H_2S]$) in the first 10 cm of the sediment (Fig. S2). The production rate of free sulfide was estimated as the upward flux towards the bottom of the suboxic zone, as calculated from Fick's first law J = - φ D$_s$ dC/dx, where φ = 0.89 is the local porosity, D$_s$ is the effective diffusion coefficient in the pore water and dC/dx is the concentration gradient (obtained by linear regression of the $\Sigma H_2 S$ depth profile). The effective diffusion coefficient was calculated as Ds = D$_{mol}$ / θ^2, where we assume that bisulfide (HS$^-$) is the dominant pore water species and the molecular diffusion coefficient D$_{mol}$ was calculated from the CRAN: marelac package as a function of temperature and salinity. A tortuosity correction θ^2 = 1-2ln(φ) was implemented. Note that this approach does not account for the local sulfate reduction within the suboxic zone, and hence, it provides a conservative estimate for the sulfate reduction rate (SRR). The monthly SRR varied between 4 and 30 mmol S m^{-2} d^{-1} over the year 2012, and reached a maximum of 30 mmol S m^{-2} d^{-1} in August, with an annual average of 10.7 mmol S m^{-2} d^{-1} or 3.9 mol S m^{-2} yr^{-1}. The diffusive oxygen uptake (DOU) at the study site was calculated in a similar way by applying Fick's first law to the oxygen depth profile just below the sediment-water interface. The monthly DOU varied between 16.9 and 58.1 mmol O$_2$ m^{-2} d^{-1}, with an annual average of 23.6 mmol O$_2$ m^{-2} d^{-1} or 8.6 mol O$_2$ m^{-2} y^{-1}.

The burial of reduced sulfur compounds was estimated from the concentrations of iron sulfides ([FeS] determined as Acid Volatile Sulfur: 0.15 mmol S g^{-1} dry sediment) and
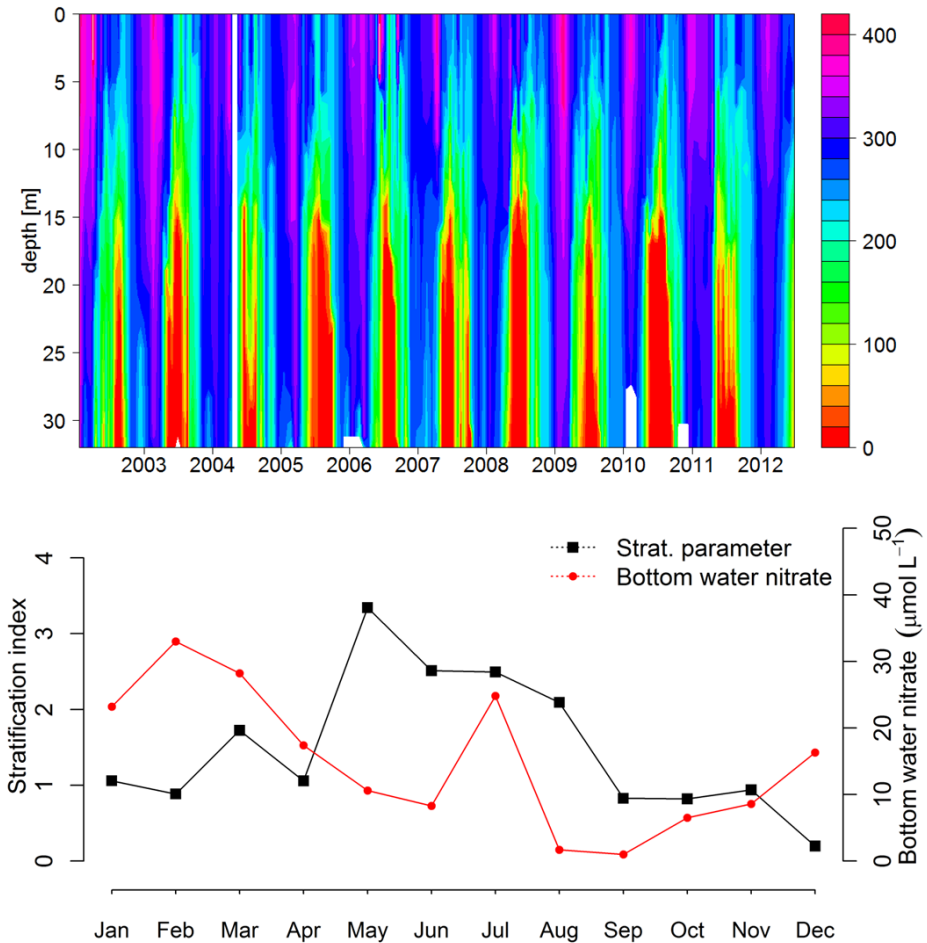
Figure S1. (A) Oxygen concentrations (μmol L^{-1}) recorded over the period 2002–2012 show a regular pattern of seasonal hypoxia in the deeper bottom waters at the Lake Grevelingen field site. Data collected by Rijkswaterstaat (Dutch Ministry of Infrastructure and the Environment). (B) Bottom water nitrate concentrations (μmol L^{-1}, red circles) and stratification index (J m^{-3}, black squares) as recorded in monthly sampling campaigns throughout 2012.

pyrite ([FeS$_2$] determined as Chromium Reducible Sulfur: 0.12 mmol S g^{-1} dry sediment) at 10 cm depth. The burial rate was calculated as F = (1-φ) w ρ ([FeS] + [FeS$_2$]) = 1.1 mol S m^{-2} yr^{-1}, where φ = 0.9 is the porosity at 10 cm depth, w is the burial velocity (2 cm yr^{-1} as determined by Pb^{210} radionuclide dating; (Malkin et al. 2014)), and ρ is the solid phase

density (2.6 g cm^{-3}). Using an average SRR of 10.7 mmol m^{-2} d^{-1}, we found that 39 % of the free sulfide produced is buried as iron sulfides or pyrite.

Accordingly, the remaining ~ 61 % of the sulfide production (2.4 mol S m^{-2} y^{-1}) must be re-oxidized to sulfate, if no free sulfide escapes the sediment. If oxygen is the sole terminal electron acceptor ($H_2S + 2O_2 \rightarrow SO_4^{2-} + 2H^+$), one needs two mole of oxygen per mole of sulfide, and so the required oxygen consumption rate (4.8 mol S m^{-2} y^{-1}) is smaller than the calculated DOU of the sediment. If sulfide re-oxidation would occur solely by nitrate-accumulating *Beggiatoaceae*, the re-oxidation of sulfide occurs in two steps: the oxidation of H_2S to S^0 by nitrate and the intracellular storage of S_0 (upon migration of *Beggiatoaceae* into the deeper suboxic zone) and then the oxidation of intracellular S^0 to sulfate by oxygen (upon migration to the oxic layer at the surface). This process ($S_0 + 3/2O_2 + H_2O \rightarrow SO_4^{2-} + 2H^+$) predicts an overall oxygen consumption of 3.6 mol O_2 m^{-2} y^{-1}, which is below the observed DOU.
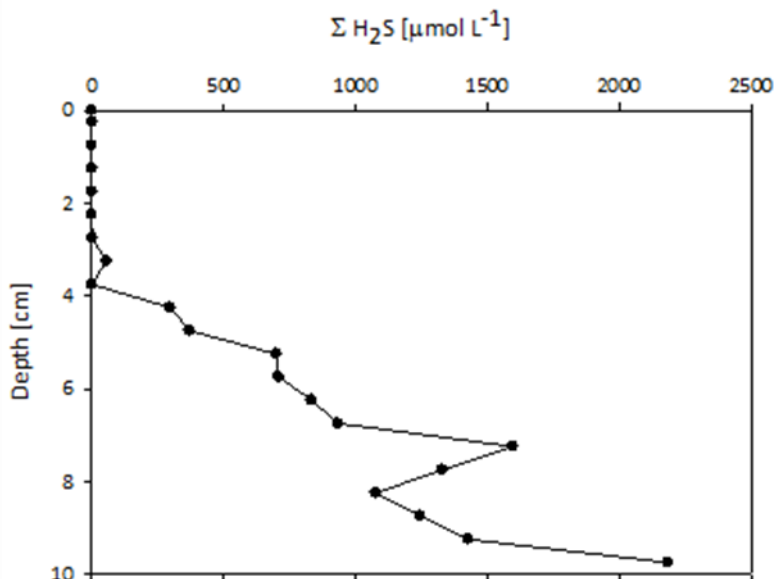
Figure S2. Sulfide concentrations in the pore water in the upper 10 cm of sediment in January. Pore water samples were obtained upon sediment centrifugation.

4.5.3. pH typology and seasonal succession of sulfur cycling pathways

To determine which sulfur-oxidation mechanisms were active through the seasonal cycle, we developed a pH signature typology. Different sulfur-oxidation pathways will release and consume protons (or more exactly, alkalinity) within different sediment horizons, and hence, they will induce a specific pH depth profile in the pore water. This

way, the pH depth profile (in combination with the O_2 and H_2S depth profiles) provides a characteristic signature of the sulfur oxidation mechanism at hand. Below we discuss 5 types of pH profiles, which each could be associated with a specific form of the sulfur cycling. In this way, micro-sensor depth profiling allows to screen which sulfur cycling pathways are active throughout the year (Fig. 1c; Fig. S3), and as discussed in the text, this revealed a rapid temporal succession of different sulfur cycling pathways at the field site.

Electrogenic sulfur oxidation (e-SOx) by cable bacteria. The electrogenic metabolism of cable bacteria induces a distinct geochemical signature in the interstitial pore water (Fig 2a), which is characterized by strong pH excursions (Nielsen et al. 2010; Schauer et al. 2014; Meysman et al. 2015). High proton consumption occurs within the shallow oxic zone due to cathodic oxygen reduction ($O2 + 4e^- + 4H^+ \rightarrow 2H_2O$), creating a pH maximum near the oxygen penetration depth. Similarly, proton production takes place within the deeper part of the suboxic zone due to anodic sulfide oxidation ($\frac{1}{2} H_2S + 2H_2O \rightarrow \frac{1}{2} SO_4^{2-} + 4e^- + 5H^+$), which generates a pH minimum at depth. This characteristic e-SOx signature (25) was recorded by micro-sensor profiling in January (Fig. S3) and February, when pH depth profiles showed a narrow maximum within the oxic zone (8.04 ± 0.21 pH units in January and February) accompanied by a broad pH-minimum near the sulfide appearance depth (pH 6.37 ± 0.17 below 20 mm depth; Fig. 2). In March, no subsurface pH-peak was detected, but acidic conditions (6.49 ± 0.13 pH units) persisted at 25-30 mm depth, while FISH data confirmed a dense population of cable bacteria present (Fig.1d). Reactive transport simulations have recently shown that at high e-SOx rates, the subsurface pH-maximum shifts towards the sediment-water interface and becomes less pronounced, making it more challenging to detect by micro-sensor profiling (Meysman et al. 2015). In April, the pH within the suboxic zone (6.84 ± 0.08) remained below 7, which we used as an operational threshold for e-SOx activity, but the pH depth profile was less characteristic and showed signs of a transition towards another sulfide oxidation regime.

Sulfur oxidation through iron cycling. The cycling of iron between reduced and oxidized forms requires solid phase mixing, which transports oxidized forms (FeOOH) into deeper sulfidic layers and brings up reduced forms of iron (e.g. FeS, Fe^{2+} adsorbed onto solids) towards oxic surface layer (Canfield et al. 1993b; Thamdrup et al. 1994). As a result of this, protons are produced in the oxic zone (e.g. $Fe^{2+} + \frac{1}{4} O_2 + 3/2H_2O \rightarrow FeOOH + 2H^+$), leading to a pH minimum near the OPD where re-oxidation takes place, and similarly, protons are consumed in deeper layers (e.g. $4FeOOH + \frac{1}{2} HS^- + 8H^+ \rightarrow 4Fe^{2+} + \frac{1}{2} SO_4^{2-} + 6H_2O$) leading to a subsurface pH increase. In reality, the redox pathways can be more complex, as there can be multiple parallel transport pathways of iron transport, as well as an intermediate cycle of manganese between iron and oxygen (Thamdrup et al. 2000). Yet overall, iron cycling leads to release of protons within the oxic surface layer and consumption of protons in the deeper suboxic zone, as confirmed by reaction transport modelling of pH distributions in marine sediments (Jourabchi et al. 2005). This

geochemical signature of metal cycling in the surface sediment was observed in the micro-sensor profiles recorded in May 2012 (Fig. S3). Although the FISH data show that cable bacteria maintained a dense population in May, the pH depth distribution (Fig. S3) suggests that e-SOx was no longer as dominant in May. Compared to January-March, the pH in the suboxic zone evolved towards more alkaline values, increasing from 6.84 ± 0.08 in April to 7.26 ± 0.07 in June (Fig. 1c). Rather than a pH-maximum, the pH depth profile in May showed a subsurface-minimum (7.57) at the OPD, followed by a small pH-increase (7.63), to subsequently decrease again (7.18) at 26 mm depth (Fig. 2). The pH profiles recorded in June were similar as in May, and hence, the period of metal cycling, as indicated by the pH typology, coincided with the higher abundances of macrofauna (Fig 1d), which may have generated the required solid phase mixing through bioturbation.
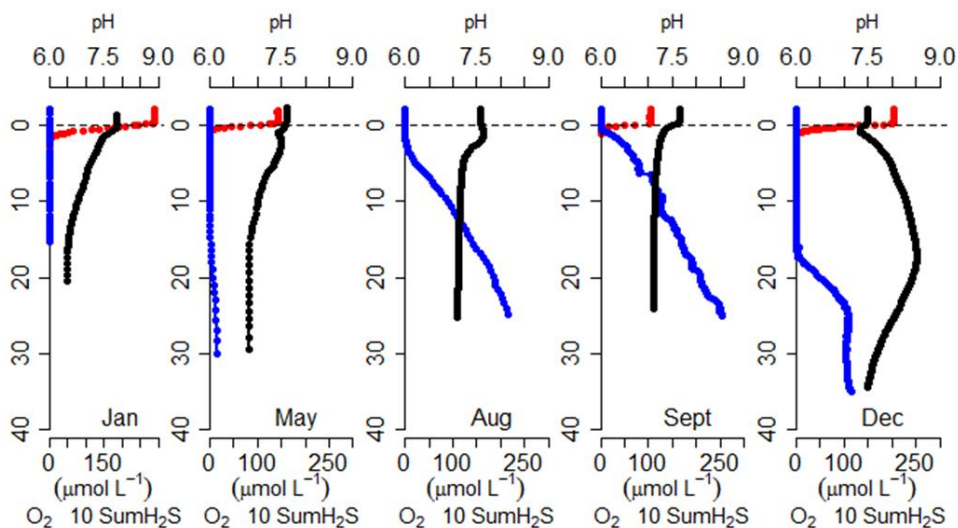
Figure S3. Pore water depth profiles of O_2 (red line), pH (black line), and ΣH_2S (blue line) at the field site in January, May, August, September, and December. These so-called geochemical signatures illustrate the different types of sulfur cycling that were active at the field site.

Summer anoxia. The establishment of low oxygen conditions (28.8 µmol L^{-1}, 11% air saturation) in the bottom water in July resulted in a clear change in the pH depth profile. The pH decreased to around 7.3 ± 0.1 pH units over the first 5 mm and subsequently remained constant with depth (Fig. S3), while the sulfide horizon migrated upwards and the sulfide depth profile switched from convex to concave. This geochemical signature suggests the production of sulfide through sulfate reduction at depth and an upward transport by molecular diffusion (Meysman et al. 2015). The pH depth profile did not exhibit the subsurface maximum, but showed a monotonous decrease, which is the expected profile when sulfate reduction is the dominant mineralization pathway. Sulfate

reduction ($2CH_2O + SO_4^{2-} \rightarrow 2HCO_3^- + H_2S$) releases dissolved inorganic carbon and alkalinity in equal proportions, which explains the gradual decrease in pH with depth.

Canonical sulfur oxidation at the O_2-H_2S interface. Right after the re-oxygenation of the bottom waters in September, oxygen and free sulfide showed a small overlapped, allowing canonical sulfur oxidation to occur (i.e. the direct redox interaction of H_2S and O_2 as defined in (Meysman et al. 2015)). The pH profile that was recorded is consistent with recent reactive transport model simulations (14), showing a monotonous decrease with depth. The pH decreased in the narrow oxic zone (~7.73) down to the oxic-anoxic interface (~7.41), where the oxidation of sulfide releases protons (e.g. $HS^- + 2 O_2 \rightarrow SO_4^{2-} + H^+$). In deeper anoxic layers, the pH became constant with depth (~7.19 below 5 mm depth), and thus stabilized at slightly lower values compared to August.

Sulfur oxidation by nitrate-accumulating Beggiatoaceae. In fall, the sediment was characterized by yet a different type of geochemical signature (Fig. 2c), which suggested that another pathway of sulfide oxidation was dominant. In the period from October to December, the pH depth profiles showed a distinct sigmoid shape, with a subsurface-minimum located at the OPD that became progressively pronounced (from 7.52 ± 0.06 to 7.28 ± 0.04), and increasingly alkaline near the sulfide horizon (from 7.79 ± 0.10 to 8.48 ± 0.05). The sigmoid pH depth profile has been previously linked to the metabolism of motile, nitrate-respiring *Beggiatoaceae* (Sayama et al. 2005; Lichtschlag et al. 2010), and reflects the proton production/consumption associated with spatial separation of the two sequential steps in sulfide oxidation (Fig. 2c). The oxidation of sulfide at depth via intracellular nitrate ($4HS^- + NO_3^-{}_{intracell} + 6H^+ \rightarrow 4S^0{}_{intracell} + NH_4^+ + 3H_2O$) consumes protons, thus explaining the broad pH-maximum at the sulfide horizon. The elemental sulfur (S^0) generated from this oxidation is stored intracellularly, and once the gliding *Beggiatoaceae* reach the oxic zone, elemental sulfur is further oxidized to sulfate using oxygen as the electron acceptor ($2S^0{}_{intracell} + 3O_2 + 2H_2O \rightarrow 2SO_4^{2-} + 4H^+$). This latter reaction produces protons, and therefore induces a pH-minimum near the OPD (Fig. 2c).

4.5.4. Interconversion of FeS and FeOOH

The depletion of the FeS pool (as shown by the AVS depth profiles) in the uppermost 3.5 cm and accumulation of iron (hydr)oxides in the first 2 cm of sediment in spring suggests conversion of FeS to FeOOH (Fig. 4b). We attribute this to dissolution of FeS ($FeS + H^+ \rightarrow Fe^{2+} + HS^-$) by the acid-generating metabolism of the cable bacteria, followed by aerobic oxidation of ferrous iron in the oxic surface sediment ($4Fe^{2+} + O_2 + 6H_2O \rightarrow 4FeOOH + 8H^+$). By fall, these iron (hydr)oxides have been converted again to FeS, as seen by the increase FeS pool and a decrease in the pool of extractable iron (hydr)oxides (Fig. 4b). We attribute this interconversion to the reduction iron (hydr)oxides by free sulfide under anoxic conditions in summer ($8FeOOH + 9HS^- + 7H^+ \rightarrow 8FeS + SO_4^{2-} + 12H_2O$). The resulting conversion was quantified by calculating the change in the

inventory $I = \int_0^L \rho_s (1-\phi) C(x) dx$ of both AVS and extractable Fe-oxides between

March and November 2012. In this ρ_s is the solid phase density (2.60 g cm^{-3}), ϕ

represents porosity, $C(x)$ is the measured concentration depth profile (in µmol g^{-1}), and L

= 4 cm is the integration depth (i.e., the depth horizon affected by metabolic FeS dissolution of cable bacteria). The calculated increase in the AVS inventory amounted to 1.17 mol Fe m^{-2}, while the observed decrease in FeOOH inventory was 0.73 mol Fe m^{-2}. Given the uncertainties associated with the operational extraction procedures for these iron phases, this suggests a nearly stoichiometric interconversion of ~ 0.95 mol Fe m^{-2} (the mean of both values) from FeOOH into FeS over the summer period.

4.5.5.   Nitrate accumulation in Beggiatoaceae filaments

Beggiatoaceae filaments were identified by microscopy based on size, motility and the presence of sulfur inclusions. To verify that the large *Beggiatoaceae* filaments observed at the field site were capable of nitrate accumulation, and hence nitrate respiration, lysis experiments were conducted as described in reference (Lichtschlag et al. 2010). Two intact sediment cores were sliced from 0 to 2 cm at depth intervals of 0.2 mm, and beyond this, every 0.5 cm down to 3 cm. The samples were stored frozen (-20 ^{o}C) for several weeks, in order to allow the lysis of any nitrate accumulating cells. Pore water was separated by centrifugation of thawed sediment samples at 3,000 x g for 10 min, and the nitrate concentration was determined in the supernatant by using standard colorimetric method on a Seal QuAAtro autoanalyzer. Nitrate was present in the pore water at high concentrations throughout the suboxic zone, with a maximum of 374 ±64 µmol L^{-1} near the surface and gradually decreasing to 8 ± 1 µmol L^{-1} at 3 cm depth (Fig. S3). These pore water concentrations strongly exceeded the bottom water nitrate concentrations (7.1 µmol L^{-1}), suggesting that the nitrate was likely contained in intracellular vacuoles of the *Beggiatoaceae*. In addition, the nitrate accumulation was measured in individual hand-picked *Beggiatoaceae* filaments. Around 40 *Beggiatoaceae* filaments (~10-20 µm of diameter) were separately picked using a glass needle, and transferred to vials with 0.25 mL of demineralized water and immediately frozen at -20°C. Nitrate was measured in the supernatant after thawing and centrifugation, as described above. The bacterial biovolume was calculated based on the average measured diameter (15 µm) and assuming a filament length of 70 µm. Based on this estimated biovolume of filaments, and assuming that 80% of the cell consists of vacuoles, the average vacuolar nitrate concentrations was 51 ± 23 mmol L^{-1}.
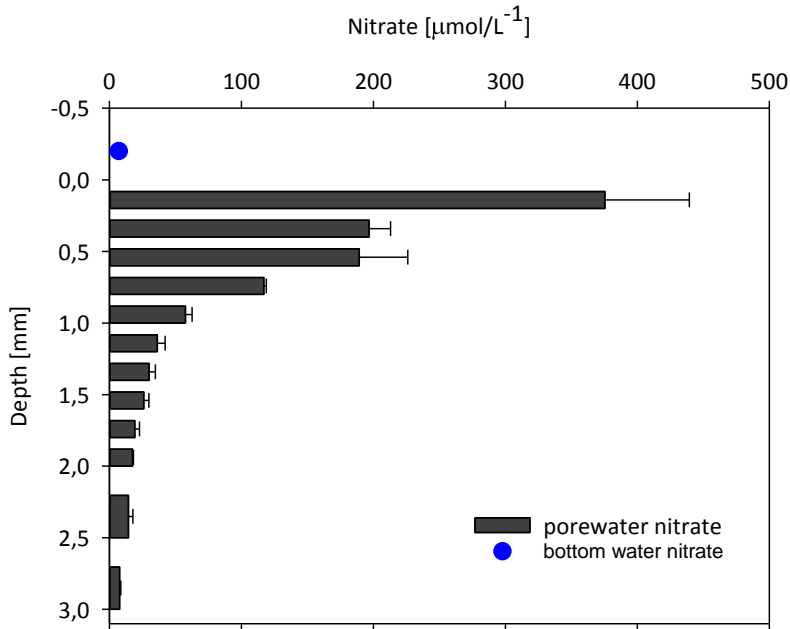
Figure S4. Nitrate concentrations (dark gray bars) in the pore water after lysis of nitrate-accumulating cells, during *Beggiatoaceae* dominance. The nitrate concentrations in the pore water were substantially (up to ~50 times) higher than in the overlying water (blue dot), suggesting intracellular nitrate accumulation by Beggiatoaceae.

This concentration is slightly lower compared to previous observations in *Beggiatoceae* in coastal sediments , reporting intracellular nitrate concentrations of 73-390 mmol L^{-1} (Mussmann et al. 2003; Preisler et al. 2007; Jørgensen et al. 2010).

4.5.6. Multi-year survey of sulfur oxidation pathways

The relative presence of sulfur oxidation pathways was surveyed each spring and fall over a time span of four years, i.e., from November 2011 to March 2015. Sampling campaigns were performed at multiple locations (3 − 6 sites, always including the current field site) within the deeper basins of Marine Lake Grevelingen (sediments > 15 m water depth subject to seasonal hypoxia; see Fig.S1a). The dominant sulfur oxidation pathway was determined based on the pH typology (Fig. S3), which was confirmed by detailed microscopic observations in a systematic fashion throughout the monthly samplings throughout 2012 at the field site (as discussed above). Three intact sediment cores were collected per site and were used for micro-sensor profiling (O_2, pH and H_2S). Each set of micro-sensor depth profiles was classified into one of three categories: (1) electrogenic

sulfur oxidation by cable bacteria as (Fig. 2a); (2) sulfur oxidation by nitrate-accumulating *Beggiatoaceae* (Fig. 2b); (3) "other", which contained micro-sensor depth profiles that did not unambiguously fit the categories (1) or (2). Note that only profiles which had a clear signature were classified in categories (1) and (2), and so when uncertain, the profile set was attributed to category (3). The relative abundance of sulfur oxidation pathways was calculated as the percentage of each category recorded during each campaign (Fig 3).

4.5.7.   <u>Ruling out alternative mechanisms of FeS to FeOOH conversion</u>

The depletion of the FeS pool in the uppermost 3.5 cm and concurrent accumulation of iron (hydr)oxides sediment in spring suggests that a conversion of FeS to FeOOH has taken place. As already noted above, we attribute this conversion to dissolution of FeS by the acid-generating metabolism of the cable bacteria, followed by aerobic oxidation of ferrous iron in the oxic surface sediment. We now examine the likelihood of two alternative mechanisms for FeOOH accumulation in the surface sediment in winter.

Storm-induced resuspension events in winter. If a resuspension event would occur, then any FeS in the surface sediment layer would be suspended in an oxic water column and could be oxidized to FeOOH. However, there are two arguments that speak against this mechanism. Firstly, if a resuspension event would cause the FeS to FeOOH oxidation, then after settling, the FeOOH formed would be uniformly distributed over the depth horizon over which FeS is depleted (~3.5 cm). However, our data show no such uniform FeOOH distribution with depth, but rather a local accumulation of FeOOH right at the sediment surface. The latter observation is hence not consistent with resuspension, but is consistent with the colonization depth of cable bacteria. The FeS to FeOOH hence is driven by dissolution of FeS by cable bacteria, subsequent diffusion of Fe^{2+} to the oxic zone, and oxidation and re-precipitation of FeOOH near the sediment. Secondly, these resuspension events cannot explain the observed growth of a dense cable bacteria population. If an FeOOH-rich surface layer would already be present prior to the presence of the cable bacteria, the development of cable bacteria would likely be hampered, as there would be no longer a source of free sulfide (their primary electron donor). Previous studies have shown that FeS dissolution and sulfate reduction are the two sources of sulfide for the e-SOx metabolism (16). If the sediment fully consists of FeOOH, it is difficult to perform e-SOx, as there is no FeS reservoir to dissolve, and no sulfate reduction ongoing (as dissimilatory iron conduction would outcompete sulfate reduction).

Strong seasonal sedimentation of allochtonous iron oxides. Given the strong accumulation of sediment at the field site, there is clearly a flux of mineral iron to the sediment jointly with other detrital matter. Lake Grevelingen is closed off from river input by a dam, and hence receives is no significant input of terrigeneous matter. However, Lake Grevelingen is in communication with the open sea via a sluice, which allows the exchange of water with the North Sea (37). Hence, the high sedimentation rates are explained by lateral input of detrital matter from the adjacent North Sea, which then settles in the more

quiescent Grevelingen, and accumulates in the deeper basins through local sediment focusing. However, seasonality in the deposition of iron minerals cannot explain the observed depth distributions of FeS and FeOOH. If deposition would be the driver, rather than the oxidation of FeS to FeOOH, then one needs a strong difference in the composition of settling particles between spring (low FeS, high FeOOH) and fall (high FeS, low FeOOH). However, in both seasons, the water column is oxygenated, and so strong differences in the composition of settling particles are unlikely. Moreover, the depth profiles of suspended matter in the water column showed no seasonality throughout 2012, which rules out strong seasonality in sedimentation. Secondly, the depth layer affected by the switch between FeOOH and FeS extends down to 3.5 cm, which far exceeds the accumulation depth over the six-month between November and March (< 1 cm). In conclusion, we contend that deposition or depositional changes cannot explain the observed depth distributions of FeS and FeOOH.

Lake Grevelingen

Photo: Silvia Hidalgo Martinez

Cable Bacteria Control Iron-Phosphorus Dynamics in Sediments of a Coastal Hypoxic Basin

Fatimah Sulu-Gambari, Dorina Seitaj, Filip J. R. Meysman, Regina Schauer, Lubos Polerecky, Caroline P. Slomp

Abstract

Phosphorus is an essential nutrient for life. The release of phosphorus from sediments is critical in sustaining phytoplankton growth in many aquatic systems and is pivotal to eutrophication and the development of bottom-water hypoxia. Conventionally, sediment phosphorus release is thought to be controlled by changes in iron-oxide reduction driven by variations in external environmental factors, such as organic matter input and bottom-water oxygen. Here, we show that internal shifts in microbial communities, and specifically the population dynamics of cable bacteria, also can induce strong seasonality in sedimentary iron-phosphorus dynamics. Field observations in a seasonally hypoxic coastal basin demonstrate that the long-range electrogenic metabolism of cable bacteria leads to a dissolution of iron sulfides in winter and spring. Subsequent oxidation of the mobilised ferrous iron with manganese oxides results in a large stock of iron-oxide-bound phosphorus below the oxic zone. In summer, when bottom-water hypoxia develops and cable bacteria are undetectable, the phosphorus associated with these iron-oxides is released, strongly increasing phosphorus availability in the water column. Future research should elucidate whether formation of iron oxide-bound phosphorus driven by cable bacteria, as observed in this study, contributes to the seasonality in iron-phosphorus cycling in aquatic sediments worldwide.

5.1. Introduction

Phosphorus (P) is a necessary constituent of organic bio-molecules such as DNA and RNA, phospholipids and ATP (Ruttenberg 2014), and may limit phytoplankton growth in both freshwater and marine ecosystems. In coastal waters, river input is typically the primary P source, while burial in sediments is the major sink. In systems subject to excessive nutrient input, which are often characterized by hypoxic bottom-waters ($O_2 < 63$ µM), P is readily remobilized from sediments (Rozan et al. 2002) . This 'internal' source of P may fuel a high primary productivity in surface waters, which then can sustain bottom-water hypoxia, even when riverine P inputs are reduced (Gustafsson et al. 2012). Phosphorus recycling from sediments has been shown to hamper recovery of coastal 'dead zones' that have developed worldwide over the past decades due to anthropogenic eutrophication (Diaz and Rosenberg 2008; Middelburg and Levin 2009).

The release of P from sediments during seasonal hypoxia is typically assumed to be the combined result of the release of P upon reductive-dissolution of iron (Fe)(oxyhydr)oxides (Mortimer 1941) (henceforth referred to as Fe-oxides) and of P stored as polyphosphate in microbial cells during oxic conditions (Gächter et al. 1988) and from degrading organic matter (OM). Conventionally, changes in sediment Fe and sulfur (S) redox chemistry are thought to be driven by seasonal variation in factors external to the sediment. In this model, increased inputs of OM, temperature-dependent stratification of the water column and a subsequent decline in bottom-water oxygen in summer, induce high sulfate-reduction rates and the conversion of sediment Fe-oxides to Fe-sulfides, leaving fewer Fe-oxides to bind P (Jensen et al. 1995; Rozan et al. 2002). Upon re-oxygenation of the surface sediment in fall and winter, the Fe-sulfides are thought to be oxidized mostly by oxygen, creating Fe-oxides that can sequester P (Schulz and Schulz 2005; Dale et al. 2013; Ruttenberg 2014). Furthermore, large sulfur-oxidizing bacteria, like *Thiomargarita* and *Beggiatoa,* are known to accumulate considerable amounts of P as polyphosphate inclusions (Schulz and Schulz 2005). The release of such intracellular reserves has been suggested to enhance benthic release of P during summer in seasonally-hypoxic sediments (Dale et al. 2013).

Recently, a novel mode of electrogenic sedimentary sulfide oxidation was described involving filamentous bacteria of the *Desulfobulbaceae* family (Nielsen et al. 2010). These cable bacteria are able to link the oxidation of free sulfide in deep anoxic sediment layers to the reduction of oxygen (Risgaard-Petersen et al. 2012; Pfeffer et al. 2012; Schauer et al. 2014) or nitrate (NO_3^-) (Marzocchi et al. 2014) in surface sediments, by shuttling electrons over centimeter-scale distances. Electrogenic sulfur oxidation by cable bacteria occurs in a wide range of marine sediments (Malkin et al. 2014), where it has the potential to strongly impact the sediment geochemistry (Risgaard-Petersen et al. 2012; Meysman et al. 2015). Laboratory experiments demonstrate that electrogenic sulfur oxidation induces acidification of the pore-water, resulting in dissolution of iron-mono-sulfide (FeS) and calcium carbonate ($CaCO_3$) in deeper sediment horizons (Risgaard-Petersen et al. 2012). In these experiments, the released Fe^{2+} partly diffused upwards to the oxic zone where it was

oxidized as Fe-oxides ($Fe(OH)_3$), and partly to deeper sulfidic layers, where it re-precipitated as FeS. Cable bacteria hence have the potential to substantially alter Fe- and S-cycling in natural sediments. However, the extent to which this occurs in the field and the possible impact on sediment P-dynamics are still completely unknown.

Here we present field data from a coastal marine basin, which demonstrate a direct link between seasonal changes in cable bacteria abundance, the formation and dissolution of FeS, and sedimentary P-dynamics.

5.2. Materials and Methods

5.2.1. Location

Our study site is a 34 m-deep basin in a marine lake (salinity ~32) in the Netherlands, with rapidly accumulating organic-rich sediments (~2 cm/yr) (Malkin et al. 2014). The water column in Lake Grevelingen is seasonally stratified (Hagens et al. 2015), which induces bottom-water O_2-depletion in summer. In 2012, oxygenated bottom-waters prevailed from January to May, followed by hypoxia from June to July, anoxia in August and the return of oxygen from September onwards (Figure 1).

5.3. Sediment and pore-water sampling

Sediment cores were collected monthly on the RV Luctor in 2012 with a gravity corer (UWITEC, Austria), using transparent PVC core-liners with 60-mm inner diameters. Each month, one core was sliced at high resolution (0.5 cm slices over 10 cm) in a N_2-purged glove-bag. Bottom-water samples were collected from the overlying water in each core. The pore-water was extracted from the sediment using centrifugation (15 min. at 4500 g). Bottom-water and pore-water samples were filtered (0.45 µm) and sub-sampled under N_2. Sub-samples for total dissolved P, Fe, Mn and Ca were acidified (37% HCl, 10 µl per ml) and analyzed with ICP-OES (Perkin Elmer Optima 3000). Pore-water analyses of P with ICP-OES and colorimetrically with a nutrient auto-analyzer (Bran and Luebbe) (Strickland and Parsons 1972), were compared for one sampling outing and found to be nearly identical, indicating most pore-water P is present as dissolved inorganic P. Sulfate was measured using a Dionex Ion Chromatograph. The relative accuracy and precision of the analyses above, as established from standards and duplicates, was always <5%.

Centrifuged sediment samples were freeze-dried, then ground in a N_2-purged glove-box. Total sediment Mn was determined by ICP-OES, following acid destruction with HF-HNO_3 (Kraal et al. 2009) . Sediment P was fractionated into exchangeable P, Fe-bound P, authigenic Ca-P, detrital P and organic P using a modified SEDEX extraction procedure (Ruttenberg 1992; Kraal et al. 2009). The relative error in the P speciation, based on duplicate analyses, was generally <5% with the exception of the detrital P and Fe-bound P, which had an error <15%. Sediment sulfur fractions were separated using the extraction method by Burton et al. (2008) and modified as described in Kraal et al. (2013). Acid-

volatile sulfur (AVS) and chromium-reducible sulfur (CRS) fractions were quantified using iodometric titrations, where duplicate samples varied less than 10% for AVS and less than 8% for CRS.

Pore-water micro-profile measurements were conducted on intact sediment cores (n = 3) within a few hours of retrieval. Profiling was conducted using commercial micro-sensors operated with a motorised micromanipulator (Unisense A.S., Denmark). Depth-profiles of O_2 (25 or 50 µm tip-diameter; detection limit < 1 µM), H_2S (50 µm tip-diameter; detection limit < 1 µM) and pH (100 or 200 µm tip-diameter electrode) were recorded following standard calibration procedures (for O_2 a 2-point calibration in air-saturated seawater (100% saturation) and at depth in anoxic sediment (0% saturation); for H_2S, a 5-point standard curve using freshly-prepared Na_2S standards; for pH, 3 NBS standards and TRIS buffer to correct for salinity, where pH values were reported on a total scale). Total H_2S ($\Sigma H_2S = H_2S + HS^-$) was calculated as in Malkin et al. (2014).

5.3.1. Bacterial Characterization

Microscopic identification of cable bacteria filaments (March, May, August and November 2012) was performed by Fluorescence In Situ Hybridization (FISH), using a *Desulfobulbaceae*-specific oligonucleotide probe[25] (DSB706; 5′-ACC CGT ATT CCT CCC GAT-3′), after staining with DAPI (1 mg/ml), as described in Schauer et al. (2014) and references therein.

To determine the biovolume of *Beggiatoaceae* filaments, intact sediment cores were sectioned within 24 hours of retrieval, at 5 mm depth for the first 4 cm and subsampled (20-30 mg) as described in chapter 4. The biovolume was determined from the length (×10) and width (×40) of all filaments found in the sample (Jørgensen et al. 2010). Cable bacteria biovolumes (mm^3 cm^{-3}) were calculated from measured filament lengths and diameters and integrated over all eight sediment layers. Polyphosphate inclusions in DAPI-stained cable bacteria and *Beggiatoaceae* filaments were visualized with a fluorescent light microscope (Leica DM4500) and identified based on visual appearance (Jørgensen et al. 2010).

5.3.2. Water Column Sampling

Discrete bottom-water samples were collected with a 12 L Niskin bottle at 32 m water-depth, and transferred from the bottle using Tygon® tubing. Bottom-water O_2 concentrations were measured by an automated Winkler titration procedure with potentiometric end-point detection (Mettler Toledo DL50 titrator and a platinum redox electrode) as described in Knap et al. (1994).

Water column subsamples were analyzed for dissolved inorganic phosphate (PO_4) on a nutrient auto-analyzer (Seal QuAAtro). Additional discrete water samples (2.5 L) were filtered (0.7 µm Whatman® glass microfiber GF/F filters) for SPM using a setup that was adjusted (vacuum-sealed) when the bottom-water became anoxic. SPM samples were then freeze-dried and fractionated for P-phases according to the modified SEDEX procedure discussed above.

5.3.3.   Flux Measurements and Calculations

Benthic fluxes of PO_4 from the sediment into the overlying water were measured in intact cores (triplicates) in shipboard closed-chamber incubations. The depth of the overlying water in each core was adjusted immediately upon retrieval to 18-20 cm above the sediment, and the water was subsequently replaced with ambient bottom-water. Replacement was conducted with minimal disturbance to the sediment, via a gas-tight tube, to prevent gas exchange with the atmosphere. Cores were promptly sealed with gas-tight lids, transferred to a temperature controlled-container and incubated at *in situ* temperature. Lids contained two sampling ports and a central stirrer to homogenize the water. Six-hour and 18-hour incubation periods were applied during summer and winter, respectively. Water samples were collected from each core at regular intervals (5 times) and fluxes were calculated as the change in $[PO_4]$ during the incubation, accounting for the enclosed sediment area and overlying water volume. Diffusive PO_4-fluxes were calculated using Fick's first law, using the dissolved $[PO_4]$ in the first 0.5 cm sediment depth interval and bottom-water $[PO_4]$ (Figure S8).

5.3.4.   Polyphosphate Quantification

Intracellular P-content of individual cable bacteria cells was estimated using nanometer-scale secondary ion mass spectrometry (NanoSIMS). The analysis was performed as described by Vasquez-Cardenas et al. (2015), using a NanoSIMS 50L instrument (Cameca, France). Filaments, hand-picked from sediment-cores treated with ^{13}C-labeled bicarbonate and propionate, were analyzed for counts of secondary ions, subsequently used to calculate the P/C ratio and the intracellular P-content of the cells. Overall, three to eight different filaments were analyzed from each treatment and zone (Supplementary Information, 1.8; Figure S9).

5.4. Results and Discussion

5.4.1.   Biogeochemical Signals of Bacteria.

In both spring and fall, a suboxic zone devoid of oxygen and free sulfide developed in the surface sediment. The suboxic zone extended from 1.5 to ca. 18 mm and 0.4 to ca. 10 mm in March and November, respectively. Microscopic examination of the sediment using Fluorescence In Situ Hybridization (FISH) revealed the presence of cable bacteria in spring, down to 40 mm depth. Micro-sensor depth-profiles of O_2, ΣH_2S and pH showed the characteristic geochemical signature of electrogenic sulfur oxidation (Risgaard-Petersen et al. 2012; Meysman et al. 2015) with a high pH near the sediment surface due to proton consumption via the reduction of oxygen ($O_2 + 4e^- + 4H^+ \rightarrow 2H_2O$), and a low pH in deeper, suboxic sediment due to proton production by the oxidation of sulfide ($0.5H_2S + 2H_2O \rightarrow 0.5SO_4^{2-} + 4e^- + 5H^+$). The absence of a distinct pH peak is consistent with high electrogenic activity in sediments characterized by a shallow oxygen-penetration-depth (chapter 4).
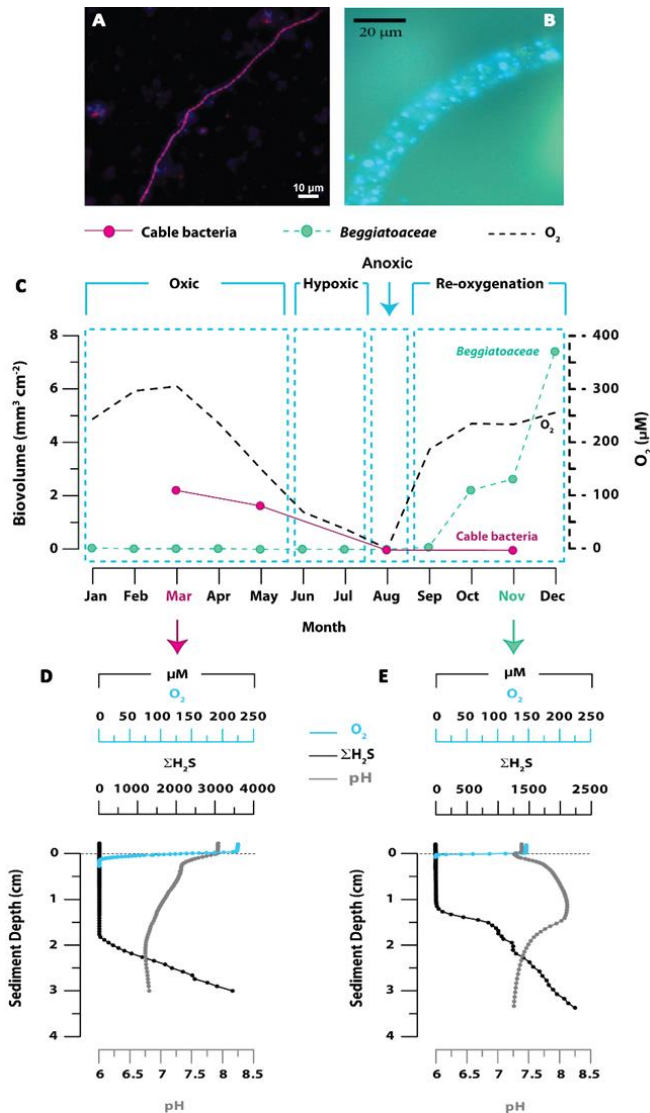
Figure 1. (A) FISH image of filamentous cable bacteria (probe DSB706). (B) *Beggiatoaceae* filament stained with DAPI as viewed with a fluorescent light microscope (Leica DM4500). (C) Temporal changes in oxygen concentrations in the bottom-water and bacterial succession at the sediment surface in 2012. The abundance of cable bacteria (pink dots) was determined in March, May, August and November only, whereas for *Beggiatoaceae* (green dots), data were obtained for each sampling month. Micro-sensor profiles of oxygen, hydrogen sulfide and pH in sediment pore water in March (D) and November (E). Cable bacteria fingerprints are characterized by a broad subsurface pH-minimum while *Beggiatoaceae* create a broad pH-maximum in the suboxic zone, reflecting the effect of bacterial succession on sediment pore-water chemistry, as both bacteria induce the formation of oxygen- and sulfide-free suboxic zones.

The abundance of active cable bacteria, as reflected by pore-water sulfate (SO_4^{2-}) profiles (Figure S1) and biovolumes (Figure 1c), declined from June onwards with the onset of hypoxia. The geochemical response to shallow-cutting of the sediment confirmed that cable bacteria were metabolically-active and the dominant sulfur-oxidizers in spring (Vasquez-Cardenas et al. 2015). After summer hypoxia, tufts of large motile S-accumulating sulfur-oxidizing bacteria (*Beggiatoaceae*) were present at the sediment surface from September to December, with extensive mat formation from October onwards (Figure 1).

Beggiatoaceae filaments were detected down to a depth of ca. 20mm in the sediment (chapter 4). Micro-sensor profiles in fall were consistent with the metabolic activity of *Beggiatoaceae*, with a suboxic zone that is characterized by a broad pH-maximum, which is most likely the result of H_2S-oxidation with nitrate ($4HS^- + NO_3^- + 6H^+ \rightarrow 4S^0 + NH_4^+ + 3H_2O$) (Sayama et al. 2005). Seasonal surveys over the period 2011-2015 show that cable bacteria are replaced by *Beggiatoaceae* in fall nearly every year. The reasons for this population shift, however, are not yet fully understood (chapter 4).
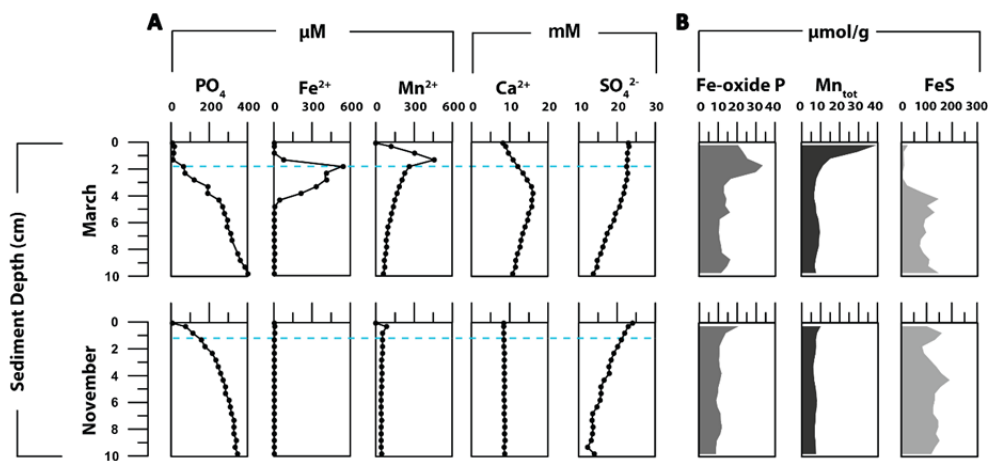
Figure 2. (A) Pore-water [PO_4], [Fe^{2+}], [Mn^{2+}], [Ca^{2+}] and [SO_4^{2-}] for March 2012, when cable bacteria are present and November 2012, when *Beggiatoaceae* are abundant in the sediment. Dashed lines indicate the depths below which hydrogen sulfide is detectable. (B) Solid-phase Fe-bound P, total Mn (Mn_{tot}), and FeS for March and November 2012.

Whether cable bacteria or *Beggiatoaceae* are the dominant sulfur-oxidizing micro-organisms has major implications for sediment Fe, S and P-dynamics at the field site. In March, profiles of pore-water Fe^{2+}, Ca^{2+} and SO_4^{2-} (Figure 2a) and sediment FeS (Figure 2b) are in line with strong dissolution of FeS and $CaCO_3$ by cable bacteria (Risgaard-

Petersen et al. 2012; Meysman et al. 2015). In contrast to previous laboratory experiments (Risgaard-Petersen et al. 2012), the dissolved Fe^{2+}, which is remobilized and diffuses upwards, does not reach the oxic sediment surface (Figure 2a), and so, iron oxidation cannot proceed aerobically. Although there is NO_3^- in the bottom-water (30 µM) (Hagens et al. 2015), iron oxidation coupled to nitrate reduction (Straub et al. 1996) is unlikely, given that the potential downward-diffusive flux of nitrate can only explain ~27% of the Fe-removal (Supplementary Information, 1.4). Instead, we propose that upward-diffusing Fe^{2+} is largely oxidized by manganese oxides (MnO_2), which are abundant in the surface sediment in March (ca. 40 µmol/g, Figure 2b; $2Fe^{2+} + MnO_2 + 2H_2O \rightarrow 2FeOOH + Mn^{2+} + 2H^+$). Consequently, Mn^{2+} accumulates in the pore-water (Figure 2a) and MnO_2 is lost from the sediment (Figure S2). Upward-diffusing PO_4, produced deeper in the sediment is removed from the pore-water through the association of P with the newly-formed Fe-oxides in the suboxic zone (Figure 2b; Figures S3, S4 and S5). In November, the dominance of *Beggiatoaceae* results in pore-water profiles typical for anoxic, sulfidic sediments, with a gradually-increasing phosphate (PO_4) concentration. Profiles of dissolved Fe^{2+}, Mn^{2+} and Ca^{2+} show little change with depth in the sediment. Sulfate concentrations decrease gradually with depth, indicating sulfate reduction. Iron sulfides are present throughout the sediment profile.

5.4.2. **Impact of Cable Bacteria on Fe-P Cycling.**

Our results demonstrate that cable bacteria have a major impact on P dynamics in Lake Grevelingen by promoting the formation of Fe-oxides and removal of pore-water P over a much broader zone than expected based on the penetration of oxygen in such organic-rich sediments. In spring, all P released to the pore-water at depth is sequestered in the sediment as Fe-oxide-bound P (Figure 2). As a consequence, there is little sediment-water exchange of phosphate (Figure 3). From late spring onwards, bottom-water de-oxygenation during seasonal stratification coincides with increased release of phosphate from the sediment and an increase in water-column phosphate (Figure 3a, b, c). A significant proportion of the phosphate efflux (~20 % for the measured flux, 40% for the calculated flux) in late spring and summer (May to August) can be explained by changes in the sedimentary pool of Fe-oxide-bound P (Figure 3c, d). In fall, when stratification ceases, oxic conditions in the bottom-water are re-established and the surface sediment is colonised by *Beggiatoaceae*. However, little build-up of Fe-oxide-bound P is observed and, critically, the efflux of phosphate from the sediment remains significant (Figure 3c). A similar link between cable bacteria and P sequestration was observed at a second site in the basin (Figures S6 and S7).

Release of P from intracellular polyphosphates in bacteria can also modulate sedimentary P-dynamics (Schulz and Schulz 2005; Dale et al. 2013), yet our data suggest that this does not play a major role at the field site. Microscopic analysis of individual filaments of cable bacteria with nanoSIMS indicates the presence of intracellular polyphosphate accumulations (Figure 4) but the amount of accumulated P is negligible compared to that associated with $Fe(OH)_3$ (0.3 mmol P m^{-2} versus 47.9 mmol P m^{-2};
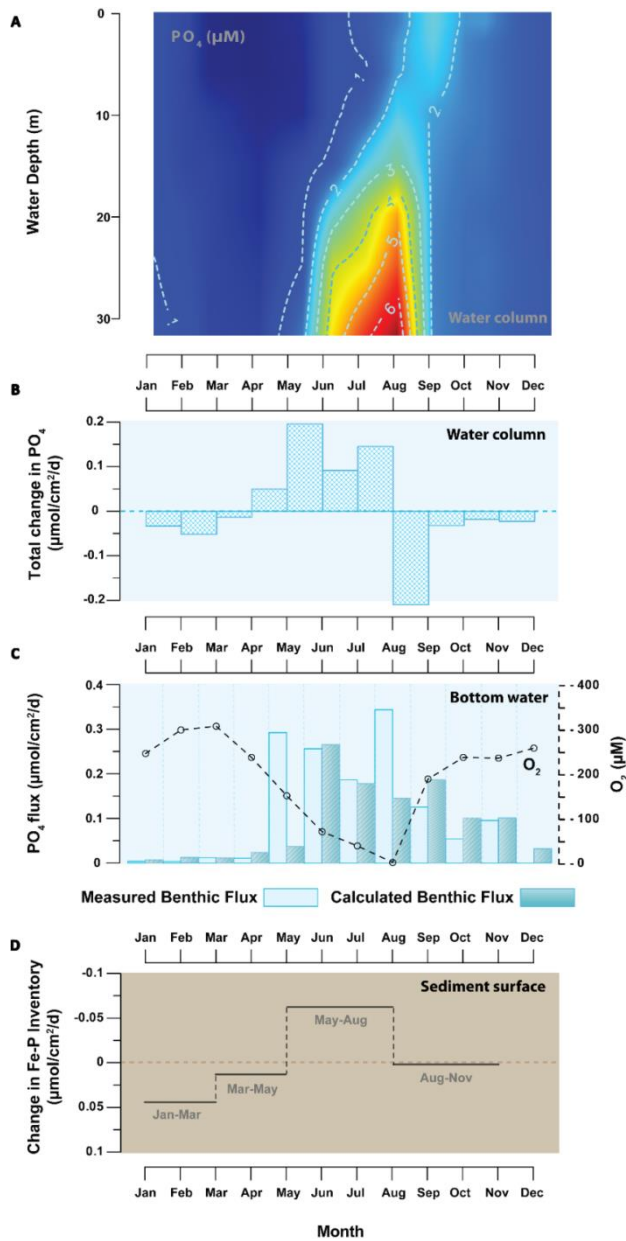
Figure 3. (A) Seasonal change in water column phosphate (in µmol L^{-1}) as a function of water depth (B) Change in phosphate in the water column in 2012 (integrated with depth; µmol cm^{-2} d^{-1}) (C) Flux of phosphate from the sediment to the water column as measured in incubations (also see Table S2) and calculated from pore-water profiles (in µmol cm^{-2} d^{-1}). (D) Change in sediment Fe-P inventory (in µmol cm^{-2} d^{-1}) in the surface sediment (0-4 cm) during 4 periods in 2012 (n.b. y-axis is inverted).

Supplementary Information, 1.8). Although *Beggiatoaceae* also contain intracellular polyphosphates (Figure 1), there is no evidence for a major impact on either the pore-water or solid-phase P-profiles (Supplementary Information, 1.9).

5.1.1. Biogeochemical Implication.

Traditionally, the seasonal build-up of Fe-oxide-P observed in aquatic sediments eg. (Mortimer 1941; Klump and Martens 1981; Rozan et al. 2002) is assumed to be controlled by changes in the input of reactive OM and bottom-water oxygenation. Our data show that cable bacteria are additional key drivers of sediment Fe-oxide-bound P formation, allowing for the conversion of FeS to Fe-oxides over a broad sediment horizon (affecting the upper 20-40 mm). In the absence of cable bacteria, this same Fe conversion process would be primarily governed by seasonal changes in the oxygen penetration depth, which only affects the top 1-2 mm of the sediment.
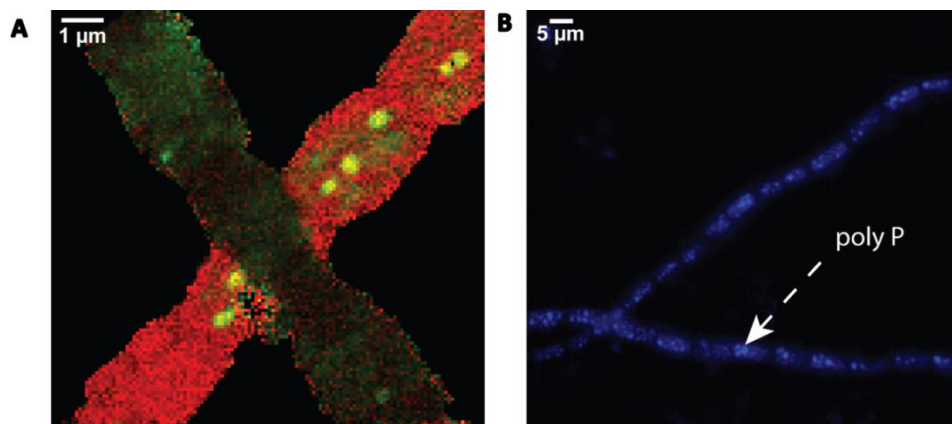
Figure 4. (A) Composite NanoSIMS image of cable bacterial cells treated with ^{13}C-labeled propionate. Intensities of the red and green channels correspond to the values of the $\frac{^{13}C}{C_{tot}}$ and $\frac{^{31}P}{C_{tot}}$ ratios, respectively. The brighter red cells have incorporated propionate and are therefore active, while the darker cells are inactive. The bright-yellow spots correspond to phosphate-rich inclusions. (B) DAPI-stained image of cable bacterial cells from the same core, examined for polyphosphate.

Therefore at our field site, we observe at least a ten-fold increase in conversion of FeS to Fe-oxides when compared to a situation without cable bacteria (Supplementary Information; 1.4). As a consequence, in sediments where cable bacteria are abundant, P retention is highly efficient.

Equally, when their activity ceases, for example due to the establishment of anoxia in the water column, the release of P from the sediment to the overlying water is amplified. Recent work shows that cable bacteria are present in a wide range of sediments, both in marine (Malkin et al. 2014) and freshwater environments (Risgaard-Petersen et al. 2015). This suggests a potential role for cable bacteria in seasonal changes in sediment Fe-P biogeochemistry in such environments and highlights the necessity for further detailed studies on the impact of cable bacteria, especially within the context of the continued worldwide expansion of areas suffering from eutrophication and bottom-water hypoxia (Diaz and Rosenberg 2008).

Supplementary Information

1.1. Monthly Changes in Pore-water Sulfate: Impact of Cable Bacteria

Pore-water depth-profiles of sulfate for January to June 2012 clearly deviate from those recorded for August to December 2012 (Figure S1).
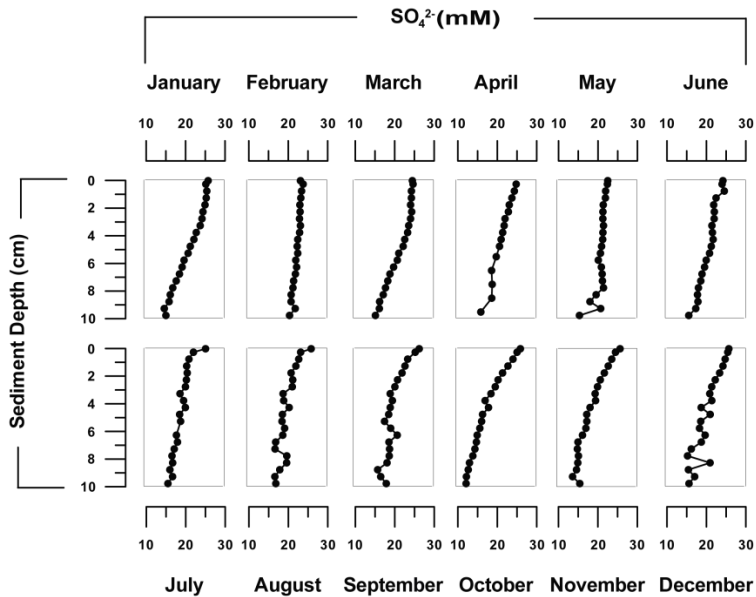
Figure S1: Seasonal variation in the profiles for sulfate in Grevelingen sediments.

The latter set of profiles show the typical decline with depth that is expected for non-bioturbated sediments, i.e. the concave curvature that results from sulfate consumption due to sulfate reduction. The sulfate depth-profiles for January to June 2012 however, either show a convex shape indicative of sulfate production in the upper 4 cm (January, march, June), or a near-linear decline with depth (February, April, May) in some cases, followed by a concave shape in line with sulfate consumption in deeper sediment layers (January, April, June). This characteristic sulfate pore-water profile has been linked to the activity of cable bacteria, based on laboratory experiments[1] and model simulations[2], where the production of sulfate in the top sediment layer results from the dissolution and oxidation of iron sulfides promoted by the strong acidification of the pore-water by cable bacteria activity. The signals for cable bacteria are most clearly developed in January and March.

134

1.2. Seasonal Variation in Solid Phase Manganese

Solid phase Mn is abundantly present in the surface sediment in spring, but is absent in summer and autumn (Figure S2).
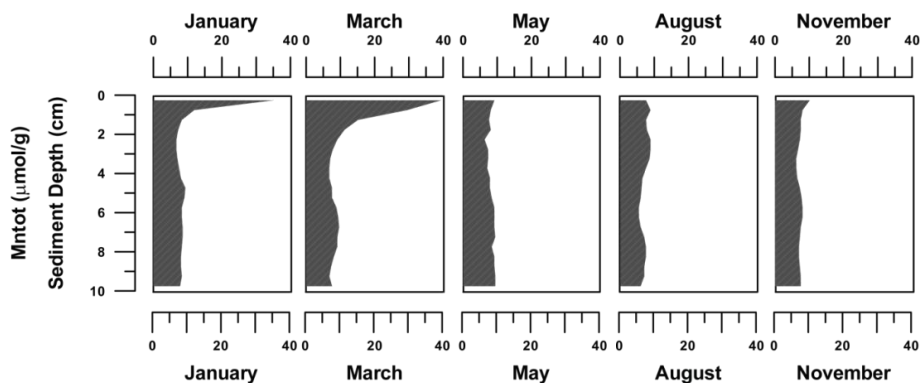
Figure S2: Depth profiles of total manganese in the sediment for January, March, May, August and November 2012, highlighting strong seasonal variation.

1.3. Seasonality in Sediment Phosphorus Forms and Fe sulfide

Depth-profiles of exchangeable P and Fe-oxide bound P in March differ greatly from those in November in 2012, but there is little change in authigenic P, detrital and organic P (Figure S3). There is substantial seasonal variation in Fe-oxide bound P and Fe-S in Grevelingen sediments from January to November 2012, where Fe-oxide-bound P is enriched in FeS-poor sediments in spring (Figure S4). The zone of FeS dissolution extends down to a depth of 2 to 4 cm in spring (Figure S4), despite a very shallow penetration depth of oxygen throughout the year (see Figure 1, chapter 4).
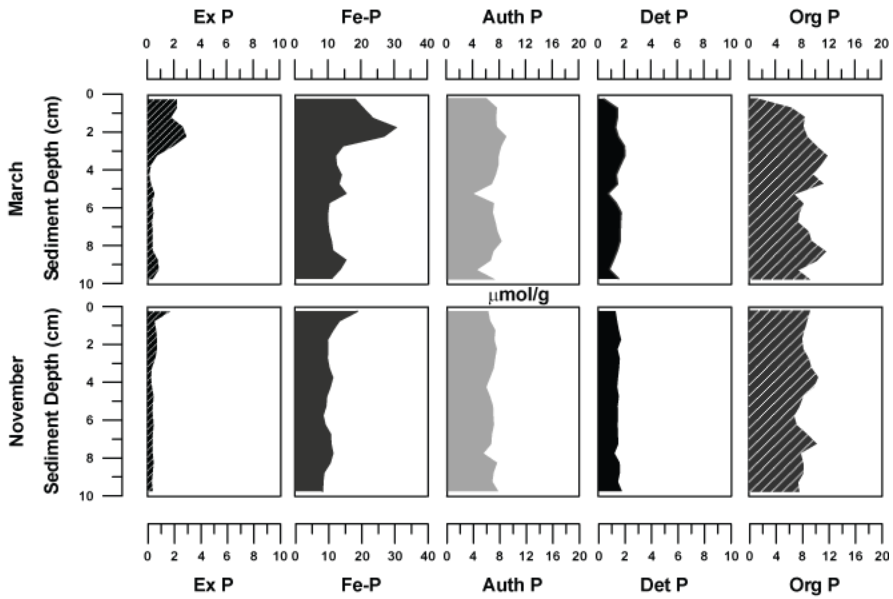
Figure S3: Sediment P forms (in µmol/g) in March and November 2012.
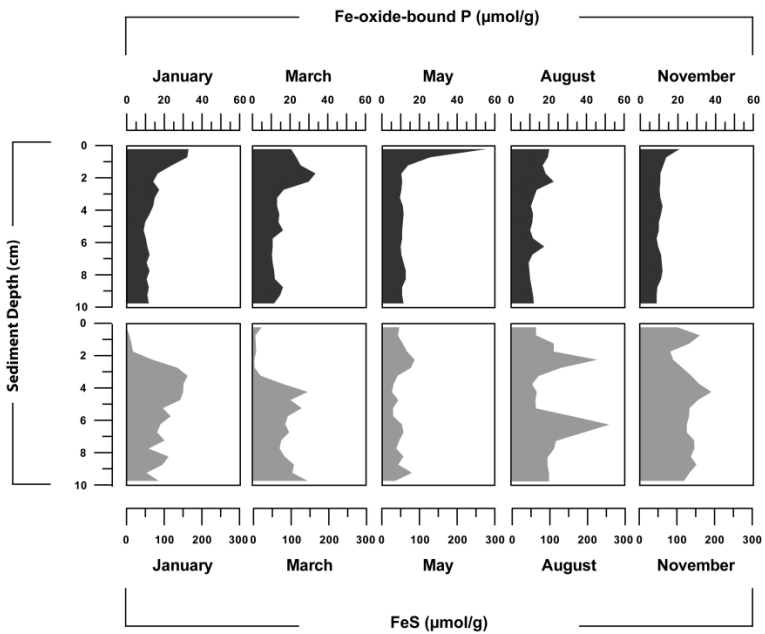
Figure S4: Depth profiles of sediment Fe-P and FeS for January, March, May, August and November 2012.

1.4. Oxidants for Fe^{2+}

Ferrous iron (Fe^{2+}) can be oxidized below the oxic zone with either nitrate or manganese oxide as an oxidant, following:

$$10Fe^{2+} + 2NO_3^- + 24H_2O \rightarrow 10Fe(OH)_3 + N_2 + 8H^+ \qquad (S1)$$

$$2Fe^{2+} + MnO_2 + 2H_2O \rightarrow 2FeOOH + Mn^{2+} + 2H^+ \qquad (S2)$$
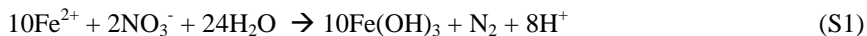
All pore-water Fe^{2+} was removed above 1.25 cm depth in March. Diffusive fluxes of Fe^{2+} and nitrate to the removal zone were calculated using diffusion coefficients taken from Boudreau (1997), corrected for the ambient temperature, salinity and porosity. The diffusive Fe^{2+} flux was estimated from the pore-water gradient in Fe^{2+} (Figure 2) at 4 mmol $m^{-2} d^{-1}$. Using the bottom-water nitrate concentration of 30 µM, and assuming the supply of nitrate through nitrification in this zone to be negligible, the maximum nitrate flux to this zone was estimated at ca. 0.22 mmol $m^{-2} d^{-1}$. Given the 5:1 stoichiometry of the reaction between Fe^{2+} and NO_3^-, this implies that at most 27% of the dissolved Fe^{2+} could be oxidized with nitrate. Manganese oxides are abundantly present in the surface sediment in March (Figures 2 and S2) and concentrations of Mn^{2+} rise with depth where Fe^{2+} is removed. Concentrations of both solutes are of the same order of magnitude. Given the 2:1 stoichiometry of the reaction between Fe^{2+} and MnO_2, this implies that sufficient manganese oxides were present to explain the oxidation of Fe^{2+}.

1.5. Fe-oxide data

Sedimentary Fe fractions were determined using the method of (Poulton and Canfield 2005), where Fe-oxides were estimated as the total of the non-sulphidized Fe pools extracted with a 1 M hydroxylamine-HCl solution in 25% v/v acetic acid and sodium dithionite solution (50 g L^{-1}), buffered to pH 4.8. The contents of Fe oxides were corrected for FeS dissolution, by subtracting the measured sulfide concentration for each sediment interval, determined as Acid Volatile Sulfide (AVS) from the S extractions. Measured Fe concentrations from duplicate analyses varied less than 5%.

There is a build-up of Fe-oxides in the surface sediments between January and March (Figure S5). From May onwards, the Fe oxides start to be removed, although an enrichment near the sediment-water interface is still visible. Low concentrations are observed in November (Figure S5). Changes in background values of Fe-oxides likely reflect spatial variations in the contribution of more refractory Fe-oxides.
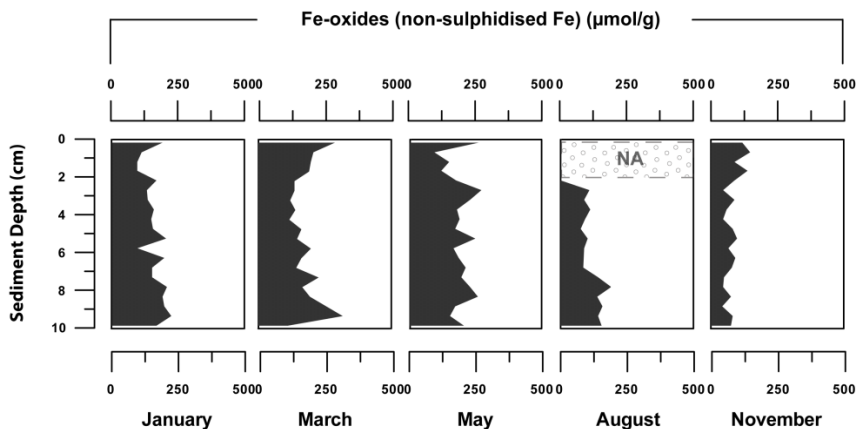
Figure S5: Depth profiles of sediment Fe-oxides for January, March, May, August and November 2012.

1.6. 1.4. Impact of cable bacteria on sedimentary P cycling at a second site in the basin

Data from an additional site (17m) in Lake Grevelingen demonstrate a direct link between seasonal changes in cable bacteria abundance and sedimentary P-dynamics. This shallower location is subject to a significantly lower sedimentation rate (~0.4 cm/yr) than the deeper site. In both spring and fall of 2012, a suboxic zone devoid of oxygen and free sulfide developed in the surface sediment at depths down to 26.1 mm and 18.2 mm respectively.

Microscopic examination of the sediment using Fluorescence In Situ Hybridization (FISH; probe DSB 706) revealed a high abundance of cable bacteria in March and May down to a depth of 40 mm and micro-sensor depth-profiles of O_2, ΣH_2S and pH showed the characteristic geochemical signature of electrogenic sulfursulfur oxidation (Figure S6). Similar to the deeper site, cable bacteria were undetected with the onset of hypoxia and from September onwards, *Beggiatoaceae* were present at the sediment surface. In March there is production of Fe^{2+}, Mn^{2+}, Ca^{2+} and SO_4^{2-} in the pore-water, accompanied by evidence for the removal of PO_4 from the pore-water just above this sedimentary horizon in spring (Figure S7a). Later on in the year, the sediment pore-water profiles are characterized by trends with depth that are typical for hypoxic sediments (Figure S7a).

Total P and total Mn are strongly enriched in the surface sediment in spring, a feature which is absent in November (Figure S7b). In March, sediment concentrations of total sulfur (Stot) decrease towards the sediment-water interface, consistent with dissolution of Fe-sulfides in the suboxic zone. In November, under more reducing sediment conditions and in the absence of cable bacteria, sulfur in the surface sediment is replenished (Figure S7b).
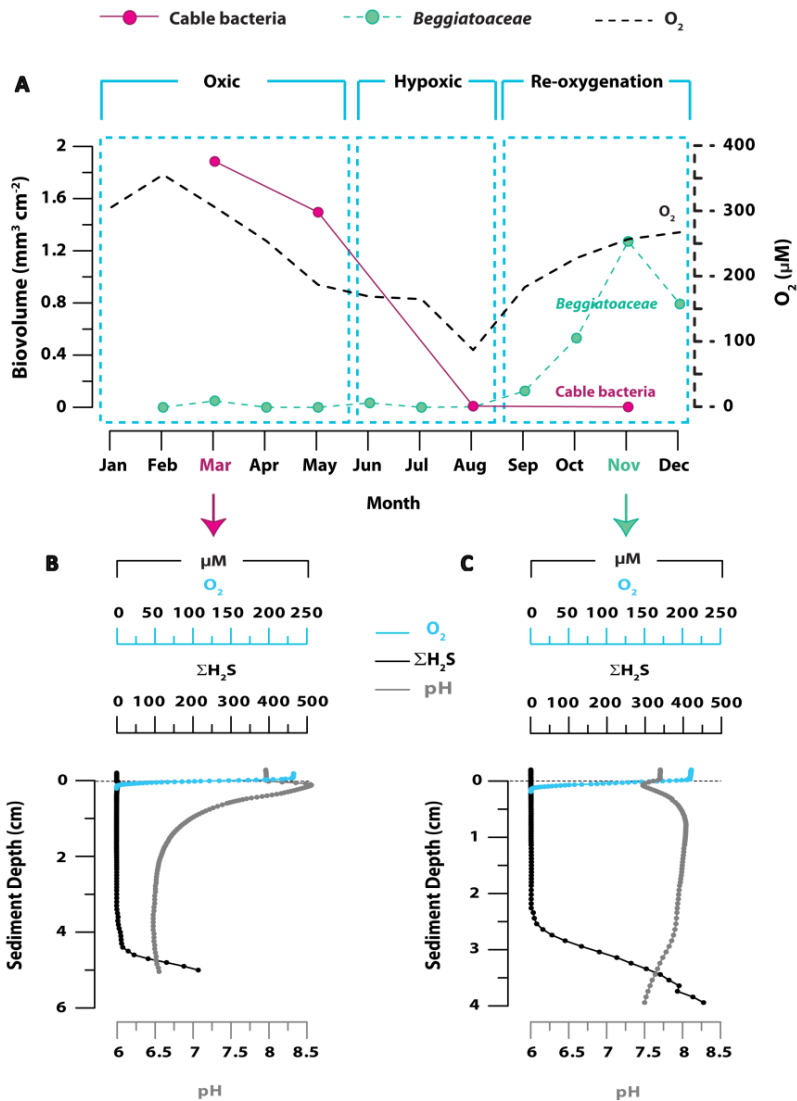
Figure S6: (A) Temporal changes in oxygen concentrations in the bottom-water and bacterial succession at the sediment surface at an additional site (17m) in 2012. The abundance of cable bacteria filaments (pink dots) was determined in March, May, August and November only, whereas for *Beggiatoaceae* (green dots) data were obtained for each sampling month. Micro-sensor profiles of oxygen, hydrogen sulfide and pH in sediment pore-water in March (B) and November (C) for the site at 17m-depth. Cable bacteria fingerprints are characterized by a broad subsurface pH-minimum while *Beggiatoaceae* create a broad pH-maximum in the suboxic zone, reflecting the effect of bacterial succession on sediment pore-water chemistry at this site, as both types of bacteria induce the formation of oxygen- and sulfide-free suboxic zones.
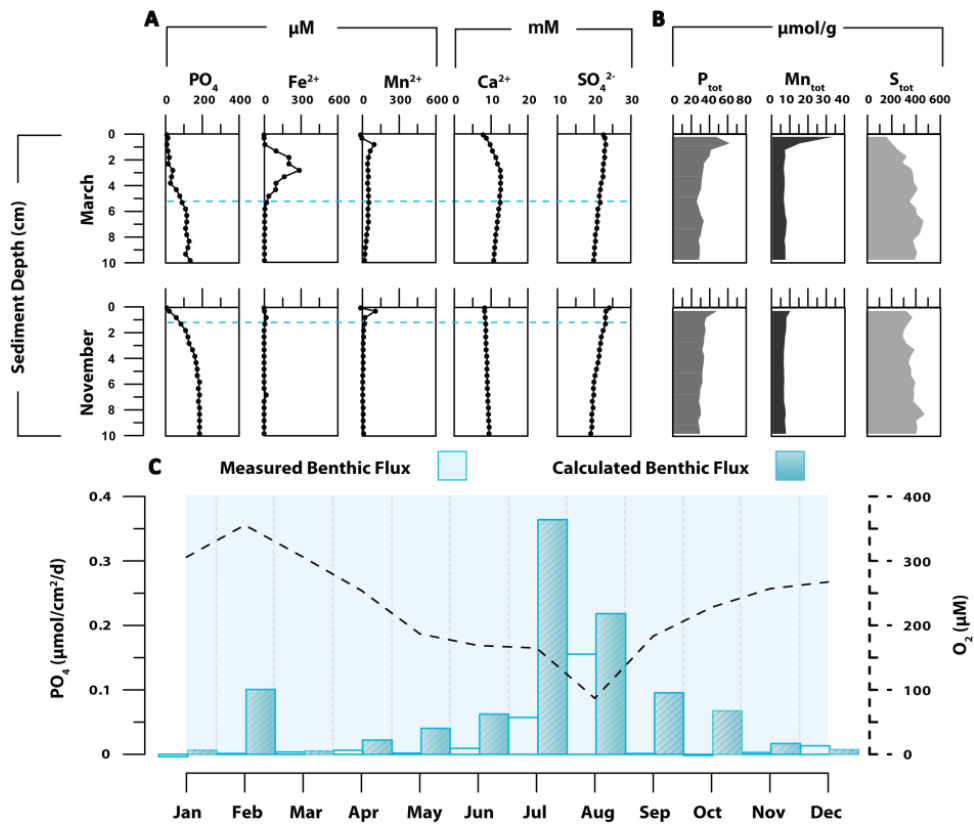
Figure S7: Geochemical imprint of cable bacteria at an additional site (17m). (A) Pore-water [PO_4], [Fe^{2+}], [Mn^{2+}], [Ca^{2+}] and [SO_4^{2-}] for March 2012, when cable bacteria are present and November 2012, when *Beggiatoaceae* are abundant in the sediment. Dashed lines indicate the depths below which hydrogen sulfide is detectable. (B) Solid-phase total P (P_{tot}), total Mn (Mn_{tot}), and total S (S_{tot}) for March and November 2012. (C) Flux of phosphate from the sediment to the water column as measured in incubations and calculated from pore-water profiles from cores collected at 17m (in μmol cm^{-2} d^{-1}).

Similar to the deep site, there is generally little release of phosphate from the sediment to the overlying water in spring (Figure S7c). From late spring onwards, the decline in bottom-water oxygen during seasonal stratification coincides with increased release of phosphate from the sediment (Figure S7c). Bottom-water PO_4 and O_2 concentrations for 2012 and 2013 in the basin show similar seasonal trends, with low concentrations of PO_4 in the oxygenated bottom-water in spring and elevated concentrations of PO_4 in summer following the onset of hypoxia (Table S1). The larger amplitude of the seasonal change in PO_4 concentrations in 2013 is likely the direct consequence of the lower bottom-water oxygen concentrations in that year. The low bottom-water PO_4 concentrations in spring of

2013 are consistent with retention of PO_4 in the sediment due to activity of the cable bacteria.

Table S1: Temporal changes in oxygen and phosphate concentrations (μmol L^{-1}) in the bottom-water in 2012 and 2013.

Bottom-water conc. (µM)	2012		2013	
	O$_2$	PO$_4$	O$_2$	PO$_4$
Jan	247.82	1.12	260.63	1.18
Feb	300.64	0.95	296.88	1.02
Mar	309.07	0.49	253.13	1.09
Apr	239.07	0.44	303.07	0.15
May	153.13	1.67	188.90	1.89
Jun	72.50	4.51	84.27	3.33
Jul	40.63	5.83	0.00	7.40
Aug	3.44	6.82	0.00	10.80
Sep	190.56	1.77	0.00	11.10
Oct	239.07	1.54	213.67	1.30
Nov	237.54	1.51	225.59	1.76
Dec	259.98	1.32	159.69	2.73

1.7. Benthic Flux Calculations

Diffusive fluxes of phosphate across the sediment-water interface were calculated from the pore-water depth-profiles, as the phosphate concentration gradient between bottom-water and topmost pore-water value (Figure S8). Fluxes were determined using diffusion coefficients taken from Boudreau (1997), corrected for the ambient temperature, salinity and porosity.

1.8. Polyphosphate in Cable Bacteria

Intracellular phosphorus (P) content in individual cells of cable bacteria was estimated using nanometer-scale secondary ion mass spectrometry (NanoSIMS). The analysis was performed as previously described by Vasquez-Cardenas et al. (2015) using a NanoSIMS 50L instrument (Cameca, France) at Utrecht University and the data processing freeware programme, Look@NanoSIMS (Polerecky et al. 2012). Two sediment cores with abundant cable bacteria were incubated with ^{13}C-labeled bicarbonate and propionate. Individual filaments were then hand-picked from the oxic (0-0.2cm depth) and suboxic zones (0.4-2.0 cm depth) and analysed for counts of secondary ions ^{12}C$^-$, ^{13}C$^-$, and ^{31}P$^-$, which were subsequently used to calculate the P/C ratio as $\frac{^{31}P}{(^{12}C + ^{13}C)}$. Overall, three to eight different
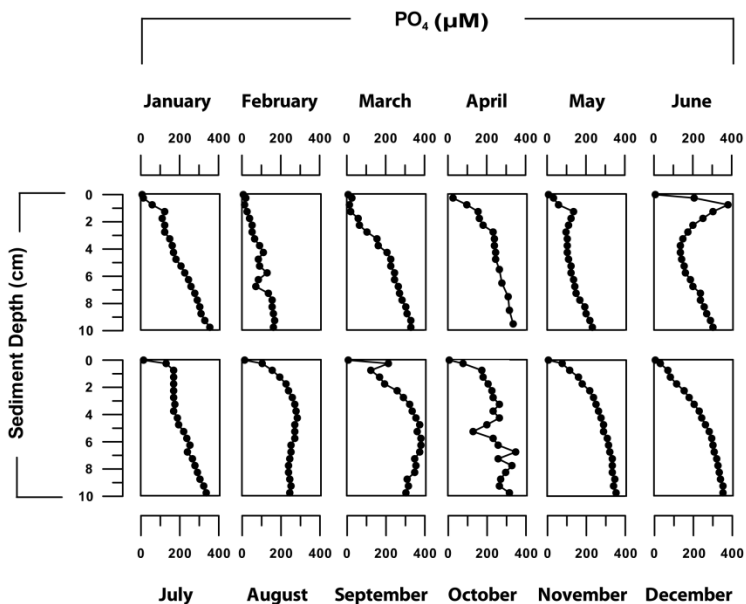
Figure S8: Profiles of pore-water phosphate for each Month in 2012, highlighting a strong seasonality in the retention and release of phosphate in the sediment.

filaments were analysed from each treatment and zone. Only active cells were used in the analysis, where the activity was determined based on their ^{13}C-enrichment in comparison to the control cells (see Vasquez-Cardenas et al. 2015). NanoSIMS images revealed that active cable bacteria contained clear P-rich inclusions (exemplary cells from the suboxic zone of the ^{13}C-proprionate incubation core are shown in Figure 3a). Based on a total of 87 individual cells and 70 P inclusions (Figure S9), we determined that the P/C ratio in inclusions was on average 5.6-fold greater than that of the rest of the cell, and that the area of an inclusion comprised on average 4.2% of the total planar cell area in the nanoSIMS image.

It is known that due to differences in ionisation behaviour of different elements the sensitivity of nanoSIMS generally varies depending on the element and the matrix from which they are mobilised by the primary ion beam. Thus, to calibrate the semi-quantitative nanoSIMS data we assumed that the average P/C ratio determined by nanoSIMS for the cell *without* inclusions (0.022; see red symbols in Figure S2) was equal to the Redfield ratio $\left(\frac{1}{106}\right)$. To make the estimation of the P/C ratio in active cells of the cable bacteria possible, we additionally assumed that this calibration was matrix-independent, i.e., the same when detecting C and P from the material comprising the cell and from the material comprising the P-rich inclusions. Taking into account that there were 2 inclusions on

142

average per cell (e.g. Figure 3a), these assumptions led to the estimated average P/C ratio of the individual cable bacteria cell of $(1 - 2 \times 0.042) \times \frac{1}{106} + 2 \times 0.042 \times \frac{5.6}{106} = 0.0131$, which is about 38% larger than the Redfield ratio.

The cable bacteria biovolume was highest in March 2012 at 2.3 mm^3 cm^{-2}. Using the empirical equation of Loferer-Krossbacher et al. (1998) (dw = 4.35 x V$^{0.86}$, where the dry weight, dw, is calculated in fg and the volume, V, is in µm3) and assuming a cellular carbon content of 50% (Schauer et al. 2014), the cable bacteria biomass was estimated at 20 mmol C m^{-2}. Using the P/C ratio estimated
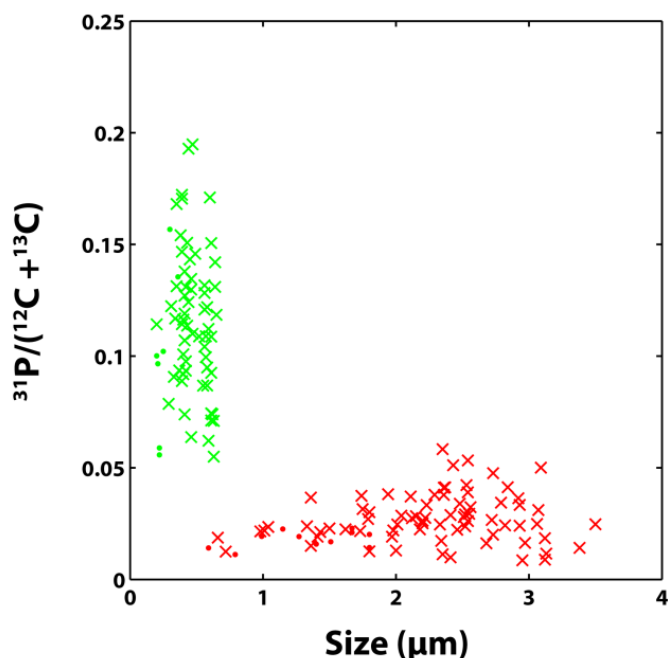
Figure S9: NanoSIMS analysis of P/C ratios for individual cable bacteria cells. Shown are P/C ratios, calculated from the measured secondary-ion counts, versus size (in µm) determined for P-rich inclusions (green) and cells without inclusions (red). Dots and crosses correspond to cells incubated with ^{13}C-bicarbonate and ^{13}C-propionate, respectively.

above, this translates to a P-content of about 0.3 mmol P m^{-2}. Thus the intracellular P-content of active cable bacteria is negligible in comparison to the change in the Fe-P inventory observed from May to August (47.9 mmol P m^{-2}). Note that this conclusion would hold even if the P/C ratio in cable bacteria estimated by nanoSIMS was grossly underestimated. For example, even if the P/C ratio was 10-fold larger than the Redfield

ratio, the sedimentary P content due to cable bacteria would amount to about 1.9 mmol P m^{-2} and would therefore still be unable to explain the observed change in the Fe-P inventory.

1.9. Impact of *Beggiatoaceae* on sedimentary P cycling

The release of large amounts of intracellular phosphate from sulfur-oxidising bacteria such as *Thiomargarita* and *Beggiatoa* can result in formation of apatite in sediments(Schulz and Schulz 2005) and may impact benthic exchange (Dale et al. 2013). Concentrations of authigenic apatite show little change with depth in the sediment (Figure S3) and are comparable to concentrations in suspended matter (e.g., 6.0 and 6.2 µmol/g for March and November, respectively). Moreover, there is no evidence for a significant impact on pore-water profiles of phosphate during months that *Beggiatoaceae* are most abundant (October to December) (Figure 1). This suggests that *Beggiatoaceae* are not significantly impacting sediment-water exchange of P nor are inducing apatite formation in these sediments to a significant extent, confirming earlier suggestions that the reported effect of sulfide-oxidising bacteria on apatite formation (Schulz and Schulz 2005; Goldhammer et al. 2010) is not ubiquitous in hypoxic marine sediments (Mort et al. 2010)**.**

Long Island Sound

Photo: Dorina Seitaj

The paradox of aerobic sulfide oxidation revisited: suboxic zone formation, redox shuttling and cryptic sulfur cycling in marine sediments

Filip J. R. Meysman and Dorina Seitaj

ABSTRACT

Sulfate reduction is the dominant pathway of organic matter mineralization in coastal sediments, and hence, vast amounts of free sulfide are produced in the pore water. Nonetheless, the surface layer of coastal sediments often exhibits a centimeter wide zone, where neither oxygen nor free sulfide are present, indicating that intense sulfide removal processes are taking place. Here we provide a comparative discussion of the three known mechanisms of sulfide removal that can lead to the formation of a suboxic zone. A first mechanism is iron and manganese shuttling enabled by bioturbation. The other two mechanisms are linked to sulfide oxidation carried out by either nitrate-storing *Beggiatoaceae* or electricity-generating cable bacteria. We provide field observations of the geochemical fingerprint from each mechanism, and implement the associated reaction mechanisms into a common reactive transport model. These model simulations reveal that the measured geochemical fingerprint can be faithfully reproduced, and that the three mechanisms can be distinguished through their pH imprint on the pore water. All three processes of suboxic zone formation are critically dependent on the presence of redox shuttling and cryptic sulfur cycling.

6.1. INTRODUCTION

Sulfate reduction is the dominant pathway of organic matter mineralization in coastal sediments, where it accounts for up to 50-75% of the overall oxidation of organic carbon (Jorgensen et al., 1982; Jorgensen, 2004; Glud, 2008). Free sulfide (H_2S) is the principal end-product of sulfate reduction, and hence, vast amounts of free sulfide are formed in marine sediments, which often leads to substantial accumulation of free sulfide in the pore water, i.e., up to millimolar levels (Jørgensen and Nelson 2004). Still, free sulfide is typically not released from the sediment to the overlying water. This occurs because in the current oceanic setting, the bottom waters are predominantly characterized by oxidizing redox conditions, and hence, plenty of soluble electron acceptors, such as oxygen (O_2) and nitrate (NO_3^-), are available for sulfide oxidation. These electron acceptors are transported into the sediment either by molecular diffusion, advective percolation induced by waves and currents, or through bio-irrigation by burrowing fauna (Aller 2014). The presence of oxygen or nitrate in the top millimeters of the sediment prevents the escape of free sulfide to the overlying water. At the same time, only a minor fraction (~3%) of the sulfide produced by sulfate reduction escapes to deeper sediments through pyrite burial (Canfield and Farquhar 2009). Because the losses to overlying water and deeper sediments are small, nearly all of the free sulfide that is generated within marine sediments by sulfate reduction must be ultimately re-oxidized back to sulfate (Jørgensen 1977; Canfield and Farquhar 2009).

Oxygen is by far the most dominant electron acceptor used in re-oxidation of reduced sulfur compounds in marine sediments. This is mainly for two main reasons. First, O_2 is thermodynamically the most favorable electron acceptor for microbial sulfur oxidation, as it provides the most free energy per mole of sulfide (Canfield 2005). As a result, micro-organisms performing aerobic oxidation have a competitive advantage over other sulfur oxidizers. Secondly, O_2 is also more readily available than NO_3^-, which is the other potent electron acceptor for sulfide oxidation. The O_2 concentrations in coastal bottom waters (250-300 μmol L^{-1}) are typically an order of magnitude higher than those of NO_3^- (10-30 μmol L^{-1}). Therefore in the present-day seafloor, most of free sulfide generated by sulfate reduction is aerobically oxidized, and this transformation can be represented by the overall reaction equation

$$H_2S + 2O_2 \rightarrow SO_4^{2-} + 2H^+ \qquad\qquad (1)$$

This reaction equation however instantly exposes what can be defined as the "aerobic sulfide oxidation paradox". Although O_2 is the principal electron acceptor that oxidizes H_2S, it has been known for long time that in most coastal sediments, the depth profiles of O_2 and H_2S do not overlap (Jørgensen and Postgate 1982). Instead, the more common situation is that a so-called "suboxic zone" is observed, i.e., a distinct sediment horizon where neither O_2 nor H_2S are detectable (Jørgensen and Postgate 1982). Within organic-

rich coastal sediments, this suboxic zone typically ranges from millimeters to centimeters. This raises the intriguing question how aerobic sulfur oxidation can still proceed, when the two key reagents (i.e., O_2 and H_2S) do not occur together.

It needs to be stressed that the aerobic sulfide oxidation paradox is far from a new insight. The problem was already clearly recognized in the early 1980's in the pioneering work of B.B. Jorgensen and coworkers on sulfur cycling in coastal sediments. In a seminal review paper (Jørgensen and Postgate 1982), it was stated that "*It is a general observation, however, that oxygen and sulfide are separated in these sediments by a zone a few centimeters deep in which neither of the two compounds can be detected. How does the oxidation take place?*". This same paper also confronts us with a remarkable bias in our observations, which still persists today: *"Research has instead been focused on the less typical environments where oxygen and sulfide do meet and coexist in detectable concentrations. It should be remembered, however, that these environments are exceptions and that studies of the typical environments of sulfide oxidation are greatly needed.*" (Jørgensen and Postgate 1982).

Furthermore, the "aerobic sulfide oxidation paradox" is no longer a true paradox anymore either. This is in large part due to the work on sulfur cycling in coastal systems by B. B. Jorgensen and co-workers, and so, the research group that first identified the paradox was also instrumental in providing solutions. Over the past few decades, a number of mechanisms have been proposed, via which aerobic oxidation of sulfide can take place in marine sediments, without sulfide and oxygen being present in the same sediment horizon. A first mechanism was uncovered during studies that examined the iron cycling in coastal and shelf sediments (Canfield et al. 1993b; Berg et al. 2003). When sediments are intensively mixed through bioturbation by infauna, oxidized iron minerals are mixed downwards and reduced iron minerals are mixed upwards. This process can create an electron shuttle between H_2S and O_2, thus forming a suboxic zone (Canfield et al. 1993b). A second mechanism emerged from the detailed investigation of the metabolism of large colorless bacteria, such as *Beggiatoa*, *Thioploca* and *Thiomargarita* (Fossing et al. 1995; Thamdrup et al. 1996; Schulz et al. 1999). Through intracellular accumulation of intermediate redox compounds (NO_3^-, elemental sulfur S^0), these large motile bacteria also generate an electron shuttle between H_2S and O_2, which equally leads to a suboxic zone. A third mechanism of suboxic zone formation has only been very recently discovered (Nielsen et al. 2010; Pfeffer et al. 2012; Malkin et al. 2014). It depends on the ability of long, filamentous sulfur-oxidizing bacteria, termed cable bacteria, to transport electrons over centimeters scale distances.

The objective here is to summarize and review our understanding of the "aerobic sulfide oxidation paradox" by putting the three known solutions of the paradox into a single conceptual geochemical framework. In addition, we tackle the important question of how to discern which particular mechanism of suboxic zone formation is active at a given location. In other words, given the observation that a suboxic zone has developed in the sediment,

how to know whether it is caused by bioturbation-driven metal cycling, intracellular redox shuttling by *Beggiatoaceae*, or long-distance electron transport by cable bacteria? We will show that these different mechanisms can be differentiated by their geochemical fingerprint. In other words, there is a characteristic set of pore water concentration depth profiles (O_2, H_2S and pH depth profiles) that uniquely represents each of the mechanisms.

6.2. MATERIAL AND METHODS

6.2.1. Terminology

During the discussion here, we will frequently refer to the terms suboxic zone, redox shuttle and cryptic sulfur cycling. Hence, it is valuable to precisely define the meaning of these concepts upfront. For instance, different definitions and interpretations of the term "suboxic zone" are used in the literature, and this has led to considerable confusion in the past – see the review by (Canfield and Thamdrup 2009), which has put this problem into focus. The confusion about the term "suboxic zone" essentially boils down to a difference between concentrations and rates. The classical view of sequential redox zonation (Froelich et al. 1979), suggests a "rate-based" perspective. In this view, the suboxic zone is defined as the horizon between the zones of oxygen reduction and sulfate reduction, and accordingly, the suboxic zone is a depth horizon where other mineralization pathways (nitrate reduction, Mn and Fe reduction) are active. However, such a rate-based definition is problematic in a number of ways. Firstly, it assumes that the mineralization pathways are strictly segregated with depth, which is often not the case (Canfield and Thamdrup 2009). For example, it has frequently been observed that sulfate reduction and iron reduction occur within the same sediment horizon (e.g. Goldhaber et al. 1977; Canfield et al. 1993), which makes the definition of the suboxic zone in terms of mineralization pathways highly ambiguous. Based on the presence of iron reduction, the sediment horizon would classify as a suboxic zone, yet based on the presence of sulfate reduction, it cannot be a suboxic zone. Secondly, the documentation of a rate-based "suboxic zone" is also operationally difficult, as it requires the carefully delineation of the different mineralization zones in the sediment. This requires detailed reaction rate measurements, which are highly laborious and challenging in comparison to the determination of pore water concentration depth profiles.

Here, we do not define the suboxic zone in terms of mineralization pathways, but in terms of pore water concentrations. The suboxic zone is simply the depth layer where both oxygen and sulfide are undetectably low (Fig. 1a). The oxygen penetration depth (OPD, operationally defined as the depth where $[O_2] < 1$ µmol L^{-1}) and the sulfide appearance depth (SAD, operationally defined as the depth where $[H_2S] > 1$ µmol L^{-1}), hence provide the upper and lower limits of the suboxic zone. Accordingly, our usage of the term suboxic zone does not make any inference about mineralization pathways that are acting. For example, sulfate reduction can take place at sizeable rates within the suboxic zone, although free sulfide is not present.

A redox shuttle refers to a redox transformation, where an intermediate redox compound continuously cycles between oxidized and reduced forms, and the oxidation and reduction steps take place in spatially segregated locations. Figure 1b shows an idealized example, where iron acts as a redox shuttle in between the oxidation of free sulfide and the reduction of oxygen. This redox shuttle is a simplified representation of the redox cycling that goes on in coastal bioturbated sediments (as discussed in more detail below). In a first step (the iron oxidation step), iron oxides (FeOOH) are formed, when ferrous iron comes (Fe^{2+}) into contact with O_2 in the top millimeters of the sediment. In a second step (the iron reduction step), these iron oxides are used to oxidize H_2S in the deeper sediment, thus producing Fe^{2+} again, which makes the cycle complete.
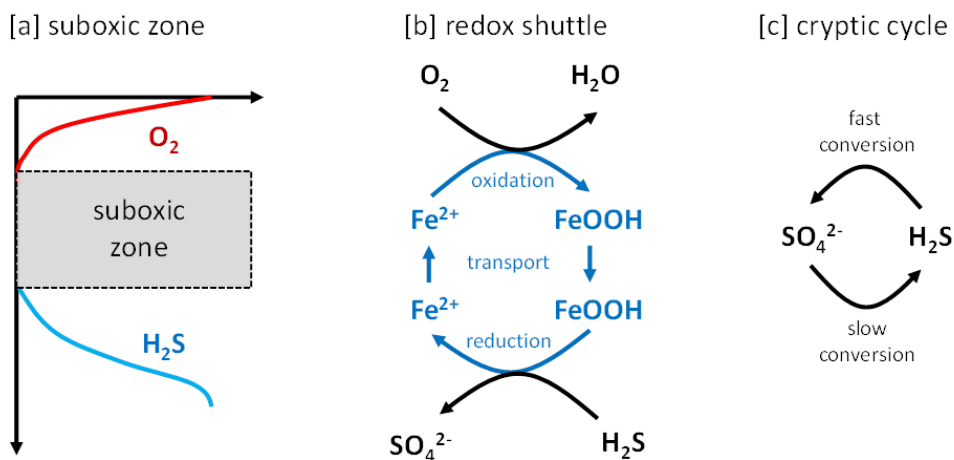
Figure 1. Definition of terminology. (A) The suboxic zone is the depth layer where both oxygen and sulfide are undetectably low. (B) A redox shuttle is a redox transformation, in which an intermediate redox compound continuously cycles between oxidized and reduced forms. The oxidation and reduction steps must take place in different locations. (C) A cryptic cycle occurs when a chemical compound (e.g. H_2S) is produced slowly by one process and rapidly consumed by another process. As a result the compound itself is not detectable in the environment.

The reduced and oxidized iron species thus function as intermediate redox species, shuttling electrons from sulfide to oxygen, hence the name redox shuttle. It is important to note that to obtain a true redox shuttle, the iron oxidation and reduction steps need to occur in different locations (Fig. 1b). Accordingly, one needs a transport mechanism for the oxidized intermediate (e.g. downward mixing of iron oxide particles) as well as for the reduced intermediate (e.g. upward diffusion of ferrous iron). If we combine the reduction and the oxidation steps, the redox shuttle cancels out, and the overall reaction equation is identical to that of aerobic sulfide oxidation Eq. (1).

A cryptic cycle occurs when a chemical compound refers is actively produced and consumed, but the compound itself is not detectable in the environment (Fig. 1c). In recent

years, more and more of these cryptic cycles have been uncovered in both the water column and sediments of the marine environment (Turchyn et al. 2006; Canfield et al. 2010; Holmkvist et al. 2011; Sivan et al. 2014). Here, our discussion will particularly focus on the cryptic cycling of free sulfide within the pore water of marine sediments. In this environment, sulfide is typically produced through sulfate reduction, and hence, free sulfide is expected to accumulate in the pore water. Yet, when free sulfide is immediately and efficiently scavenged by some efficient removal process (e.g. microbial oxidation back to sulfate – see Fig. 1c), the pore water concentration of free sulfide can remain below the detection limit, despite substantial sulfide production. In general, two conditions are required for a cryptic cycle to occur. Firstly, a close spatial coupling between production and consumption processes is needed. Secondly, the oxidative consumption step requires a fast kinetics and a high affinity for free sulfide. Stated otherwise, the production step must be rate limiting, otherwise accumulation would occur in the pore water, and hence, free sulfide would become eventually detectable by common analytical methods. It is important to note the difference between a redox shuttle and a cryptic cycle. Although redox reactions can be involved in cryptic cycling, this must not be necessarily the case (e.g. dissolution and precipitation reactions can also be involved in cryptic cycling).

6.2.2. Dataset

Our goal is here to differentiate four mechanisms of sulfur oxidation by means of their geochemical fingerprint. Here, we define a "geochemical fingerprint" as a particular combination of concentration depth profiles of O_2, H_2S and pH in the pore water (see Meysman et al. 2015; chapter 4). To this end, pore water data were collected by microsensor profiling in Long Island Sound (USA). Long Island Sound (LIS) is a shallow estuarine basin, which is divided into a western, central, and eastern region (Aller 1994). Sediment samples were collected at two sites. The first site was located in the central part of LIS (40° 56 696 N, 73° 13 786W; Smithtown Bay, 15 m depth) which is characterized by bioturbated sediments (Aller 1994) with porosity of 0.8. The second site was located in Port Jefferson harbor (40°57 55 2 N, 73°05 08 4 W; 10 m depth) and the sediments were muddy (porosity 0.88) and had a smell of free sulfide. Sediment at the two stations was retrieved using a Soutar style box corer, and afterwards was carefully subsampled by manually inserting PVC core liners (4 cm inner diameter, 10 cm length) into the sediment. The undisturbed sediment cores were transferred to the laboratory and kept in the dark at room temperature, which was closed to the *in situ* bottom water temperature and during the experiment time oscillated only by 2°C (22-24 °C). The intact sediment samples were incubated with constant aeration of the overlying water and microsensor profiling was started within 4 hours from retrieval. Three replicate cores were analyzed for each station.

In addition, to the intact sediment cores, an incubation experiment was performed. The top 10 cm of the sediment from Port Jefferson harbor was collected, homogenized, and repacked into PVC cores (4 cm inner diameter, 10 cm length). Sediment cores were

subsequently incubated at room temperature in a darkened incubation tank with seawater from the field site (salinity 27). During incubations, the overlying water was kept at 100% air saturation by continuous air bubbling. After a period of overnight equilibration, microsensor profiling was performed on triplicate sediment cores every day, in order to track the potential for electrogenic sulfur oxidation in these sediments.

Microsensor depth profiling was performed using commercial micro-electrodes (Unisense A.S., Denmark) for O_2 (25 or 50-µm tip; Unisense), pH (200-µm tip diameter), H_2S (50-µm tip diameter). Oxygen depth profiles were made at 25-50 µm resolution, with a 2-point calibration made in air-saturated seawater (100% saturation) and at depth in anoxic sediment (0% saturation). For H_2S and pH, depth profiles were made at 200 µm resolution in the oxic zone, and 400 or 600 µm resolution below. Calibrations for pH were made with three NBS standards and a TRIS buffer to correct for salinity effects (Dickson et al. 2007). The pH is reported on the total scale. For H_2S, a 5-point calibration was made using Na_2S standards, which were prepared freshly for each experiment, and concentration of the Na_2S stock solution was determined spectrophotometrically (Cline 1969). ΣH_2S was calculated from H_2S based on pH measured at the same depth using the R package AquaEnv (Hofmann et al. 2010), with the relations of Millero (1995) for the thermodynamic equilibrium constants of H_2S.

6.2.3.   Model formulation

The geochemical fingerprints of four mechanisms of sedimentary sulfur oxidation were emulated by means of model simulations. To this end, we implemented a model description of the biogeochemical cycling in a typical coastal sediment. This model is an extension of the reactive transport model recently developed by Meysman et al. (2015) for simulating long-distance electron transport by cable bacteria in marine sediment, which also includes a description of canonical sulfur oxidation, which takes place when sulfide oxidation and oxygen reduction occur within the same location (i.e at the oxic-anoxic interface). This model was extended with the other two mechanisms (iron shuttling, nitrate-accumulating *Beggiatoaceae*). The model extension was done by including suitable reactions and transport processes for sulfur oxidation by nitrate-accumulating *Beggiatoaceae*, as well as sulfur oxidation through a redox shuttle based on bioturbation-driven iron cycling (the model description and numerical solution procedure is fully detailed in the supplementary information). Most importantly, the simulations presented here for the four mechanisms of sulfide oxidation are based on the same underlying reactive transport model. The different modes of sulfur oxidation can be individually turned on and off by changing suitable parameter values, i.e., by modulating the associated kinetic constants (in the case of nitrate-accumulating bacteria and cable bacteria) or transport coefficients (iron shuttling is turned off by setting the bio-mixing intensity to zero).

6.3. RESULTS
6.3.1. <u>Different mechanisms of suboxic zone formation</u>

We will sequentially discuss the four distinct sulfur oxidation pathways in marine sediments (Figure 2). Three of these sulfur oxidation pathways lead to the formation of a suboxic zone. These four different sulfur oxidation pathways impose a specific "geochemical fingerprint" on the pore water, that is, a characteristic set of O_2, pH, and H_2S profiles which can be determined by microsensor profiling. Figure 3 summarizes the field observations of this geochemical fingerprint as well as the corresponding reactive transport model simulations.

[1] Canonical sulfur oxidation at the O_2-H_2S interface. In certain coastal systems, free sulfide is able to diffuse upwards to the sediment surface, and comes into contact with oxygen, so that the depth profiles of O_2 and H_2S overlap. Under these conditions, O_2 and H_2S coexist in the pore water, and canonical sulfide oxidation (CSO) can occur, which is represented by the overall redox reaction (Fig. 2a):

$$H_2S + 2O_2 \rightarrow SO_4^{2-} + 2H^+ \tag{2}$$

The process is typically observed in sediments with a high local supply of free sulfide. These include coastal sediments receiving high organic carbon loadings (Glud et al. 2003; Jørgensen and Nelson 2004), hydrothermal vents and cold seeps (Jørgensen and Nelson 2004; Beer et al. 2006; Lichtschlag et al. 2010; Grünke et al. 2012), and hot sulfur springs (Kuenen 1975). Canonical sulfide oxidation occurs either chemically (Millero et al. 1987; Gartman et al. 2011) or biologically (i.e. mediated by colorless sulfur oxidizing bacteria, positioned at the oxic-sulfidic interface (Jørgensen and Revsbech 1983). Chemical oxidation of sulfide does not generally lead to the production of sulfate, but forms intermediates such as elemental sulfur and thiosulfate (Gartman et al. 2011). In contrast, biological sulfide oxidation typically proceeds all the way to sulfate (Kuenen 1985; Zopfi et al. 2008).

In most cases, microbes are able to kinetically outcompete the chemical oxidation pathway, and as a result, canonical sulfur oxidation is typically microbially mediated (Jorgensen et al., 1982; Jannasch et al., 1991; Zopfi et al., 2001; Canfield et al., 2005; Luther et al., 2011). Among the colorless sulfur bacteria, the unicellular bacteria belonging to the genera *Thiobacillus* and *Thiomicrospira* (Robertson and Kuenen 2006) and filamentous bacteria belonging to the *Beggiatoaceae* family are known to catalyze canonical sulfide oxidation (Jørgensen and Nelson 2004).

The geochemical fingerprint imposed by CSO on the pore water is illustrated in Fig. 3. This geochemical fingerprint is characterized by (1) the absence of a suboxic zone, i.e., no separation between the depth at which O_2 disappears and the depth where H_2S appears, and (2) a decrease of the pH in the oxic zone down to the oxic-anoxic interface. Beneath the oxygen penetration depth, the pH slightly increases, after which the pH depth profile

becomes constant in deeper anoxic layers. This observed geochemical fingerprint has been previously observed by Jørgensen and Revsbech (1983), during micro-electrode recordings in a white mat of *Beggiatoa* spp. that grew on the surface of an organic-rich sediments.

The most informative feature of the geochemical fingerprint is the pH depth profile. The shape of the pH depth profile in marine sediments is essentially governed by the local acid-base dynamics in the pore water (Hofmann et al. 2010). The resulting pH depth profile can be understood by identifying the zones where dissolved inorganic carbon (DIC) is consumed/produced in addition to the zones where alkalinity (A_T) is consumed/produced (Fig 3. 5th column). An increase in A_T (at constant DIC) will generally increase the pH, while adversely, an increase of DIC (at constant A_T) will decrease the pH. The drop in pH within the oxic zone can be explained by aerobic heterotrophic respiration ($CH_2O + O_2 \rightarrow CO_2 + H_2O$), which produces DIC but does not produce A_T. Because canonical sulfur oxidation is governed by fast (microbial) kinetics, its activity is sharply concentrated near the oxygen penetration depth. The rate of CSO peaks at the interface between O_2 and H_2S, and hence, the process results in strong consumption of A_T within a narrow zone around the oxic-anoxic transition (Fig. 3; 4th column). This explains the sharp transition in the pH depth profile near the OPD. In deeper zone, sulfide is produced through sulfate reduction ($CH_2O + \frac{1}{2} SO_4^{2-} + H^+ \rightarrow \frac{1}{2} H_2S + CO_2 + H_2O$), which produces alkalinity and hence stabilizes the pH profile at depth.

[2] Electrogenic sulfur oxidation by cable bacteria. Cable bacteria have only been recently discovered (Pfeffer et al. 2012), and are long filamentous sulfur oxidizing bacteria, belonging to the genera Electrothrix and Electronema within the Deltaproteobacteria (Trojan et al. 2016). Their most remarkable aspect is that they possess a unique metabolic lifestyle, referred to as electrogenic sulfur oxidation (e-SOx), which is based on the capability of performing long-distance electron transport (Nielsen et al. 2010). Cable bacteria oxidize sulfide in deeper sediments and conduct the resulting electrons along their longitudinal axis up to the oxic zone, where the electrons are used in the reduction of oxygen (see Fig. 2b; the process is reviewed in detail in Nielsen and Risgaard-Petersen 2015).

Cable bacteria have recently been documented in a number of natural settings, including organic-rich coastal sediments in the southern North Sea (Malkin et al. 2014; chapter 4), saltmarshes (Larsen et al. 2015; Rao et al. 2016), mangrove sediments in Australia (Burdorf et al. 2016) and a riverine sediment in Denmark (Risgaard-Petersen et al. 2015). Field observations are still scarce, but gene sequence archives suggest a broader cosmopolitan distribution, leading to the hypothesis that cable bacteria are likely active in a variety of sediments, as long as the bottom waters are oxygenated and the sediment sustains a sufficiently high sulfide production (Malkin et al. 2014). Overall, the basic ecology of cable

[a] canonical sulfur oxidation

Oxic Zone

O_2

$\frac{1}{2}H_2S + O_2 \rightarrow \frac{1}{2}SO_4^{2-} + H^+$

Sulfidic Zone

H_2S

[b] cable bacteria

Oxic Zone

O_2

$O_2 + 4e^- + 4H^+ \rightarrow 2H_2O$

Suboxic Zone

electron transport

Sulfidic Zone

$\frac{1}{2}H_2S + 2H_2O$
$\rightarrow \frac{1}{2}SO_4^{2-} + 4e^- + 5H^+$

H_2S

[c] NO_3-accumulating Beggiatoa

Oxic Zone

O_2

$S^0 + \frac{3}{2}O_2 + H_2O \rightarrow SO_4^{2-} + 2H^+$

Suboxic Zone

NO_3

S_0

$4H_2S + NO_3^- + 2H^+$
$\rightarrow 4S^0 + NH_4^+ + 3H_2O$

Sulfidic Zone

H_2S

[d] bioturbation & Fe cycling

Oxic Zone

O_2

$4Fe^{2+} + O_2 + 6H_2O$
$\rightarrow 4FeOOH + 8H^+$

Suboxic Zone

FeOOH

Fe^{2+}

$4FeOOH + \frac{1}{2}H_2S + 7H^+$
$\rightarrow 4Fe^{2+} + \frac{1}{2}SO_4^{2-} + 6H_2O$

Sulfidic Zone

H_2S

Figure 2. Four different modes of "aerobic" sulfur oxidation in marine sediments. (A) Canonical sulfur oxidation which occurs right at the oxic-sulfidic interface. (B) Electrogenic sulfur oxidation mediated by cable bacteria. (C) Sulfur oxidation by large motile filamentous bacteria (e.g. Beggiatoa or Thioploca) that accumulate nitrate and elemental sulfur. (D) Sulfur oxidation driven by a metal shuttle, which is itself sustained by particle mixing through infauna.

bacteria, including their life history, distribution, and the geochemical consequences of their metabolism, is only beginning to be unraveled (Nielsen and Risgaard-Petersen 2015). The specific geochemical fingerprint imposed by e-SOx has been investigated in detail by Meysman et al. (2015) and is illustrated in Figure 3. The fingerprint of e-SOx differs strongly from that of canonical sulfur oxidation. The pH depth profile has a clear maximum at the oxic-anoxic transition and a pronounced pH minimum much deeper in the anoxic zone (Nielsen et al. 2010; Fig. 3, field observations and model simulation). In addition, there is a prominent suboxic zone, separating the shallow depth where O_2 disappears and the deeper sediment horizon where H_2S appears. Laboratory incubations (Nielsen et al. 2010; Pfeffer et al. 2012; Schauer et al. 2014) as well as field observations (Malkin et al. 2014; chapter 4; Burdorf et al. 2016) indicate that this suboxic zone is typically 10-30 millimeters wide.

The characteristic shape of the pH depth profile in sediments with cable bacteria activity is again explained by the local acid-base dynamics in the pore water (see Meysman et al. 2015 for details). Deeper in the sediment, sulfide is consumed by the anodic half-reactions of e-SOx

$$\tfrac{1}{2}H_2S + 2H_2O \rightarrow \tfrac{1}{2}SO_4^{2-} + 4e^- + 5H^+ \tag{3}$$
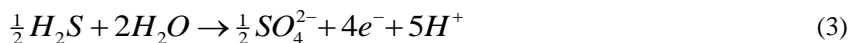
This process induces a large consumption of alkalinity (10 mole of alkalinity per mole of H_2S), thus creating the observed pH minimum. The acidification of the pore water is substantial (pH values down to 6; Fig. 3), and occurs throughout the suboxic zone. Within the surface sediment, the electrons are used to reduce oxygen in the cathodic half-reaction

$$O_2 + 4e^- + 4H^+ \rightarrow 2H_2O \tag{4}$$

This reaction produces large amounts of alkalinity (4 mole of alkalinity per mole of O_2), and this way, it creates a pH maximum within the oxic zone. Overall, the large pH excursions in the pH depth profile are essentially a consequence of the spatial segregation of the two half-reactions in e-SOx. The proton release during anodic sulfide oxidation takes place within a very different depth zone than the proton consumption during cathodic oxygen reduction. Both the acidifying effect within the suboxic zone and the elevated pH within the oxic zone are characteristic for e-SOx, as no other natural process is known to generate a similar pH distribution in marine sediments (Meysman et al. 2015).
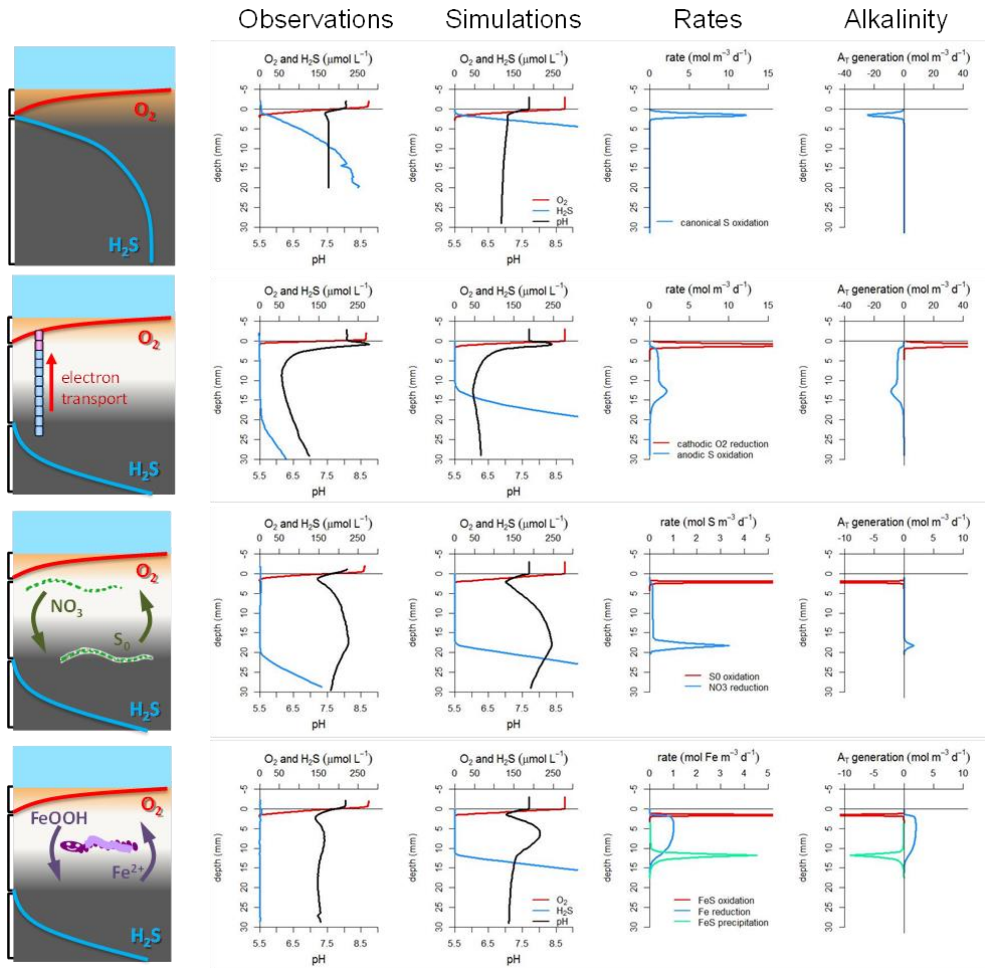
Figure 3. A comparison of the geochemical fingerprint of the four different modes of "aerobic" sulfur oxidation. Observations = Typical microsensor depth profiles of O_2 (red line), pH (black line) and ΣH_2S (blue line) as obtained within sediments from Long Island Sound. Simulations = Recreation of these microsensor depth profiles by means of reactive transport model. Rates = Reaction rates simulated by the reactive transport model. Alkalinity = Alkalinity production rate of selected reactions as simulated by the reactive transport model (line colours correspond to reacton rates depicted in previous column). Origin of observational data: (A) Canonical sulfur oxidation: homogenized sediment from muddy station in LIS incubated in the laboratory (B) Cable bacteria: homogenized sediment retrieved from a muddy station in LIS and further incubated in the laboratory (C) NO_3-accumulating *Beggiatoa*: field observation on intact sediment in muddy station in LIS. (D) Metal shuttling: field observation on intact sediment from station 5 in LIS.

[4] Sulfur oxidation by nitrate-accumulating bacteria. Large motile colorless sulfur bacteria, including members of the genus *Beggiatoa* and *Thioploca*, are also known to

create a suboxic zone in marine sediments (Sayama et al. 2005; Preisler et al. 2007; Lichtschlag et al. 2010). These filamentous bacteria generate a redox shuttle between H_2S and O_2 by combining gliding motility with the intracellular accumulation of intermediate redox compounds (NO_3, S^0). The conceptual model of this metabolism is displayed in Fig. 2 for *Beggiatoa* (the mechanism in *Thioploca* is conceptually similar). In a first step, nitrate is removed from the ambient pore water near the sediment-water interface, and stored in intracellular vacuoles

$$NO_3^- \rightarrow \left\{NO_3^-\right\}_{\text{intracell}} \tag{5}$$

By means of their gliding motility, the *Beggiatoa* subsequently migrate deeper into the sediment, until they reach the sulfidic zone (Dunker et al. 2011). Within this deeper horizon, the intracellular nitrate is used to oxidize free sulfide to elemental sulfur (S^0), which is also stored intracellularly.

$$\left\{NO_3^-\right\}_{\text{intracell}} + 4H_2S + 2H^+ \rightarrow NH_4^+ + 4\left\{S^0\right\}_{\text{intracell}} + 3H_2O \tag{6}$$
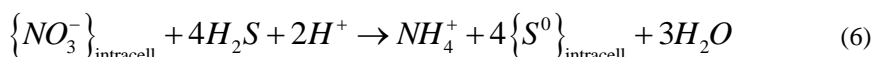
Afterwards, the *Beggiatoa* migrate up again to the oxic zone near the sediment-water interface, where they oxidize their internal elemental sulfur reservoir to sulfate.

$$\left\{S_0\right\}_{\text{intracell}} + \tfrac{3}{2}O_2 + H_2O \rightarrow SO_4^{2-} + 2H^+ \tag{7}$$
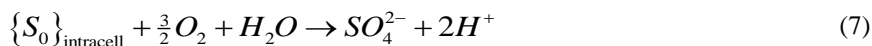
The cyclic migration pattern of *Beggiatoa* causes a net downward transport of nitrate and a upward transport of elemental sulfur. In essence this process works like a redox shuttle, where electrons are shuttled upwards via elemental sulfur, and electron acceptor capacity is shuttled downwards through nitrate.

The concept that large filamentous bacteria can oxidize sulfide with nitrate was developed in 1994, when mats of *Thioploca* were studied on the continental shelf off central Chile, revealing intracellular nitrate concentrations up to 500 mM (Fossing et al. 1995). *Thioploca* are abundant on the seafloor along the Pacific coast of South America (Gallardo 1977), where they occur at a zone where coastal upwelling provides high nitrate levels in the bottom water, and high productivity provides a large input of organic matter to the sediment thus stimulating high rates of sulfide production through sulfate reduction (Ferdelman et al. 1997). Subsequently the mechanism of sulfide oxidation with nitrate was confirmed in other large sulfur oxidizing bacteria, including *Beggiatoa* and *Thiomargarita* (see reviews (Jørgensen and Gallardo 1999; Schulz and Jørgensen 2001; Jørgensen and Nelson 2004). The nitrate accumulation explains why these bacteria grow to giant sizes, as the intracellular space is largely occupied by large vacuoles in which the nitrate is stored.

At the same time, the white appearance of these bacteria is explained by the intracellular accumulation of smaller granules of elemental sulfur.

The metabolism of motile nitrate-accumulating sulfur oxidizers also imposes a specific geochemical fingerprint upon the porewater (Fig. 3). The pH profile shows a distinct sigmoid shape (Sayama et al. 2005; Preisler et al. 2007; Lichtschlag et al. 2010), which is caused by the spatial separation of the two sequential steps in sulfide oxidation. The oxidation of sulfide via nitrate at depth Eq. (6) consumes protons, and hence produces alkalinity, thus causing a broad pH maximum at the sulfide appearance depth (Fig. 3). Similarly, the further oxidation of elemental sulfur to sulfate via Eq. (7), produces protons and consumes alkalinity, inducing a pH minimum near the oxygen penetration depth (Fig. 3).

[5] Sulfur oxidation through metal shuttling. A third and final way to create a suboxic zone involves sulfide removal through a redox shuttle involving iron and/or manganese (hydr)oxides (Aller and Rude 1988; Canfield et al. 1993b), which we abbreviate here as "sulfur oxidation by metal shuttling". The process is illustrated by the conceptual scheme in Fig 2. Metal oxides are transported downwards into the sediment by bioturbation and/or physical mixing by waves and currents, and these oxides interact with H_2S at depth to form metal sulfides (mostly iron mono-sulfides FeS and pyrite FeS_2). These metal sulfides are then transported upwards again by solid phase mixing, where they are re-oxidized near the sediment-water interface upon contact with oxygen. It should be noted that in most sediments, the network of redox transformations will be more complex than the simplified redox shuttle depicted in Figure 2. For example, in some environments (e.g. chapter 5) a double redox shuttle can be active, where iron (hydr)oxides (FeOOH) are first reduced by H_2S, the ferrous iron Fe^{2+} released subsequently migrates upwards, and is oxidized by manganese oxides (MnO_2). The reduced Mn^{2+} that is released in its turn diffuses upwards, and is oxidized with O_2, completing the cycle.

The creation of a suboxic zone by metal shuttling has been documented from a range of coastal environments (Jørgensen et al. 1990; Thamdrup et al. 1994; Kostka et al. 2002; Kristiansen et al. 2002; Kristensen et al. 2003) and seems to be the most widespread mechanism of suboxic zone formation in the coastal zone. The reason for this is that a large proportion of coastal sediments are inhabited by large burrowing infauna, which induce bio-mixing of the solid phase (Meysman et al. 2006; Kristensen et al. 2012a). As already emphasized above, the creation of a suboxic zone by metal shuttling is critically dependent on (1) the availability of metal (hydr)oxides in the sediment and (2) the intensity of solid phase mixing (Aller and Rude 1988; Canfield et al. 1993b). The latter process is required for the downward transport of metal oxides (e.g. FeOOH), as well as the upward transport of reduced metal compounds (e.g. FeS, FeS_2 or Fe^{2+} adsorbed onto solid particles; Berg et al. 2003).

When the metal shuttling mechanism is active, the associated pH depth profile shows a subsurface minimum at the OPD, followed by a pH increase in the following centimeters, to subsequently decrease again near the SAD, and stabilize at an asymptotic value in deeper layers (Fig.3D, left). Model simulations have previously shown that this pH depth profile is associated with metal shuttling (Jourabchi et al., 2005), and the reactive transport simulations performed here confirm this. The pH minimum in the oxic zone (Fig. 3) can be linked to the formation of iron (hydr)oxides (FeOOH), through the aerobic oxidation of ferrous iron or iron sulfide

$$Fe^{2+} + \tfrac{1}{4}O_2 + \tfrac{3}{2}H_2O \rightarrow FeOOH + 2H^+ \tag{8}$$

$$FeS + \frac{9}{4}O_2 + \frac{3}{2}H_2O \rightarrow FeOOH + SO_4^{2-} + 2H^+ \tag{9}$$
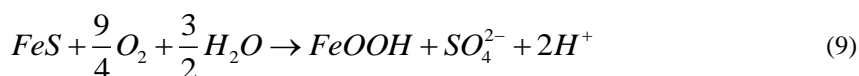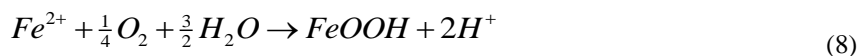
Both of these reactions generate protons, and hence consume alkalinity. The solid iron (hydr)oxides are transported downwards and reduced (Canfield et al. 1993b; Thamdrup et al. 1994), either biotically, through dissimilatory reduction with organic matter,

$$\{CH_2O\}_f + 4FeOOH + 7H^+ \rightarrow HCO_3^- + 4Fe^{2+} + 6H_2O \tag{10}$$

or abiotically, through the reduction with free sulfide

$$H_2S + 8FeOOH + 14H^+ \rightarrow SO_4^{2-} + 8Fe^{2+} + 12H_2O \tag{11}$$
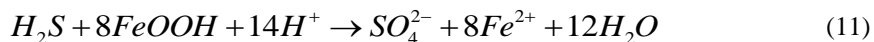
Both reactions take place within the suboxic zone and create large amounts of alkalinity, which increases the pH in the suboxic zone. In a final step, the ferrous iron in the pore water reacts with the free sulfide to form iron sulfides.

$$Fe^{2+} + H_2S \rightarrow FeS + 2H^+ \tag{12}$$

This reaction takes principally place near at the sulfide appearance depth (SAD), and forms a sink for free sulfide diffusing from deeper depths. Iron sulfide precipitation consumes alkalinity, thus explaining the observed decrease in pH near the SAD, after which the pH remains constant with depth. .

6.4. DISCUSSION

6.4.1. <u>Suboxic zone formation</u>

The "aerobic sulfide oxidation paradox" is based on the observation that O_2 is the principal electron acceptor for the oxidation H_2S in marine sediments, while in most environments a wide suboxic zone is present and so the depth profiles of O_2 and H_2S do not overlap (Jørgensen and Postgate 1982). As a consequence, O_2 and H_2S molecules appear to be engaged in a redox reaction without ever being in physical contact. If this reaction were to occur in a homogeneous and sterile laboratory reactor, it would indeed be puzzling, but in the more complex biogeochemical setting of seafloor, the solution of the paradox is rather straightforward. The defining feature of a redox reaction is that electrons are passed on from the electron donor (H_2S) to the electron acceptor (O_2). Accordingly, the paradox can be resolved if an intermediate process is at work, which suitably enables the necessary electron transfer from free sulfide to oxygen across the suboxic zone. In marine sediments, three such mechanisms have been identified: bioturbation-driven metal cycling, sulfur oxidation by nitrate-accumulating bacteria and electrogenic sulfur oxidation by cable bacteria.

Sulfide oxidation through metal cycling is based on a redox shuttle mechanism where oxidized and reduced forms of iron or manganese act as intermediate redox species, shuttling electrons from sulfide to oxygen. Figure 4a illustrates the mechanism for iron cycling in bioturbated coastal sediments. At depth, the iron oxides are reduced to form ferrous iron, which subsequently can follow three separate routes. In a first pathway, the ferrous iron is directly transported upwards by molecular diffusion in the pore water, and when reaching the sediment surface, it becomes oxidized with oxygen. By combining all reactions involved in the redox shuttle, the aerobic oxidation of sulfide as the overall reaction is recovered.

Iron reduction $\quad H_2S + 8FeOOH + 14H^+ \rightarrow SO_4^{2-} + 8Fe^{2+} + 12H_2O$

Ferrous iron oxidation $\quad 8Fe^{2+} + 2O_2 + 12H_2O \rightarrow 8FeOOH + 16H^+$

Overall: Aerobic sulfide oxidation $\quad H_2S + 2O_2 \rightarrow SO_4^{2-} + 2H^+$
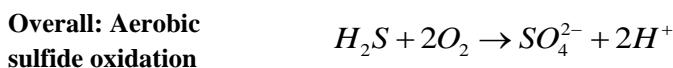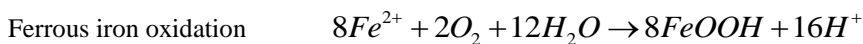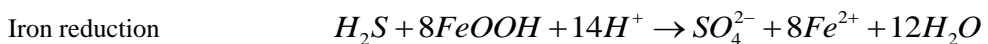
Alternatively, the ferrous iron can also be adsorbed onto sediment particles, and the sorbed iron is subsequently transported upwards by bioturbation to the oxic zone. Model simulations suggest that this adsorbed transport of ferrous iron could be more quantitatively important than the transport via molecular diffusion (Berg et al. 2003). In a third scenario,

the ferrous iron comes into contact with free sulfide and precipitates as iron sulfide. Bioturbation then transports the iron sulfides to the oxic zone, where they are oxidized to iron oxides upon contact with O_2. By combining all the reactions involved, we find that the intermediate species cancel out, so that eventually, the overall reaction again simplifies to the aerobic oxidation of sulfide.

Iron reduction	$H_2S + 8FeOOH + 14H^+ \rightarrow SO_4^{2-} + 8Fe^{2+} + 12H_2O$
Iron sulfide precipitation	$8Fe^{2+} + 8H_2S \rightarrow 8FeS + 16H^+$
Iron sulfide oxidation	$8FeS + 18O_2 + 12H_2O \rightarrow 8FeOOH + 8SO_4^{2-} + 16H^+$
Overall: Aerobic sulfide oxidation	$9H_2S + 18O_2 \rightarrow 9SO_4^{2-} + 18H^+$
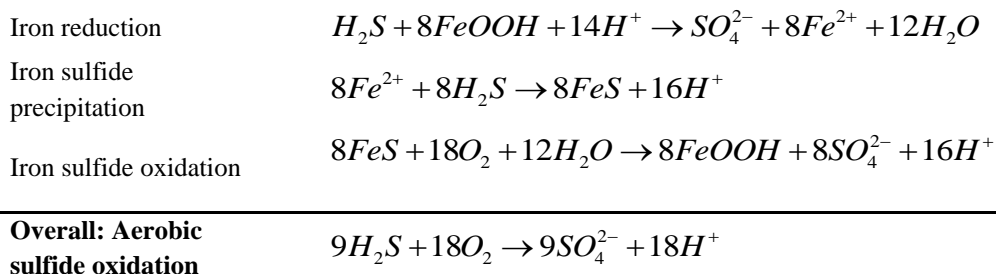
Note that particle mixing through bioturbation is essential to keep the redox shuttle ongoing. Particle mixing transports the oxidized forms of iron (e.g. FeOOH) downwards in the sediment and the reduced forms of iron (e.g. FeS, adsorbed Fe^{2+}) upwards.
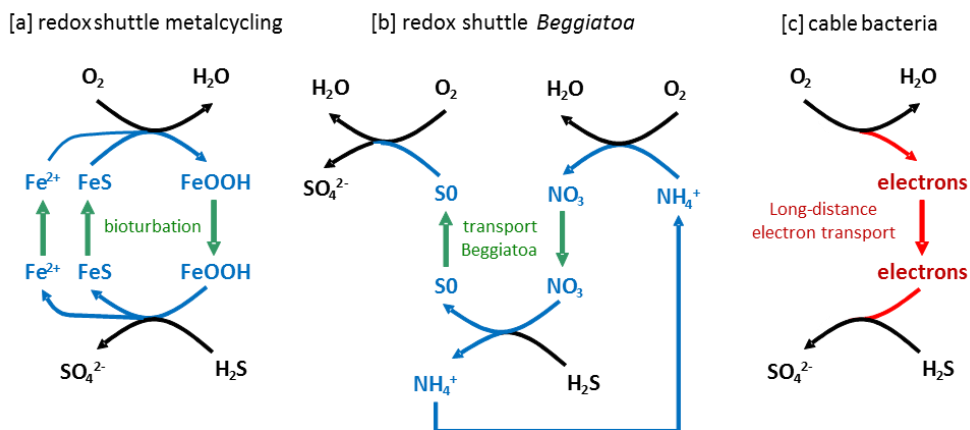
Figure 4. A comparison of three types of redox shuttling that sustain the formation of a suboxic zone. (A) In bioturbated sediments, the redox shuttle is driven by the transport of oxidized and reduced forms of metal compounds such as iron and manganese. (B) In sediments with NO3-accumulating bacteria the transport of oxidized and reduced compounds occurs inside the cells of the large motile bacteria. The redox shuttle is slightly more complex as it involves both nitrogen and sulfur compounds. (C) Cable bacteria facilitate aerobic sulfur oxidation by means of long-distance electron transport. The electrons that are exchanged between H_2S and O_2 are no longer "packed" inside redox compounds, but are directly transferred through conduction along the longitudinal axis of the long cable bacteria filaments.

Sulfide oxidation via large nitrate-accumulating bacteria is also based on a redox shuttle mechanism (Fig. 4b). The interactions are however slightly more complex compared to metal cycling case, as the redox cycling now involves two elements (nitrogen and sulfur). The transport of the intermediate redox species is mediated by the continuous up and down migration of the large bacteria. Elemental sulfur is produced from the oxidation of H_2S with nitrate and accumulates as intracellular granules in the cytoplasm of the bacteria. When the bacteria migrate upwards the S^0 is further oxidized to sulfate. Nitrate also accumulates in the intracellular space of the large bacteria, and is transported downwards as the bacteria migrate into deeper sediment layers. The ammonium that is produced during the reduction of nitrate with H_2S will diffusive upwards, and will be oxidized back to nitrate in the oxic zone. By combining all the reactions involved, the intermediate species cancel out, and the overall reaction reduces to aerobic sulfide oxidation, as required for a proper redox shuttle.

Nitrate uptake	$NO_3^- \rightarrow \left\{ NO_3^- \right\}_{\text{intracell}}$
Nitrate reduction	$\left\{ NO_3^- \right\}_{\text{intracell}} + 4H_2S + 2H^+ \rightarrow NH_4^+ + 4\left\{ S^0 \right\}_{\text{intracell}} + 3H_2O$
Elemental sulfur oxidation	$4\left\{ S_0 \right\}_{\text{intracell}} + 6O_2 + 4H_2O \rightarrow 4SO_4^{2-} + 8H^+$
Ammonium oxidation	$NH_4^+ + 2O_2 \rightarrow NO_3^- + 2H^+ + H_2O$
Overall: Aerobic sulfide oxidation	$4H_2S + 8O_2 \rightarrow 4SO_4^{2-} + 8H^+$
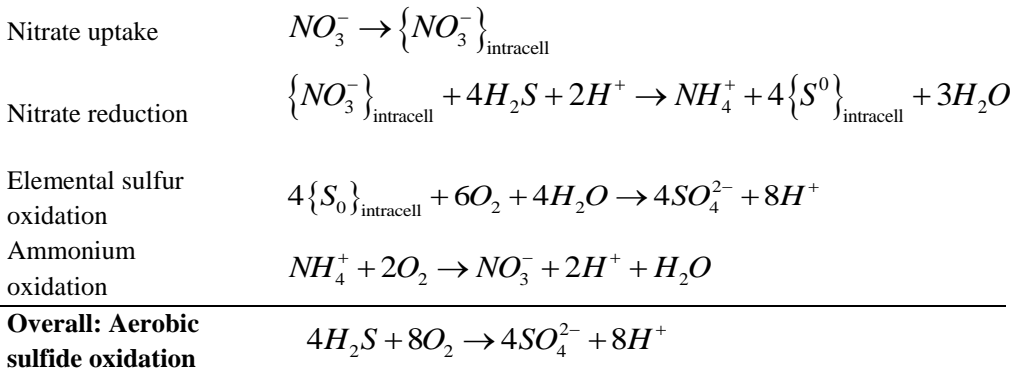
Finally, electrogenic sulfide oxidation by cable bacteria also creates a suboxic zone, but does not fit the conventional definition of a redox shuttle. This is because the necessary electron transport no longer occurs via intermediate redox species, but through the direct conduction of electrons from H_2S to O_2 along the longitudinal axis of the filamentous cable bacteria (Nielsen and Risgaard-Petersen 2015). In other words, the electrons are no longer "stored" into redox species and transported, but are directly transferred. By combining the two half-reactions of the electron shuttle mechanism, the overall reaction also becomes aerobic sulfide oxidation.

Anodic sulfide oxidation	$\frac{1}{2}H_2S + 2H_2O \rightarrow \frac{1}{2}SO_4^{2-} + 4e^- + 5H^+$
Cathodic oxygen reduction	$O_2 + 4e^- + 4H^+ \rightarrow 2H_2O$
Overall: Aerobic sulfide oxidation	$\frac{1}{2}H_2S + 2O_2 \rightarrow \frac{1}{2}SO_4^{2-} + H^+$
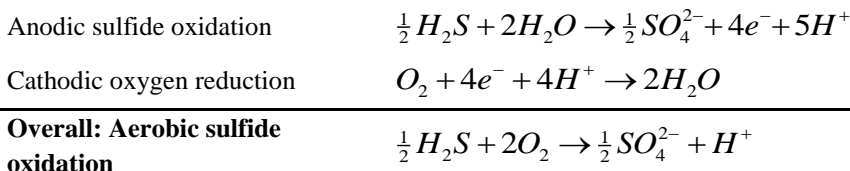
In coastal systems, the suboxic zone may range from only few millimeters down to tens of centimeters (Table 1). Intrinsic differences between the three known mechanisms of the suboxic zone formation may explain these observed differences in the extent of the suboxic zone. As already noted above, sulfur oxidation by metal shuttling is critically dependent on the transport of solid metal compounds (Aller and Rude 1988; Jørgensen and Nelson 2004). Our model simulations confirm that the depth of the suboxic zone is set by the mixing depth of bioturbation, which is essentially determined by the depth to which burrowing fauna live in marine sediments. Boudreau (1992) estimated a global mean mixing depth of 9.8 ± 4.5 cm. However, crustaceans (e.g. callianassid shrimp) and some polychaete species (e.g. *Allita virens*) are capable of burrowing up to several tens of cm sediment depth (Ziebis et al. 1996). Overall, bioturbation-driven metal shuttling typically creates wide suoboxic zones. Nitrate-accumulating *Beggiatoa* and cable bacteria lead to the formation of smaller suboxic zones, which are typically on the order of a few centimeters at most (Mussmann et al., 2003; Malkin et al., 2003). In the case of nitrate-accumulating *Beggiatoa*, the depth of the suboxic zone appears to be limited by the capability of the *Beggiatoa* to glide via cyclic movements between oxic and sulfidic zone (Dunker et al. 2011). In the case of cable bacteria, the depth limitation seems to be related to the capability of transferring electrons over long distances, i.e., the inherent conductivity of the organic structures that guide the electron transport inside the cable bacteria.

6.1.1. pH fingerprint as an indicator of suboxic zone formation

In this study we have examined the four known mechanisms of aerobic sulfur oxidation in marine sediments: electrogenic sulfur oxidation, sulfur oxidation by nitrate-accumulating bacteria, and sulfur oxidation by metal shuttling. Each of these mechanisms relies on redox reactions that release and consume protons (or more exactly, consume and produce alkalinity) within different sediment horizons. As a result, these three mechanisms impose a specific pH depth profile upon the pore water. Foremost, the pH depth profile of electrogenic sulfur oxidation is highly distinct: it induces a subsurface pH maximum at the OPD and the substantial acidification within the suboxic zone (Nielsen et al. 2010; Meysman et al. 2015). These two features readily distinguish the pH fingerprint of e-SOx from those generated by the other sulfide oxidation mechanisms. Secondly, the pH depth profile associated with sulfur oxidation by nitrate-accumulating bacteria is characterized by a subsurface pH minimum near the oxygen penetration depth followed by a pH maximum near the sulfide appearance depth (Sayama et al. 2005). At first sight, this pH depth profile resembles that created by sulfur oxidation through metal shuttling, which also shows a pH minimum near the oxygen penetration depth followed by a pH increase in deeper layers. However, the location of the pH maximum at depth is crucially different, allowing to distinguish both phenomena.

Table 1. Research studies reporting the formation of a suboxic zone.

Site	Water depth (m)	Suboxic zone thickness (cm)	Mechanism	Reference
Lake Grevelingen, The Netherlands	34	1.8	e-SOx	Malkin et al., 2014
Boknis Eck, Baltic Sea	28	10	Large NO_3^- accumulating bacteria	Dale et al., 2011
Aarhus Bay, Denmark	15	2-10	Metal shuttling via bioturbation	Jørgensen et al. 1990; Moeslund and Thamdrup, 1994; Fossing et al. 1994
Limfjorden, Denmark	4-12	3.5	Large NO_3^- accumulating bacteria	Jorgensen 1977
Kattegat, Denmark	73	40	Metal shuttling via bioturbation	Jørgensen et al. 1990
Skagerrak, Denmark	200	20	Metal shuttling via bioturbation	Jørgensen et al. 1990
Great Belt, Baltic Sea	17	6	Metal shuttling via bioturbation	Jørgensen et al. 1990
Salt marsh sediments	intertidal	4-5.5	Metal shuttling via bioturbation	Thamdrup et al. 1994; Kostka et al. 2002
Salt marsh sediments, The Netherlands	intertidal	2	e-SOx	Malkin and Meysman, 2014
Rehoboth Bay, Delaware, US	1	2	Metal shuttling via bioturbation	Rozan et al. 2002
Fjord Kaeby Fed, Denmark	2.2	6	Metal shuttling via bioturbation	Kristensen et al. 2003
Falleesstrand lagoon, Denmark	1	6	Metal shuttling via bioturbation	Kristiansen et al. 2002
Loch Duin fjord, Scotland	120	25	Unknown	Mortimer et al. 2002
Upwelling area off Chile	24	1	Large NO_3^- accumulating bacteria	Zopfi et al. 2008

In the case of metal cycling, the maximum in pH is located in the center of the suboxic zone (Jourabchi et al. 2005), while when nitrate-accumulating bacteria are active, the pH maximum occurs near the SAD at the bottom of the suboxic zone.

Overall, the pH depth profile (in combination with the O_2 and H_2S depth profiles) appears to provide a distinct biogeochemical fingerprint for the mechanism of suboxic zone at hand. Clearly, in a number of situations, and particularly under *in situ* conditions, the fingerprint will not be as clear-cut as the "endmember" examples presented here. The model simulations here assume that (1) sulfur oxidation is dominated by one particular mechanism and (2) the sediment geochemistry resides in a steady state. Therefore, hybrid pH profiles may be encountered, when multiple sulfide oxidation pathways are active, or when the sediment biogeochemistry is in transition from one dominant pathway to the next. Yet overall, the pH fingerprinting typology presented here allows to identify the dominant

pathways that are responsible for the formation of the suboxic zone in a given coastal sediment. This approach was already successfully applied in chapter 4 to unravel the seasonal dynamics in the dominant sulfur-oxidation pathway in Lake Grevelingen.

6.1.2. Suboxic zone formation and cryptic sulfur cycling

The term "cryptic sulfur cycling" was firstly coined in 2010 to designate the strongly coupled sulfur and nitrogen cycling that occurred within the oxygen minimum zone (OMZ) in the pacific off the coast of Chile (Canfield et al. 2010). The water column within this OMZ shows a substantial suboxic zone with low concentrations of both O_2 (< 13 nM) and H_2S (< 0.1 μM). Still within this suboxic zone substantial rates of sulfate reduction were measured, but no accumulation of sulfide was observed within the water column, suggesting a tightly coupled sulfide removal process. It was suggested that the reduction of nitrate to nitrite was responsible for the sulfide oxidation, although the actual details of the coupling between sulfate oxidation and nitrate reduction remain elusive (Canfield et al. 2010).

Previous to this, similar phenomena had already been documented in marine sediments, though other terminology was used than the term "cryptic sulfur cycling". For example, a cryptic sulfur cycle has been invoked to explain the discrepancy between sulfate reduction rate measurements and the net sulfate consumption rate derived from sulfate porewater depth profiles e.g. (Holmer et al. 2003) in addition to explaining peculiar responses in sulfate isotopes eg. (Turchyn et al. 2006). Still, these type of reports are scarce, and as a result, the impression might arise that cryptic sulfur cycling is a rather rare phenomenon in marine sediments. Here, we contend that this would be a misconception. Cryptic sulfur cycling is actually a very common phenomenon in the surface layer coastal and continental shelf sediments. This is because the creation of a suboxic zone is commonly observed in these environments, and each of the three known mechanisms of suboxic zone formation essentially gives rise to cryptic sulfur cycling (Table 2).

Table 2. Summary of different forms of "aerobic" sulfur oxidation in marine sediments. It is indicated (1) whether a particular mechanism induces the formation of a suboxic zone (2) whether it is based on a redox shuttle, and (3) whether the mechanism gives rise to cryptic sulfur cycling

	suboxic zone formation	redox shuttle	cryptic sulfur cycling
Canonical S oxidation	-	-	-
Electrogenic S oxidation	+	**Electron shuttle**	+
NO_3^--accumulating bacteria	+	+	+
Bioturbation-driven metal cycling	+	+	?

In sediments with nitrate-accumulating *Begggiatoa*, high rates of sulfate reduction have been detected (Preisler et al. 2007). The fact that the sulfide is not present at detectable concentrations, while sulfate reduction occurs at high rates, indicates that *Begggiatoa* must have a high affinity for sulfide, ensuring that sulfide is removed before it is capable of accumulating in the pore water. At present no direct measurements are available for the affinity of *Begggiatoa* towards sulfide, but our model simulations allow to estimate a low K_m value = 1e+6 mol^{-1} m^3 yr^{-1} for sulfide uptake (Sup Mat). In a similar fashion, sulfate reduction has been measured in the suboxic zone of electrogenic sediments incorporating cable bacteria (Risgaard-Petersen et al. 2012). While *Begggiatoa* only rely on sulfide originating from sulfate reduction, cable bacteria have access to two sources of sulfide. Due to the strong acidification of the pore water, iron monosulfides (FeS) go into dissolution (Rao et al. 2016), which provides a second supply route of free sulfide. The existence of a suboxic zone implies that cable bacteria must also have a high affinity for sulfide. This is confirmed by our model analysis here, which suggest a low K_m value = 1.4e+8 mol^{-1} m^3 yr^{-1} for sulfide uptake by cable bacteria (Sup. Mat).

Finally, cryptic sulfur cycling is also likely in sediments where the suboxic zone is sustained by metal shuttling, although it is not strictly necessary from a theoretical point of view. If redox pathways would be sufficiently competitive so they become exclusive, then only dissimilatory iron conduction would occur in the suboxic zone, and sulfate reduction would be displaced to the deeper sediment horizon where sulfide accumulates. This sequential occurrence of organic matter mineralization pathways with depth is the central idea underlying the long-held conceptual model of the redox cascade (Froelich et al. 1979). However, there are various indications that this model of sequential electron acceptor does not necessary reflect the actual distribution of electron acceptor use, particularly in coastal sediments (Goldhaber et al. 1977; Canfield et al. 1993b). First of all, iron (oxyhydr)oxides in coastal sediments comprise a complex mixture of various iron minerals with different reactivities (Poulton and Canfield 2005). Only the most reactive iron oxides are preferentially consumed before sulfate, while others are consumed simultaneously with sulfate, thus providing an overlap between dissolved iron reduction and sulfate reduction (Postma and Jakobsen 1996). Secondly, coastal sediments are characterized by substantial horizontal redox gradients and sediment heterogeneity, e.g. due to burrow networks, which allows different redox conditions and mineralization pathways to occur in the same depth layer (Aller 1977). In a one–dimensional representation, as in the diagenetic model employed here, such three-dimensional heterogeneity will show up as a depth overlap in mineralization pathways.

6.2. SUMMARY and CONCLUSION

The "aerobic sulfide oxidation paradox" is based on the observation that most sulfide in sediments is removed through oxidation with oxygen, though oxygen and sulfide are never

in contact, as they are separated by a wide suboxic zone. In marine sediments, three mechanisms enable the necessary electron transfer from free sulfide to oxygen across the suboxic zone: bioturbation-driven metal cycling, sulfur oxidation by nitrate-accumulating bacteria and electrogenic sulfur oxidation by cable bacteria.

Sulfide oxidation through metal cycling is based on a redox shuttle mechanism where oxidized and reduced forms of iron or manganese act as intermediate redox species, shuttling electrons from sulfide to oxygen, and is strictly dependent on particle mixing through bioturbation. A redox shuttle mechanism is used also by large nitrate-accumulating bacteria, which enable sulfide oxidation by transporting intracellularly intermediate redox species (nitrogen and sulfur) and continuous up and down migration traversing the suboxic zone. Cable bacteria do not make use of intermediate redox species, but enable aerobic sulfide oxidation by means of long-distance electron transport, via direct conduction of electrons from H_2S to O_2 along the longitudinal axis of the filamentous cable bacteria.

All three mechanisms contribute to the formation of a subxic zone in coastal sediment, and can be differentiated by their pH imprint on the pore water, as demonstrated by field observations and reactive transport modelling. These insights provide a better understanding and guidance as to the different mechanisms of sulfide oxidation and suboxic zone formation in the seafloor.

Supplementary Information: model formulation

Mass balance equations

The depth profiles of solutes and solids are respectively described by the mass balance equations (Boudreau 1997; Meysman et al. 2005)

$$
\begin{cases}
\varphi \dfrac{\partial C_i}{\partial t} = \dfrac{\partial}{\partial z}\left(\varphi D_i \dfrac{\partial C_i}{\partial z} - \varphi v C_i \right) + \sum_k \nu_{i,k} R_k & (13) \\[2em]
(1-\varphi)\dfrac{\partial S_i}{\partial t} = \dfrac{\partial}{\partial z}\left((1-\varphi) D_B(z) \dfrac{\partial S_i}{\partial z} - (1-\varphi) w S_i \right) + \sum_k \nu_{i,k} R_k
\end{cases}
$$

In this, C_i represents the concentration of a solute in the pore water, S_i is the concentration of a solid component, z is the depth into the sediment and φ the porosity. The model includes a set of transport processes that is characteristic for a cohesive, non-permeable coastal sediment: (1) solute diffusion in the pore water (effective diffusion coefficient D_i), (2) downward advection due to sediment accumulation (sedimentation velocity at $v = w = 0.2$ cm yr-1), (3) bio-mixing by infauna (biodiffusivity coefficient D_b). However, pore water advection, characteristic for permeable sediments, is not incorporated.

Transport processes

The parameterization of the transport processes follows the standard treatment of early diagenesis and is adapted to a typical coastal setting (see Meysman et. al (2015) for details). The solute flux due to molecular diffusion and advection is described by Fick's first law (Fick, 1855),

$$
J_D = -\varphi D_i \frac{\partial C}{\partial z} + \varphi v C \tag{14}
$$

where the effective diffusion coefficient is written as $D_i = D_0 / \theta^2$, with D_0 the molecular diffusivity of the solute and $\theta^2 = 1 - 2\ln(\varphi)$ is a correction factor for sediment tortuosity (Boudreau 1996). The molecular diffusion coefficient D_0 is calculated as a function of the salinity S and temperature T using the R package CRAN: marelac (Soetaert 2010), which implements the constitutive relations listed in Boudreau (1997). The selected values are S = 35 and T=10°C.

To keep the model analysis tractable, sediment compaction is ignored, and so the porosity is taken to be constant with depth ($\varphi = 0.8$, a typical value for surface sediment in coastal environments). The absence of compaction also implies that the burial velocity of the pore water and the solid phase is identical. We fixed the sedimentation velocity at

$v = w$ = 0.2 cm yr^{-1}, which represents a typical accumulation regime for coastal environments (the coastal range is 0.01 to 0.5 cm yr^{-1} as in Boudreau 1997 and Mouret et al. 2009).

Bioturbation represents all faunal activities affecting the chemical composition of the sediment environment, and generally involves two components (Meysman et al. 2006; Kristensen et al. 2012b): (1) the physical reworking of the sediment matrix through burrowing activities, which in general leads to enhanced solid particle transport, here referred to as bio-mixing, and (2) the enhanced transport of pore water solutes due to burrow ventilation activities, which is referred to as bio-irrigation. Following the conventional description (Boudreau 1997), bio-mixing is described as a diffusive process (see Meysman et al. 2010 for a theoretical justification)

$$J_b = -(1-\varphi)D_b \frac{\partial S}{\partial z} \tag{15}$$

Benthic fauna are dependent on food resources that settle from the overlying water, and so their ecology is tightly associated to the sediment-water interface (SWI). Accordingly, the most intense sediment reworking activity occurs in the top sediment layer, and subsequently decreases with depth (Boudreau 1998). To describe this depth dependency, the biodiffusivity coefficient (D_b) follows a sigmoidal depth profile (Fig. 1a)

$$D_b(z) = D_{b,0} \exp\left(-\frac{(z-x_L)}{0.25x_{bm}}\right) \Bigg/ \left(1 + \exp\left(-\frac{(z-x_L)}{0.25x_{bm}}\right)\right) \tag{16}$$

where $D_{b,0}$ is the biodiffusivity at the SWI, x_L is the depth of the mixed layer and x_{bm} is an attenuation coefficient determining the width of the transition zone from mixed to unmixed sediment horizons. The biodiffusivity remains constant up to a depth of $x_L - x_{bm}/2$, after which it decreases to zero at $x_L + x_{bm}/2$.

Reaction processes

In addition to transport, concentration depth profiles are also influenced by a set of biogeochemical reactions, where R_k represents the reaction rate and $v_{i,k}$ denotes the stoichiometric coefficient of the i-th species in the k-th reaction. The baseline model includes a simplified set of reactions (n=14), which provide a description of organic matter degradation and sulfur cycling in a coastal sediment. Organic matter is subject to three mineralization pathways: aerobic respiration (AR), dissimilatory iron reduction (DIR) and

sulfate reduction (SR) (Table S1). Denitrification, methane formation and the reduction of manganese (hydr)oxides are not included, as these typically provide a smaller contribution to the total mineralization rate (Thamdrup 2000). The sequential usage of electron acceptors based on thermodynamic free energy gain (AR > DIR > SR) is implemented via a conventional limitation-inhibition formulation (Soetaert et al. 1996; Table S2).

The model contains a simplified iron and sulfur cycle (Table S1). Canonical sulfur oxidation (CSO) is the main default pathway of free sulfide oxidation, and is always turned on. Hence, CSO always competes with other pathways of sulfide oxidation, when these are present. The reduction of iron (oxyhydr)oxides releases ferrous iron (Fe^{2+}), which can become reoxidised by oxygen, or precipitate as iron sulfide. Similarly, free sulfide can be reoxidised by iron (oxyhydr)oxides or precipitate as iron sulfide (Reaction R9-10, 12-13; Table S1). Iron sulfides (FeS) can be further oxidized in the presence of oxygen (Reaction R11; Table S1). The kinetic rate expression of all re-oxidation processes are described by standard second-order rate laws (Boudreau 1997; Table S2). The precipitation/dissolution of calcium carbonate acts as a buffer against pH excursions (reactions K6 and K8 in Table S1). The kinetics of dissolution and precipitation of FeS and $CaCO_3$ follows the standard rate laws, where the reaction rate becomes dependent on the saturation state of the pore water (Van Cappellen and Wang 1995; Meysman et al. 2003; Table S2).

The model implements a new description of the metabolism of nitrate-accumulating *Beggiatoa*. The model includes the nitrate concentration in the pore water as well as the intracellular nitrate concentration as separate state variables. The uptake of nitrate is described as transfer from the pore water to the intracellular environments

$$NO_3^- \rightarrow \left\{NO_3^-\right\}_{\text{intracell}} \tag{17}$$

The nitrate uptake rate of the bacteria increases with the ambient nitrate concentration, and is slowed down when the intracellular vacuoles became saturated. The kinetics of this reaction is described via a second order rate law featuring both the intracellular nitrate concentration and the ambient free sulfide concentration in the pore water (Table S2). The reduction of nitrate

$$\left\{NO_3^-\right\}_{\text{intracell}} + 4H_2S + 2H^+ \rightarrow NH_4^+ + 4\left\{S_0\right\}_{\text{intracell}} + 3H_2O \tag{18}$$

The aerobic oxidation of the intracellular S^0 that is formed is also described by a second order rate law, featuring both the intracellular S^0 concentration as well as the ambient oxygen concentration. No attempt was made to model the random movement of individual *Beggiatoaceae* filaments. Instead, a decription was implemented that emulates the directional population-level transport of intracellular nitrate and elemental sulfur. This

172

was done via an advective formultion. The intracellular nitrate was given an advection velocity $v_{NO_3^-}$ = 50 cm yr^{-1} directed downwards, while the elemental sulfur was given an advection velocity v_{S^0} = 100 cm yr^{-1} directed upwards.

To describe the pH dynamics in the pore water, the biogeochemical model was equipped with a pH calculation procedure (see full details in Meysman et al., 2015). The modelled set of acid-base dissociation reactions includes the carbonate, borate, sulfide and water equilibria (reactions AB1-AB5, Table S1). The equilibrium constants for the acid-base reactions were calculated as a function of temperature and salinity using AquaEnv, a dedicated R-package for acid-base and CO2 system calculations (Hofmann et al., 2010). Specifically, for the carbonate equilibria, we used the relationships provided by Millero et al. (2006).

Numerical solution

The open-source programming language R was used to implement a numerical solution procedure for the partial differential equations Eqns. (13), following the procedures of Soetaert and Meysman (2012) and Meysman et al. (2015). The spatial derivatives within the partial differential equations Eqns. (13) were expanded over the sediment grid using finite differences by using the R package CRAN:ReacTran (see Soetaert and Meysman 2012 for details). This sediment grid was generated by dividing the sediment domain (thickness L = 10 cm) into 200 sediment layers of variable thickness, with a higher resolution near the sediment-water interface where most intense geochemical cycling takes place (the first layer was 0.005 cm thick and the thickness of the following layers increases with a factor 1.018). The resulting set of ordinary differential equations was integrated using the stiff equation solver vode using the package CRAN:deSolve (Soetaert et al. 2010). All model simulations were run for a sufficiently long time period (1000 yr) to allow them to reach a steady-state situation.

Table S1. List of biogeochemical reactions included in the sediment model. K-type reactions denotes "Kinetic reactions", E-type reactions stand for "Electrogenic reactions", while AB-type reactions correspond to "Acid-Base dissociation reactions".

	Mineralization	
OM1	Aerobic respiration	$CH_2O + O_2 \rightarrow HCO_3^- + H^+$
OM2	Iron reduction	$\{CH_2O\}_f + 4FeOOH + 7H^+ \rightarrow HCO_3^- + 4Fe^{2+} + 6H_2O$
OM3	Sulfate reduction	$CH_2O + \frac{1}{2}SO_4^{2-} \rightarrow HCO_3^- + \frac{1}{2}HS^- + \frac{1}{2}H^+$
	Iron cycling	
I1	Ferrous iron oxidation	$Fe^{2+} + \frac{1}{4}O_2 + \frac{3}{2}H_2O \rightarrow FeOOH + 2H^+$
I2	Iron sulfide oxidation	$FeS + \frac{9}{4}O_2 + \frac{3}{2}H_2O \rightarrow FeOOH + SO_4^{2-} + 2H^+$
I3	Sulfidic iron reduction	$HS^- + 8FeOOH + 15H^+ \rightarrow SO_4^{2-} + 8Fe^{2+} + 12H_2O$
	Iron cycling	
M1	Carbonate precipitation	$Ca^{2+} + HCO_3^- \rightarrow CaCO_3 + H^+$
M2	Carbonate dissolution	$CaCO_3 + H^+ \rightarrow Ca^{2+} + HCO_3^-$
M3	Iron sulfide precipitation	$Fe^{2+} + HS^- \rightarrow FeS + H^+$
M4	Iron sulfide dissolution	$FeS + H^+ \rightarrow Fe^{2+} + HS^-$
	Acid –base reactions	
AB1	Carbon dioxide dissociation	$CO_2 + H_2O \rightarrow HCO_3^- + H^+$
AB2	Bicarbonate dissociation	$HCO_3^- \rightarrow CO_3^{2-} + H^+$
AB3	Borate dissociation	$B(OH)_3 + H_2O \rightarrow B(OH)_4^- + H^+$
AB4	Sulfide dissociation	$H_2S \rightarrow HS^- + H^+$
AB5	Water dissociation	$H_2O \rightarrow OH^- + H^+$
	Canonical sulfur oxidation	
C1	Canonical sulfur oxidation	$\frac{1}{2}HS^- + O_2 \rightarrow \frac{1}{2}SO_4^{2-} + \frac{1}{2}H^+$
	Beggiatoa	
B1	Nitrate accumulation	$NO_3^- \rightarrow \{NO_3^-\}_{intracell}$
B2	Nitrate reduction	$\{NO_3^-\}_{intracell} + 4H_2S + 2H^+ \rightarrow NH_4^+ + 4\{S_0\}_{intracell} + 3H_2O$
B3	Elemental S oxidation	$\{S_0\}_{intracell} + \frac{3}{2}O_2 + H_2O \rightarrow SO_4^{2-} + 2H^+$
	Electrogenic sulfur oxidation	
E1	Cathodic oxygen reduction	$O_2 + 4e^- + 4H^+ \rightarrow 2H_2O$
E2	Anodic sulfide oxidation	$\frac{1}{2}HS^- + 2H_2O \rightarrow \frac{1}{2}SO_4^{2-} + 4e^- + 4.5H^+$

Table S2. List of kinetic rate expressions for the reactions included in the model. The rate expressions for kinetic reactions K1-K8 are standard formulations used in sediment biogeochemical models (Soetaert et al., 1996; Van Cappelen & Wang, 1996; Boudreau, 1996; Meysman et al, 2003). The rate expressions for electrochemical half-reactions E1 and E2 are newly introduced here (see text for details).

	Reaction	Kinetic rate expression
K1	Aerobic respiration	$R = (1-\phi)k_{\min}\left[CH_2O\right]\dfrac{\left[O_2\right]}{\left[O_2\right]+K_{O_2}}$
K2	Iron reduction	$R = (1-\phi)k_{\min}\left[CH_2O\right]\dfrac{\left[FeOOH\right]}{\left[FeOOH\right]+K_{FeOOH}}\dfrac{K_{O_2}}{\left[O_2\right]+K_{O_2}}$
K2	Sulfate reduction	$R = (1-\phi)k_{\min}\left[CH_2O\right]\dfrac{\left[SO_4^{2-}\right]}{\left[SO_4^{2-}\right]+K_{SO_4^{2-}}}\dfrac{K_{FeOOH}}{\left[FeOOH\right]+K_{FeOOH}}\dfrac{K_{O_2}}{\left[O_2\right]+K_{O_2}}$
K4	Ferrous iron oxidation	$R = \phi k_{FIO}\left[Fe^{2+}\right]\left[O_2\right]$
K5	Carbonate precipitation	$R = (1-\phi)k_{CP}\left(\left[Ca^{2+}\right]\left[CO_3^{2-}\right]/K_{CaCO_3}^{SP}-1\right)^{n_{CP}}$
K6	Carbonate dissolution	$R = (1-\phi)k_{CD}\left[CaCO_3\right]\left(1-\left[Ca^{2+}\right]\left[CO_3^{2-}\right]/K_{CaCO_3}^{SP}\right)^{n_{CD}}$
K7	Iron sulfide precipitation	$R = (1-\phi)k_{ISP}\left(\dfrac{\left[Fe^{2+}\right]\left[HS^-\right]}{\left[H^+\right]K_{FeS}^{SP}}-1\right)^{n_{ISP}}$
K8	Iron sulfide dissolution	$R = (1-\phi)k_{ISD}\left[FeS\right]\left(1-\dfrac{\left[Fe^{2+}\right]\left[HS^-\right]}{\left[H^+\right]K_{FeS}^{SP}}\right)^{n_{ISD}}$
C1	Canonical sulfur oxidation	$R = \phi k_{CSO}\left[O_2\right]\left[HS^-\right]$
I1	Sulfidic iron reduction	$R = (1-\phi)k_{SIR}\left[FeOOH\right]\left[HS^-\right]$
I2	Iron sulfide oxidation	$R = (1-\phi)k_{ISO}\left[O_2\right]\left[FeS\right]$
B1	Nitrate uptake	$R = \phi k_{NU}\left[NO_3^-\right]\dfrac{\{NO_3^-\}_{int}^{sat}}{\{NO_3^-\}_{int}^{sat}+\left[\{NO_3^-\}_{int}\right]}$
B2	Nitrate reduction	$R = \phi k_{NR}\left[\{NO_3^-\}_{int}\right]\left[HS^-\right]$
B3	Elemental S oxidation	$R = \phi k_{ESO}\left[\{S^0\}_{int}\right]\left[O_2\right]$
E1	Cathodic oxygen reduction	$R = \phi k_{COR}\left[O_2\right]\left[X_{charged}\right]$
E2	Anodic sulfide oxidation	$R = \phi k_{ASO}\left[HS^-\right]\left[X_{free}\right]$

Table S3. List of parameters included in the model. Solid phase concentrations are expressed per unit volume of solid phase. The concentration of charge carriers E_T is expressed per bulk volume of sediment. "Method" refers to the procedure by which parameter values are constrained: A = Measurements, B = Literature values, C = Sensitivity analysis, D = Microscopy data, E = Model Fitting. References: [1] Malkin et al. (2014) [2] Unpublished data from Lake Grevelingen field site [3] Soetaert et al (1996) [4] Boudreau (1997) [5] Meysman et al. (2003) [6] Van Capellen and Wang (1996), [7] Rickard (2006). (*) The concentration of charge carriers is expressed per unit volume of bulk sediment.

ENVIRONMENTAL PARAMETERS	Symbol	Value	Units	Method	References
Temperature	T	10	ºC	A	[1]
Salinity	S	32	-	A	[1]
Pressure	P	1.013	bar	A	[1]
Porosity	ϕ	0.8	-	A	[1]
Depth of sediment domain	L	5	cm	-	
Number of grid layers	N	100		-	
BIOGEOCHEMICAL PARAMETERS	**Symbol**	**Value**	**Units**	**Method**	**References**
Mineralization constant	k_{min}	1	yr^{-1}	B	[3], [4]
Oxygen saturation constant	K_{O_2}	0.001	mol m^{-3}	B	[5]
FeOOH saturation constant	K_{FeOOH}	10.4	mol m^{-3}	B	[5]
Sulfate saturation constant	$K_{SO_4^{2-}}$	0.9	mol m^{-3}	B	[5]
Ferrous iron oxidation	k_{FIO}	1e+07	mol^{-1} m^3	B	[5], [6]
CaCO$_3$ precipitation rate	k_{CP}	0	mol m^{-3}		
CaCO$_3$ dissolution rate	k_{CD}	10	yr^{-1}	B	[5]
FeS precipitation rate	k_{ISP}	1e+4	mol m^{-3}	B	[5]
FeS dissolution rate	k_{ISD}	3	yr^{-1}	B	[5]
Solubility CaCO3	$K_{CaCO_3}^{SP}$	0.39	(mol m^{-3})^2	B	[5]
Solubility FeS	K_{FeS}^{SP}	3.16	mol m^{-3}	B	[7]
CANONICAL S OXIDATION	**Symbo**	**Value**	**Units**	**Met**	**References**
Canonical sulfur oxidation	k_{CSO}	1e+7	mol^{-1} m^3	B	[5], [6]
IRON SHUTTLE	**Symbo**	**Value**	**Units**	**Met**	**References**
Bio-mixing intensity	D_B	4	cm^2 yr^{-1}	C	This work
Sedimentation velocity	v_{sed}	0.2	cm yr^{-1}	C	This work
Sulfidic iron reduction	k_{SIR}	494	mol^{-1} m^3	D	This work
Iron sulfide oxidation	k_{ISO}	1e+7	mol^{-1} m^3	E	This work
BEGGIATOA	**Symbo**	**Value**	**Units**	**Met**	**References**
Migration velocity	v_{mig}	100	cm yr^{-1}	C	This work
Nitrate uptake	k_{NU}	5e+4	mol^{-1} m^3	C	This work
Internal nitrate saturation	$\{NO_3^-\}_{i...}^{sat}$	0.2	mol m^{-3}	D	This work
Nitrate reduction	k_{NR}	1e+7	mol^{-1} m^3	D	This work
Elemental sulfur oxidation	k_{ESO}	1e+6	mol^{-1} m^3	E	This work
ELECTROGENIC	**Symbo**	**Value**	**Units**	**Met**	**References**
Cathodic oxygen reduction	k_{COR}	1.4e+8	mol^{-1} m^3	C	This work
Anodic sulfide oxidation	k_{ASO}	1.4e+8	mol^{-1} m^3	C	This work
Concentration charge	X_T	0.029	mol m^{-3}	D	This work
Diffusion coefficient	D_X	8.4e+4	cm^2 yr^{-1}	E	This work

Lake Grevelingen. Photo: Ilja Kocken

GENERAL DISCUSSION

7.1. Factors controlling hypoxia and euxinia

The seasonal depletion of oxygen in the bottom waters of coastal systems (coastal hypoxia) is an increasingly occuring phenomenon worldwide. Under certain circumstances, the removal of oxygen from the bottom water is also accompanied by the accumulation of free sulfide (euxinia), which is harmful for marine life. Marine ecosystems above hypoxic bottom waters are typically also locations of intense fishing activity, and hence their ecosystem functioning is of economical relevance. Therefore, it is urgent to understand how internal and external factors interact in causing hypoxia, not only to create a baseline understanding of these systems (prior to the shifts likely induced by global change) but also for providing suggestions for water management and policy.

Despite a number of studies conducted in hypoxic systems, it remains poorly understood what factors regulate the oxygen and sulfide concentrations in the bottom waters. Environmental factors, such as seasonal temperature variations (driving seasonal stratification) and nutrient input (driving primary production) are typically considered to be the major drivers of oxygen limitation in coastal systems. In addition to these external drivers, this study shows that internal factors such as sedimentary biogeochemical cycling mediated by microbes may also play a crucial role in regulating oxygen and sulfide concentrations in the water column.

To fully understand the complex condition of hypoxia in marine systems, it is necessary to perform multidisciplinary studies (i.e. investigating the geochemistry, physics/hydrodynamics and biology) over multiple seasons and years, in order to properly account for seasonal and interannual variability. In this thesis, such a detailed study was conducted on the water chemistry and sediment biogeochemistry in the seasonally hypoxic Lake Grevelingen. The resulting dataset allowed the evaluation of the role of sediments in nutrient regeneration and effluxes to the water column, and the development of bottom water hypoxia. Sediments are crucial in the development (or not) of sulfidic bottom waters, and this capability is strongly linked to the presence of a suboxic zone.

7.2. A new perspective on biogeochemical cycling in Lake Grevelingen

Lake Grevelingen was formed in 1971, after the construction of seaward and landward dams, which transformed the former Grevelingen estuary into a marine lake. The subsequent rapid transformation of the Grevelingen ecosystem attracted the attention of both scientists and the Dutch Environmental Agency (Rijkswaterstaat). Given the recreational relevance of Lake Grevelingen, the Dutch Environmental Agency established a monitoring program which performed monthly transects of the water column chemistry (GTSO measurements of O_2, temperature, and salinity).

At the same time, the ecology and geochemistry of the water column and sediments were extensively investigated in the decade that followed the closure of the dam (Nienhuis and van Ierland 1978; Lindeboom and Merks 1983; Bakker and De Vries 1984; Bannink and Van Der Meulen 1984; de Vries 1984; Nienhuis and Huis in 't Veld 1984). These

178

studies documented the occurrence of bottom water anoxia during spring and summer, which was linked to temperature and salinity stratification of the water column (Bakker and De Vries 1984). After this decade of intense ecological research into Lake Grevelingen, scientific attention however diminished. In the early 2000's, the Dutch Environmental Agency recognized that the seasonal bottom water oxygen depletion in Lake Grevelingen was a water quality problem, and started to consider remediation strategies. Currently, the agency is evaluating interventions aiming to improve the water quality and reduce the occurrence of hypoxia in the Grevelingen. The most important measure is to re-introduce a tidal regime and increase the flushing rate across the sluice in the seaward dam. As part of this investigation, a numerical model was developed, which aimed to predict the evolution of hypoxia in the Grevelingen under different scenarios of water exchange with the North Sea (Nolte and Spiteri 2011). This model predicted that the introduction of a tidal amplitude of 40 cm would significantly decrease the area affected by seasonal hypoxia in Lake Grevelingen.

As in other systems suffering from seasonal hypoxia, the bottom water depletion in Lake Grevelingen is caused by stratification (chapter 2) and increased oxygen consumption due to respiration in the water column and the sediment (chapter 3). However the source of the organic matter that is respired in the bottom waters of Lake Grevelingen is different compared to other coastal systems. Classically, bottom water depletion is linked to increased nutrient input from lands (eutrophication). However, compared to other Dutch coastal sytems, Lake Grevelingen is low in nutrients, and so eutrophication does not seem the main driver of seasonal hypoxia in Lake Grevelingen. Instead, Lake Grevelingen appears to act as a large sediment trap for fine silt and organic matter that is imported from the North Sea. The coastal waters of the North Sea have high concentrations of fine suspended matter, because of strong curents (over 1 m s^{-1}) and large tidel amplitudes (> 4 m). Once this North Sea water enters Grevelingen, it encounters the calmer conditions with low current velocities and no tides, so that the suspended matter floculates and sinks out as marine snow in the deeper basins (Fig. 1). As a result of the investigatons in this thesis, we conjecture that this marine snow imposes an important oxygen demand on the bottom waters of Lake Grevelingen. Accordingly, the oxygen demand is not exclusively driven by internal primary production (as in eutrophied systems), but is largely driven by an import of external organic matter due to the sediment trap mechanism.

Therefore, this thesis suggests that an increase in flushing rates will not necessarily cease the occurrence of summer hypoxia in Lake Grevelingen. Flushing with oxygenated North Sea water introduces oxygen in the water, but also introduces large amounts of suspended material. Therefore, not only the oxygen supply is increased, but also the oxygen demand. Long-term data show that the opening of the sluice in 1979 caused an increase in primary production due to external input of N (Nienhuis and Huis in 't Veld 1984) and also an increase in POC, with an import estimated to be 10 g C m^{-2} y^{-1} (de Vries 1984). In chapters 2 and 3, based on the carbon and O$_2$ balances, we suggest that Den Osse basin

functions as a sediment trap that retains the suspended material transported from the North Sea, which is accumulated in the sediments at the bottom of the basin (Fig. 1). I believe a similar mechanism occurs also in the other deep basins with the main gully, and the accumulation decreases with the distance from the seaward sluice. Moreover, in Chapter 2 we demonstrated that sediments are a major sink for oxygen, and are responsible for up to 30% of the total oxygen consumption within the Den Osse basin. These estimations were based on calculations that include measured respiration rates in the water column. Such rates carry an intrinsic uncertainty due to methodological issues (Hagens et al. 2015) and the measurements remain to be repeated in the future, for possible confirmation.
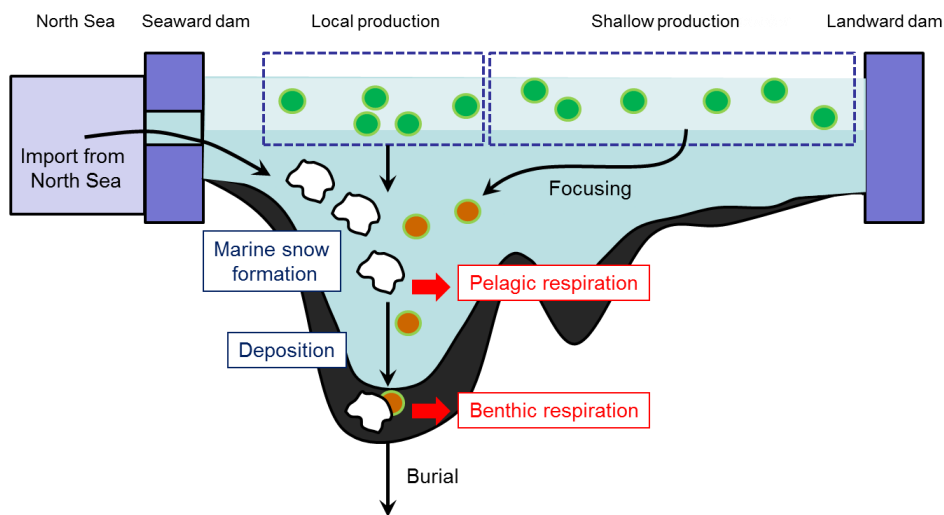
Figure 1. Schematic of organic matter cycling in Lake Grevelingen. See text for details.

Similar primary production rates were previously measured by de Vries (1984) during earlier investigation in Lake Grevelingen. This early study pointed out a discrepancy between respirations rates measured via benthic oxygen fluxes and primary production assessed via the ^{14}C-incubation method (de Vries 1984). Altogether these studies suggest that the excessive respiration compared to the *in situ* production rates point towards an external transport of organic material, likely from the adjacent North Sea. Hence, an increase in the flushing rates could lead to more trapping of fine material, thus enhancing respiration rates within the deep basins, leading to a rapid consumption of oxygen and hence possibly exacerbating hypoxia.

7.3. Amplified O_2 debt dynamics in seasonally hypoxic systems

In shallow coastal environments, the ratio between water volume and sediment area is low compared to the deep sea, and as a result, sediments can play a major role in the overall biogeochemical cycling of the coastal zone (Therkildsen and Lomstein, 1993). The sediment compartment is a hotspot for respiration, as up to 50-70 % of the organic matter produced in the water column can be mineralized in the sediment (Jørgensen 1977, 1982). Such high mineralization rates have an impact not only on nutrient cycling, but also on the oxygen dynamics. Therefore, coastal sediments are sites of intensified oxygen consumption, and constitute a major sink of oxygen within aquatic systems (Glud 2008). Furthermore, in freshwater lakes, or locked marine basins with a low ratio between the water volume and sediment area, sediments may be the major compartment of oxygen utilization, being responsible for up to 80% of the total oxygen consumption (Cornett and Rigler 1987; Pace and Prairie 2005). This contribution of sediments to the total oxygen consumption might be crucial in systems prone to hypoxia, as sedimentary oxygen consumption could potentially cause or exacerbate hypoxia, in periods with limited bottom water renewal (Middelburg and Levin 2009).

Within the sediment compartment, oxygen is consumed via aerobic respiration or re-oxidation or reduced compounds (Glud 2008). The oxygen required to reoxidize the reduced compounds that transiently accumulate in the sediment is defined as 'oxygen debt' (Pamatmat 1971). This oxygen debtmechanim has been recognized since long time as an important source of oxygen utilization in the sediment (Martens and Klump 1984; Chanton et al. 1987; Boynton et al. 1990; Rasmussen and Jorgensen 1992; Moeslund et al. 1994; Brady et al. 2013). In temperate marine systems organic matter mineralization, and consequently oxygen consumption displays a clear seasonal cycle. Seasonal patterns in sedimentary oxygen consumption are often complex and difficult to understand, as they are affected by simultaneous and interdependent processes (Glud, 2008). The sediment oxygen consumption is typically estimated via close-core sediment incubations that quantify the flux of oxygen at the sediment-water interface, commonly defined as total oxygen uptake (TOU). This method has been largely used in combination with water column chemistry in previous studies conducted in seasonally hypoxic sites eg. (Jørgensen 1980; Boynton et al. 1990; Koop et al. 1990; Cowan et al. 1996; Hammond et al. 1999; Bonaglia et al. 2014). Although this is a consolidated method, the measure of the TOU does not allow a full understanding of the dynamics of oxygen utilization. To overcome this limitation, in chapter 2, we complement the TOU measurements with water column chemistry and sediment geochemistry data, as well as microbial activity evidence. As a result, we show
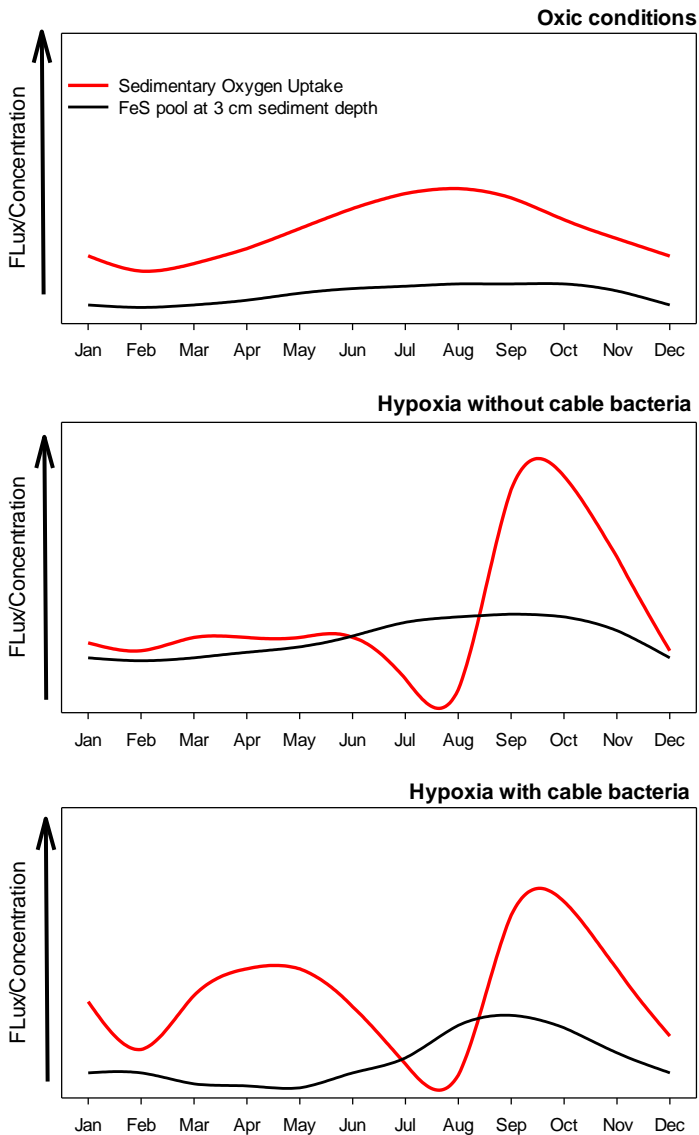
Figure 2. Impact of cable bacteria on oxygen debt dynamics. Seasonal variations of sedimentary FeS stock in the uppermost 3 cm of sediment (black line), and Total oxygen Uptake (red line; TOU) (upper panel) in systems with yearlong oxic conditions in the bottom water, (middle panel) in systems affected by hypoxia in the bottom water and without cable bacteria activity in the sediment and (lower panel) under hypoxic setting and with activity of cable bacteria. Cable bacteria deplete the FeS stock in spring and lower the oxygen debt in fall.

that the strong seasonality in sedimentary oxygen consumption in Lake Grevelingen is induced by an oxygen debt within the sediment. Moreover, we have shown for the first time, that the seasonal oxygen debt cycle works in an unexpected way. These dynamics are not controlled by external environmental factors (such as seasonal variation in bottom water temperature or input of organic matter), but instead, they are governed by seasonality in the presence and activity of key microbial players in the sediment.

Specifically, we have found that the metabolism of cable bacteria plays a crucial role in the sedimentary oxygen dynamics. Cable bacteria enhance the sedimentary oxygen consumption in winter by oxidizing the FeS in surficial sediments. The oxidation of FeS is the major source of the oxygen debt in Lake Grevelingen sediments, and hence variations in the FeS concentration cause pronounced changes in the oxygen debt dynamics. Accordingly, by depleting the iron sulfides in the sediment, cable bacteria lower the potential oxygen debt formed in the benthic compartment. In temperate systems as Lake Grevelingen, the oxygen debt is typically fulfilled in fall, via the reoxidation of the reduced compounds with oxygen, which causes an enhancement of the sedimentary oxygen consumption. Hence, by depleting the FeS pool in spring, cable bacteria reduce the overall oxygen debt of the systems, and indirectly lower the sedimentary oxygen consumption taking place in fall.

It became only possible to unravel this remarkable oxygen dynamics via high temporal resolution sampling campaigns, which combined not only geochemical approaches, but also microbiological data. Studies in seasonally hypoxic systems are typically concentrated around the period of oxygen depletion. In chapter 2 we show that processes taking place before and after the hypoxic period are equally crucial in determining the response of the systems to hypoxia, as they affect the composition of the surficial sediment, and the concentrations of the oxygen-consuming compounds.

7.4. Suboxic zone formation and pH fingerprinting

Coastal sediments are sites of intense sulfate reduction, which generates vast amounts of free sulfide that accumulate in the porewater. In the present-day seafloor, most of the sulfide is oxidized by oxygen. However, the associated reaction of this oxidation requires the direct contact between oxygen and sulfide, and thus gives rise to what we refer here to as the "aerobic sulfide oxidation paradox". Although oxygen is the principal electron acceptor oxidizing free sulfide, it has been known for a long time that in most coastal sediments, the depth profiles of O_2 and H_2S do not overlap (Jorgensen, 1982). Instead, the more common situation is that a so-called "suboxic zone" i.e., a distinct sediment horizon where neither O_2 nor H_2S are detectable (Froelich et al. 1979), is observed.

The suboxic zone is a layer within marine sediments where both oxygen and sulfide are absent. Since its first explicit recognition by Froelich et al. (1979), the presence of the suboxic zone has been frequently documented in biogeochemical studies conducted in the coastal zone (e. g. Thamdrup et al. 1994; Aller 1994; Dale et al. 2011) as well as in the

deep sea eg. (Reimers 1996; Zopfi et al. 2008; Lichtschlag et al. 2010). These studies demonstrate that the presence of a suboxic layer is a widespread phenomenon in the seafloor.

Within organic-rich coastal sediments, characterized by high rates of sulfate reduction, the suboxic zone thickness typically ranges from millimeters to centimeters. This raises the intriguing question how aerobic sulfur oxidation can still proceed, when the two key reagents (i.e., O_2 and H_2S) do not co-occur in space. In Chapter 6 we review the known mechanisms via which aerobic oxidation of sulfide can take place in marine sediments, and that lead to the formation of a suboxic zone. Three major mechanisms have been documented: (1) bioturbation, (2) the metabolism of nitrate-accumulating *Beggiatoaceae* and (3) the electrogenic metabolism of cable bacteria.
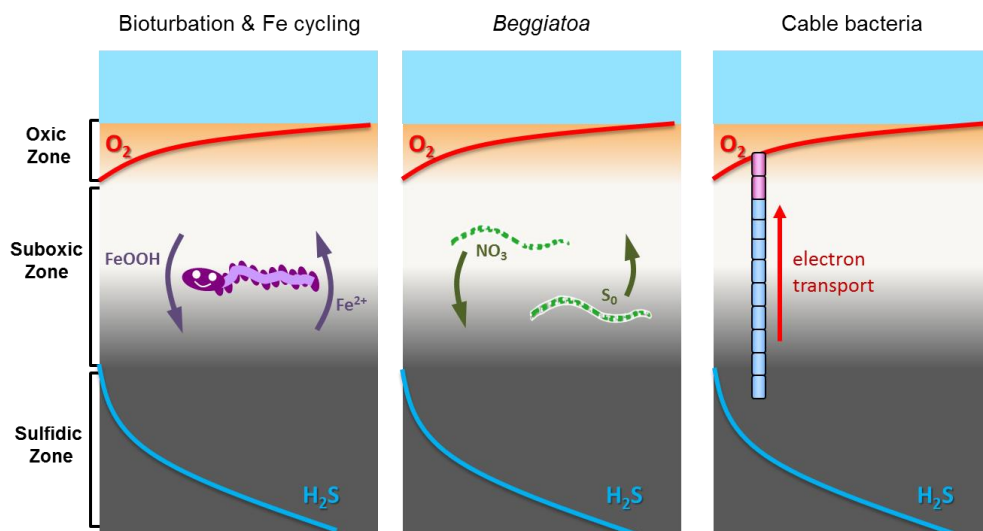
Figure 3. Schematic of aerobic sulfide oxidation enabled by bioturbation-driven metal cycling (left), sulfur oxidation by nitrate-accumulating bacteria (middle) and electrogenic sulfur oxidation by cable bacteria (right).

When sediments are intensively mixed through bioturbation by infauna, oxidized iron minerals are mixed downwards and reduced iron minerals are mixed upwards, and this can create an electron shuttle between H_2S and O_2, thus forming a suboxic zone (Canfield et al. 1993b). A second mechanism emerged from the detailed investigation of the metabolism of large colorless bacteria, such as *Beggiatoaceae* (McHatton et al. 1996; Schulz and Jørgensen 2001; Mussmann et al. 2003; Sayama et al. 2005). Through intracellular accumulation of intermediate redox compounds (NO_3, S^0), these large motile bacteria also generate an electron shuttle between H_2S and O_2, which equally leads to a suboxic zone. A

184

third mechanism of suboxic zone formation has only been very recently discovered (Nielsen et al. 2010). It depends on the ability of long, filamentous sulfur-oxidizing bacteria, termed cable bacteria, to transport electrons over centimeters scale distances. Although very distinct, these three mechanisms share the capability of bringing together electron donor and acceptor, which otherwise would be remotely distributed over the sediment layers. Such abilities equip the players of these three mechanisms with an undoubtful advantage over the canonical sulfide oxidation that can function only via direct contact between oxygen and sulfide.

In addition, we developed a conceptual and numerical model that, based on the depth distribution of three solutes (O_2, pH and H_2S) allows to distinguish which of these three mechanism actually creates the suboxic zone in a given sediment (Fig. 3). This thesis hence provides a new tool to diagnose the dominant mechanism that has created the suboxic zone. This analysis was developed by combining observations (microsensor profiling) with numerical modelling (reactive transport description of pore water chemistry) and specific microscopical investigations (i.e. light microscopy form fauna and *Beggiatoaceae* and FISH in the case of cable bacteria). One remaining challenge is natural variability, as natural sediment samples display spatial heterogeneity in the distribution of geochemical compounds and biological species. In addition, different biogeochemical processes may co-occur in natural samples.

The ecological significance of the suboxic zone is that it constitutes a buffer layer against the release of sulfide to the bottom water. Sulfide can be released in the bottom water only after that the sulfide horizon diffuses upwards towards the sediment surface and progressively depletes the thickness of the suboxic zone. This process may take from days to few months, depending on the thickness of the suboxic zone, the concentration of the reactive minerals, and the biological rates of sulfide oxidation. Such effect may be crucial in seasonally hypoxic sites (as for instance Lake Grevelingen) as it may impede the release of sulfide to the bottom water for a long enough time before that the oxygen returns to the systems. Such a buffering effect avoids the consequent toxic effects on the living organisms, and offers a surface where fauna can recolonize.

7.5. Cable bacteria influence the biogeochemical cycling of both sediment and water column

Cable bacteria have only recently been discovered from marine sediments (Nielsen et al. 2010; Pfeffer et al. 2012). These filamentous bacteria couple the oxidation of free sulfide at centimeters depth within the sediment to the reduction of oxygen at the surface by conducting electrons along their longitudinal axis (Nielsen and Risgaard-Petersen 2015). Knowledge on the role of cable bacteria in sediment geochemistry (Risgaard-Petersen et al. 2012; Meysman et al. 2015; Rao et al. 2016) and in the ecology of marine systems is rapidly growing (Malkin et al. 2014; chapter 4, 5). Cable bacteria have been documented to

naturally occur in a range of marine settings, including also seasonally hypoxic systems (Malkin et al. 2014).

A detailed seasonal study showed that cable bacteria are abundant in the sediments of Lake Grevelingen during winter and spring, prior to the onset of hypoxia in the bottom waters (chapters 4, 5). Hypoxic conditions in the bottom water combined with high sulfate reduction rates lead to the accumulation of free sulfide in surficial sediments. However, bottom waters are rich in oxygen throughout the rest of the year, and hence, the combination of oxic water and sulfidic sediments allows for cable bacteria to reach a high abundance. Cable bacteria do not only thrive in seasonally hypoxic sediments, but their metabolism strongly impacts the sedimentary geochemical cycling in these systems (chapter 4, 5).

In previous laboratory investigations (Risgaard-Petersen et al. 2012; Rao et al. 2016) and model studies (Meysman et al. 2015), it was proposed that cable bacteria cause dissolution of iron sulfides in this sediment layer by imposing acidic conditions in the porewater of the suboxic zone. In this way, these bacteria are able to indirectly 'extract' sulfide from iron sulfides, which constitutes a large pool of reduced sulfur within marine sediments. In this thesis, iron sulfide dissolution driven by cable bacteria was shown – for the first time – to occur under natural conditions (chapter 4). In spring, during maximal activity of cable bacteria, the low pH conditions imposed by the electrogenic oxidation of sulfide, caused the dissolution of the iron sulfides in the suboxic zone (Fig. 4). A secondary effect of such dissolution was the mobilization of reduced iron, which could later on re-precipitate as a layer of reactive iron hydr(oxides) near the sediment surface. The presence of the oxidized iron pool became crucial during summer anoxia, as it could efficiently bind the large amounts of sulfide that were being produced via sulfate reduction during the summer months. The precipitation of free sulfide lowered its concentration in the porewater and it ultimately impeded the release of sulfide to the bottom water, avoiding the possible toxic effect for the living fauna. In this way, the pool of reactive iron constituted a 'firewall' against the release of sulfide to the bottom water (chapter 4). Given that the formation of the reactive iron layer was indirectly induced by the electrogenic metabolism of cable bacteria, these microorganisms were responsible for triggering a 'firewall' mechanism in Lake Grevelingen sediments.

The removal of sulfide from the porewater and bottom water has consequences not only for S and Fe cycling, but also on other biogeochemical cycles. The iron hydr(oxides) layer contained also a large stock of iron-oxide-bound phosphorus, which was then released to the water column upon the reduction of the iron (hydr)oxides in summer (chapter 5). Such release of phosphorus from the sediment increased availability of this element in the water column. These results challenge the classical paradigm that changes in input of reactive organic matter and oxygen supply to surface sediments predominantly control the seasonal
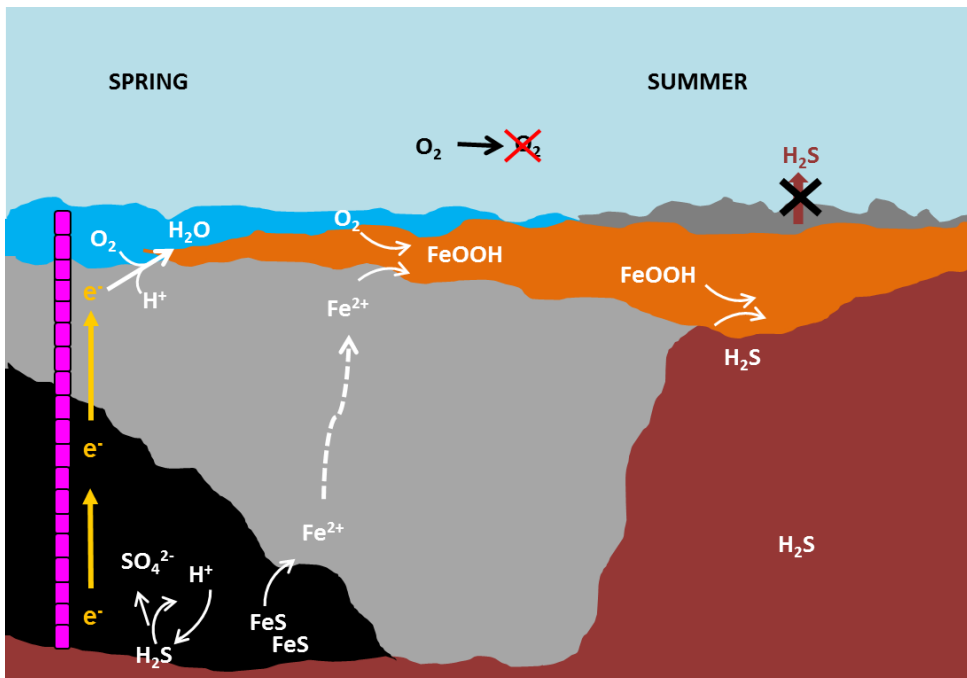
Figure 4. In spring, cable bacteria abound in the top centimeters of the sediment and oxidize hydrogen sulfide. The electrons from sulfide oxidation are passed to the sediment surface through internal electric 'wires' and donated to oxygen (blue). The hydrogen sulfide is derived from concurrent sulfate reduction but also from dissolution of a large storage of iron sulfide (black). Protons from the anodic oxidation process promote further dissolution of iron sulfide, and the dissolved ferrous iron diffuses to the surface where it reacts with oxygen to form a crust of iron hydroxide (orange). When oxygen depletion develops in late summer and sulfate reduction intensifies, the iron 'firewall' is ready to capture the hydrogen sulfide that accumulates in the sediment (dark red). Modified from Nielsen (2016).

build-up of Fe-oxide-P observed in aquatic sediments. Instead, cable bacteria are the key drivers of sediment Fe-oxide-bound P formation, allowing for a highly efficient P retention in the sediment.

Overall, during winter and late spring, sulfide was mainly removed biologically via e-SOx from cable bacteria, and also chemically upon reaction with the iron hydr(oxides) whose formation was induced by cable bacteria. Hence, cable bacteria were the main players of sulfide oxidation in Lake Grevelingen sediments, and such sulfide removal process had a potential detoxifying effect on the the benthic environment. The detoxification of the surface sediment could potentially promote the recolonization of benthic fauna in the following months, and hence, might have positive repercussion an ecosystem scale. The reestablishment of a bioturbation activity after a successful recolonization of fauna may

replenish the surface sediment with reactive minerals, which can act as an additional buffer against the accumulation of sulfide, potentially strengthening the buffering capacity of the sediments towards sulfide.

7.6. **Competition among filamentous S-oxidizing bacteria**

During a five yearlong survey we investigated the distribution of cable bacteria and *Beggiatoaceae* in different sites within Lake Grevelingen (chapter 4). At a particular deep site experiencing seasonal oxygen depletion (S1 in this thesis), the two bacterial groups were following a temporal succession, where *Beggiatoaceae* were dominant in autumn after summer hypoxia, while cable bacteria become dominant throughout late winter and spring (Fig. 5). Such temporal succession suggests that each of them was competitively successful at different periods of the year. Accordingly, the two filamentous S-oxidizing bacteria appeared to be competing for the same geochemical niche in these sediments.

The filamentous cable bacteria and large *Beggiatoaceae* (> 20 μm of diameter) are both able to access spatially segregated pools of electron acceptors and donors, but utilize entirely different strategies. Cable bacteria have developed a unique capability, whereby via electrical currents, they can exploit the oxidation of sulfide occurring at centimeters depth within the sediment and tap into the oxygen pool present at the sediment surface (Nielsen et al. 2010; Pfeffer et al. 2012). Like cable bacteria, large *Beggiatoaceae* are capable of harvesting free sulfide at centimeters depth, but they do so by transporting nitrate inside intracellular vacuoles to the sulfidic zone (Schulz and Jørgensen 2001; Mussmann et al. 2003; Sayama et al. 2005). Nitrate is a powerful electron acceptor, and once transported to the sulfidic zone which is rich in electron donors but lacks oxidative species, it can sustain bacterial growth.

Whether these two bacterial groups create or are able to exploit the suboxic zone, observations from Lake Grevelingen (chapter 4) and Tokyo Bay (Sayama 2011) suggest that cable bacteria and *Beggiatoaceae* likely compete for the same resources. The nature and modalities of such competition remain to be further investigated. Here, I briefly discuss the environmental and internal population factors that might govern the outcome of this microbial competition.

A first factor controlling this microbial competition might be the electron acceptor availability. *Beggiatoaaceae* are adapted to low oxygen concentrations and show phobic behavior to oxygen concentrations > 5% saturation. Cable bacteria thrive at fully oxic conditions, although they have been found to survive at lower oxygen conditions (Laurine Burdorf personal communication). Another electron acceptor that can be potentially used by both bacteria is nitrate. Marzocchi et al. (2014) recently established via laboratory incubations that cable bacteria may develop in sediments where oxygen in the overlying water has been replaced with nitrate. On the other side, *Beggiatoaaceae* are known to perform sulfide oxidation via intracellular nitrate vacuoles (Mussmann et al. 2003; Sayama
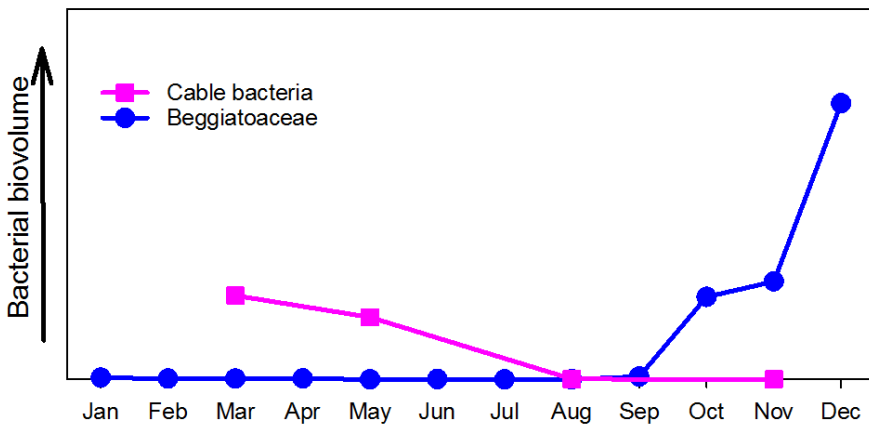
Figure 7. Biovolume distribution of cable bacteria and Beggiatoaceae at S1 sediments throughout 2012. Cable bacteria were enumerated in March, May, August, and November; Beggiatoaceae were counted monthly over the entire year 2012.

et al. 2005). Such capability would potentially give them a competitive advantage over the cable bacteria.

A second factor could be the electron donor availability. Both bacteria are capable of harvesting energy from the oxidation of free sulfide generated by sulfate reduction within the sediment. *Beggiatoaceae* are known to be able to cope with high concentrations of free sulfide (up to mM levels), but there are no studies reporting on the tolerance of cable bacteria to sulfide concentrations. I believe that the form of sulfide is more important rather than the absolute concentration. Therefore, the speciation of the electron donor might be a key factor in the competition between the two bacterial groups. Cable bacteria have access to an extra supply of sulfide which is originated by the dissolution of the iron sulfides. This reduced form of sulfides is typically abundant in marine sediments and cable bacteria induce their dissolution, and hence the release of free sulfide, by imposing acidic condition into the porewater. Accordingly, cable bacteria may harvest sulfide from an 'extra' source compared to *Beggiatoaaceae*. However, laboratory studies have shown that the rapid growth of the cable bacteria population occurs in concert with the depletion of the iron sulfide pool and both events are followed by a fast decline of the cable bacteria abundance (Schauer et al. 2014). A comparable condition was observed in Lake Grevelingen (S1, chapter 4) in March, suggesting that the depletion of the iron sulfides stock may have caused to the disappearance of cable bacteria at the sampling site. Hence, the competitive advantage of cable bacteria linked to the capability of utilizing this 'extra' sulfide source

may last up to few months, in absence of replenishment via iron and sulfur cycling or external transport.

Although cable bacteria and *Beggiatoaceae* make use of different strategies to spatially connect the electron donor and acceptor, they both need to traverse the suboxic zone to access these compounds. Hence, the thickness of the suboxic zone might be a crucial factor in the competition between the two bacteria. *Beggiatoaceae* use negative chemotactic responses to confine their distribution between the boundaries of oxygen/nitrate and sulfide. In order to glide towards sulfide and afterwards find their way back to the sediment surface, where they may replenish their nitrate vacuoles they rely on simple random walks to move within the suboxic zone (Dunker et al. 2011). *Beggiatoaceae* therefore spend a time that is 100 time longer than the period required to cross the suboxic zone in a straight line (Dunker et al. 2011). Although sulfide does not accumulate at detectable concentrations in the suboxic zone, radiotracer studies have demonstrated that large amounts of this reduced species are being produced via microbial sulfate reduction (Jørgensen et al. 2010). Hence, within the suboxic zone *Beggiatoaceae* are not limited by the electron donor, but by the amount of electron acceptor they carry to the anoxic zone.

The concentrations of the intracellular nitrate will hence determine the period the *Beggiatoaceae* can survive in the suboxic zone, and hence, the length of the zone that can traverse (Dunker et al. 2011). Preisler et al. (2007) estimated that the *Beggiatoaceae* could remain motile for 21 days within the suboxic zone of coastal sediments, whereas at the Lake Grevelingen site (S1) we estimated that the *Beggiatoaceae* could survive for around 4 days before depleting their reservoir of 51 mmol L^{-1} (assuming a nitrate consumption of 13 mmol L^{-1} d^{-1}; Preisler et al. 2007). Our estimations likely underestimate the real potential of nitrate storage from the *Beggiatoaceae* at the field site (chapter 4), due to the low number of filaments and replicates used for our analysis.

Further measurements are hence required to elucidate the nitrate storage capability of *Beggiatoaceae* in the Lake Grevelingen sediments. At present, little is known on the depth limit at which cable bacteria can expand their network. Field studies have shown that cable bacteria can expand up to 6 cm depth in the sediment.

Cable bacteria activity is sensitive to mechanical disturbance of the filament network (Pfeffer et al. 2012), and initially it was proposed that bioturbation could be a factor limiting the distribution of cable bacteria in natural sediments (Malkin et al. 2014). However, more recent field studies have shown that cables successfully colonize bioturbated coastal sediments (Malkin et al. 2016). Therefore, it is likely that physical disturbance is not a major factor affecting the competition between cable bacteria and *Beggiatoaceae*.

In conclusion, in terms of the electron donor availability, low oxygen concentrations in the bottom water favour the growth of *Beggiatoaceae*, as they can thrive at these conditions and are more efficient than cable bacteria in utilizing nitrate for respiration. The speciation of the electron donor plays a role as well, as cable bacteria, contrary to the *Beggiatoaceae,*

are able to exploit the sedimentary iron sulfide stock. However, such capability represents only a short term competitive advantage, as cable bacteria deplete the stock in few months period. *Beggiatoaceae* face a depth limit at which they can extend their exploration for free sulfide, as after a certain depth the population typically collapses as the filaments run out of nitrate. In this way, the geochemical niche becomes suddenly free, but does not imply that it can be colonized by cable bacteria as they are known to grow starting from an overlap between oxygen and sulfide. Only in the eventuality that this conditions is followed by environmental events that for instance resuspend the sediment and bring in contact oxygen and sulfide then cable bacteria might establish (as hypothesized in Chapter 4). Based on these considerations, I speculate that *Beggiatoaceae* would be more successful in reduced sulfidic sediments underlying hypoxic to anoxic bottom waters, whereas cable bacteria could rapidly colonize anoxic sediment that are suddenly covered by oxygenated waters.

However, my consideration are based on field data, which are typically difficult to interpret, as they depend on multiple and interdependent environmental and internal factors. Moreover, variability in spatial distribution of the geochemical species and patchy distribution of bacteria might mask the governing factors. In this thesis I focused on the temporal succession of the two bacterial groups at a specific field site (S1). We rarely found the two bacterial groups coexisting in the same site, but intriguingly, a site located only 500 m apart from this site (S2; chapter 2) was always dominated by *Beggiatoaceae*. This suggests that the nature and form of this competition remains to be consolidated by specific laboratory experiments.

Popularizing summary: Electrical microbes protect coastal areas from toxic nightmare

When coastal areas suffer from oxygen depletion, sulfide is released from the seafloor, a chemical compound that is highly toxic for marine life. Luckily, this scenario is not often observed, but it was unclear why. Researchers from the Royal Netherlands Institute of Sea Research, Utrecht University and the Vrije Universiteit Brussel have now discovered that electricity-generating bacteria act as a kind of guardian angels and prevent sulfide from escaping the sediment. This discovery is important in helping designing strategies of how coastal ecosystems can cope with future climate change.

Why are toxic nightmares so rare?

Oceanographers have known for long time that under the right conditions, the bottom waters of coastal areas can turn into a real chemical nightmare. In some places, the oxygen gradually disappears from the bottom waters during summer months, and on top of that, the sediments underneath start accumulating hydrogen sulfide, a chemical that is known for its odor of "rotten eggs", and which is highly toxic to marine life. The situation becomes disastrous when this hydrogen sulfide gas is released from the sediments, and mixed into the overlying water. Such sulfide eruptions are known from a few places in the world, such as the coast of Namibia, where massive cohorts of lobsters have been observed to flee the sea, crawling onto the beach to avoid the poisonous gas in the water. 'The ecological and fisheries impact of these sulfide cataclysms can be enormous, but luckily, they are really exceptional' explains team leader Prof. dr. ir. Filip Meysman 'The problem was that we didn't really understand why these events are so rare. It's good to know that you're lucky, but it is much better to know why you're lucky. Our study now demonstrates that there is a natural "firewall" mechanism in place that delays or even prevents the escape of sulfide from sediments. This way, coastal systems that are susceptible to oxygen depletion are protected from the horrid environmental degradation that comes with sulfide release."

Saved by electricity

The mechanism was discovered in Lake Grevelingen, a coastal basin in the south of the Netherlands, which experiences strong oxygen depletion in the deeper waters every summer. "In 2012, we went out on a research ship every month, and made a very detailed study of the chemistry and microbiology of the sediments in Lake Grevelingen" explains PhD student Dorina Seitaj, the lead author of the study. "What we found was really amazing. In spring, the seafloor was colonized by high densities of long, filamentous electricity-generating bacteria. These so-called cable bacteria were only discovered a few years ago, and are able to send an electrical current along their body over centimeter distances. This electrical metabolism allows them to mobilize large quantities of iron deeper in the seafloor." The dissolved iron then moves upwards and precipitates as an

orange iron crust near the sediment surface. In summer, high quantities of sulfide are generated within the sediment, but the sulfide cannot escape the sediment. Fatimah Suluh-Gambari, responsible for the sediment chemistry in the research project, clarifies: "The iron crust deposited by the cable bacteria has a high binding capacity for sulfide, and so it acts as a firewall against sulfide, sealing the sediment and preventing the release of sulfide into the overlying water."

Global effect

Over the last 5 years, the research team has organized regular field trips to Lake Grevelingen, demonstrating that the electricity-generating bacteria are always present in spring, and so the firewall mechanism is a yearly recurring phenomenon. This is good news for the local oyster fisheries in Lake Grevelingen, as it reduces the risk of mass mortality due to upwelling of deeper toxic waters. Moreover, members of the same research team have recently demonstrated that cable bacteria are also abundant in many other coastal systems worldwide. Therefore, the firewall mechanism may be widespread in other coastal systems that are suffering oxygen depletion in summer. This is particularly relevant, as the frequency and intensity of coastal oxygen depletion is increasing. This is linked to an increased input of nutrients from land to the coastal zone in combination with warmer seawater resulting from climate change.

Popularizerende samenvatting: Electrische bacteriën beschermen kustgebieden tegen giframp

    Wanneer in de zomer de zuurstof daalt in het water van kustgebieden, kan er sulfide ontsnappen uit de zeebodem, een chemische stof die zeer toxisch is voor het leven in zee. Gelukkig genoeg gebeurt dit slechts zeer uitzonderlijk. Onderzoekers van het Koninklijk Nederlands Instituut voor Onderzoek der Zee, Utrecht Universiteit en de Vrije Universiteit Brussel hebben ontdekt dat elektriciteit-producerende bacteriën als een soort beschermengel optreden door er voor te zorgen dat de sulfide niet ontsnapt uit het sediment. De ontdekking gebeurde in het Grevelingen meer (Zeeland) en is goed nieuws voor de lokale oesterkwekers. Wereldwijd helpt het onderzoek in het wapenen van kustecosystemen tegen de gevolgen van klimaatverandering.

Waarom zo zeldzaam?

Oceanografen weten reeds lang dat onder de juiste omstandigheden in de zomer, het diepere water van kustgebieden zich kan omvormen tot een chemische nachtmerrie. Nabij de zeebodem verdwijnt dan de zuurstof uit het water, en tegelijkertijd, stapelt sulfide gas zich op in het onderliggende sediment. Sulfide is een chemisch stof die ruikt naar rotte eieren, en die zeer toxisch is voor het leven in zee. De situatie wordt echt rampzalig voor het ecosysteem wanneer deze sulfide ontsnapt uit de zeebodem, en opgewerveld wordt in het bovenliggende water. Dergelijke sulfide uitbarstingen zijn bekend van slechts een aantal plekken in de wereld, zoals voor de kust van Namibië, waarbij ganse cohorten van kreeften de zee uitvluchten, en redding zoeken op het strand om te ontsnappen aan het giftige goedje. "Gelukkig komt dit zeer zelden voor, want wanneer sulfide ontsnapt uit zeebodem is dit steeds een catastrofe voor het lokale ecosysteem en de bijhorende visserij" legt Prof. dr. ir. Filip Meysman uit, het hoofd van het onderzoeksteam. "Het probleem is dat we niet goed begrepen waarom er zo weinig sulfide ontsnapt. Het is goed om te weten dat je geluk hebt, maar het is nog beter om te weten waarom je geluk hebt. Onze studie toont aan dat er een natuurlijke proces aan het werk is dat sulfide verhindert om te ontsnappen uit de zeebodem."

Gered door electriciteit

Het mechanisme werd ontrafeld na intens onderzoek in de Grevelingen, een zout meer in Zeeland dat in verbinding staat met de Noordzee, en waar elke zomer het diepere water zuurstofloos wordt. "In 2012 zijn we elke maand uitgevaren met ons onderzoeksschip, en hebben we een zeer gedetailleerde studie uitgevoerd van de chemie en microbiologie in de sedimenten van het Grevelingen meer" legt Dorina Seitaj uit, doctoraatsstudent en eerste auteur van de publicatie. "Het was een echte verassing wat we ontdekten. In de lente werd de zeebodem gekoloniseerd door lange, draadvormige bacteriën die elektriciteit produceren en geleiden. Deze zogenaamde kabelbacteriën zijn slechts recent ontdekt, en zijn in staat

om een elektrische stroom te geleiden over een afstand van centimeters." Door hun elektrische manier van ademhalen zorgen kabelbacteriën ervoor dat een grote hoeveelheid ijzer wordt gemobiliseerd in de zeebodem. Dit opgeloste ijzer migreert vervolgens naar boven en slaat neer als een oranje laag nabij het oppervlak van het sediment. Fatimah Suluh-Gambari, verantwoordelijk voor de sediment geochemie in het project, legt nader uit: "Ijzer heeft een zeer sterke bindingcapaciteit voor sulfide. De ijzerlaag die door de kabel bacteriën is aangemaakt verzegeld als het ware het sediment, zodat de sulfide niet naar het bovenliggende water kan. Sulfide wordt dus in grote hoeveelheden aangemaakt in de zeebodem, maar kan niet ontsnappen, waardoor een toxische ramp vermeden wordt."

Wereldwijd effect

De laatste vijf jaar heeft het onderzoeksteam regelmatig onderzoek uitgevoerd in het Grevelingen meer, en daarbij werd duidelijk dat elektriciteits-producerende kabel bacteriën elke lente weer terugkeren. Dit is zeer goed nieuws voor de lokale oesterkwekers in het Grevelingen meer, omdat dit de kans sterk verkleint dat dieper sulfide-rijk water opborrelt in de zomer, en zo massale sterfte veroorzaakt in de ondiep gelegen oesterbedden. Leden van hetzelfde onderzoeksteam hebben onlangs ook aangetoond dat kabel bacteriën in kustsystemen overal ter wereld voorkomen. Het "beschermengel" mechanisme komt dus waarschijnlijk ook voor in vele andere gebieden die te maken hebben met zuurstofgebrek. Dit is zeer belangrijk aangezien het aantal meldingen van zuurstofloosheid in kustgebieden sterk toeneemt. Deze trend is gelinkt aan een verhoogde afvoer van voedingsstoffen via rivieren en warmer zeewater onder invloed van klimaatverandering

.

REFERENCES

Aller, R. C. 1977. The influence of macrobenthos on chemical diagenesis of marine sediments. Yale University.

Aller, R. C. 1988. Benthic fauna and biogeochemical processes in marine sediments, p. 301–338. *In* T.H. Blackburn and J. Sorensen [eds.], Nitrogen cycling in coastal marine environments. John Wiley and Sons, New York.

Aller, R. C. 1994. The sedimentary Mn cycle in Long Island Sound: Its role as intermediate oxidant and the influence of bioturbation, O2, and Corg flux on diagenetic reaction balances. J. Mar. Res. **52**: 259–295.

Aller, R. C. 2001. Transport and Reactions in the Bioirrigated Zone., p. 269–301. *In* The Benthic Boundary Layer: Transport Processes and Biogeochemistry. eds., Oxford University Press, Oxford.

Aller, R. C. 2014. Sedimentary Diagenesis, Depositional Environments, and Benthic Fluxes, p. 293–334. *In* H.D.H. and K.K. Turekian [ed.], Treatise on Geochemistry. Elsevier, Oxford.

Aller, R. C., and P. D. Rude. 1988. Complete oxidation of solid phase sulfides by manganese and bacteria in anoxic marine sediments. Geochim. Cosmochim. Acta **52**: 751–765.

Anderson, J. J., and A. H. Devol. 1987. Extent and intensity of the anoxic zone in basins and fjords. Deep Sea Res. Part A, Oceanogr. Res. Pap. **34**: 927–944.

Andersson, L., and L. Rydberg. 1988. Trends in nutrient and oxygen conditions within the kattegat: Effects of local nutrient supply. Estuar. Coast. Shelf Sci. **26**: 559–579.

Archer, D., and A. Devol. 1992. Benthic oxygen fluxes on the Washington shelf and slope : A comparison of in situ microelectrode and chamber flux measurements. Limnol. Oceanogr. **37**: 614–629.

Bakker, C., and I. De Vries. 1984. Phytoplankton- and nutrient dynamics in saline lake grevelingen (SW Netherlands) under different hydrodynamical conditions in 1978-1980. Netherlands J. Sea Res. **18**: 191–220.

Bannink, B. A., and J. H. M. Van Der Meulen. 1984. Lake Grevelingen: from an estuary to a saline lake. an introduction. J. Sea Res. **18**: 179–190.

Banta, G., M. Holmer, M. Jensen, and E. Kristensen. 1999. Effects of two polychaete worms, Nereis diversicolor and Arenicola marina, on aerobic and anaerobic decomposition in a sandy marine sediment. Aquat. Microb. Ecol. **19**: 189–204.

Beer, D. De, E. Sauter, H. Niemann, N. Kaul, U. Witte, and M. Schlu. 2006. In situ fluxes and zonation of microbial activity in surface sediments of the Ha ̊ kon Mosby Mud Volcano. Limnol. Oceanogr. **51**: 1315–1331.

Berg, P., S. Rysgaard, and B. O. Thamdrup. 2003. Dynamic Modeling of Early Diagenesis and Nutrient Cycling. A Case Study in an Arctic Marine Sediment. Arctic **303**: 905–955.

Berner, R. A. 1970. Sedimentary Pyrite Formation. Am. J. Sci. **268**: 1–23.

Berner, R. a., and J. T. Westrich. 1985. Bioturbation and the early diagenesis of carbon and sulfur. Am. J. Sci. **285**: 193–206.

196

Boesch, D. F., and N. N. Rabalais. 1991. Effects of hypoxia on continental shelf benthos: comparisons between the New York Bight and the Northern Gulf of Mexico. Geol. Soc. London, Spec. Publ. **58**: 27–34.

Bonaglia, S., B. Deutsch, M. Bartoli, H. K. Marchant, and V. Brüchert. 2014. Seasonal oxygen, nitrogen and phosphorus benthic cycling along an impacted Baltic Sea estuary: Regulation and spatial patterns. Biogeochemistry **119**: 139–160.

Boudreau, B. P. 1992. Mean mixed depth of sediments: The wherefore and the why. Limnol. Oceanogr. **46**: 524–526.

Boudreau, B. P. 1996. The diffusive tortuosity of fine-grained unlithified sediments. Geochim. Cosmochim. Acta **60**: 3139–3142.

Boudreau, B. P. 1997. Diagenetic Models and their Implementation, Springer-Verlag Berlin Heidelberg New York.

Boudreau, B. P. 1998. Mean Mixed Depth of Sediments: the Wherefore and the Why. Limnol. Oceanogr. **43**: 524–526.

Bouldin, D. R. 1968. Models for Describing the Diffusion of Oxygen Mud-Water Interface. J. Ecol. **56**: 77–87.

Boynton, W. R., and W. M. Kemp. 2000. Influence of river flow and nutrient loads on selected ecosystem processes: A synthesis of Chesapeake Bay data. Estuar. Sci. A Synth. Approach to Res. Pract. 269–298.

Boynton, W. R., W. M. Kemp, J. M. Barnes, J. L. W. Cowan, S. E. Stammerjohn, L. L. Matteson, F. M. Rohland, and M. Marvin. 1990. Long-Term Characteristics and nends of Benthic Oxygen and Nutrient Fluxes in the Maryland Portion of Chesapeake Bay. *New Perspectives in the Chesapeake System: A Research and Management Partnership.* Chesapeake Research Consortium Publication. 239–354.

Brady, D. C., J. M. Testa, D. M. Di Toro, W. R. Boynton, and W. M. Kemp. 2013. Sediment flux modeling: Calibration and application for coastal systems. Estuar. Coast. Shelf Sci. **117**: 107–124.

Brüchert, V., B. Currie, and K. R. Peard. 2009. Hydrogen sulphide and methane emissions on the central Namibian shelf. Prog. Oceanogr. **83**: 169–179.

Brüchert, V., B. Currie, K. R. Peard, U. Lass, R. Endler, ArneD, Ubecke, E. Julies, ThomasLeipe, and and S. Zitzmann. 2006. Biogeochemical and physical control on shelf anoxia and water column hydrogen sulphide in the Benguel a coastal upwelling system off Namibia, p. 161–193. *In* Past and Present Water Column Anoxia.

Burdorf, L. D. W., S. Hidalgo-Martinez, P. L. M. Cook, and F. J. R. Meysman. 2016. Long-distance electron transport by cable bacteria in mangrove sediments. Mar. Ecol. Prog. Ser. **545**: 1–8.

Burton, E. D., L. a. Sullivan, R. T. Bush, S. G. Johnston, and A. F. Keene. 2008. A simple and inexpensive chromium-reducible sulfur method for acid-sulfate soils. Appl. Geochemistry **23**: 2759–2766.

Cai, W., and C. Reimers. 1995. Benthic oxygen flux, bottom water oxygen concentration and core top organic carbon content in the deep northeast Pacific Ocean. Deep Sea

Res. Part I Oceanogr. Res. Pap. **42**: 1681–1699.

Cai, W.-J., X. Hu, W.-J. Huang, M. C. Murrell, J. C. Lehrter, S. E. Lohrenz, W.-C. Chou, W. Zhai, J. T. Hollibaugh, Y. Wang, P. Zhao, X. Guo, K. Gundersen, M. Dai, and G.-C. Gong. 2011. Acidification of subsurface coastal waters enhanced by eutrophication. Nat. Geosci. **4**: 766–770.

Cai, W.-J., and F. L. Sayles. 1996. Oxygen penetration depths and fluxes in marine sediments. Mar. Chem. **52**: 123–131.

Canfield, D. E. 1993. Organic matter oxidation in marine sediments, p. 333–363. *In* C.L. Wollast R, Mackenzie FT [ed.], Interactions of C, N, P, and S biogeochemical cycles and global change.

Canfield, D. E. 2005. The early history of atmospheric oxygen: homage to Robert M. Garrels. Annu. Rev. Earth Planet. Sci. **33**: 1–36.

Canfield, D. E., and J. Farquhar. 2009. Animal evolution, bioturbation, and the sulfate concentration of the oceans. Proc. Natl. Acad. Sci. U. S. A. **106**: 8123–8127.

Canfield, D. E., B. B. Jorgensen, H. Fossing, R. Glud, J. Gundersen, N. B. Ramsing, B. Thamdrup, J. W. Hansen, L. P. Nielsen, and P. O. Hall. 1993a. Pathways of organic carbon oxidation in three continental margin sediments. Mar. Geol. **113**: 27–40.

Canfield, D. E., F. J. Stewart, B. Thamdrup, L. De Brabandere, T. Dalsgaard, E. F. Delong, N. P. Revsbech, and O. Ulloa. 2010. A cryptic sulfur cycle in oxygen-minimum-zone waters off the Chilean coast. Science **330**: 1375–1378.

Canfield, D. E., and B. Thamdrup. 2009. Towards a consistent classification scheme for geochemical environments, or, why we wish the term "suboxic" would go away. Geobiology **7**: 385–392.

Canfield, D. E., B. Thamdrup, and J. W. Hansen. 1993b. The anaerobic degradation of organic matter in Danish coastal sediments: iron reduction, manganese reduction, and sulfate reduction. Geochim. Cosmochim. Acta **57**: 3867–83.

Van Cappellen, P., and Y. Wang. 1995. Metal cycling in surface sediments: Modeling the interplay of transport and reaction, p. 21–64. *In* H.E. Allen [ed.], Metal Contaminated Aquatic Sediments. Ann Arbor Press.

Carstensen, J., J. H. Andersen, B. G. Gustafsson, and D. J. Conley. 2014a. Deoxygenation of the Baltic Sea during the last century. Proc. Natl. Acad. Sci. **111**: 5628–5633.

Carstensen, J., D. J. Conley, E. Bonsdorff, B. G. Gustafsson, S. Hietanen, U. Janas, T. Jilbert, A. Maximov, A. Norkko, J. Norkko, D. C. Reed, C. P. Slomp, K. Timmermann, and M. Voss. 2014b. Hypoxia in the Baltic Sea: Biogeochemical cycles, benthic fauna, and management. Ambio **43**: 26–36.

Cembella, A. D., N. J. Antia, and P. J. Harrison. 1982. The utilization of inorganic and organic phosphorous compounds as nutrients by eukaryotic microalgae: a multidisciplinary perspective: part 1. Crit. Rev. Microbiol. **10**: 317–391.

Chanton, J. P., C. S. Martens, U. S. G. Survey, and M. B. Goldhaber. 1987. Biogeochemical cycling in an organic-rich coastal marine basin. 7. Sulfur mass balance, oxygen uptake and sulfide retention. Geochim. Cosmochim. Acta **51**: 1187–

1199.

Cite, B. J. not to. 2004. Edited by, p. 63–81. *In* and T.W.L. J. P. Amend, K. J.Edwards [ed.], Sulfide oxidation in marine sediments: geochemistry meets microbiology.

Cline, J. 1969. Spectrophotometric determination of hydrogen sulfide in natural waters. Limnol. Oceanogr. 454–458.

Codispoti, L. a. 2005. Suboxic respiration in the oceanic water column, p. 225–247. *In* P.W. PA DelGiorgio [ed.], Respiration in aquatic ecosystems. New York: Oxford Univ. Press.

Codispoti, L. a, J. a Brandes, J. P. Christensen, a H. Devol, S. W. a Naqvi, H. W. Paerl, and T. Yoshinari. 2001. The oceanic fixed nitrogen and nitrous oxide budgets : Moving targets as we enter the anthropocene? Sci. Mar. **65**: 85–105.

Van Colen, C., F. Montserrat, M. Vincx, P. Herman, T. Ysebaert, and S. Degraer. 2008. Macrobenthic recovery from hypoxia in an estuarine tidal mudflat. Mar. Ecol. Prog. Ser. **372**: 31–42.

Conley, D. J., S. Björck, E. Bonsdorff, J. Carstensen, G. Destouni, B. G. Gustafsson, S. Hietanen, M. Kortekaas, H. Kuosa, H. E. M. Meier, K. N. B. Müller-Karoulis, A. Norkko, G. Nürnberg, H. Pitkänen, N. N. Rabalais, R. Rosenberg, O. P. Savchuk, C. P. Slomp, M. Voss, F. Wulff, and L. Zillen. 2009. Hypoxia-Related Processes in the Baltic Sea. Environ. Sci. Technol. **43**: 3412–3420.

Conley, D. J., J. Carstensen, G. Ærtebjerg, P. B. Christensen, T. Dalsgaard, J. L. S. Hansen, and A. B. Josefson. 2007. Long-Term Changes and Impacts of Hypoxia in Danish Coastal Waters. Ecol. Appl. **17**: S165–S184.

Cornett, R. J., and F. H. Rigler. 1987. Decomposition of Seston in the Hyolimnion. Can. J. Fish. Aquat. Sci. **44**: 146–151.

Cowan, J. L. W., J. R. Pennock, and W. R. Boynton. 1996. Seasonal and interannual patterns of sediment-water nutrient and oxygen fluxes in Mobile Bay, Alabama (USA): Regulating factors and ecological significance. Mar. Ecol. Prog. Ser. **141**: 229–245.

Cowan, L. W. and B. 1996. Sediment-Water Oxygen and Nutrient Exchanges Along the Longitudinal Axis of Chesapeake Bay : Seasonal Patterns , Controlling Factors and Ecological Significance. Estuaries **19**: 562–580.

Dale, A. W., V. J. Bertics, T. Treude, S. Sommer, and K. Wallmann. 2013. Modeling benthic-pelagic nutrient exchange processes and porewater distributions in a seasonally-hypoxic sediment: evidence for massive phosphate release by Beggiatoa? Biogeosciences Discuss. **9**: 11517–11575.

Dale, a. W., S. Sommer, L. Bohlen, T. Treude, V. J. Bertics, H. W. Bange, O. Pfannkuche, T. Schorp, M. Mattsdotter, and K. Wallmann. 2011. Rates and regulation of nitrogen cycling in seasonally hypoxic sediments during winter (Boknis Eck, SW Baltic Sea): Sensitivity to environmental variables. Estuar. Coast. Shelf Sci. **95**: 14–28.

Dauer, D. M., A. J. Rodi, and J. A. Ranasinghe. 1992. Effects of Low Dissolved Oxygen Events on the Macrobenthos of the Lower Chesapeake Bay. Estuaries **15**: 384.

REFERENCES

Delaney, M. L. 1998. Phosphorus accumulation in marine sediments and the oceanic phosphorus cycle. Global Biogeochem. Cycles **12**: 563.

Diaz, R. J. 2001. Overview of hypoxia around the world. J. Environ. Qual. **30**: 275–281.

Diaz, R. J., and R. Rosenberg. 1995. Marine Benthic Hypoxia : a review of its icological effects and the behavioural responses of benthic macrofauna. Oceanogr. Mar. Biol. Annu. Rev. **33**: 245–303.

Diaz, R. J., and R. Rosenberg. 2008. Spreading dead zones and consequences for marine ecosystems. Science (80-.). **321**: 926–9.

Dickson, A. G., C. L. Sabine, and J. R. Christian. 2007. Guide to Best Practices for Ocean CO2 15 Measurements, PICES special publication, 3, North Pacific Marine Science Organization Place: Sidney, British Columbia.

Donders, T. H., E. Guasti, F. P. M. Bunnik, and H. van Aken. 2012. Impact van de Brouwersdam op zuurstofcondities in de Grevelingen; reconstructies uit natuurlijke sediment archieven.

Dunker, R., H. Røy, A. Kamp, and B. B. Jørgensen. 2011. Motility patterns of filamentous sulfur bacteria, Beggiatoa spp. FEMS Microbiol. Ecol. **77**: 176–85.

Ekau, W., H. Auel, H. O. Portner, and D. Gilbert. 2010. Impacts of hypoxia on the structure and processes in pelagic communities (zooplankton, macro-invertebrates and fish). Biogeosciences **7**: 1669–1699.

Falkowski, P. G., T. Algeo, and L. a. Codispoti. 2011. Ocean De - oxygen - ation : Past , Present , and Future. EOS, Trans. Am. Geophys. Union **92**: 409–420.

Feistel, R. 2008. A Gibbs function for seawater thermodynamics for −6 to 80°C and salinity up to 120gkg–1. Deep Sea Res. Part I Oceanogr. Res. Pap. **55**: 1639–1671.

Fenchel, T. 1996. Worm burrows and oxic microniches in marine sediments. 1. Spatial and temporal scales. Mar. Biol. **127**: 289–295.

Ferdelman, T. G., C. Lee, S. Pantoja, J. Harder, B. M. Bebout, and H. Fossing. 1997. Sulphate reduction and methanogenesis in a Thioploca-dominated sediment off the coast of Chile. Geochim. Cosmochim. Acta **61**: 3065–3079.

Fick, A. 1855. Uber Diffusion. Ann. Phys. (N. Y). **94**: 59–86.

Follmi, K. 1996. The phosphorus cycle, phosphogenesis and marine phosphate-rich deposits. Earth-Science Rev. **40**: 55–124.

Fossing, H., V. a. Gallardo, B. B. Jørgensen, M. Hüttel, L. P. Nielsen, H. Schulz, D. E. Canfield, S. Forster, R. N. Glud, J. K. Gundersen, J. Küver, N. B. Ramsing, a. Teske, B. Thamdrup, and O. Ulloa. 1995. Concentration and transport of nitrate by the mat-forming sulphur   bacterium Thioploca. Nature **374**: 713–715.

Froelich, P. N., M. A. Arthur, W. C. Burnett, M. Deakin, V. Hensley, R. Jahnke, L. Kaul, K. H. Kim, K. Roe, A. Soutar, and C. Vathakanon. 1988. Early diagenesis of organic matter in Peru continental margin sediments: Phosphorite precipitation. Mar. Geol. **80**: 309–343.

Froelich, P. N. N., G. P. P. Klinkhammer, M. L. L. Bender, N. a. A. Luedtke, G. R. R. Heath, D. Cullen, P. Dauphin, D. Hammond, B. Hartman, and V. Maynard. 1979.

Early oxidation of organic matter in pelagic sediments of the eastern equatorial Atlantic: suboxic diagenesis. Geochim. Cosmochim. Acta **43**: 1075–1090.

Gächter, R., J. S. Meyer, and A. Mares. 1988. Contribution of bacteria to release and fixation of phosphorus in lake sediments. Limnol. Oceanogr. **33**: 1542–1558.

Gallardo, V. A. 1977. Large benthic microbial communities in sulphide biota under Peru– Chile Subsurface Countercurrent. Nature **268**: 331–332.

Gartman, A., M. Yücel, A. S. Madison, D. W. Chu, S. Ma, C. P. Janzen, E. L. Becker, R. a. Beinart, P. R. Girguis, and G. W. Luther. 2011. Sulfide Oxidation across Diffuse Flow Zones of Hydrothermal Vents. Aquat. Geochemistry **17**: 583–601.

Giordani, G., R. Azzoni, and P. Viaroli. 2008. A rapid assessment of the sedimentary buffering capacity towards free sulphides. Hydrobiologia **611**: 55–66.

Glazer, B. T., G. W. Luther, S. K. Konovalov, G. E. Friederich, R. E. Trouwborst, and A. S. Romanov. 2006. Spatial and temporal variability of the Black Sea suboxic zone. Deep. Res. Part II Top. Stud. Oceanogr. **53**: 1756–1768.

Glud, R. N. 2008. Oxygen dynamics of marine sediments. Mar. Biol. Res. **4**: 243–289.

Glud, R. N., J. K. Gundersen, H. Røy, and B. B. Jørgensen. 2003. Seasonal dynamics of benthic O2 uptake in a semienclosed bay: Importance of diffusion and faunal activity. Limnol. Oceanogr. **48**: 1265–1276.

Glud, R. N., B. Thamdrup, H. Stahl, F. Wenzhoefer, A. Glud, H. Nomaki, K. Oguri, N. P. Revsbech, and H. Kitazato. 2009. Nitrogen cycling in a deep ocean margin sediment (Sagami Bay, Japan). Limnol. Oceanogr. **54**: 723–734.

Goldhaber, M., R. C. Aller, J. Cochran, J. Rosenfeld, C. Martens, and R. A. Berner. 1977. Sulfate reduction, diffusion and bioturbation in long island sound sediments: report of the foam group. Am. J. Sci. **277**: 193–237.

Goldhammer, T., V. Brüchert, T. G. Ferdelman, and M. Zabel. 2010. Microbial sequestration of phosphorus in anoxic upwelling sediments. Nat. Geosci. **3**: 557–561.

Greenwood, N., E. R. Parker, L. Fernand, D. B. Sivyer, K. Weston, S. J. Painting, S. Kröger, R. M. Forster, H. E. Lees, D. K. Mills, and R. W. P. M. Laane. 2010. Detection of low bottom water oxygen concentrations in the North Sea; implications for monitoring and assessment of ecosystem health. Biogeosciences **7**: 1357–1373.

Gruber, N. 2008. The Marine Nitrogen Cycle, p. 1–50. *In* E.C. DG Capone, DA Bronk, MR Mulholland [ed.], Nitrogen in the Marine Environment. Burlington, MA: Academic.

Grünke, S., a. Lichtschlag, D. de Beer, J. Felden, V. Salman, a. Ramette, H. N. Schulz-Vogt, and a. Boetius. 2012. Mats of psychrophilic thiotrophic bacteria associated with cold seeps of the Barents Sea. Biogeosciences **9**: 2947–2960.

Gustafsson, B. G., F. Schenk, T. Blenckner, K. Eilola, H. E. M. Meier, B. M??ller-Karulis, T. Neumann, T. Ruoho-Airola, O. P. Savchuk, and E. Zorita. 2012. Reconstructing the development of baltic sea eutrophication 1850-2006. Ambio **41**: 534–548.

Hagens, M., C. P. Slomp, F. J. R. Meysman, D. Seitaj, J. Harlay, a V Borges, and J. J. Middelburg. 2015. Biogeochemical processes and buffering capacity concurrently affect acidification in a seasonally hypoxic coastal marine basin. Biogeosciences **12**:

1561–1583.

Hall, P. O. J., L. G. Onderson, M. M. R. Van Der Loeff, B. Sundby, and S. F. G. Westerlund. 1989. Oxygen uptake kinetics in the benthic boundary layer. Limnol. Oceanogr. **34**: 734–746.

Hamerlynck, O., K. Hostens, J. Mees, R. V. Arellano, A. Cattrijsse, and J. A. van de Vyver, P Craeymeersch. 1992. The ebb tidal delta of the Grevelingen: a man-made nursery for flatshif? Netherlands J. Sea Res. **30**: 191–200.

Hammond, D. ., P. Giordani, W. . Berelson, and R. Poletti. 1999. Diagenesis of carbon and nutrients and benthic exchange in sediments of the Northern Adriatic Sea. Mar. Chem. **66**: 53–79.

Hedges, J., and R. Keil. 1995. Sedimentary organic matter preservation: an assessment and speculative synthesis. Mar. Chem. **49**: 81–115.

Heijs, S. K., H. M. Jonkers, H. Van Gemerden, B. E. M. Schaub, and L. J. Stal. 1999. The Buffering Capacity Towards Free Sulphide in Sediments of a Coastal Lagoon (Bassin d ' Arcachon , France)— the Relative Importance of Chemical and. Estuar. Coast. Shelf Sci. 21–35.

Helly, J. J., and L. A. Levin. 2004. Global distribution of naturally occurring marine hypoxia on continental margins. Deep. Res. Part I Oceanogr. Res. Pap. **51**: 1159–1168.

Hofmann, A. F., K. Soetaert, J. J. Middelburg, and F. J. R. Meysman. 2010. AquaEnv: An aquatic acid-base modelling environment in R,.

Holland, a. F., A. T. Shaughnessy, and M. H. Hiegel. 1987. Long-term variation in mesohaline Chesapeake Bay macrobenthos: Spatial and temporal patterns. Estuaries **10**: 227–245.

Holmer, M., C. M. Duarte, and N. Marbá. 2003. Sulfur cycling and seagrass (Posidonia oceanica) status in carbonate sediments. 223–239.

Holmkvist, L., T. G. Ferdelman, and B. B. Jørgensen. 2011. A cryptic sulfur cycle driven by iron in the methane zone of marine sediment (Aarhus Bay, Denmark). Geochim. Cosmochim. Acta **75**: 3581–3599.

Ingall, E. D., R. M. Bustin, and P. Van Cappellen. 1993. Influence of water column anoxia on the burial and preservation of carbon and phosphorus in marine shales. Geochim. Cosmochim. Acta **57**: 303–316.

Ingall, E., and R. Jahnke. 1994. Evidence for enhanced phosphorus regeneration from marine sediments overlain by oxygen depleted waters. Geochim. Cosmochim. Acta **58**: 2571–2575.

Jannasch, H. W., C. O. Wirsen, and S. J. Molyneaux. 1991. Chemoautotrophic sulfur-oxidizing bacteria from the Black Sea. Deep Sea Res. Part A. Oceanogr. Res. Pap. **38**: S1105–S1120.

Jäntti, H., and S. Hietanen. 2012. The effects of hypoxia on sediment nitrogen cycling in the Baltic Sea. Ambio **41**: 161–9.

Jensen, H. S., P. B. Mortensen, F. O. Andersen, E. Rasmussen, and a. Jensen. 1995.

Phosphorus cycling in a coastal marine sediment, Aarhus Bay, Denmark. Limnol. Oceanogr. **40**: 908–917.

Jilbert, T., C. P. Slomp, B. G. Gustafsson, and W. Boer. 2011. Beyond the Fe-P-redox connection: preferential regeneration of phosphorus from organic matter as a key control on Baltic Sea nutrient cycles. Biogeosciences **8**: 1699–1720.

Jørgensen, B. B. 1977. The sulfur cycle of a coastal marine sediment (Limfjorden, Denmark). Limnol. Oceanogr. **22**: 814–832.

Jørgensen, B. B. 1980. Seasonal oxygen depletion in the bottom waters of a Danish depletion and its effect on the benthic community. Oikos **34**: 68–76.

Jørgensen, B. B. 1982. Mineralization of organic matter in the sea bed – the role of sulphate reduction. Nature **296**: 643–645.

Jørgensen, B. B. 1983. Processes at the sediment–water interface., p. 477–509. *In* B.& R.B.C. Bolin [ed.], The Major Biogeochemical Cycles and Their Interactions. SCOPE 21, Stockholm.

Jørgensen, B. B. 1996. Case Study - Aarhus Bay, p. 137–154. *In* K. Richardson and B.B. Jørgensen [eds.], Eutrophication in Coastal Marine Ecosystems. Coastal and Estuarine Studies. American Geophysical Union, Washington D.C., USA.

Jørgensen, B. B., M. Bang, and T. H. Blackburn. 1990. Anaerobic Mineralization in Marine-Sediments From the Baltic-Sea-North-Sea Transition. Mar. Ecol. Ser. **59**: 39–54.

Jørgensen, B. B., R. Dunker, S. Grünke, and H. Røy. 2010. Filamentous sulfur bacteria, Beggiatoa spp., in arctic marine sediments (Svalbard, 79 degrees N). FEMS Microbiol. Ecol. **73**: 500–13.

Jørgensen, B. B., H. Fossing, C. O. Wirsen, and H. W. Jannasch. 1991. Sulfide oxidation in the anoxic Black Sea chemocline. Deep Sea Res. Part A. Oceanogr. Res. Pap. **38**: S1083–S1103.

Jørgensen, B. B., and V. A. Gallardo. 1999. Thioploca spp.: Filamentous sulfur bacteria with nitrate vacuoles. FEMS Microbiol. Ecol. **28**: 301–313.

Jørgensen, B. B., and D. J. Des Marais. 2008. The Diffusive Boundary Layer of Sediments : Oxygen Microgradients Over a Microbial Mat The diffusive boundary layer of sediments : Oxygen microgradients over a microbial mat. Limnol. Oceanogr. **35**: 1343–1355.

Jørgensen, B. B., and D. C. Nelson. 2004. Sulfide oxidation in marine sediments: geochemistry meets microbiology, p. 283–284. *In* J.P. Amend, K. J.Edwards, and T.W. Lyons [eds.], Sulfur biogeochemistry—past and present. The Geochemical Society of America.

Jørgensen, B. B., and J. R. Postgate. 1982. Ecology of the Bacteria of the Sulphur Cycle with Special Reference to Anoxic-Oxic Interface Environments. Philos. Trans. R. Soc. B Biol. Sci. **298**: 543–561.

Jørgensen, B. B., and N. P. Revsbech. 1983. Colorless Sulfur Bacteria, Beggiatoa spp. and Thiovulum spp., in O2 and H2S Microgradients. Appl. Environ. Microbiol. **45**: 1261–

1270.

Jourabchi, P., P. Van Cappellen, and P. Regnier. 2005. Quantitative interpretation of pH distributions in aquatic sediments: A reaction-transport modeling approach. Am. J. Sci. **305**: 919–956.

Joye, S. B., and J. T. Hollibaugh. 1995. Influence of Sulfide Inhibition of Nitrification on Nitrogen Regeneration in Sediments. Sci. (washingt. D C) **270**: 623–625.

Justić, D., T. Legović, and L. Rottini-Sandrini. 1987. Trends in oxygen content 1911–1984 and occurrence of benthic mortality in the northern Adriatic Sea. Estuar. Coast. Shelf Sci. **25**: 435–445.

Kana, T. M., C. Darkangelo, M. D. Hunt, J. B. Oldham, G. E. Bennett, and J. C. Cornwell. 1994. Membrane inlet mass spectrometer for rapid high-precision determination of N2, O2, and Ar in environmental water samples. Anal. Chem. **66**: 4166–4170.

Kana, T. M., M. B. Sullivan, J. C. Cornwell, and K. M. Groszkowski. 1998. Denitrification in estuarine sediments determined by membrane inlet mass spectrometry. Limnol. Oceanogr. **43**: 334–339.

Karlson, K., R. Rosenberg, and E. Bonsdorff. 2002. Temporal and spatial large-scale effects of eutrophication and oxygen deficiency on benthic fauna in Scandinavian and Baltic waters - a review. Oceanogr. Mar. Biol. Annu. Rev. 427–489.

Kartal, B., M. M. M. Kuypers, G. Lavik, J. Schalk, H. J. M. Op Den Camp, M. S. M. Jetten, and M. Strous. 2007. Anammox bacteria disguised as denitrifiers: Nitrate reduction to dinitrogen gas via nitrite and ammonium. Environ. Microbiol. **9**: 635–642.

Keeling, R. F., A. Körtzinger, and N. Gruber. 2010. Ocean Deoxygenation in a Warming World. Ann. Rev. Mar. Sci. **2**: 199–229.

Kemp, W. M., W. R. Boynton, J. E. Adolf, D. F. Boesch, W. C. Boicourt, G. Brush, J. C. Cornwell, T. R. Fisher, P. M. Glibert, J. D. Hagy, L. W. Harding, E. D. Houde, D. G. Kimmel, W. D. Miller, R. I. E. Newell, M. R. Roman, E. M. Smith, and J. C. Stevenson. 2005. Eutrophication of Chesapeake Bay: Historical trends and ecological interactions. Mar. Ecol. Prog. Ser. **303**: 1–29.

Kemp, W. M., P. Sampou, J. Caffrey, M. Mayer, K. Henriksen, and W. R. Boynton. 1990. Ammonium recycling versus denitrification in Chesapeake Bay sediments. Limnol. Oceanogr. **35**: 1545–1563.

Kemp, W. M., J. M. Testa, D. J. Conley, D. Gilbert, and J. D. Hagy. 2009. Temporal responses of coastal hypoxia to nutrient loading and physical controls. Biogeosciences **6**: 2985–3008.

Klump, J. V., and C. S. Martens. 1981. Biogeochemical cycling in an organic rich coastal marine basin—II. Nutrient sediment-water exchange processes. Geochim. Cosmochim. Acta **45**: 101–121.

Knap, A., A. Michaels, and A. Close. 1994. The JGOFS Protocols.

Konovalov, S. K., and J. W. Murray. 2001. Variations in the chemistry of the Black Sea on a time scale of decades (1960-1995). J. Mar. Syst. **31**: 217–243.

Koop, K., W. R. Boynton, F. Wulff, and R. Carman. 1990. Sediment-water oxygen and

nutrient exchanges along a depth gradient in the Baltic Sea. Mar. Ecol. Prog. Ser. **63**: 65–77.

Kostka, J. E., B. Gribsholt, E. Petrie, D. Dalton, H. Skelton, and E. Kristensen. 2002. The rates and pathways of carbon oxidation in bioturbated saltmarsh sediments. Limnol. Oceanogr. **47**: 230–240.

Kraal, P., E. D. Burton, and R. T. Bush. 2013. Iron monosulfide accumulation and pyrite formation in eutrophic estuarine sediments. Geochim. Cosmochim. Acta **122**: 75–88.

Kraal, P., C. P. Slomp, A. Forster, M. M. M. Kuypers, and S. A. 2009. Pyrite oxidation during sample storage determines phosphorus fractionation in carbonate-poor anoxic sediments. Geochim. Cosmochim. Acta **73**: 3277–3290.

Kristensen, E. 2000. Organic matter diagenesis at the oxic/anoxic interface in coastal marine sediments, with emphasis on the role of burrowing animals. Hydrobiologia **426**: 1–24.

Kristensen, E. 2001. Impact of polychaetes (Nereis spp. and Arenicola marina) on carbon biogeochemistry in coastal marine sediments. Geochem. Trans. **2**: 92.

Kristensen, E., and J. E. Kostka. 2005. Macrofaunal burrows and irrigation in marine sediment: microbiological and biogeochemical interactions. Interact. between macro-Microorg. Mar. sediments 125–157.

Kristensen, E., K. D. Kristiansen, and M. H. Jensen. 2003. Temporal behavior of manganese and iron in a sandy coastal sediment exposed to water column anoxia. Estuaries **26**: 690–699.

Kristensen, E., G. Penha-Lopes, M. Delefosse, T. Valdemarsen, C. O. Quintana, and G. T. Banta. 2012a. What is bioturbation? the need for a precise definition for fauna in aquatic sciences. Mar. Ecol. Prog. Ser. **446**: 285–302.

Kristensen, E., G. Penha-Lopes, M. Delefosse, T. Valdemarsen, C. O. Quintana, and G. T. Banta. 2012b. What is bioturbation? the need for a precise definition for fauna in aquatic sciences. Mar. Ecol. Prog. Ser. **446**: 285–302.

Kristiansen, K. D., E. Kristensen, and M. H. Jensen. 2002. The influence of water column hypoxia on the behaviour of manganase and iron in sandy coastal marine sediment. Est. Coast. Shelf. Sci. **55**: 645–654.

Kuenen. 1975. Colourless sulfur bacteria and their role in the sulfur cycle. Plant Soil **76**: 49–76.

Kuenen. 1985. Microbial interactions among Aerobic and Anaerobic Sulphur-Oxidizing Bacteria. B. chapeter

Lam, P., and M. M. M. Kuypers. 2011. Microbial nitrogen cycling processes in oxygen minimum zones. Ann. Rev. Mar. Sci. **3**: 317–345.

Landing, W. M., and K. W. Bruland. 1987. The contrasting biogeochemistry of iron and manganese in the Pacific Ocean. Geochim. Cosmochim. Acta **51**: 29–43.

Larsen, S., L. P. Nielsen, and A. Schramm. 2015. Cable bacteria associated with long-distance electron transport in New England salt marsh sediment. Environ. Microbiol. Rep. **7**: 175–179.

REFERENCES

Lavik, G., T. Stührmann, V. Brüchert, A. Van der Plas, V. Mohrholz, P. Lam, M. Mussmann, B. M. Fuchs, R. Amann, U. Lass, and M. M. M. Kuypers. 2009. Detoxification of sulphidic African shelf waters by blooming chemolithotrophs. Nature **457**: 581–4.

Lehrter, J. C., D. L. Beddick, R. Devereux, D. F. Yates, and M. C. Murrell. 2011. Sediment-water fluxes of dissolved inorganic carbon, O2, nutrients, and N2 from the hypoxic region of the Louisiana continental shelf. Biogeochemistry **109**: 233–252.

Levin, L. A., W. Ekau, a. J. Gooday, F. Jorissen, J. J. Middelburg, S. W. a. Naqvi, C. Neira, N. N. Rabalais, and J. Zhang. 2009. Effects of natural and human-induced hypoxia on coastal benthos. Biogeosciences **6**: 2063–2098.

Lewis, B. L., and W. M. Landing. 1992. The investigation of dissolved and suspended-particulate trace metal fractionation in the Black Sea. Mar. Chem. **40**: 105–141.

Lichtschlag, A., J. Felden, and V. Bru. 2010. Geochemical processes and chemosynthetic primary production in different thiotrophic mats of the Hakon Mosby Mud Volcano (Barents Sea). Limnol. Oceanogr. **55**: 931–949.

Lindeboom, H. J., and A. G. A. Merks. 1983. Annual changes in nutrient, DOC and POC concentrations and their relationship with chemical and biological processes in a closed estuary. Mitt. Geol. Paläont. Inst. Univ. Hambg. **55**: 315–329.

Livingstone, D. M., and D. M. Imboden. 1996. The prediction of hypolimnetic oxygen profiles: a plea for a deductive approach. Can. J. Fish. Aquat. Sci. **53**: 924–932.

Llans, R. J. 1992. Effects of Hypoxia on Estuarine Benthos: the Lower Rappahannock River (Chesapeake Bay), a Case Study. Est. Coast. Shelf. Sci. **35**: 491–515.

Loferer-Krossbacher, M., J. Klima, and R. Psenner. 1998. Determination of bacterial cell dry mass by transmission electron microscopy and densitometric image analysis. Appl. Environ. Microbiol. **64**: 688–694.

Luther, G. W., A. J. Findlay, D. J. MacDonald, S. M. Owings, T. E. Hanson, R. A. Beinart, and P. R. Girguis. 2011. Thermodynamics and kinetics of sulfide oxidation by oxygen: A look at inorganically controlled reactions and biologically mediated processes in the environment. Front. Microbiol. **2**: 1–9.

Luther, G. W., A. Giblin, R. W. Howarth, and R. a. Ryans. 1982. Pyrite and oxidized iron mineral phases formed from pyrite oxidation in salt marsh and estuarine sediments. Geochim. Cosmochim. Acta **46**: 2665–2669.

Malkin, S. Y., A. M. Rao, D. Seitaj, D. Vasquez-Cardenas, E.-M. Zetsche, S. Hidalgo-Martinez, H. T. Boschker, and F. J. Meysman. 2014. Natural occurrence of microbial sulphur oxidation by long-range electron transport in the seafloor. ISME J. **8**: 1843–1854.

Manning, C. C., R. C. Hamme, and A. Bourbonnais. 2010. Impact of deep-water renewal events on fixed nitrogen loss from seasonally-anoxic Saanich Inlet. Mar. Chem. **122**: 1–10.

Martens, C. S., and J. Klump. 1984. Biogeochemical cycling in an organic-rich coastal marine basin 4. An organic carbon budget for sediments dominated by sulfate

206

reduction and methanogenesis. Geochim. Cosmochim. Acta **48**: 1987–2004.

Marzocchi, U., D. Trojan, S. Larsen, R. Louise Meyer, N. Peter Revsbech, A. Schramm, L. Peter Nielsen, and N. Risgaard-Petersen. 2014. Electric coupling between distant nitrate reduction and sulfide oxidation in marine sediment. ISME J. **8**: 1682–1690.

McCarthy, M. J., K. S. McNeal, J. W. Morse, and W. S. Gardner. 2008. Bottom-water hypoxia effects on sediment-water interface nitrogen transformations in a seasonally hypoxic, shallow bay (Corpus Christi Bay, TX, USA). Estuaries and Coasts **31**: 521–531.

McCave, I. N., R. J. Bryant, H. F. Cook, and C. A. Coughanowr. 1986. Evaluation of a Laser-Diffraction-Size Analyzer for Use with Natural Sediments. J. Sediment. Res. **56**: 561–564.

McHatton, S. C., J. P. Barry, H. W. Jannasch, and D. C. Nelson. 1996. High Nitrate Concentrations in Vacuolate, Autotrophic Marine Beggiatoa spp. Appl. Environ. Microbiol. **62**: 954–8.

Meire, L., K. E. R. Soetaert, and F. J. R. Meysman. 2013. Impact of global change on coastal oxygen dynamics and risk of hypoxia. Biogeosciences **10**: 2633–2653.

Meysman, F. J. R., B. P. Boudreau, and J. J. Middelburg. 2005. Modeling reactive transport in sediments subject to bioturbation and compaction. Geochim. Cosmochim. Acta **69**: 3601–3617.

Meysman, F. J. R., B. P. Boudreau, and J. J. Middelburg. 2010a. When and why does bioturbation lead to diffusive mixing ? J. Mar. Res. **68**: 881–920.

Meysman, F. J. R., O. S. Galaktionov, R. N. Glud, and J. J. Middelburg. 2010b. Oxygen penetration around burrows and roots in aquatic sediments. J. Mar. Res. **68**: 309–336.

Meysman, F. J. R., J. J. Middelburg, and C. H. R. Heip. 2006. Bioturbation: a fresh look at Darwin's last idea. Trends Ecol. Evol. **21**: 688–695.

Meysman, F. J. R., J. J. Middelburg, P. M. J. Herman, and C. H. R. Heip. 2003. Reactive transport in surface sediments. II. Media: an object-oriented problem-solving environment for early diagenesis. Comput. Geosci. **29**: 301–318.

Meysman, F. J. R., N. Risgaard-Petersen, S. Y. Malkin, and L. P. Nielsen. 2015. The geochemical fingerprint of microbial long-distance electron transport in the seafloor. Geochim. Cosmochim. Acta **152**: 122–142.

Middelburg, J. J., and L. A. Levin. 2009. Coastal hypoxia and sediment biogeochemistry. Biogeosciences **6**: 1273–1293.

Middelburg, J. J., K. Soetaert, P. M. J. Herman, and C. H. R. Heip. 1996. Denitrification in marine sediments : A model study. Glob. Biogeochem. cyles

Millero, F. J. 1995. Thermodynamics of the carbon dioxide system in the ocean. Geochim. Cosmochim. Acta **59**: 661–677.

Millero, F. J., S. Hubinger, M. Fernandez, and S. Garnett. 1987. Oxidation of H2S in Seawater as a Function of Temperature, pH, and Ionic Strength. Environ. Sci .Technol. **21**: 439–443.

Moeslund, L., B. Thamdrup, and B. B. Jørgensen. 1994. Sulfur and iron cycling in a coastal

sediment: Radiotracer studies and seasonal dynamics. Biogeochemistry **27**: 129–152.

Moodley, L., J. J. Middelburg, P. M. J. Herman, K. Soetaert, and G. J. de Lange. 2005. Oxygenation and organic-matter preservation in marine sediments: Direct experimental evidence from ancient organic carbon-rich deposits. Geology **33**: 889–892.

Morrison, J. M., L. a. Codispoti, S. L. Smith, K. Wishner, C. Flagg, W. D. Gardner, S. Gaurin, S. W. a. Naqvi, V. Manghnani, L. Prosperie, and J. S. Gundersen. 1999. The oxygen minimum zone in the Arabian Sea during 1995. Deep. Res. Part Ii-Topical Stud. Oceanogr. **46**: 1903–1931.

Mort, H. P., C. P. Slomp, B. G. Gustafsson, and T. J. Andersen. 2010. Phosphorus recycling and burial in Baltic Sea sediments with contrasting redox conditions. Geochim. Cosmochim. Acta **74**: 1350–1362.

Mortimer, C. H. 1941. The Exchange of Dissolved Substances between mud and water in lakes. J. Ecol. **30**: 147–201.

Mouret, A., P. Anschutz, P. Lecroart, G. Chaillou, C. Hyacinthe, J. Deborde, F. J. Jorissen, B. Deflandre, S. Schmidt, and J. Jouanneau. 2009. Benthic geochemistry of manganese in the Bay of Biscay , and sediment mass accumulation rate. Geo-Mar Lett **29**: 133–149.

Mucci, A., M. Starr, D. Gilbert, and B. Sundby. 2011. Acidification of Lower St. Lawrence Estuary Bottom Waters. Atmosphere-Ocean **49**: 206–218.

Mulder, A., A. A. van de Graaf, L. A. Robertson, and J. G. Kuenen. 1995. Anaerobic ammonium oxidation discovered in a denitrifying fluidized bed reactor. FEMS Microbiol. Ecol. **16**: 177–183.

Murray, J., K. Stewart, S. Kassakian, M. Krynytzky, D. Dijulio, and J. W. Murray. 2007. Oxic, suboxic, and anoxic conditions in the Black Sea, p. 1–21. *In* The Black Sea Flood Question: Changes in Coastline, Climate, and Human Settlement.

Mussmann, M., H. N. Schulz, B. Strotmann, T. Kjaer, L. P. Nielsen, R. a Rosselló-Mora, R. I. Amann, and B. B. Jørgensen. 2003. Phylogeny and distribution of nitrate-storing Beggiatoa spp. in coastal marine sediments. Environ. Microbiol. **5**: 523–33.

Neubacher, E. C., R. E. Parker, and M. Trimmer. 2011. Short-term hypoxia alters the balance of the nitrogen cycle in coastal sediments. Limnol. Oceanogr. **56**: 651–665.

Nielsen, L. P. 2016. Ecology: Electrical Cable Bacteria Save Marine Life. Curr. Biol. **26**: R32–R33.

Nielsen, L. P., and N. Risgaard-Petersen. 2015. Rethinking Sediment Biogeochemistry After the Discovery of Electric Currents. Ann. Rev. Mar. Sci. **7**: 425–442.

Nielsen, L. P., N. Risgaard-Petersen, H. Fossing, P. B. Christensen, and M. Sayama. 2010. Electric currents couple spatially separated biogeochemical processes in marine sediment. Nature **463**: 1071–4.

Nienhuis, P. H., and J. C. Huis in 't Veld. 1984. Grevelingen: from an estuary to a saline lake. Water Sci. Technol. **16**: 27–50.

Nienhuis, P. H., and E. T. van Ierland. 1978. Consumption of eelgrass, zostera marina, by

birds and invertebrates during the growing season in lake grevelingen (SW Netherlands). Netherlands J. Sea Res. **12**: 180–194.

Noffke, A., S. Sommer, A. W. Dale, P. O. J. Hall, and O. Pfannkuche. 2016. Benthic nutrient fluxes in the Eastern Gotland Basin (Baltic Sea) with particular focus on microbial mat ecosystems. J. Mar. Syst. **158**: 1–12.

Nolte, A. J., and C. Spiteri. 2011. Effect van herintroductie van getij op waterkwaliteit en ecologische toestand van het Grevelingenmeer.

Oguz, T., J. W. Murray, and A. E. Callahan. 2001. Modeling redox cycling across the suboxic-anoxic interface zone in the Black Sea. Deep. Res. Part I Oceanogr. Res. Pap. **48**: 761–787.

Pace, M., and Y. Prairie. 2005. Respiration in lakes, p. 103–121. *In* P.J. le. B. Williams and P.A. Del Giorgio [eds.], Respiration in aquatic ecosystems. Oxford University Press.

Pamatmat, M. M. 1971. Oxygen Consumption by the Seabed. VI. Seasonal Cycle of Chemical Oxidation and Respiration in Puget Sound. Int. Rev. Hydrobiol. **56**: 769–739.

Paulmier, A., and D. Ruiz-Pino. 2009. Oxygen minimum zones (OMZs) in the modern ocean. Prog. Oceanogr. **80**: 113–128.

Pearson, T. H., and R. Rosenberg. 1978. Macrobenthic succession in relation to organic enrichment and pollution of the marine environment. Oceanogr. Mar. Biol. Annu. Rev. **16**: 229–311.

Pfeffer, C., S. Larsen, J. Song, M. Dong, F. Besenbacher, R. L. Meyer, K. U. Kjeldsen, L. Schreiber, Y. a Gorby, M. Y. El-Naggar, K. M. Leung, A. Schramm, N. Risgaard-Petersen, and L. P. Nielsen. 2012. Filamentous bacteria transport electrons over centimetre distances. Nature **491**: 218–21.

Ploug, H., and B. B. Jørgensen. 1999. A net-jet flow system for mass transfer and microsensor studies of sinking aggregates. Mar. Ecol. Prog. Ser. **176**: 279–290.

Polerecky, L., B. Adam, J. Milucka, N. Musat, T. Vagner, and M. Kuypers. 2012. Look@NanoSIMS-a tool for the analysis of nanoSIMS data in environmental microbiology. Environ. Microbiol. **14**: 1009–1023.

Postma, D., and R. Jakobsen. 1996. Redox zonation: Equilibrium constraints on the Fe(III)/SO4-reduction interface. Geochim. Cosmochim. Acta **60**: 3169–3175.

Poulton, S. W., and D. E. Canfield. 2005. Development of a sequential extraction procedure for iron: Implications for iron partitioning in continentally derived particulates. Chem. Geol. **214**: 209–221.

Preisler, A., D. de Beer, A. Lichtschlag, G. Lavik, A. Boetius, and B. B. Jørgensen. 2007. Biological and chemical sulfide oxidation in a Beggiatoa inhabited marine sediment. ISME J. **1**: 341–53.

Rabalais, N. N., R. J. Díaz, L. a. Levin, R. E. Turner, D. Gilbert, and J. Zhang. 2010. Dynamics and distribution of natural and human-caused hypoxia. Biogeosciences **7**: 585–619.

Rabalais, N. N., R. E. Turner, B. K. Sen Gupta, D. F. Boesch, P. Chapman, and M. C.

Murrell. 2007. Hypoxia in the northern Gulf of Mexico: does the science support the plan to reduce, mitigate, and control hypoxia? Estuaries and Coasts **30**: 753–772.

Rabalais, N. N., R. E. Turner, and W. J. Wiseman. 2002. Gulf of Mexico Hypoxia, a.K.a. "the Dead Zone." Annu. Rev. Ecol. Syst. **33**: 235–263.

Rabouille, C., L. Denis, K. Dedieu, G. Stora, B. Lansard, and C. Grenz. 2003. Oxygen demand in coastal marine sediments: Comparing in situ microelectrodes and laboratory core incubations. J. Exp. Mar. Bio. Ecol. **285**–**286**: 49–69.

Rao, A. M. F., S. Y. Malkin, S. Hidalgo-Martinez, and F. J. R. Meysman. 2016. The impact of electrogenic sulfide oxidation on elemental cycling and solute fluxes in coastal sediment. Geochim. Cosmochim. Acta **172**: 265–286.

Rasmussen, H., and B. B. Jorgensen. 1992. Microelectrode studies of seasonal oxygen uptake in a coastal sediment : role of molecular diffusion. Mar. Ecol. Prog. Ser. **81**: 289–303.

Reed, D. C., C. P. Slomp, and B. G. Gustafsson. 2011. Sedimentary phosphorus dynamics and the evolution of bottom-water hypoxia: A coupled benthic-pelagic model of a coastal system. Limnol. Oceanogr. **56**: 1075–1092.

Reimers, C. E. 1996. Porewater pH and authigenic phases formed in the uppermost sediments of the Santa Barbara Basin. Geochim. Cosmochim. Acta **60**: 4037–4057.

Rickard, D., and G. W. Luther. 2007. Chemistry of iron sulfides,.

Risgaard-Petersen, N., M. Kristiansen, R. B. Frederiksen, A. L. Dittmer, J. T. Bjerg, D. Trojan, L. Schreiber, L. R. Damgaard, A. Schramm, and L. P. Nielsen. 2015. Cable bacteria in freshwater sediments. Appl. Environ. Microbiol. **81**: 6003–6011.

Risgaard-Petersen, N., A. Revil, P. Meister, and L. P. Nielsen. 2012. Sulfur, iron-, and calcium cycling associated with natural electric currents running through marine sediment. Geochim. Cosmochim. Acta **92**: 1–13.

Ritter, C., and P. a. Montagna. 1999. Seasonal Hypoxia and Models of Benthic Response in a Texas Bay. Estuaries **22**: 7–20.

Roberts, K. L., V. M. Eate, B. D. Eyre, D. P. Holland, and P. L. M. Cook. 2012. Hypoxic events stimulate nitrogen recycling in a shallow salt-wedge estuary: The Yarra River Estuary, Australia. Limnol. Oceanogr. **57**: 1427–1442.

Robertson and Kuenen. 2006. The Genus Thiobacillus, p. 812–827. *In* Procaryotes.

Romero-Ramirez, A., A. Grémare, M. Desmalades, and J. C. Duchêne. 2013. Semi-automatic analysis and interpretation of sediment profile images. Environ. Model. Softw. **47**: 42–54.

Rosenberg, R. 1990. Negative Oxygen Trends in Swedish Coastal Bottom Waters. Mar. Pollut. Bull. **21**: 335–339.

Rosenberg, R., S. Agrenius, B. Hellman, H. C. Nilsson, and K. Norling. 2002. Recovery of marine benthic habitats and fauna in a Swedish fjord following improved oxygen conditions. Mar. Ecol. Prog. Ser. **234**: 43–53.

Rosenberg, R., and H. C. Nilsson. 2005. Deterioration of soft-bottom benthos along the Swedish Skagerrak coast. J. Sea Res. **54**: 231–242.

Rosenberg, R., H. C. Nilsson, and R. J. Diaz. 2001. Response of Benthic Fauna and Changing Sediment Redox Profiles over a Hypoxic Gradient. Estuar. Coast. Shelf Sci. **53**: 343–350.

Rowe, G. T., M. E. C. Kaegi, J. W. Morse, G. S. Boland, E. G. Escobar Briones, H. Heights, M. M. Service, and N. Orleans. 2002. Sediment community metabolism associated with continental shelf hypoxia, Northern Gulf of Mexico. Estuaries **25**: 1097–1106.

Rozan, T. F., M. Taillefert, R. E. Trouwborst, B. T. Glazer, S. Ma, J. Herszage, L. M. Valdes, K. S. Price, and G. W. I. Luther. 2002. Iron-sulfur-phosphorus cycling in the sediments of a shallow coastal bay: Implications for sediment nutrient release and benthic macroalgal blooms. Limnol. Oceanogr. **47**: 1346–1354.

Ruttenberg, K. C. 1992. Development of a sequential extraction method for different forms of phosphorus in marine sediments. Limnol. Oceanogr. **37**: 1460–1482.

Ruttenberg, K. C. 2014. The Global Phosphorus Cycle, Elsevier: Oxford.

Van Santvoort, P. J. M., G. J. De Lange, J. Thomson, S. Colley, F. J. R. Meysman, and C. P. Slomp. 2002. Oxidation and origin of organic matter in surficial Eastern Mediterranean hemipelagic sediments. Aquat. Geochemistry **8**: 153–175.

Sayama, M. 2011. Seasonal dynamics of sulfide oxidation processes in Tokyo Bay dead zone sediment. Goldschmidt Abstr. 1804.

Sayama, M., N. Risgaard-petersen, L. P. Nielsen, H. Fossing, and P. B. Christensen. 2005. Impact of Bacterial NO3− Transport on Sediment Biogeochemistry. **71**: 3–6.

Schauer, R., N. Risgaard-Petersen, K. U. Kjeldsen, J. J. Tataru Bjerg, B. B Jørgensen, A. Schramm, and L. P. Nielsen. 2014. Succession of cable bacteria and electric currents in marine sediment. ISME J. **8**: 1–9.

Schulz, H. N., and B. B. Jørgensen. 2001. Big bacteria. Annu. Rev. Microbiol. **55**: 105–137.

Schulz, H. N., and H. D. Schulz. 2005. Large sulfur bacteria and the formation of phosphorite. Science (80-.). **307**: 416–418.

Schulz, H. N., B. T, F. TG, M. MH, J. Teske A, and O. BB. 1999. Dense Populations of a Giant Sulfur Bacterium in Namibian Shelf Sediments. Science (80-.). **284**: 493–495.

Scranton, M. I., G.T. Taylor, R. Thunell, C. R. Benitez-Nelson, F. Muller-Karger, K. Fanning, L. Lorenzoni, E. Montes, R. Varela, and nd Y. and Astor. 2014. Interannual and Subdecadal Variability in the Nutrient Geochemistry of the Cariaco Basin. Oceanography **27**: 148–159.

Seitaj, D., R. Schauer, F. Sulu-Gambari, S. Hidalgo-Martinez, S. Y. Malkin, L. D. W. Burdorf, C. P. Slomp, and F. J. R. Meysman. 2015. Cable bacteria generate a firewall against euxinia in seasonally hypoxic basins. Proc. Natl. Acad. Sci. **112**: 13278–13283.

Simpson, J. H. 1981. The shelf-sea fronts: implications of their existence and behaviour. Philos. Trans. R. Soc. A Math. Phys. Eng. Sci. **302**: 531–543.

Sivan, O., G. Antler, A. V Turchyn, J. J. Marlow, and V. J. Orphan. 2014. Iron oxides

stimulate sulfate-driven anaerobic methane oxidation in seeps. 4139–4147.

Slomp, C. P. 2011. Phosphorus Cycling in the Estuarine and Coastal Zones: Sources, Sinks, and Transformations, p. 201–230. *In* E.W. and D. McLusky [ed.], Treatise on Estuarine and Coastal Science. Elsevier Inc.

Slomp, C. P., S. J. Van der Gaast, and W. Van Raaphorst. 1996. Phosphorus binding by poorly crystalline iron oxides in North Sea sediments. Mar. Chem. **52**: 55–73.

Slomp, C. P., J. F. P. Malschaert, L. Lohse, and W. Van Raaphorst. 1997. Iron and manganese cycling in different sedimentary environments on the North Sea continental margin. Cont. Shelf Res. **17**: 1083–1117.

Smith, K. L. 1973. Respiration of a Sublittoral Community. Ecology **54**: 1065–1075.

Soetaert, K., P. M. J. Herman, and J. J. Middelburg. 1996a. Dynamic response of deep-sea sediments to seasonal variations: A model. Limnol. Oceanogr. **41**: 1651–1668.

Soetaert, K., P. M. J. Herman, and J. J. Middelburg. 1996b. A model of early diagenetic processes from the shelf To abyssal depths. Geochim. Cosmochim. Acta **60**: 1019–1040.

Soetaert, K., P. M. J. Herman, J. J. Middelburg, and C. Heip. 1998. Assessing organic matter mineralization, degradability and mixing rate in an ocean margin sediment (Northeast Atlantic) by diagenetic modeling. J. Mar. Res. **56**: 519–534.

Soetaert, K., and F. Meysman. 2012. Reactive transport in aquatic ecosystems: Rapid model prototyping in the open source software R. Environ. Model. Softw. **32**: 49–60.

Soetaert, K., and J. J. Middelburg. 2009. Modeling eutrophication and oligotrophication of shallow-water marine systems: the importance of sediments under stratified and well-mixed conditions. Hydrobiologia **629**: 239–254.

Soetaert, K., J. J. Middelburg, P. M. J. Herman, and K. Buis. 2000. On the coupling of benthic and pelagic biogeochemical models. Earth Sci. Rev. **51**: 173–201.

Soetaert, K., T. Petzoldt, and F. J. R. Meysman. 2010a. marelac: Tools for Aquatic Sciences R package version 2.1.

Soetaert, K., T. Petzoldt, and R. W. Setzer. 2010b. Package deSolve : Solving Initial Value Differential Equations in R. J. Stat. Softw. **33**: 1–25.

Stachowitsch, M. 1991. Anoxia in the Northern Adriatic Sea: rapid death, slow recovery. Geol. Soc. London, Spec. Publ. **58**: 119–129.

Steckbauer, A., C. M. Duarte, J. Carstensen, R. Vaquer-Sunyer, and D. J. Conley. 2011. Ecosystem impacts of hypoxia: thresholds of hypoxia and pathways to recovery. Environ. Res. Lett. **6**: 25003.

Stramma, L., G. C. Johnson, J. Sprintall, and V. Mohrholz. 2008. Expanding Oxygen-Minimum Zones in the Tropical Oceans. Science (80-.). **320**: 655–659.

Straub, K. L., M. Benz, B. Schink, and F. Widdel. 1996. Anaerobic, nitrate-dependent microbial oxidation of ferrous iron. Appl. Environ. Microbiol. **62**: 1458–60.

Strickland, J. D., and T. R. Parsons. 1972. A Practical Handbook of Seawater Analysis, p. 310. *In* Bulletin (Fisheries Research Board of Canada): Ottawa.

Sulu-Gambari, F., D. Seitaj, F. J. R. Meysman, R. Schauer, L. Polerecky, and C. P. Slomp.

212

2016. Cable Bacteria Control Iron-Phosphorus Dynamics in Sediments of a Coastal Hypoxic Basin. Environ. Sci. Technol. **50**: 227–1233.

Sunda, W. G., and W. J. Cai. 2012. Eutrophication induced CO2-acidification of subsurface coastal waters: Interactive effects of temperature, salinity, and atmospheric P CO2. Environ. Sci. Technol. **46**: 10651–10659.

Sundby, B. 1992. The phosphorus cycle in coastal marine sediments. Limnol. Oceanogr. **37**: 1129–1145.

Sverdrup, H. U. 1953. On conditions for the vernal blooming of phytoplankton. J. du Cons. **18**: 287–295.

Testa, J. M., and W. M. Kemp. 2011. Oxygen – Dynamics and Biogeochemical Consequences, p. 163–200. *In* Wolanski E and McLusky DS (eds.) Treatise on Estuarine and Coastal Science. Waltham: Academic Press.

Testa, J. M., and W. M. Kemp. 2012. Hypoxia-induced shifts in nitrogen and phosphorus cycling in Chesapeake Bay. Limnol. Oceanogr. **57**: 835–850.

Testa, J. M., and W. M. Kemp. 2014. Spatial and Temporal Patterns of Winter-Spring Oxygen Depletion in Chesapeake Bay Bottom Water. Estuaries and Coasts **37**: 1432–1448.

Thamdrup, B. 2000. Bacterial Manganese and Iron Reduction in Aquatic Sediments, p. 41–84. *In* B. Schink [ed.], Advances in Microbial Ecology. Luwer Academic/Plenum Publishers.

Thamdrup, B., D. E. Canfield, T. G. Ferdelman, R. N. Glud, and J. K. Gundersen. 1996. A biogeochemical survey of the anoxic basin Golfo Dulce, Costa Rica. Rev. Biol. Trop. **44**: 19–33.

Thamdrup, B., H. Fossing, and B. B. Jørgensen. 1994. Manganese, iron and sulfur cycling in a coastal marine sediment, Aarhus bay, Denmark. Geochim. Cosmochim. Acta **58**: 5115–5129.

Thamdrup, B., M. M. Jensen, O. Ulloa, L. Farı, and R. Escribano. 2006. Anaerobic ammonium oxidation in the oxygen-deficient waters off northern Chile. Limnol. Ocean. **51**: 2145–2156.

Thamdrup, B., R. Rosselló-Mora, and R. Amann. 2000. Microbial manganese and sulfate reduction in Black Sea shelf sediments. Appl. Environ. Microbiol. **66**: 2888–97.

Thamdrup, B., J. Wu, and B. B. Jörgensen. 1998. Temperature dependence of aerobic respiration in a coastal sediment. FEMS Microbiol. Ecol. **25**: 189–200.

Therkildsen, M. S., and B. A. Lomstein. 1993. Seasonal variation in net benthic C-mineralization in a shallow estuary. FEMS Microbiol. Ecol. **12**: 131–142.

Trojan, D., L. Schreiber, J. T. Bjerg, A. Bøggild, and T. Yang. 2016. A Taxonomic framework for cable bacteria and proposal of the candidate genera Electrothrix and Electronema. Syst. Appl. Microbiol. , doi:10.1016/j.syapm.2016.05.006

Tryggestad, S., K. A. Selanger, J. P. Mathisen, and Ø. Johansen. 1983. Extreme Bottom Currents in the North Sea., p. 148–158. *In* J. Sündermann [ed.], North Sea dynamics.

Turchyn, A. V., O. Sivan, and D. P. Schrag. 2006. Oxygen isotopic composition of sulfate

in deep sea pore fluid: Evidence for rapid sulfur cycling. Geobiology **4**: 191–201.

Turner, R. E., N. N. Rabalais, and D. Justic. 2008. Gulf of Mexico hypoxia: alternate states and a legacy. Environ. Sci. Technol. **42**: 2323–7.

Ulloa, O., D. E. Canfield, E. F. DeLong, R. M. Letelier, and F. J. Stewart. 2012. Microbial oceanography of anoxic oxygen minimum zones. Proc. Natl. Acad. Sci. **109**: 15996–16003.

Vahtera, E., D. J. Conley, B. G. Gustafsson, H. Kuosa, H. Pitkänen, O. P. Savchuk, T. Tamminen, M. Viitasalo, M. Voss, N. Wasmund, and F. Wulff. 2007. Internal ecosystem feedbacks enhance nitrogen-fixing cyanobacteria blooms and complicate management in the Baltic Sea. R. Swedish Acad. Sci. **36**: 186–94.

Vaquer-Sunyer, R., and C. M. Duarte. 2008. Thresholds of hypoxia for marine biodiversity. Proc. Natl. Acad. Sci. U. S. A. **105**: 15452–7.

Vasquez-Cardenas, D., J. van de Vossenberg, L. Polerecky, S. Y. Malkin, R. Schauer, S. Hidalgo-Martinez, V. Confurius, J. J. Middelburg, F. J. Meysman, and H. T. Boschker. 2015. Microbial carbon metabolism associated with electrogenic sulphur oxidation in coastal sediments. ISME J. 1–13.

de Vries, I. 1984. The carbon balance of a saline lake (lake Grevelingen, The Netherlands). Netherlands J. Sea Res. **18**: 511–528.

Wenzhöfer, F., and R. N. Glud. 2004. Small-scale spatial and temporal variability in coastal benthic O-2 dynamics: Effects of fauna activity. Limnol. Oceanogr. **49**: 1471–1481.

Wenzhöfer and Glud. 2002. Benthic carbon mineralization in the Atlantic: a synthesis based on in situ data from the last decade. Deep Sea Res. I **49**: 1255–1279.

Wetsteyn, L. P. M. J. 2011. Grevelingenmeer: meer kwetsbaar? Lelystad, The Netherlands.

Zaikova, E., D. a. Walsh, C. P. Stilwell, W. W. Mohn, P. D. Tortell, and S. J. Hallam. 2010. Microbial community dynamics in a seasonally anoxic fjord: Saanich Inlet, British Columbia. Environ. Microbiol. **12**: 172–191.

Zhang, J., D. Gilbert, a. J. Gooday, L. Levin, S. W. a. Naqvi, J. J. Middelburg, M. Scranton, W. Ekau, a. Peña, B. Dewitte, T. Oguz, P. M. S. Monteiro, E. Urban, N. N. Rabalais, V. Ittekkot, W. M. Kemp, O. Ulloa, R. Elmgren, E. Escobar-Briones, and a. K. Van der Plas. 2010. Natural and human-induced hypoxia and consequences for coastal areas: synthesis and future development. Biogeosciences **7**: 1443–1467.

Ziebis, W., S. Forster, M. Huettel, and B. B. Jørgensen. 1996. Complex burrows of the mud shrimp Callianassa truncata and their geochemical impact in the sea bed. Nature **382**: 619–622.

Zijl, F., and A. Nolte. 2006. Delft Hydraulics.

Zilius, M., M. Bartoli, D. Daunys, R. Pilkaityte, and a. Razinkovas. 2012. Patterns of benthic oxygen uptake in a hypertrophic lagoon: spatial variability and controlling factors. Hydrobiologia **699**: 85–98.

Zopfi, J., M. E. Böttcher, and B. B. Jørgensen. 2008. Biogeochemistry of sulfur and iron in Thioploca-colonized surface sediments in the upwelling area off central chile. Geochim. Cosmochim. Acta **72**: 827–843.

Zopfi, J., T. G. Ferdelman, B. B. Jorgensen, A. Teske, and B. Thamdrup. 2001. Influence of water column dynamics on sulfide oxidation and other major biogeochemical processes in the chemocline of Mariager Fjord (Denmark). Mar. Chem. **74**: 29–51.

CURRICULUM VITAE

Name	Dorina Seitaj
Date of birth	01/08/1983
Nationality	Italian, Albanian
Tel	+31 (0) 647225040
E-mail	dorina.seitaj@gmail.com

EDUCATION

2011 - present **PhD-researcher**, Department of Ecosystem Studies, Royal Netherlands Institute for Sea Research (NIOZ), Yerseke, The Netherlands. PhD research project funded by the Darwin Center for Biogeosciences.

2007 - 2010 **MSc. in Environmental Sciences and Technologies (cum laude)**, University of Parma, Italy. Dissertation title: "*Ecological consequences of changing water regimes: Po River and Po Delta ecosystems*".

2004 - 2007 **BSc. in Environmental and Landscape Sciences and Technologies (cum laude)**, University of Parma, Italy. Dissertation title: *"Analysis of the role of macrophytic vegetation in two fluvial segments of the Mincio River: seasonal evolution of the O_2, CO_2 and nutrient mass balances".*

PUBLICATIONS

Seitaj D, Sulu-Gambari F, Burdorf LDW, Romero-Ramirez A, Maire O, Malkin SY, Slomp CP, Meysman FJR. Sedimentary oxygen dynamics in a seasonally hypoxic basin, *Limnology and Oceanography* in press.

Sulu-Gambari F, **Seitaj D**, Behrends T, Banerjee D, Meysman FJR, Slomp CP. Impact of Cable Bacteria on Sedimentary Iron and Manganese Dynamics in a Seasonally-Hypoxic Marine Basin, *Geochimica et Cosmochimica Acta,* 2016, 49-69.

Sulu-Gambari F, **Seitaj D**, Meysman FJR, Schauer R, Slomp CP (2016). Cable Bacteria Control Iron-Phosphorus Dynamics in Sediments of a Coastal Hypoxic Basin. *Environ. Sci. Technol.,* 2016, 50 (3), pp 1227–1233, doi:10.1021/acs.est.5b04369.

Seitaj D, Schauer R, Sulu-Gambari F, Malkin SY, Hidalgo-Martinez S, Slomp CP, Meysman FJR (2015). Cable bacteria generate a firewall against euxinia in seasonally hypoxic basins, *PNAS*, 2016, 112 (43), pp 13278–13283, doi: 10.1073/pnas.1510152112.

Hagens M, Slomp C, Meysman FJR, **Seitaj D**, Harlay J, Borges AV, Middelburg JJ (2015). Biogeochemical processes and buffering capacity concurrently affect acidification in a seasonally hypoxic coastal marine basin. *Biogeosciences*, 12, 15827-15887.

Malkin SY, Rao A, **Seitaj D**, Vasquez-Cardenas D, Zetsche E, Hidalgo-Martinez S, Boschker HTS, Meysman FJR (2014). Natural occurrence of microbial sulfur oxidation by long-range electron transport in the seafloor. *ISME Journal*, doi: 10.1038/ismej.2014.41.

MANUSCRIPTS SUBMITTED

Malkin SY, **Seitaj D**, Burdorf LDW, Nieuwhof S, Hidalgo-Martinez S, Tramper A, Geeraert N, de Stigter H, Meysman FJR. Electrogenic sulfide oxidation by cable bacteria in a bivalve reef sediment*s*, revision in progress at *Limnology and Oceanography*.

Burdorf LD, Tramper A, **Seitaj D**, Meire L, Hidalgo Martinez S, Zetsche E-M, Boschker HTS, Meysman FJR. Global distribution of cable bacteria, submited to *Biogeosciences*.

MANUSCRIPTS IN PREPARATION

Meysman FJR, **Seitaj D**. The paradox of aerobic sulfide oxidation revisited: suboxic zone formation, redox shuttling and cryptic sulfur cycling in marine sediments, in prep.

Seitaj D, Hagens M, Veuger B, Slomp CP, Meysman FJR. Biogeochemcial cycling in Lake Grevelingen, in prep.

Lipsewers AY, Vasquez-Cardenas D, **Seitaj D**, Sinninghe Damsté J, Meysman FJR, Villanueva L, Boschker HTS. Chemolithoautotrophic bacterial communities in sediments, in prep.

ORAL PRESENTATIONS

Seitaj D, Meysman FJR. Microbial innovation and the quest for electron donors in marine sediments. Aquatic Sciences Meeting, Granada, Spain, 22-27 February 2015.

Seitaj D, Aller RC, Soto-Neira J, Zhu Q, Meysman FJR. Hunting for cable bacteria in Long Island Sound. Second international workshop on Microbial long-distance electron transport, Antwerp, Belgium, 27–30 October 2014.

Seitaj D, Malkin SY, Schauer R, Meysman FJR. Efficient sulfide detoxification in seasonally hypoxic sediments by competing S-oxidizing bacteria. International colloquium on Low Oxygen Environments In Marine, Estuarine And Fresh Waters, Liege, Belgium, 05–09 May 2014.

Seitaj D, Malkin SY, Schauer R, Meysman FJR. Competition for Sulfide in Marine Sediments: Electrogenic Filamentous Bacteria Versus *Beggiatoa*. Goldschmidt 2013 conference, Florence, Italy, 25-30 August 2013.

Seitaj D, Malkin SY, Schauer R, Meysman FJR. The electrifying competition for sulfide in marine sediments: electrogenic filamentous bacteria versus *Beggiatoa*. Darwin Days, Conference of Darwin center for Biogeosciences, Utrecht, The Netherlands, 18 April 2013.

Seitaj D, Malkin SY, Schauer R, Meysman FJR. Competition for sulfide between electrogenic filamentous bacteria versus *Beggiatoa*. First International workshop on long distance electron transport. Oemborgen, Denmark, 14-17 April 2013.

POSTER PRESENTATIONS

Seitaj D, Malkin SY, Meysman FJR. Bacterial battles in hypoxic sediments. NIOZ Science Days, Texel, The Netherlands, 4-5 June 2014

Seitaj D, Malkin SY, Meysman FJR. Microbial sulfide oxidation in seasonally hypoxic coastal sediments: competition between electrogenic filamentous bacteria and *Beggiatoa*. Ocean Science meeting, Hawai, United States, 23-28 February 2014.

Seitaj D, Gambari F, Malkin SY, Slomp CP, Meysman FJR. Sulfide oxidation in hypoxic sediments: two competing microbial processes. NIOZ Science Days, Noordwijkerhout, The Netherlands, 4-5 June 2013.